

COMSAT
Technical Review

Volume 11 Number 2 Fall 1981

Advisory Board Joseph V. Charyk
William W. Hagerty
John V. Harrington
B. I. Edelson
Sidney Metzger

Editorial Board Pier L. Bargellini, Chairman
Ali E. Atia
S. J. Campanella
William L. Cook
C. Dorian
H. W. Fliieger
Jorge C. Fuenzalida
William J. Getsinger
R. W. Kreutel
Robert K. Kwan
Akos G. Revesz
George R. Welti

Editorial Staff Robert E. Bernier
MANAGING EDITOR
Margaret B. Jacocks
Elizabeth Christie
Pearl Coleman
Suzanne F. Metzger
TECHNICAL EDITORS
Edgar Bolen
PRODUCTION
Tina L. Arthur
CIRCULATION

COMSAT TECHNICAL REVIEW is published twice a year by Communications Satellite Corporation (COMSAT). Subscriptions, which include the two issues published within a calendar year, are: one year, \$7 U.S.; two years, \$12; three years, \$15; single copies, \$5; article reprints, \$1. Make checks payable to COMSAT and address to Treasurer's Office, Communications Satellite Corporation, 950 L'Enfant Plaza, S.W., Washington, D.C. 20024 U.S.A.

©COMMUNICATIONS SATELLITE CORPORATION 1982
COMSAT IS A TRADE MARK AND SERVICE MARK
OF THE COMMUNICATIONS SATELLITE CORPORATION

COMSAT TECHNICAL REVIEW

Volume 11 Number 2, Fall 1981

- 195 A DIRECT BROADCAST SATELLITE SYSTEM FOR THE UNITED STATES **L. M. Keane**, Editor
- 202 REGULATORY CONSIDERATIONS **E. E. Reinhart**
- 215 SYSTEM CHARACTERISTICS **E. R. Martin**
- 227 SATELLITE CHARACTERISTICS **E. R. Martin**
- 241 HOME EQUIPMENT TERMINAL CHARACTERISTICS
D.L. Durand
- 248 UP-LINK AND GROUND CONTROL FACILITIES **D. L. Durand**
- 255 DBS/FS FREQUENCY SHARING **J. E. Whitworth**
- 267 SBS SYSTEM EVOLUTION **W. H. Curry, Jr.**
- 293 4/6-GHZ IONOSPHERIC SCINTILLATION MEASUREMENTS DURING THE PEAK OF SUNSPOT CYCLE 21 **D. J. Fang and M. S. Pontes**
- 321 GENERALIZED DIELECTRIC RESONATOR FILTERS **A. E. Atia and R. R. Bonetti**
- 345 ANALYSIS OF THROUGHPUT EFFICIENCY AND DELAY IN ARQ SYSTEMS **D. M. Chitre**
- 369 FREQUENCY AND TIME COORDINATION VIA SATELLITE
L. Veenstra, J. Kaiser, C. Costain, W. Klepczynski, and D. Allan
- 403 FABRICATION TECHNIQUES OF LIGHTWEIGHT INVAR MICROWAVE FILTERS **H. I. Gerson**
- 421 CTR NOTES
SUMMARY OF THE SBS SATELLITE COMMUNICATIONS PERFORMANCE SPECIFICATIONS **G. G. Churan and W. E. Leavitt** 421
SOLAR ABSORPTANCE DEGRADATION OF AN UNCLEANED RADIATOR **N. L. Hyman** 433
19- AND 28-GHZ HIGH POWER/EFFICIENCY IMPATT AMPLIFIERS **S. M. Chou** 441
- 459 TRANSLATIONS OF ABSTRACTS
FRENCH 459 SPANISH 463

Foreword

This issue of *COMSAT Technical Review* presents a series of papers related to the Direct Broadcast Satellite System planned by the Satellite Television Corporation (STC), a COMSAT subsidiary.

The papers describe the proposed system, articulate some of the issues surrounding introduction of this new service, and outline its broad scope.

The success of STC's satellite-to-home pay television service will depend heavily on a careful combination of various critical technological elements. Recent developments in spacecraft components such as long life, reliable and efficient high power amplifiers and satellite antennas producing precisely shaped beams are of great importance. Equally significant will be the availability of high performance, ultra reliable, low cost receiving and decoding equipment which will permit individual control of transmissions received by the subscribers.

After the unparalleled advances of the past fifteen years in international and domestic satellite communications, in which COMSAT has played a leading role, STC is now prepared to face with confidence the challenge posed by this new broadcasting satellite service.

J. V. Charyk

A direct broadcast satellite system for the United States

L. M. KEANE, Editor

(Manuscript received August 18, 1981)

Abstract

This series of papers describes the first commercial direct broadcast satellite (DBS) service proposed for the United States. System elements are defined as they are presently conceived, and the major engineering tradeoffs made during development of the system configuration are discussed. Services to be offered and their expected characteristics are indicated. Orbit and spectrum utilization matters are considered in connection with worldwide radio conferences dealing with DBS planning. Analyses and measurements to determine the most effective means by which DBS and other domestic (terrestrial fixed) services can band share are also presented.

Introduction

On December 17, 1980, Satellite Television Corporation (STC)* applied for authorization from the U.S. Federal Communications

* STC is a wholly owned subsidiary of the Communications Satellite Corporation (COMSAT).

Abbreviations and acronyms used in this series of papers are defined on Page 265.

Commission (FCC) to build the first commercially supported DBS system for the United States. At the time of this writing, the FCC had accepted that application and invited public comments. Following receipt of an appropriate construction permit, DBS service will be available in the eastern United States in 1985-1986.

Over the past decade, significant progress has been made toward broadcasting television programs by satellite to receiving terminals that are simple enough for installation and operation at individual residences. This kind of reception has been demonstrated with the joint U.S./Canadian experimental Communications Technology Satellite (CTS) [1] and Japan's Broadcasting Satellite for Experimental Purposes (BSE) [2]. Development of prototype home receiving equipment and high-powered satellite transmitters for these experiments, as well as for other planned direct broadcast satellite applications, has provided a technological basis for the consideration of commercial direct broadcast satellite service.

Planned service

STC's broadcast service will include three channels of advertising-free television throughout the contiguous United States (CONUS) and to the major populated areas of Alaska and Hawaii.* Revenues will be obtained by viewer subscription to the basic service and to optional offerings. As currently conceived, basic programming will include movies, plays, concerts, nightclub acts, opera, dance, sports, children's shows, public affairs, and educational programs. Certain broadcast materials, targeted at narrow segments of the public that are not now adequately served, may be offered on a pay-per-series or pay-per-program basis. Since each satellite will broadcast to large areas, roughly the size of a whole U.S. time zone, widely scattered viewers with common interests can be combined into sufficiently large audiences to support these specialized programs. Major emphasis will be given to such "narrowcasting." For example, special programming might be offered to keep accountants abreast of developments in their field.

Stereophonic sound (using the viewer's conventional stereo amplifier and speaker system), and a second audio channel for a foreign language

* In its FCC application, STC requested authority to implement the first phase of the system for the provision of service to an area approximating the Eastern Time Zone in the United States. However, since STC plans to provide nationwide coverage in the future, this paper describes the complete system.

sound track will be optional features available to subscribers. STC also plans to offer optional teletext and captioning services, and to experiment with high-definition, large-screen television services, which will require special receiving equipment.

Because the proposed service will be supported by viewer subscriptions rather than by advertising, satellite transmissions will be scrambled to prevent unauthorized reception. Signals from the spacecraft will be received at subscriber residences by home equipment which includes an antenna and outdoor and indoor electronic units. This home equipment will receive and process the satellite transmissions for compatible reception and display on conventional U.S. television receivers. An addressable descrambler incorporated in the indoor unit can be controlled via the satellite to permit the receipt of optional programs or series. It can also be used to disengage nonpaying customers.

System summary

Major elements of the planned nationwide system are depicted in Figure 1. Four operating satellites will be spaced 20° apart along the geostationary arc (115°W, 135°W, 155°W, 175°W longitude). These locations were selected to achieve maximum satellite capacity and to permit spectrum reuse while providing acceptable eclipse times and elevation angles.

In addition to the four operating satellites, two in-orbit spares are planned for the nationwide implementation. The spares will be stationed at 115.05°W and 175.05°W longitude to restore service quickly in highly populated areas of the East and West Coasts if a satellite malfunction occurs. Failure of the 135°W or the 155°W satellite will necessitate repositioning one of the spares, a process that requires several days to a week.

The satellites will serve areas in the CONUS corresponding approximately to the size of the time zones. Satellite down-link transmissions will be in the 12-GHz broadcasting satellite service (BSS) band with a typical equivalent isotropic radiated power (e.i.r.p.) of 57 dBW. Once the satellites are on station, all operational up-links will be in the 17-GHz band.

Satellite broadcast transmissions will be received at individual residences by the home equipment units shown in Figure 2. Typically, the outdoor unit will consist of a 0.75-m diameter parabolic receiving

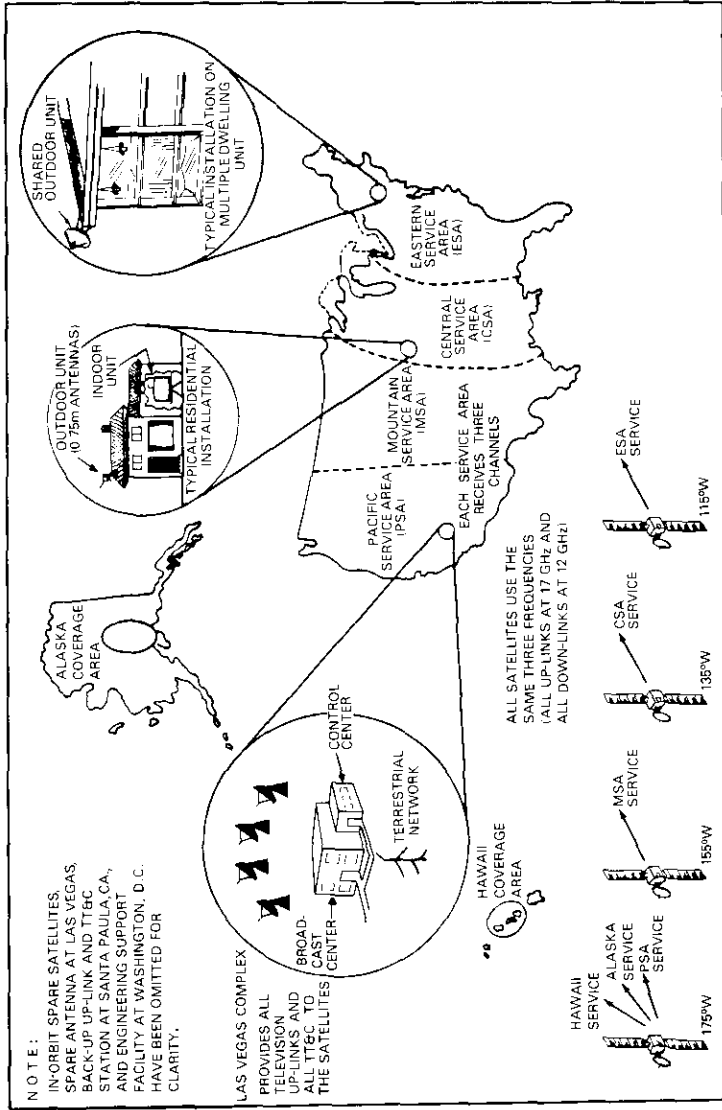


Figure 1. System Configuration

antenna and its attached microwave electronics; in some areas, antennas of 0.9- and 0.6-m diameter will be used to equalize grade of reception and/or reduce costs. The antennas may be mounted on rooftops, sidewalks, gable ends, or on the ground; however, in all cases, they must have an unobstructed view of the satellite. A cable connects the outdoor unit to an indoor unit that amplifies, demodulates, descrambles, and remodulates the received signal to allow compatible video reception by a conventional television set.

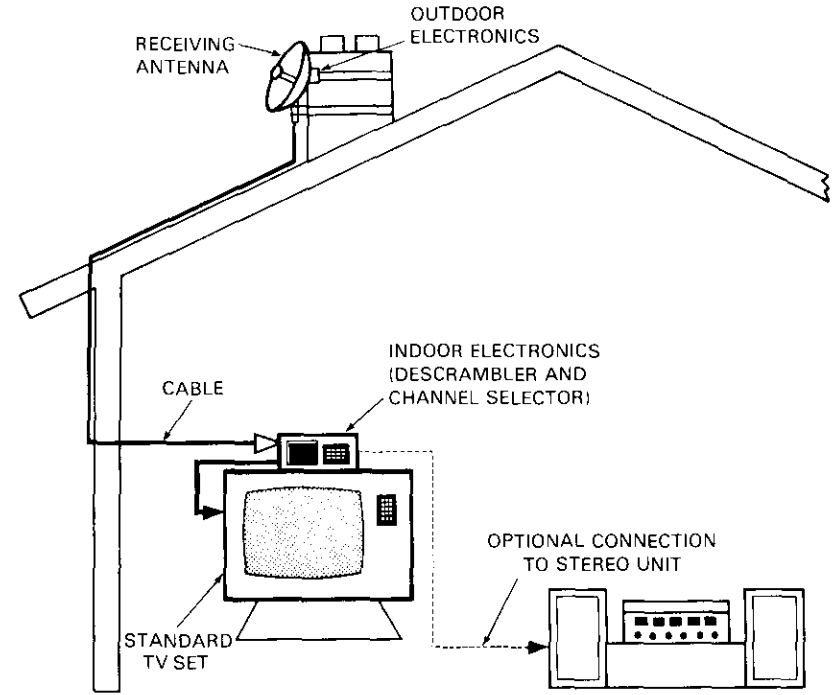


Figure 2. Typical Residential Installation

Multiple dwelling units (*e.g.*, apartment buildings and condominiums) will use equipment similar to that required for individual reception. It will also be feasible to deliver programming to cable headends with very simple receiving equipment.

The satellites are in the PAM-D mass class and will be launched on the Space Shuttle. However, the Space Shuttle may not be able to

accommodate the launch schedule of all the satellites, particularly the early ones, so the spacecraft will also be compatible with a shared launch on the ARIANE III launch vehicle. The satellites will generate prime DC power of approximately 1700 W at end of life (over 2000 W at beginning of life). Three operating traveling wave tube amplifiers (TWTAs) will feed a shaped beam transmitting antenna. Each TWTA will have 185 W RF power output at end of life. The transmit antenna patterns will be tailored to the contours of the areas served to improve transmission efficiency and minimize any signals radiated over foreign territories.

All the satellites will have a receive coverage area that extends from Los Angeles, California, to Las Vegas, Nevada. A Broadcast Center and System Control Facility near Las Vegas will have four operating 11-m diameter antennas and one redundant antenna to reliably feed and control the satellites. The spare satellites will be controlled with the same antennas used to feed and control adjacent satellites.

The Broadcast Center, which will provide program up-links to the satellites, will have studio facilities, video tape/film processing equipment, and related functional capabilities. Most programming will be stored on film or tape, but interconnections with the terrestrial microwave network will allow occasional live programming to originate from outside the Broadcast Center.

The System Control Facility will include a satellite control center and will perform telemetry, tracking and command (TT&C) functions. Additional equipment will be housed at this installation for system testing, and to activate subscriber home equipment, change the level of programming to existing customers, and coordinate subscriber billing functions. Backup feeder and TT&C facilities are also planned at Santa Paula, California.

An engineering support facility in Washington, D.C., will provide for overview of satellite control, orbital mechanics computations, special analyses and processing of telemetry, and access to specialized personnel in the event of spacecraft malfunction. All ground-based facilities will be connected by terrestrial full-period and dial-up voice/data links.

In mid-1983, a Regional Administrative Radio Conference (RARC-83) is scheduled to plan the BSS for ITU Region 2. Specific allotments (e.g., frequencies, polarizations, and orbital locations) are expected to be made to individual administrations. Because STC's application with the FCC seeks authorization to begin construction before RARC-83,

certain system parameters may change to conform with allotments made to the United States.

Domestic policy has not been fully developed to determine how the 12-GHz band will be shared with terrestrial fixed services, which are co-primary users in Region 2 in the International Table of Frequency Allocations. In the United States, some 1,700 licenses have already been granted in the 12.2-12.7-GHz band to private operational users. Fixed-service transmissions will cause significant interference into DBS home receivers if they are operated at or near the same frequencies. Domestic policy regarding band sharing between BSS and fixed-service users could also have an impact on the system characteristics.

The material presented in this series relies heavily on Volume 3 of STC's DBS application to the FCC,* which was the product of diverse engineering contributions from STC, COMSAT, COMSAT GENERAL, and COMSAT Laboratories.

References

- [1] J. Kaiser et al., "Small Earth Terminals at 12/14 GHz," *COMSAT Technical Review*, Vol. 9, No. 2B, Fall 1979, pp. 549-601.
- [2] J. Ichikawa et al., "Experimental Results of Japanese BSE Program in the First Year," AIAA paper No. 80-0569.

Leo M. Keane received a B.S. in electrical engineering from M.I.T., and an M.S. in electrical engineering from Northeastern University. He is presently Vice President, Engineering, of Satellite Television Corporation. Prior to the establishment of STC, Mr. Keane was Director of Advanced Systems Development for COMSAT General, where he was responsible for MARISAT and AEROSAT system development. Prior to joining COMSAT in 1971, Mr. Keane was Chief of the Telecommunications Division of DOT's Transportation System Center, and Chief of Communications and Navigation Programs at NASA's Electronics Research Center.



*Application of Satellite Television Corporation for a Satellite-to-Home Subscription Television Service, December 17, 1980.

Regulatory considerations

E. E. REINHART

Introduction

The general characteristics of STC's direct broadcasting satellite system have been strongly influenced by international regulatory actions taken over the past 10 years at three World Administrative Radio Conferences (WARCS) of the International Telecommunication Union (ITU). Final specifications for some system characteristics, including satellite orbital positions, carrier frequencies, and polarizations, must await the decisions of RARC-83, the regional conference scheduled for 1983.

This paper indicates how the various international regulatory actions have shaped the design of the STC system and describes the steps being taken to resolve the technical issues confronting RARC-83. Separate sections are devoted to the three WARCS.

WARC-ST

The most basic international actions affecting the BSS were taken in 1971 at the World Administrative Radio Conference for Space Telecommunication (WARC-ST). This conference defined the BSS as "a radio-communication service in which signals transmitted or retransmitted by space stations are intended for direct reception by the general public," and distinguished two types of reception: individual, which employs simple domestic installations, particularly those possessing small antennas; and community, which is characterized by receiving equipment, which, in some cases, may be complex and have antennas larger than those used for individual reception. Community reception is intended for use by a group of the general public at one location, or through a distribution system covering a limited area.

As with the terrestrial broadcasting service, all BSS transmissions are from the transmitter to the receiver. Hence, all BSS frequency allocations are in the down-link direction, which means that the up-

link transmissions to a broadcasting satellite (the so-called feeder link) must use frequencies allocated to the fixed-satellite service (FSS) in the same way that terrestrial broadcasting stations depend on microwave relay links in the terrestrial fixed service (FS) or, more recently, on satellite circuits in the FSS.

WARC-ST also provided the BSS with its first frequency allocations in bands near 0.7, 2.6, 12, 23, 42, and 85 GHz. Probably the most far-reaching action of WARC-ST for the BSS, however, was the adoption of Resolution Spa 2-2, which decreed that stations in the broadcasting-satellite service be established and operated in accordance with agreements and associated plans adopted by world or regional administrative conferences. Planning was justified in Resolution Spa 2-2 to make the best use of the geostationary-satellite orbit and of the frequency bands allocated to the BSS. Broadcasting satellites could not be repositioned economically after a great number of small directional antennas had been pointed at them. Moreover, European proponents of BSS planning argued that, since broadcasting-satellite systems would not be implemented for many years, terrestrial services with allocations in the same band could not be implemented without causing interference, unless the frequencies and orbital positions of future broadcasting satellites were known.

WARC-77

The 1977 World Broadcasting-Satellite Administrative Radio Conference (WARC-77) was the first of the planning conferences envisioned in Resolution Spa 2-2 [1]. Its purpose was to plan the BSS in the 12-GHz allocations that consisted of the 11.7- to 12.5-GHz band in Region 1 and the 11.7- to 12.2-GHz band in Regions 2 and 3.* The administrations disagreed about what the plan should specify, and how much of the world it should include. Most European nations contended that the plan should be worldwide and should specify, *a priori*, detailed system characteristics to meet the future channel and service area requirements identified by each ITU member administration. The European countries maintained that such an *a priori* plan was needed to provide guaranteed access for the broadcasting-satellite systems of developing nations, in addition to the reasons cited in connection with

Abbreviations and acronyms used in this series of papers are defined on Page 265.

*Region 1 includes Africa, Europe, the USSR, and Mongolia; Region 2 includes the Americas and Greenland; and Region 3 covers Asia (except for the USSR and Mongolia), Australia, and the Southwest Pacific.

Resolution Spa 2-2. A guarantee was considered necessary to prevent developed nations from using all of the desirable orbital positions and frequencies before the developing nations could launch their own systems.

The United States and a few other administrations were opposed to *a priori* planning at WARC-77 because countries would be restrained by unrealistic long-term projections and technology that would be obsolete, uneconomic, and wasteful of the orbit-spectrum resource long before most allotments were utilized. Even worse, the use of the entire resource to provide allotments to all administrations, regardless of size or need, would mean that most of the resource would remain unused and would preclude subsequent plan modifications to accommodate new or changed needs.

Instead of *a priori* planning, the United States favored an approach called "evolutionary planning" in which detailed characteristics of a broadcasting satellite system would not be specified by an administration until construction could be authorized. Such specifications would conform to planning principles and technical guidelines established at the conference to ensure efficient use of the orbit-spectrum resource.

For the countries in Regions 1 and 3, a detailed *a priori* plan was developed and incorporated into the Final Acts of WARC-77. In contrast, the countries in Region 2 postponed planning for at least 5 years and resolved to convene a Regional Administrative Radio Conference (RARC-83) for that purpose. The plan developed by Regions 1 and 3 includes 35 orbital positions, 40 frequencies, and both senses of circular polarization. It was decided to use orbital positions spaced nearly uniformly at 6° intervals from 37° W longitude eastward to 160° W longitude.* Channel frequencies are uniformly spaced at 19.18-MHz intervals from 11,727.48 MHz to 12,475.5 MHz. Since a 27-MHz bandwidth per channel was assumed, adjacent channels overlap, with guard bands of 14 MHz at the lower band edge (11.7 GHz) and 11 MHz at the upper band edge (12.5 GHz in Region 1 and 12.2 GHz in Region 3).

These resources provided allotments to 252 service areas in 150 countries and territories. Each allotment consisted of specified values for the following:

a. an orbital position,

*The positions at 116° and 164° E longitude and between 170° E and 160° W longitude are not used.

b. one or more channel numbers in the aforementioned frequency plan for TV carriers, and for each channel:

- the boresight of the satellite transmitting antenna,
- the half-power beamwidths and orientation corresponding to the major and minor axes of the elliptical cross-section of the satellite transmitting antenna beam,
- the sense of polarization of the antenna, and
- the e.i.r.p. in the direction of maximum radiation.

The plan was formulated on the collateral assumption that all systems will adhere to uniform specifications on a number of additional system parameters corresponding to individual reception of a high-quality TV picture. As discussed below, these include receiving antenna beamwidth, receiving figure-of-merit G/T, reference patterns for the copolarized and cross-polarized components of the transmitting and receiving antennas, type of modulation and necessary bandwidth, type and amount of energy dispersal, antenna pointing tolerances, and satellite stationkeeping tolerances.

The allotments themselves are then planned to satisfy a number of other conditions. For example, the orbital position should be far enough west of the standard-time meridian through the service area to defer power loss caused by solar eclipse near the equinoxes until after the normal broadcast day; yet it must be far enough east to maintain a minimum satellite elevation angle throughout the service area. The number of channels should accommodate the anticipated needs of the service area over the 15-year lifetime of the plan. In addition, the satellite pointing direction, elliptical-beam dimensions, and orientation should produce the minimum footprint that just covers the service area. The sense of polarization should be the same for all service areas of a given administration. Finally, the e.i.r.p. should produce a carrier-to-noise ratio (C/N) of 14 dB throughout the service area for 99 percent of the worst month.

The number of channels per service area ranged from one to eight with most Region 1 service areas receiving five channels and most Region 3 service areas, four channels. The number of service areas per country ranged from 1 to 35 with most countries having only one.*

*Note that the smallest islands and principalities received the same size allotment as most European countries (*i.e.*, five channels from one orbital position into one service area.)

However, the largest countries received proportionately larger allotments as shown in Table 1.

TABLE 1. ALLOTMENTS TO LARGEST COUNTRIES

COUNTRY	SERVICE AREAS	ORBITAL POSITIONS	TOTAL CHANNELS
China	35	3	55
USSR	21	5	65
India	12	2	48
Australia	6	2	36
Indonesia	5	2	20
Pakistan	5	1	11
Sudan	3	1	15

In the plan for Regions 1 and 3, each of the channels from 1 to 24* was used in allotments to an average of 30 different service areas administered by perhaps 25 different countries. Frequencies were rarely reused from a given orbital position, typically for two widely separated service areas using opposite senses of polarization. In the more heavily used parts of the orbit serving Europe and Africa, each orbital position was used in 5-channel allotments to approximately 12 service areas.

The specific values of the system technical characteristics assumed in formulating the plan are of special interest because WARC-77 proposed similar characteristics for Region 2 systems, and because STC's system design is modeled after the Region 2 proposals. The Region 1 and 3 system characteristics are shown in Table 2 and Figures 1 and 2. The Region 2 characteristics differ from these only in necessary bandwidth, guard band bandwidth, earth station antenna characteristics, and in the power flux density for individual reception as shown in Table 3 and Figure 3.

Probably the most important difference in the Region 2 characteristics is that an 18-MHz bandwidth was chosen for individual reception of the 525-line television signals used in most Region 2 countries.† This is to be compared with the 27-MHz bandwidth for the 625-line signals

*Channels 25 to 40 were used less often since they were available only to Region 1 countries.

†Note that, although Jamaica and Uruguay have adopted 625-line TV standard "N," the video baseband is the same as for the 525-line standard "M" used in other Region 2 countries.

TABLE 2. TECHNICAL CHARACTERISTICS OF BROADCASTING SATELLITES ASSUMED FOR THE PLAN IN REGIONS 1 AND 3

CHARACTERISTIC	VALUE	REFERENCE*
Frequency Band (GHz)	11.7–12.5 (Region 1), 11.7–12.2 (Region 3)	
Channel Spacing (MHz)	19.18	3.5.1
Minimum Channel Spacing on Same Antenna (MHz)	38.36	3.5.3
Channel Grouping	Channels within a single antenna beam assigned within 400 MHz where possible	3.5.2
Guard Bands (MHz)		
Lower	14	3.8.2
Upper	11	3.8.2
RF Channel Bandwidth (MHz)	27	3.8
Modulation & Signal Processing	FM of video (plus sound on FM subcarrier); preemphasis as in CCIR Rec. 406	3.1
Energy Dispersal (kHz peak to peak)	600 (~22 dB reduction in power flux density in any 4-kHz band)	3.18
Polarization	Circular Direct (RH or CW) and indirect (LH or CCW) (same senses in different beams to same service area where possible)	3.2.2
Cross-Polarization Component Relative to Copolarized (dB)	-27 (Rain Zones 1 and 2) -30 (Rain Zones 3, 4, and 5)	2.3
Thermal Noise Objective C/N (dB)	14 (99% of worst month) (Propagation loss up to 2 dB must be taken into account)	3.3 2.1.2.2
Interference Objective C/I (dB)		
Co-channel	31 (99% of worst month)	3.4
Adjacent	15 (99% of worst month)	3.4
Earth Station Figure of Merit G/T (dB/K)		
Individual Reception	6	3.6
Community Reception	14	3.6

*Refer to the indicated paragraph of Annex 8 of the Final Acts of the Conference.

TABLE 2. TECHNICAL CHARACTERISTICS OF BROADCASTING SATELLITES ASSUMED FOR THE PLAN IN REGIONS 1 AND 3 (CONTINUED)

CHARACTERISTIC	VALUE	REFERENCE*
Antenna Beamwidth (deg)		
Individual Reception	2 (0.9-m dia.)	3.7.1a
Community Reception	1 (1.8-m dia.)	3.7.1b
Reference Pattern	See Figure 1	3.7.2
Minimum Angle of Elevation (deg)	20-40 depending on terrain and rain climate	3.12
Power Flux Density (pfd) (dBW/m ²)		
(Edge of coverage area) (99% of worst month)		
Individual Reception	-103	3.16
Community Reception	-111	3.16
Maximum difference between on-axis pfd and edge of service area (dB)	3	3.17
Maximum Change During Satellite Lifetime (dB)	0.25	3.15
Satellite antenna		
Transmit Reference Pattern	See Figure 2	3.13.3
Half-Power Beamwidth (deg)	0.6 minimum	3.13.2
Shape	Circular or elliptical	3.13.1
Gain (a and b are major and minor axis half-power beamwidths, respectively)	27.843/ab	3.13.1
Pointing Accuracy (deg)	±0.1	3.14.1
Angular Rotation of Elliptical Beams (max) (deg)	2	3.14.1
Satellite Spacing (deg)	6	3.10
Stationkeeping (N-S & E-W) (deg)	±0.1	3.11

*Refer to the indicated paragraph of Annex 8 of the Final Acts of the Conference.

used by most countries in Regions 1 and 3. The ratio of these RF bandwidths is about equal to the ratio of the video bandwidths of the two types of TV signals.

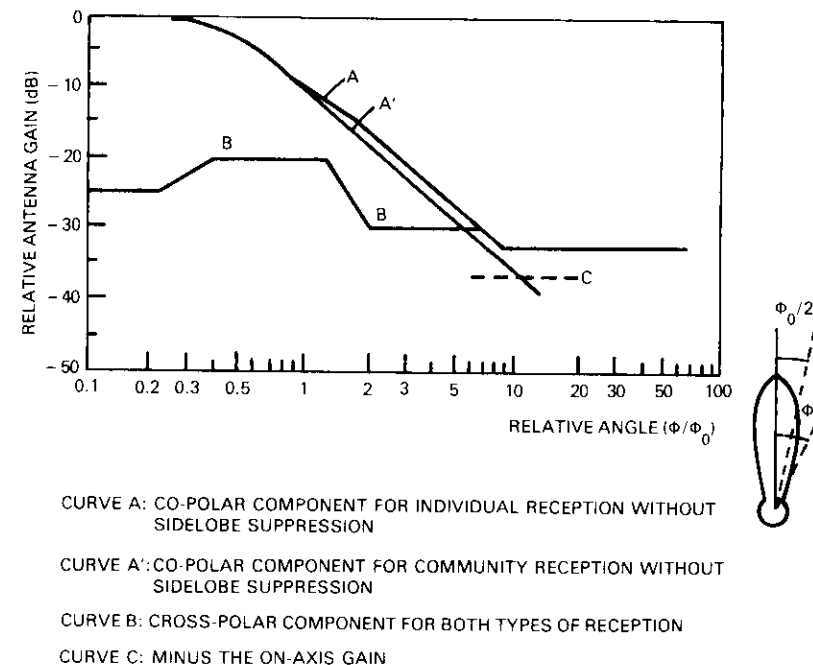
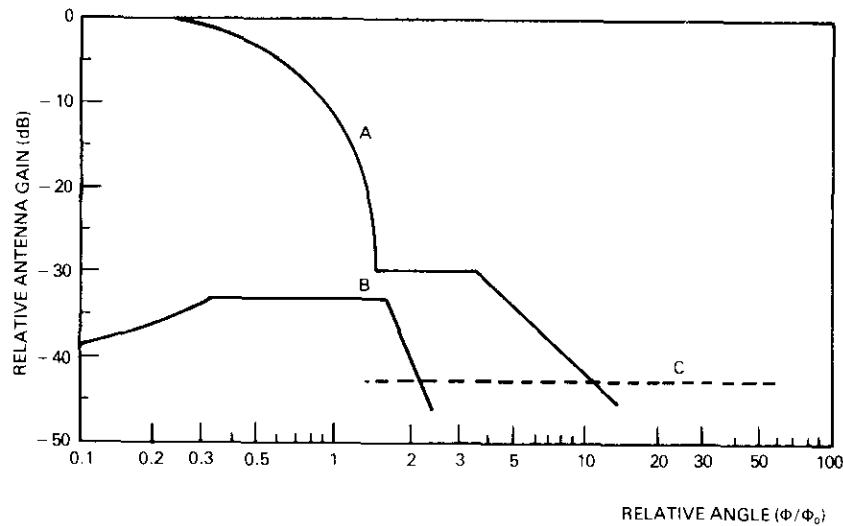


Figure 1. Reference Patterns for Copolarized and Cross-polarized Components for Receiving Antenna

Although Region 2 countries postponed the preparation of any plan until RARC-83, they adopted provisions at WARC-77 to permit the introduction of Region 2 broadcasting satellite systems before 1983. These included a requirement to use system characteristics equivalent to those recommended at WARC-77 for planning in Region 2.

Another key feature of the interim provisions dealt with the fact that in Region 2 only, the 12-GHz BSS allocation was shared on a primary basis with the FSS. To allow each of the two services access to the entire allocated band, WARC-77 specified two orbital arc segments in which the BSS would be primary and the FSS secondary: 75°-100° W (75°-95° W for the U.S., Canada, and Mexico) and 140°-170° W. Outside these arc segments, the FSS would be primary and the Region 2 BSS secondary, subject to the following limitations:

- Provision must be made between 55° and 60° W for a broadcasting satellite to serve Greenland.
- Broadcasting satellites can be located anywhere in the BSS



CURVE A: CO-POLAR COMPONENT
 CURVE B: CROSS-POLAR COMPONENT
 CURVE C: MINUS THE ON-AXIS GAIN

Figure 2. Reference Patterns for Copolarized and Cross-polarized Components for Satellite Transmitting Antenna

arc segments, but FSS satellites must be positioned far away to ensure mutual interference protection.

c. FSS systems serving Region 2 must accept interference produced by Region 1 broadcasting satellites operating in accordance with the Region 1 and 3 plan.

WARC-79

The 1979 World Administrative Radio Conference (WARC-79) was the first ITU conference in 20 years with the authority to revise the allocations, technical regulations, and regulatory procedures for all radiocommunication services and in all frequency bands [2], [3]. WARC-79 used this authority to take the following actions of significance to BSS planning:

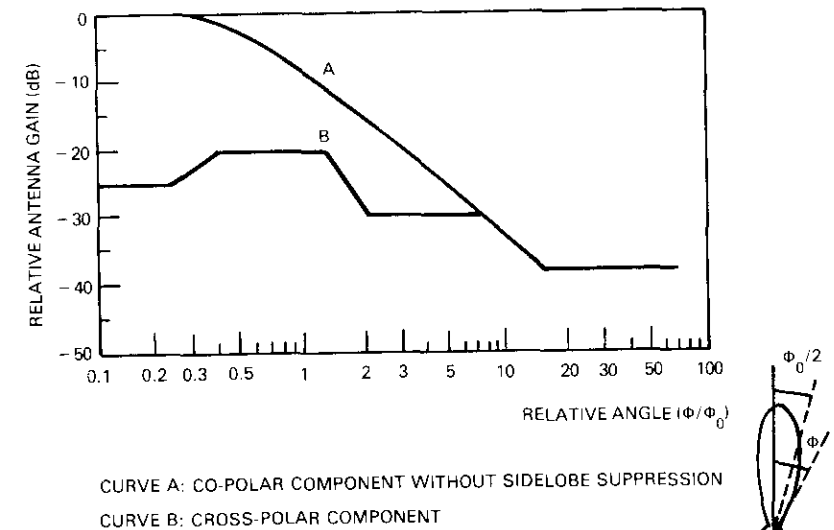
a. Reaffirmed WARC-ST Resolution Spa 2-2 by incorporating it without significant change into Resolution 507 of the Final Acts of the Conference.

TABLE 3. CHARACTERISTICS OF SYSTEMS IN REGION 2 THAT DIFFER FROM THOSE IN REGIONS 1 AND 3*

CHARACTERISTIC	VALUE	REFERENCE†
Frequency Band (GHz)	11.7 to 12.2	
RF Bandwidth (MHz)		
Individual Reception	18	3.8
Community Reception	23	3.8
Guard Band (MHz)		
Lower	12	3.9.2
Upper	9	3.9.2
Earth Station Half-Power Beamwidth (deg)	1.8 (1-m diam)	3.7.1a
Reference Pattern	See Figure 3	3.7.2
Power Flux Density (dBW/m ²) (Edge of Coverage Area) (99% Worst Month)		
Individual Reception	-105	3.16

*All characteristics for Region 2 systems are provisional. Definitive choices will be made at RARC-83.

†Refer to the indicated paragraph of Annex 8 of the Final Acts of the Conference.



CURVE A: CO-POLAR COMPONENT WITHOUT SIDELobe SUPPRESSION
 CURVE B: CROSS-POLAR COMPONENT

Figure 3. Reference Patterns for Copolarized and Cross-polarized Components for Receiving Antenna for Individual Reception in Region 2

b. Incorporated the WARC-77 Plan for Region 1 and 3 broadcasting satellites into the international radio regulations as Appendix 30.

c. Adopted Resolution 101 calling for a WARC to plan feeder links for the Region 1 and 3 plan.

d. Allocated three new FSS up-link bands with usage limited to feeder links for broadcasting satellites in the 12-GHz band: 10.7–11.7 GHz in Region 1; 14.5–14.8 GHz except for Europe; and 17.3 to 18.1 GHz worldwide.

e. Adopted Resolution 3 (BP)* on the use of the geostationary orbit and the planning of space services. This resolution calls for a two-session WARC; the first session would decide which space services and frequency bands should be planned and the nature of planning to be used, and the second session would conduct the planning. This WARC, which has been scheduled for 1985 and 1987, could decide to plan other BSS bands as called for in Resolution 507. It also could substitute for the feeder-link planning conference called for in Resolution 101.

WARC-79 also took several allocation actions of great importance to planning for the BSS in Region 2. It extended the existing Region 3 BSS allocation in the 22.5- to 23-GHz band to Region 2. As the next BSS band above 12 GHz, this allocation is sometimes viewed as a logical candidate for the introduction of new services such as high-definition television (HDTV). Also, it shifted the existing 11.7- to 12.2-GHz BSS allocation to the 12.1- to 12.7-GHz band and extended the upper edge of the existing 11.7- to 12.2-GHz FSS band to 12.3 GHz.

Several important footnotes apply to these allocations. Footnote 841 (3787B) provides that the resultant 200-MHz overlap of the BSS and FSS bands will be eliminated at RARC-83 by creating two subbands and allocating the lower subband to the FSS and the upper to the BSS. Footnote 839 (3787) provides that Region 2 use of these bands will be limited to national and subregional systems. Footnote 843 (3787E) notes that Region 2 space services, existing or planned prior to RARC-83, should not impose restrictions on the elaboration of the Region 2 plan for the BSS. Footnote 844 (3787D) similarly enjoins existing and future Region 2 terrestrial services from restricting elaboration of the

*The designations in parentheses are the temporary identifications used during WARC-79; they are included because such designations are still in common use.

RARC-83 plan and from causing harmful interference to BSS systems operating in accordance with the plan. Footnote 836 (3787A) allows transponders on space stations in the 11.7- to 12.1-GHz FSS band (plus the portion of the 12.1- to 12.3-GHz band ultimately allocated exclusively to the FSS) to be used additionally for transmissions in the BSS with a maximum e.i.r.p. of 53 dBW per TV channel provided that such transmissions do not cause greater interference or require greater interference protection than the coordinated FSS assignments. Finally, footnote 846 (3787F) allows assignments to BSS space stations made in accordance with the RARC-83 plan to be used for FSS down-link transmissions provided that such transmissions do not cause more interference or require greater interference protection than that needed for the planned BSS transmissions.

Finally, WARC-79 passed Resolution 701(CH), which defined the terms of reference for RARC-83. It extends most of the WARC-77 interim provisions for establishing Region 2 BSS systems prior to RARC-83, but eliminates the arc-segmentation provision since the foregoing allocation actions eliminate frequency sharing between the BSS and the FSS. This resolution also repeats the WARC-77 requirement that the Region 2 planning conference prepare a detailed frequency assignments and orbital positions plan for the BSS based on individual reception and ensuring that the service requirements of Region 2 countries are met in an equitable manner with a guaranteed minimum of four channels per country. However, Resolution 701 extends the scope of the planning envisioned at WARC-77 by requiring that RARC-83 also plan the feeder links associated with the 12-GHz BSS links. For this purpose, it is specified that the feeder link plan will occupy a part of the 17.3- to 18.1-GHz band equal in bandwidth to that used in the 12-GHz BSS plan.

References

- [1] R. S. Gould and E. E. Reinhart, "The 1977 WARC on Broadcasting Satellites: Spectrum Management Aspects and Implications," *IEEE Transactions on Electromagnetic Compatibility*, Vol. EMS-19, No. 3, Pt. II, August 1977, pp. 171–178.
- [2] C. Dorian et al., "The 1979 World Administration Radio Conference and Satellite Communications," *COMSAT Technical Review*, Vol. 10, No. 1, Spring 1980, pp. 1–26.
- [3] E. E. Reinhart et al., "The Impact of WARC-79 on the Broadcasting Satellite Service," *IEEE Transactions on Communications*, Vol. COM-29, No. 8, August 1981, pp. 1193–1209.



Mr. Reinhart received his B.A. and M.A. degrees in physics from the University of California, Berkeley. He did further graduate work in physics and electrical engineering at Cornell University, Ithaca, New York. He is currently Director of Spectrum Management, Satellite Television Corporation, where he is engaged in preparations for the 1983 Regional Administrative Conference (RARC-83). After joining COMSAT in 1977, he served as Manager of CCIR/WARC activities, where he coordinated COMSAT's technical contributions to U.S.

preparations for the 1979 WARC. He also chaired the FCC's Service Working Group on Broadcasting Satellites and was a delegate to the Special Preparatory Meeting of the International Radio Consultative Committee (CCIR), as well as to WARC. Mr. Reinhart served on both the Allocations and Regulatory Procedures Committees at WARC.

System characteristics

E.R. MARTIN

Broadcast transmissions

STC's transmission plan provides for high quality reception of National Television System Committee (NTSC) color video signals with their associated audio and control subcarrier. Quality objectives and system parameters are generally consistent with those adopted for Region 2 in the Final Acts of WARC-77 and incorporated in the Final Acts of WARC-79. Changes have been made in the technical characteristics described in Annex 8 of the Final Acts of WARC-77 in order to achieve STC's quality objectives at minimum cost, and maximum power and spectrum efficiency. Frequency modulation (FM) will be used to minimize the cost and complexity of home equipment.

TRANSMISSION PARAMETERS

STC's planned transmission parameters are summarized in Table 1. A second audio channel is provided which may be used for stereo sound (with a standard stereo amplifier and speakers) or for a second language track. The access control channel is used to address the home descramblers.

The color video signal is combined with a digital subcarrier and then frequency modulated onto an RF carrier. The deviation selected is consistent with the link quality objectives presented in the following section. Relative power levels of the video and digital subcarrier have been balanced to provide comparable thresholds. The composite signal deviation is greater than that implied by Carson's Rule for a 16-MHz bandwidth. The level of "overdeviation" selected provides improved clear sky signal-to-noise (S/N) without noticeable degradation of the video performance by impulse noise. The 16-MHz bandwidth was selected in preference to a wider bandwidth in order to minimize the satellite power required to ensure a reasonable fade margin above the home equipment receiver threshold.

Abbreviations and acronyms used in this series of papers are defined on Page 265.

TABLE 1. PLANNED TRANSMISSION PARAMETERS

Video Baseband	CCIR Standard M with NTSC Color
Audio/Control Subcarrier Inputs	1 ea. Basic Program; Audio Bandwidth = 13 kHz 1 ea. Stereo or Second Language; Audio Bandwidth = 13 kHz 1 ea. Access Control Channel; Bit Rate = 62 kbit/s
Audio Encoding	PCM, Bit Rate = 315 kbit/s/ch
Composite Bit Rate	692 kbit/s
Modulation	QPSK
Frequency	5.5 MHz
Amplitude	0.12-V rms before emphasis at 1V p-p video reference point
Emphasis	525 lines per CCIR Rec. 405-1
Video Deviation	10 MHz p-p
IF Bandwidth	16 MHz
Up-Link Frequency	17.3–18.1 GHz band
Down-Link Frequency	12.2–12.7 GHz band

PERFORMANCE OBJECTIVES

The overall quality objective was to provide an excellent picture normally, and to assure an acceptable picture under all precipitation conditions except the heaviest downpour. Baseline link objectives are defined in terms of both predetection filtered carrier-to-noise (C/N) over a 16-MHz radio frequency bandwidth, and demodulated video (peak-to-peak luminance) S/N (rms weighted) using the recommended deemphasis and weighting characteristics for system M as specified in CCIR Report 637-1. (See XII Recommendations and Reports of the CCIR, Kyoto, 1978.) The link quality objectives are:

- a. For 99 percent of the month with the worst precipitation:

$$C/N \geq 14 \text{ dB}$$

$$S/N \geq 42 \text{ dB};$$

- b. For 99.8 percent of the month with the worst precipitation:

$$C/N \geq 10 \text{ dB}$$

$$S/N \geq 37 \text{ dB}$$

where S/N corresponds to 45 and 40 dB, respectively, when sync tip is included in the peak-to-peak signal.

Viewer ratings in the TASO Report [1] suggest that more than 50 percent of viewers would rate a 42-dB S/N picture "excellent." Since this rating applies to performance 99 percent of the time during the month with the heaviest rain, the same rating is expected virtually all of the time from the majority of STC's customers throughout the United States. Simulations of planned link operating characteristics have confirmed the generally excellent picture quality. The TASO results also imply that a 37-dB S/N picture would be rated as "fine" or better by more than 50 percent of viewers.

Worst-month statistics normally are related to average year statistics by a factor of four (*i.e.*, 99 percent worst month equates with 99.75 percent average year, and 99.8 percent worst month equates with 99.95 percent average year). Since the second quality objective ($C/N \geq 10$ dB) corresponds to the nominal threshold of an FM demodulator, the receive C/N is expected to be above threshold for all but about 4.4 hours per year (0.05 percent of the year) for locations where these minimum objectives are just met. Periods below threshold will generally consist of degraded but viewable television. Actual outages (*e.g.*, loss of picture synchronization or a virtually unintelligible picture) are expected to occur for a much smaller period of time.

To compensate for the wide variation in precipitation throughout the country (all five rain climatic zones exist in the United States), satellite e.i.r.p. will be specified area by area. Figure 1 shows the e.i.r.p. requirements for one service area to illustrate the range of variation.*

Three home antenna diameters in the 0.6- to 0.9-m range will be employed. A 0.9-m antenna can improve the grade of service in heavy rainfall areas and/or at edge of coverage, and 0.6-m units can reduce the cost of earth terminals whenever the satellite actual e.i.r.p. appreciably exceeds the nominal required value. For the typical location, a 0.75-m antenna will provide adequate margin. Expected (clear weather) G/T (gain-to-noise temperature) values in respect to antenna diameter are presented in Table 2.

* These requirements vary with rain attenuation and range loss from the satellites to the points shown in the figures. Rain attenuation has been based on the 0.25 percent precipitation exceedance for the points shown; these statistics are based on data available for about 125 cities in the U.S. The 0.25 percent exceedance corresponds to link quality objective *a* expressed earlier (*i.e.*, 99 percent of the worst month or 99.75 percent of the year).

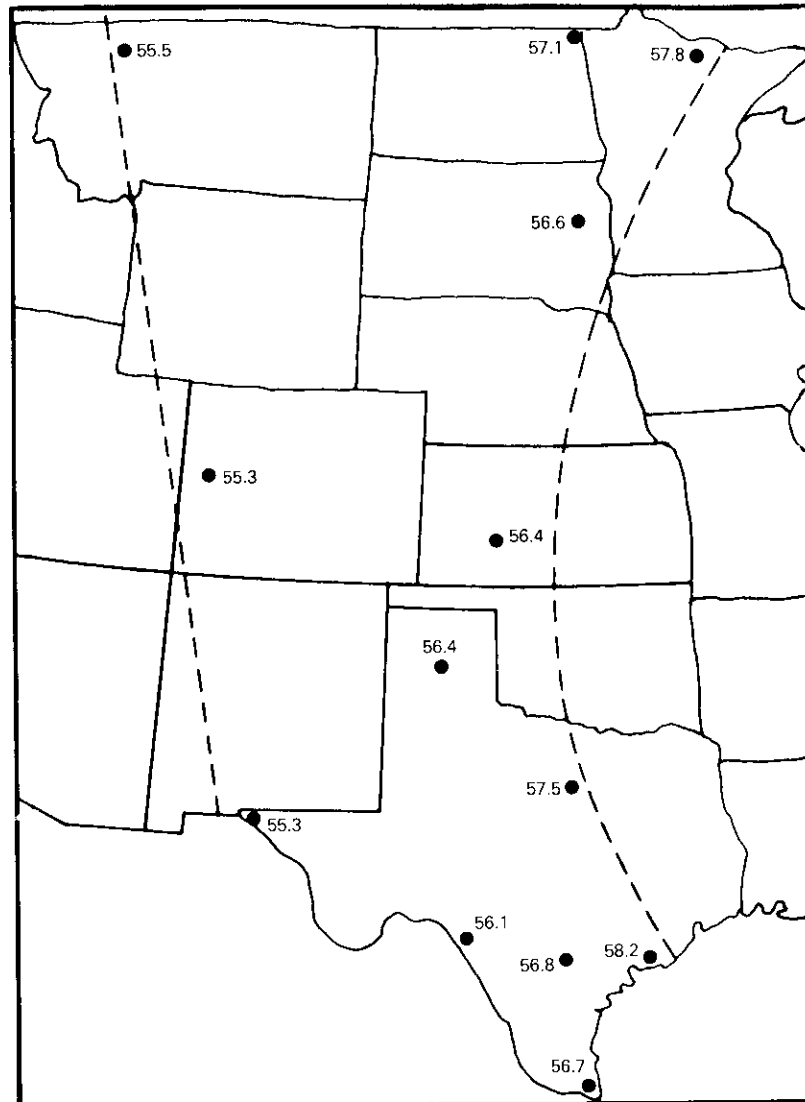


Figure 1. Minimum e.i.r.p. (dBW) for Mountain Service Area Locations

TABLE 2. CLEAR WEATHER G/T VALUES FOR HOME EQUIPMENT*

PARAMETERS	ANTENNA DIAMETERS (m)		
	0.6	0.75	0.9
Peak Gain (dB)	34.9	36.8	38.4
Noise Temperature (dB/K)	27.4	27.4	27.4
Boresight G/T (dB/K)	7.5	9.4	11.0
Pointing Loss (0.5° pointing error) (dB)	<u>0.4</u>	<u>0.6</u>	<u>0.9</u>
Net G/T (dB/K)	7.1	8.8	10.1

* Values are based on the following assumptions: antenna efficiency, 50%; noise temperature (at antenna flange) for clear weather sky noise, 9 K; for background antenna noise, 10 K; and for receiver noise (NF = 4.5 dB), 527 K. The total noise temperature is 546 K.

LINK ANALYSIS

STC's reference link design assumes the baseline 0.75-m antenna for home equipment and a typical satellite transmit e.i.r.p. of 57 dBW. The trade-offs that led to this choice of values (as opposed, for example, to a lower e.i.r.p. and a higher G/T) were based predominantly on the desire to minimize overall system cost, including the cost of millions of home equipment units which STC plans to purchase for lease to subscribers. Because of the large number of home terminals involved (5 to 7 million are expected nationally over a 7-year service period, either owned or leased by STC's subscribers), the overall cost is dominated by the investment in home terminals, which will greatly exceed the investment in launched satellites.

Following extensive discussions with equipment manufacturers and other experts, a 4.5-dB receiver noise figure and a 0.75-m antenna were selected as cost-effective, reference-receive terminal parameters. This noise figure can be achieved with receivers using direct conversion (mixer) or a GaAs field effect transistor (FET) preamplifier (both types currently exhibit comparable noise figure performance), and includes a manufacturing margin that should allow high manufacturing yields with automated production methods.

The resulting net G/T of approximately 9 dB/K for a reference-receive terminal is consistent with a 57-dBW baseline e.i.r.p. and the desired link quality objectives. This required e.i.r.p. is about the maximum value that can be considered for coverage of a CONUS time zone because of satellite TWTA considerations (see satellite description in the following section).

A reference link budget is shown in Table 3. Up-link earth station e.i.r.p. and the arid conditions of Las Vegas assure that the down-link noise budget will be degraded by less than 0.2 dB except for a few minutes per year. Under clear sky conditions there is a total link margin of 5.9 dB above the nominal receiver threshold C/N of 10 dB. However, because fading conditions lead to sky noise increases, which also reduce home equipment G/T, an atmosphere attenuation of only 5 dB is allowable before threshold is reached (see Table 3, under 5-dB Rain Attenuation).

Expected satellite e.i.r.p. in many areas of the country will be greater than required, since the satellite antenna is expected to provide minimum e.i.r.p. near the edge of coverage and excess e.i.r.p. well inside the coverage area. Because of this, the margin above threshold in many locations will be greater than required to achieve link quality objectives. For example, in Cincinnati, Ohio, the expected clear sky down-link margin above threshold is 7.0 dB. With this performance, Cincinnati terminals would operate below threshold ($C/N < 10$ dB) for

TABLE 3. REFERENCE LINK BUDGET

a. Up-Link		
Earth Station e.i.r.p.		86.6 dBW
Free Space Loss (17.6 GHz, 48° Elev.)		208.9 dB
Assumed Rain Attenuation		12.0 dB
Satellite G/T		+ 7.7 dB/K
Up-Link C/KT		102.0 dB-Hz
b. Down-Link		
	Atmospheric Condition	
	Clear	5-dB Rain Attenuation
Satellite e.i.r.p.	57.0 dBW	57.0 dBW
Free Space Loss (12.5 GHz, 30° Elev.)	206.1 dB	206.1 dB
Atmospheric Attenuation	0.14 dB	5.0 dB
Home Receiver G/T (0.75 m)	9.4 dB/K	8.1 dB/K
Receiver Pointing Loss (0.5° error)	0.6 dB	0.6 dB
Polarization Mismatch Loss (average)	0.04 dB	0.04 dB
Down-Link C/KT	88.1 dB-Hz	82.0 dB-Hz
Overall C/KT	87.9 dB-Hz	82.0 dB-Hz
Overall C/N (in 16 MHz)	15.9 dB	10.0 dB
Reference Threshold C/N	10.0 dB	10.0 dB
Margin Over Threshold	5.9 dB	0.0 dB

only 2.6 hours per average year and would exhibit a C/N of more than 14.8 dB (42.8-dB S/N) for 99 percent of the worst month.

The Cincinnati example characterizes expected signal quality under typical environmental conditions, and the effects of heavy precipitation on expected periods of operation below threshold, assuming a 0.75-m receiving antenna. Other locations have been similarly analyzed to determine the duration of below-threshold reception expected in an average year as a function of home equipment antenna diameter. The results are presented in Table 4. Above-threshold operation for 99.95 percent of an average year, (*i.e.*, below-threshold duration for less than 4.4 hours per year) is satisfied at most locations with appropriately sized home equipment antennas. For rainy areas like the Gulf Coast and Florida, the number of hours below threshold is somewhat higher.

Operating frequencies

The satellites can be designed to transmit normal 16-MHz television programming on practically any three center frequencies in the 12.2- to 12.7-GHz band, and to receive on practically any three center frequencies in the 17.3- to 18.1-GHz band. The contemplated design assumes a single translation frequency of 5,100 MHz in the expectation that the Region 2 plan developed at RARC-83 will adopt this value.

Specific center frequencies for the three channels have been tentatively selected in terms of their compatibility with existing terrestrial fixed service assignments in the United States and with an HDTV experimental package to be incorporated in the satellites. However, to allow the use of alternative channel frequencies, which may be allotted to the United States at the RARC-83, terms will be included in the satellite construction contract to permit changes of the satellite RF filters and the translation frequency as necessary. A channel-to-channel center frequency separation of 40 MHz or more would be required because of satellite output filter design constraints.

Service areas

The broadcast service areas in CONUS and in Alaska and Hawaii are shown in Figure 2. STC selected service areas approximately the size of CONUS time zones to allow DBS implementations with existing space technology and to better accommodate audience preferences (developed over thirty years of conventional television broadcasting) for certain types of programming at specific times.

A service area generally the size of a time zone will require satellite transmitter RF power per channel in the order of 150-200 W. A 200-W

TABLE 4. HOURS PER AVERAGE YEAR IN WHICH RECEIVED SIGNAL IS BELOW THRESHOLD

LOCATION	HOME EQUIPMENT ANTENNA DIAMETER (m)		
	0.6	0.75	0.9
Eastern Service Area			
Atlanta, Georgia	5.2	3.7	2.9
Boston, Massachusetts	4.6	3.2	2.2
Buffalo, New York	2.4	1.8	1.4
Caribou, Maine	8.5	3.0	1.7
Charleston, South Carolina	18.0	13.1	9.5
Cincinnati, Ohio	4.0	2.6	2.0
Detroit, Michigan	7.7	3.0	2.0
Lexington, Kentucky	5.1	3.5	2.7
Miami, Florida	19.8	14.9	11.4
New York, New York	4.5	3.2	2.3
Washington, D.C.	5.4	3.7	3.0
Central Service Area			
Chicago, Illinois	6.0	3.4	2.4
Dallas, Texas	11.6	7.0	5.2
Duluth, Minnesota	6.7	2.6	1.9
Houston, Texas	18.1	12.3	8.5
Memphis, Tennessee	7.7	5.3	4.0
Mobile, Alabama	18.1	13.4	9.5
St. Louis, Missouri	5.6	3.8	3.0
Topeka, Kansas	8.1	5.0	3.8
Mountain Service Area			
Albuquerque, New Mexico	2.0	<1	<1
Austin, Texas	8.4	4.9	3.8
Denver, Colorado	<1	<1	<1
El Paso, Texas	3.5	1.4	<1
Fargo, North Dakota	7.0	4.0	3.1
Helena, Montana	6.3	2.0	<1
Wichita, Kansas	16.0	7.1	4.3
Pacific Service Area			
Boise, Idaho	1.6	<1	<1
Los Angeles, California	4.8	1.9	<1
Portland, Oregon	4.3	2.1	1.6
San Francisco, California	5.2	1.8	1.0
Seattle, Washington	7.6	3.0	1.9
Tucson, Arizona	7.4	3.2	1.9

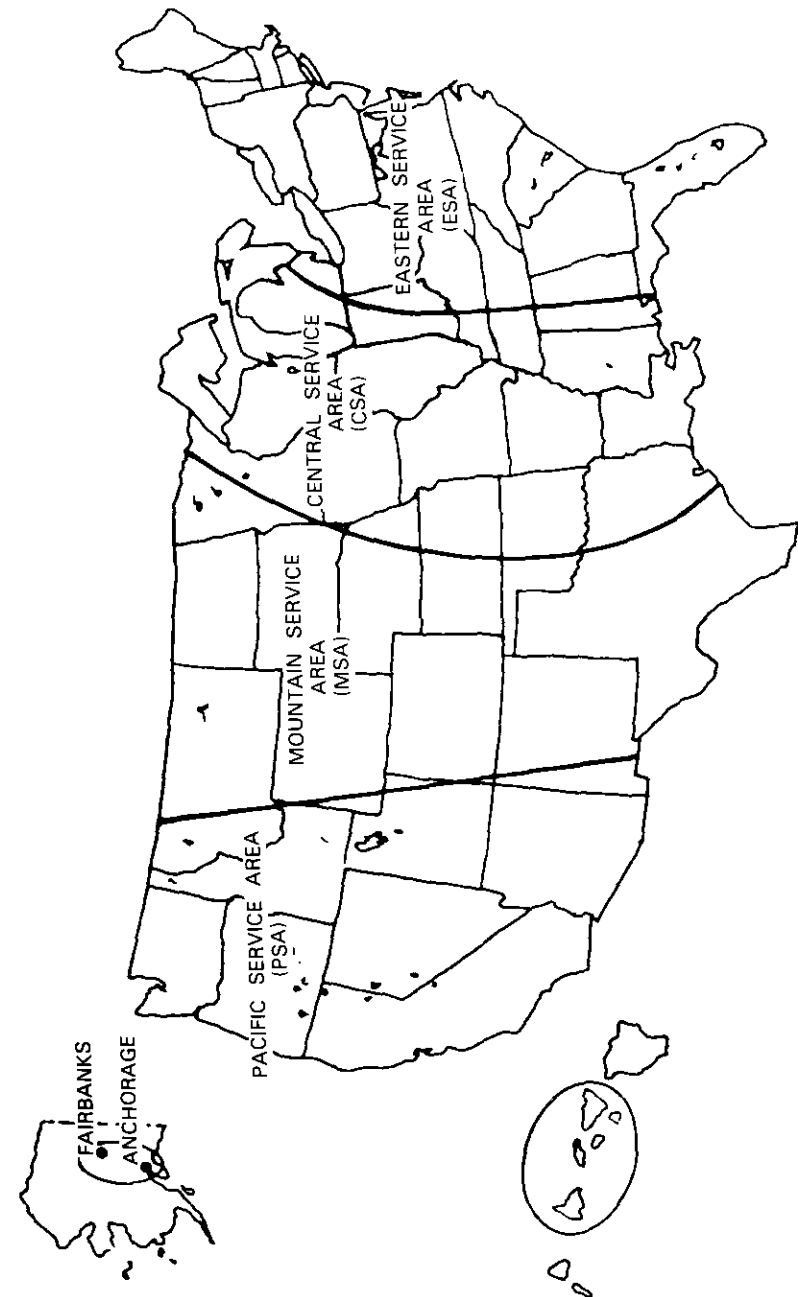


Figure 2. CONUS Service Areas and Coverage of Alaska and Hawaii

TWTA is about the largest, based on current information, that can be predicted to be available in the near future with adequate (7-year) long-life and reliability characteristics. If a service area equal to two time zones (the size of half CONUS) were considered, the RF power requirement would approximately double, raising a serious question as to the ability to provide such a transmitter from the standpoint of lifetime and reliability. Smaller service areas (e.g., spot-beam areas) introduce some inefficiencies in terms of spectrum utilization because a frequency is not used over its full potential coverage area, and power utilization because antenna pointing tolerances are relatively large in comparison with the service area.

Since CONUS service areas should be approximately the size of a time zone, their detailed characteristics were synthesized in order to achieve comparable minimum performance in each service area using a given size spacecraft transmitter amplifier. To achieve this, the coverage areas should be nearly of equal size when projected back to the satellite, except for a "normalizing" correction factor to accommodate excess rain attenuation statistics and slant range differences.* With such a performance equalization objective, the optimum partitioning of CONUS is dependent on the particular satellite orbital locations assumed and on the minimum acceptable elevation angle required for the home terminals. Considering the orbit locations chosen (see next section), the planned use of shaped beams, and the required area-by-area e.i.r.p., the four service areas that meet the aforementioned goal are shown in Figure 2.

The PSA is limited by elevation angle constraints (the home terminals along its eastern edge have an elevation angle of about 10°), and its projected normalized area is smaller than that of the other three service areas. This situation permits use of a fraction of the power from the PSA satellite transmitter to provide 0.6° spot-beam service to Alaska and Hawaii, respectively. A 0.6° -spot beam over Alaska and another over Hawaii, plus the CONUS Pacific coverage area, result in a composite coverage area which, when normalized, is about equal to the normalized coverage area of each of the other three CONUS service areas.

The receive service area from Las Vegas to Los Angeles was selected because the small coverage size leads to high satellite antenna gains

*Inclusion of rainfall statistics tends to make predominantly arid service areas somewhat larger than heavy precipitation areas.

(and a correspondingly high satellite G/T) and because it is in rain climatic zone 5. This allows the earth station to utilize transmitters of modest power (e.g., 200 W per channel) yet still provide sufficient power margin on the up-link to operate at the desired performance level except for a few minutes per year. The ability to operate at 17 GHz with modestly sized transmitters and without a diversity site reduces cost and enhances the system's operational efficiency. In addition, since the bulk of the source material anticipated for broadcast will be on video tape or film, there is little need for broader receive coverage.

Orbit locations

STC adopted the four orbit locations of 175° , 155° , 135° and 115° W on the basis that this set represents:

- a. A very cost-efficient implementation from the point of view of spectrum and orbital arc utilization;
- b. A practically achievable implementation in terms of the required technology; and
- c. A cost-effective approach for a fixed level of service, and one that is comparable in cost to other possible system configurations.

Several generic system configurations, including one-and two-satellite approaches, were studied, each with differing orbit location requirements, but with the common requirement of acceptable home equipment elevation angles and a westward satellite location for eclipse protection. A four-satellite implementation was eventually chosen after it was determined that its orbit/spectrum efficiency was equivalent to or better than that of the other configurations studied, and its space segment cost was comparable to the only other two-satellite approach that would provide the same channel capacity. Furthermore, the four-satellite approach permitted the introduction of DBS on a phased basis with the smallest practical increment, resulting in minimum initial costs. Early service, marketing, billing, installation, and maintenance problems also become more manageable.

The selected four-orbit locations are separated by 20° to permit reuse of frequencies without exceeding established interference criteria, and are located sufficiently west so that eclipses do not start until after 1:00 a.m. in the areas served, compatible with acceptable elevation angle constraints.

The selected orbit locations should not adversely affect other countries in Region 2 and, in fact, should prove beneficial when orbit/spectrum efficiency considerations are introduced. Given the more northerly latitude of Canada relative to the United States (which leads to lower elevation angles) and Canada's more easterly extension, and considering that most of the other countries in Region 2 are east of the United States, the preferred orbit locations for these countries will be in the 70°W to 145°W orbital sector. A two-satellite approach for the United States would place all channel requirements for all CONUS service areas inside this "high demand" orbital sector, while a four-satellite approach would place the MSA and PSA requirements outside this sector at 155°W and 175°W. Thus, use of these four- rather than two- or one-orbit locations will be at little or no cost to other countries in Region 2.

To account for any reasonable RARC-83 results, terms will be included in the satellite construction contract to permit realignment of the antenna subsystem on the satellite to accommodate orbit locations allotted to the United States that may be different from those proposed by STC.

High definition television capability

A 100- and a 28-MHz passband mode of operation will be included in the satellites, available by ground command to experiment with HDTV during periods when normal broadcast transmissions are terminated. This experimental capability will be made available to qualified parties interested in the development of HDTV specifications and standards.

STC expects eventual market development of a home television system with substantially higher resolution than that of the present NTSC system, and with large screens. Although the market for such a system is poorly defined at present, and there are no national standards for HDTV, the experimental transmission capability included in STC's DBS satellites is expected to stimulate the development of standards in this area and eventually the establishment of a market.

Acknowledgments

Major engineering contributions to this paper were made by D. Swearingen of COMSAT and P. Ebert of COMSAT General.

Reference

- [1] *Engineering Aspects of Television Allocations*, Report of the Television Allocation Study Organization to the Federal Communications Commission, March 16, 1959.

Satellite characteristics

E. R. MARTIN

General

Many of the system parameters presented in the previous section were chosen on the basis of iterative analyses that considered satellite constraints, as well as BSS recommendations of previous ITU conferences. Specifically, the size of the transmit service areas, the e.i.r.p. requirements, and the number of channels have significant impact on satellite characteristics. These factors were combined with information on achievable spacecraft technology to produce the type of satellite described in this paper.

Spacecraft will be procured using specifications based primarily on performance requirements (for example, e.i.r.p. and G/T) and not on any specific design. Therefore, spacecraft contractors will have considerable flexibility in designing the satellites. To characterize the system, a baseline spacecraft design was synthesized and analyzed in sufficient depth to ensure that all projected performance requirements can in effect be met. Elements of the baseline spacecraft will be described to illustrate a typical implementation. Such a representation, however, is only one of many possible alternatives which contractors may choose to meet STC's performance requirements.

All satellites will be essentially the same. A capability will exist whereby ground command controls each satellite so that it can be reconfigured to serve either of two service areas, provided that the correct orbital location is chosen. The satellite design used to serve the Eastern Service Area (ESA) from 115° can be reconfigured and relocated at 135° to serve the Central Service Area (CSA), and vice versa; similarly, the satellite design used to serve the Mountain Service Area (MSA) can also provide Pacific Service Area (PSA) service, and vice versa. The only difference between these two satellite designs is in the antenna beam-forming networks which will be described later. For the nationwide implementation, two operational satellites and a spare of one satellite design will be used for ESA/CSA service, and two operational satellites and a spare of a slightly different satellite design will be used for PSA/MSA service.

Abbreviations and acronyms used in this series of papers are defined on Page 265.

Performance requirements have been carefully selected so that the satellites can be built without reliance on unproven technology. Although substantial engineering development is required for certain spacecraft elements, contractors should be able to build most satellite components from existing, flight-qualified designs. This approach allows the satellites to be procured under a fixed-price contract and minimizes the probability of delayed deliveries and in-orbit anomalies. Table 1 summarizes the satellite characteristics.

TABLE 1. SATELLITE CHARACTERISTICS

Mission	Television broadcast for individual reception
Launch Vehicle	STS/PAM-D and ARIANE
Initial Mass on Station	650 kg
Satellite Mission Life	7 years
North-South Stationkeeping	$\pm 0.1^\circ$ or better
East-West Stationkeeping	$\pm 0.1^\circ$ or better*
Longitudinal Repositioning	One at 3° per day or more at slower rates
Prime Power	1,700 W end of life
Redundancy	100% all active electronic elements
Stabilization	Spin- or body-stabilized
Broadcast Channels	Three standard video—16-MHz bandwidth, two (alternative) HDTV channels—28-MHz and 100-MHz bandwidth
Eclipse Capability	None
Receive Service Area	Los Angeles/Las Vegas
Transmit Service Areas	See Figure 2 of previous paper
Frequency Bands	Transmit: 12.2 to 12.7 GHz Receive: 17.3 to 18.1 GHz
Minimum e.i.r.p. per Channel	Varies locally commensurate with rain attenuation statistics and range loss. Ranges between 58.2 and 55.1 dBW.
Minimum Broadcast RF Output Power per Channel	185 W end of life
Saturation Flux Density per Channel	-88.1 dBW/m ² at 17.3 GHz
Satellite Communications Subsystem G/T	7.7 dB/K minimum
Polarization	Transmit: RHCP for ESA LHCP for CSA RHCP for MSA LHCP for PSA Receive: Orthogonal to transmit

* Stationkeeping of each in-orbit spare relative to its nearby operating satellite will be adequate to maintain nominal intersatellite spacing of 0.05° .

Launch vehicle interface and spacecraft configuration

The satellites will be compatible with two different launch vehicles. NASA's Space Transportation System (STS, also referred to as the Shuttle) will use a PAM-D booster to carry the spacecraft from the Shuttle's orbit into transfer orbit. The present STS flight availability may not accommodate the launch schedule of all satellites, particularly the early one(s). Accordingly, the satellite design will also be compatible with a shared launch (*i.e.*, an STC satellite and another satellite) on the ARIANE launch vehicle. Although the mass of STC's satellites is compatible with that of a Delta launch vehicle, the volumetric configuration is expected to exceed the dimensional constraints of that vehicle.

After a satellite is injected into transfer orbit by the launch system, final injection into a nominally geostationary orbit will be accomplished by an apogee kick motor (AKM) incorporated in the satellite.

Spacecraft manufacturers will be permitted to propose either spin- or body-stabilized designs, which must meet all specified performance requirements. STC's baseline spacecraft has assumed a body-stabilized design because it appears that the high power required (about 1,700 W) may be more easily achieved with the large, deployed solar arrays typical of body-stabilized spacecraft.

Spacecraft mass and size are limited by launch vehicle constraints. The STS/PAM-D will place a maximum mass of approximately 1,247 kg into transfer orbit. The ARIANE Type III launch vehicle will be capable of launching two satellites simultaneously, each having a weight that corresponds approximately to this amount. Based on the performance of applicable AKMs, and considering the liquid propellant required prior to achieving the desired geosynchronous orbit, spacecraft mass at the start of service (after apogee motor firing) will be about 650 kg.

The spacecraft dimensions are constrained by both the ARIANE shroud dimensions and the requirement that it can be configured for a vertical launch in the STS (*i.e.*, PAM-D and apogee motor thrust axes orthogonal to the STS Orbiter longitudinal axis). The satellite is expected to have an approximately cylindrical envelope during launch, with a maximum diameter of about 2.9 m and a height of about 2.3 m.

In geosynchronous orbit, the satellite dimensions are expected to be dominated by the antenna and the solar arrays. STC's baseline satellite has one deployed antenna reflector measuring 2.9 m in diameter and two symmetrically deployed solar arrays, each measuring about 7 m by 1.5 m.

Table 2 gives a representative mass budget for the satellite. For the assumed STS/PAM-D launch, the AKM mass is approximately 595 kg with a propellant loading of 560 kg (for an ARIANE launch, the apogee motor would carry about 100 kg less propellant). The antennas weigh 44 kg, of which about half is budgeted for the reflector and its deployment mechanism, and the other half for the feeds and beam-forming networks necessary to produce the desired antenna beams. For all subsystems except communications and power, the mass estimates are based on existing hardware being used or proposed for other satellite programs. Therefore, the contingency mass in the budget provides adequate margins primarily for the communications and power subsystems.

TABLE 2. REPRESENTATIVE SATELLITE MASS BUDGET

ITEM	MASS (kg)
Launch Vehicle Capability*	1,236
AKM Consumables	560
Hydrazine Propellant (plus pressurant)	129
Dry Satellite	547
Communications Electronics	93
Communications Antenna	44
Telemetry, Tracking, and Command	20
Electric Power	104
Attitude Control†	49
Reaction Control (dry)	23
Structure	70
Thermal Control	25
AKM Case at Burnout	35
Balance and Miscellaneous	38
Contingency	46

* Assumes an optimized STS/PAM-D launch with modified transfer orbit characteristics.

† Includes 5 kg budgeted to offset solar torques induced by single antenna reflector.

Design life

The design requirement for the mission life of the satellites is seven years. This estimate is determined by a conservative evaluation of the effect of the synchronous orbit environment on the solar cell arrays, charge-discharge cycling effects on the life of the batteries, and the mass allocated to propellant for spacecraft stationkeeping. To achieve the desired probability of survival for seven years, all spacecraft equipment will be redundant where possible. Parts will be derated in

their applications, and materials and processes will be selected so that aging or wear-out effects will not adversely affect spacecraft performance.

Communications subsystem

Figure 1 is a typical block diagram of the communications subsystem of the ESA/CSA satellite, excluding redundant elements. The satellite design for MSA/PSA service would differ only in the receive and transmit antenna beam-forming networks. This block diagram shows a single-conversion transponder, with the receiver translating the 17-GHz up-link signals directly to the 12-GHz down-link frequency band.

Up-link signals are received by the antenna beam covering the Los Angeles-Las Vegas area and a wideband receiver. It is expected that at least two redundant wideband receivers will be provided. All receivers will have high sensitivity, good linearity characteristics, and excellent translation frequency stability. Net translation frequency error, including initial setting tolerance, will be better than ± 10 parts in 10^6 over the operating life-time of the satellite. Short-term stability will be better than ± 1 part in 10^6 .

Following amplification and down-conversion, the signals are fed to the input multiplexer where each channel is individually filtered prior to amplification by a TWT. Normal broadcast transmissions use the filters labeled CH.A, CH.B, and CH.C, but HDTV filters of wider bandwidth (28 and 100 MHz) can be switched in when such experimental transmissions are used.

Each satellite will have three operating transmitters whose individual outputs can be turned on and off by ground command for emission control. The TWTAs are expected to have a minimum output power of about 185 W at end of life. At least three additional TWTAs will be provided for redundancy. Based on discussions with TWT suppliers and other experts, it is believed that these power levels are near the maximum that can be achieved with present or near-term technology in such devices without sacrificing reliability and/or lifetime. The power level of these TWTAs is approximately the same as that used successfully on the CTS satellite. In addition, TWT manufacturers are engaged in considerable efforts on units of this power level. Yet, the TWTAs are considered the most critical elements of the satellite and will receive special attention to ensure timely availability of satisfactory units.

The TWTAs will not be needed for broadcasting during eclipse periods. However, because of concerns related to the effect of on/off transients on TWT life, the TWTAs will incorporate an eclipse standby mode that will keep the cathode at near operating temperatures.

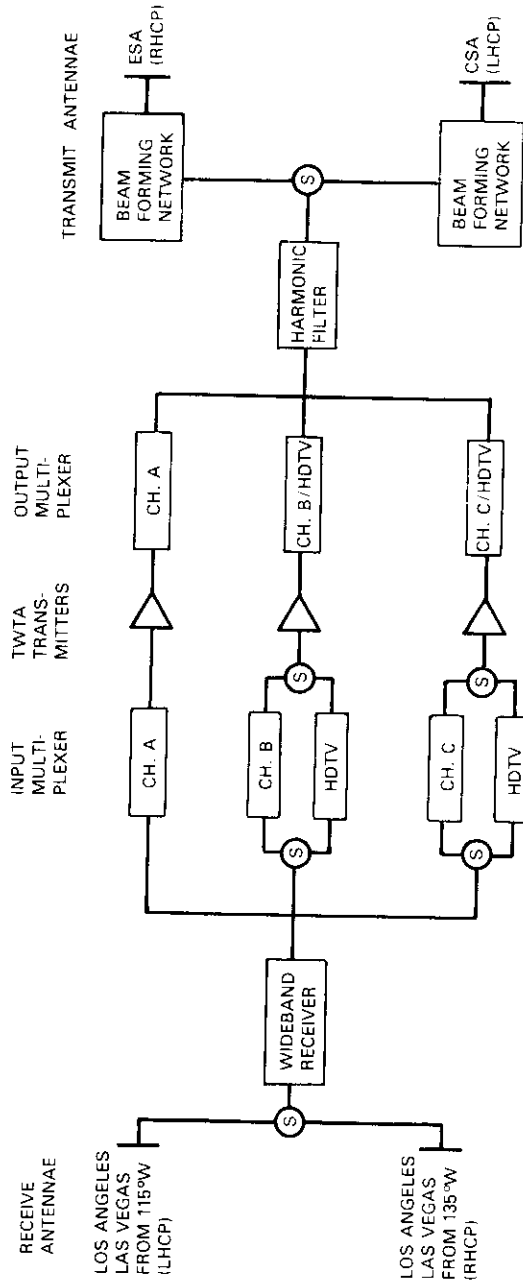


Figure 1. Representative Communications Subsystem Block Diagram (ESA/CSA Spacecraft)

The TWTA outputs are combined in the output multiplexer. The multiplexer filters are sources of potentially large RF losses which can be minimized by adequately separating the channels. High passband efficiency is particularly important because excessive losses would require TWTA's with higher power levels (which would result in reliability/lifetime implications for the TWTA's and mass/power implications for the satellite) and create increased thermal loads on the output filters. Two of the output multiplexer filters are expected to have passbands of about 28 MHz, and the third of about 100 MHz; thus, the same output filters will be used for normal and HDTV transmissions.

The multiplexed RF output is passed through a harmonic filter to attenuate out-of-band emissions and through the beam-forming network required to develop the requisite shaped transmit beam pattern.

ANTENNA ASSEMBLY

Beam-forming networks are part of the antenna assembly, which provides shaped beams to CONUS service areas. Compared to simple beams of circular or elliptical cross section, shaped beams provide more efficient use of RF power because their patterns can be tailored to closely follow irregular contours; this minimizes the RF power wasted outside the service area, and consequently, enhances the net RF power falling over the service area. In terms of interference, shaped beams also reduce the radiation falling over other countries to the maximum practicable extent.

The baseline antenna configuration employs a parabolic reflector with a diameter of approximately 2.9 m. This reflector is fed by a cluster of feed horns, which are in turn connected to the two beam-forming networks shown in Figure 1. If the satellite is used to provide service to the ESA, all of the satellite's output RF power is fed to the ESA beam-forming network where it is divided into 16 unequal parts to feed 16 separate feed horns. The weighted illumination of the reflector by the 16 contiguous horns leads to a pattern that closely follows the contours of the ESA (Figure 2). If the satellite is used to provide service to the CSA, the satellite's RF power is fed to the CSA beam-forming network and to a set of feeds to create a CSA-shaped beam* (Figure 3).

*Since the CSA broadcasts operate in LHCP (which is orthogonal to the ESA transmissions), the feed horns may be shared by feeding the RHCP port of the feeds for ESA transmissions and the LHCP port for CSA transmissions. This could reduce mass/power on the satellite.

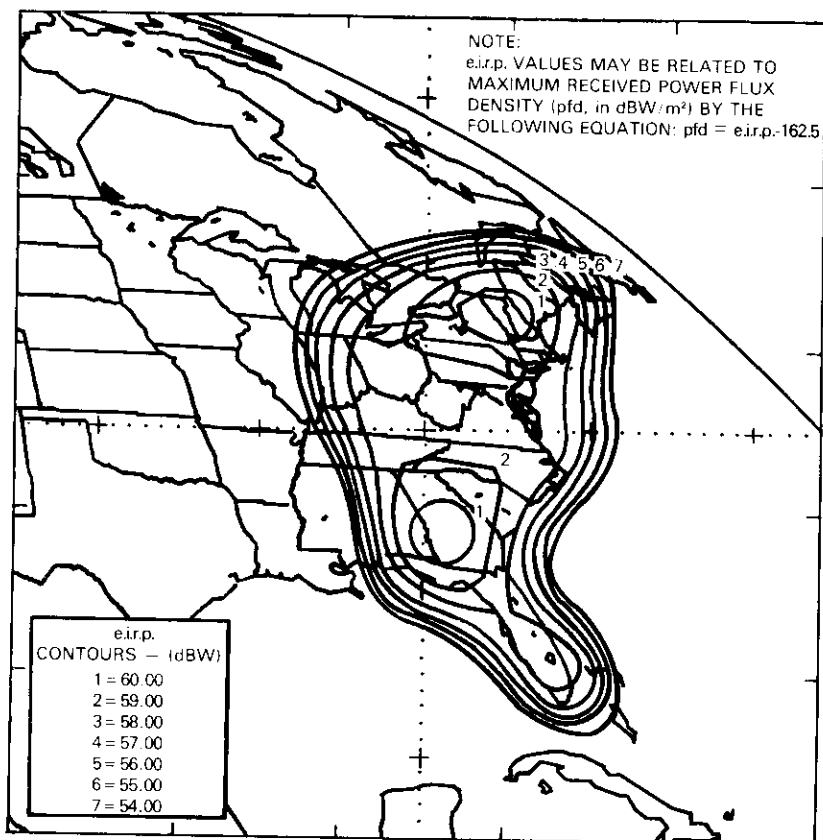


Figure 2. Computer-Predicted e.i.r.p. Contours for ESA Beam

These patterns have been designed to provide the minimum required e.i.r.p. at the edges of coverage, with sufficient margin for satellite pointing error tolerances. Since the antenna gain increases towards the center of the coverage areas, most locations will obtain e.i.r.p. values greater than those required to meet the minimum performance objectives.

All communications receive and transmit functions are performed by the single 2.9-m reflector. Although the final characteristics of the satellite antenna subsystem are subject to variations depending on the selected spacecraft design, the above-mentioned baseline antenna is

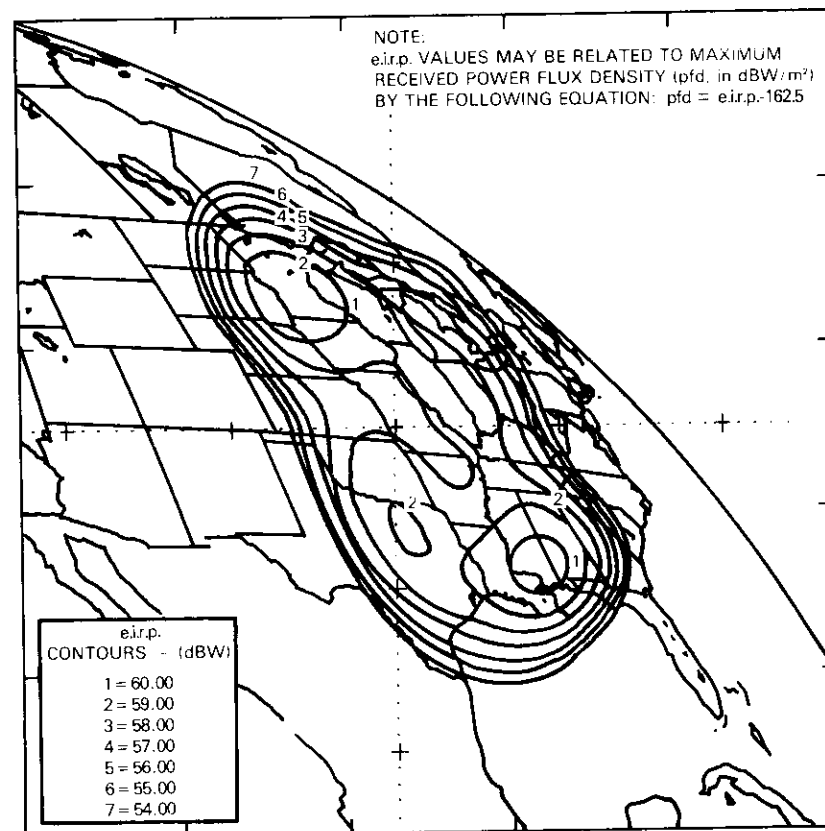


Figure 3. Computer-Predicted e.i.r.p. Contours for CSA Beam

typical of possible approaches that may be implemented.

Since the incorporation of four beam-forming networks would significantly increase satellite mass and complexity, STC will permit the spacecraft contractor to provide some spacecraft equipped with ESA and CSA beam-forming networks and other spacecraft equipped with MSA and PSA beam-forming networks, rather than require a single design that could accommodate any U.S. service area by ground command and orbit repositioning.

As noted earlier, the shaped-beam satellite antenna offers an important advantage because it reduces unintentional spillover into other

nations.* In this respect, Appendix A compares shaped and elliptical beams.

Table 3 shows the e.i.r.p. power budget, including all losses from the TWTA to the antenna, for the typical ESA edge-of-coverage e.i.r.p. of 57 dBW.

TABLE 3. SATELLITE E.I.R.P. BUDGET (TYPICAL)

End-of-Life TWTA Output Power	22.7 dBW
Output Multiplexer and Harmonic Filter Losses	-0.7 dB
Line and Switch Losses	-0.5 dB
Antenna Losses (e.g., beam-forming network and feeds)	-1.5 dB
Minimum Edge of Coverage Antenna Gain (includes pointing error losses)	37.0 dB
Minimum e.i.r.p.	57.0 dBW

Other subsystems

The remainder of the satellite subsystems are similar to those of other communications satellites. Notable variations include the large power level (about 1700 W at end of life); the comparatively low battery mass (eclipse power is used only for housekeeping loads and to keep the TWTAs warm); the fairly tight attitude control expected (of the order of $\pm 0.07^\circ$ for roll and pitch and 0.5° for yaw to maximize antenna gain and thus minimize the TWTA power level); and the advanced thermal control devices, such as heat pipes, that are anticipated to cope with the high thermal dissipation of the TWTAs and the TWTA turn off/turn on thermal transients that occur during eclipses.

APPENDIX A. Comparison of shaped versus elliptical satellite beams

Shaped-beam patterns of a 2.9-m satellite reflector used to generate ESA coverage have been synthesized and off-axis performance compared with that of an elliptical beam optimized for the same service

area and generated by a 1-m reflector. These results represent only one implementation, but provide information which is believed to typify possible off-axis envelope improvements under similar geometric conditions.

Figures A1 and A2 show analytically predicted gain contours for the shaped-beam antenna (operating from a satellite at 115°W) over specific segments of the earth's surface, and gain contours of an optimized elliptical antenna beam (a 3° by 2° ellipse with semi-major axis 20° counterclockwise from a north-south direction using BSS satellite antenna characteristics adopted at WARC-77). Edge of coverage gain is 35 dB for the shaped beam and 33.5 dB for the elliptical beam. A pointing error of 0.1° has been accounted for in the contours shown.

To compare the relative e.i.r.p. of the elliptical and shaped-beam implementations, the shaped-beam antenna gain contours should be reduced by 1.5 dB, based on the assumption that the minimum edge of coverage e.i.r.p. for both implementations would be equalized. The resultant modified gain values are proportional to e.i.r.p. for each approach. As an example, contour 4 of the shaped beam should be reduced to 6.5 dB for comparison with the elliptical beam contours.

Figures A1 and A2 show that the shaped beam offers substantial pattern improvements. For example, over Colombia the shaped beam's highest comparative gain is near 0 dB (1.7 minus 1.5), while the elliptical beam's highest gain is about 17 dB; over Haiti/Santo Domingo and Venezuela, the improvement is near 22 dB.

These figures represent only one case, namely, a particular shaped beam compared with a designated elliptical beam covering a particular service area from a specific orbital position, and the results only apply over the earth segments shown. Although the results provide some measure of trends, and it is believed that a properly designed shaped beam always provides improved off-axis envelope (to a gain about 35 dB below the antenna's maximum gain) over an equivalent elliptical antenna, analysis of a different case may lead to comparative results more or less pronounced than those shown here.

Note that large service areas are well suited for shaped beams because their size is much larger than the individual "beamlets" used to form a shaped beam (the 2.9-m reflector generates sixteen 0.6° beamlets to form the ESA shaped beam). A shaped beam for a smaller service area, such as one of the Central American countries, would probably not be practical, since it requires an extremely large satellite reflector.

*ITU Radio Regulation No. 428A provides that: "In devising the characteristics of a space station in the broadcasting-satellite service, all technical means available shall be used to reduce, to the maximum extent practicable, the radiation over the territory of other countries unless an agreement has been previously reached with such countries."

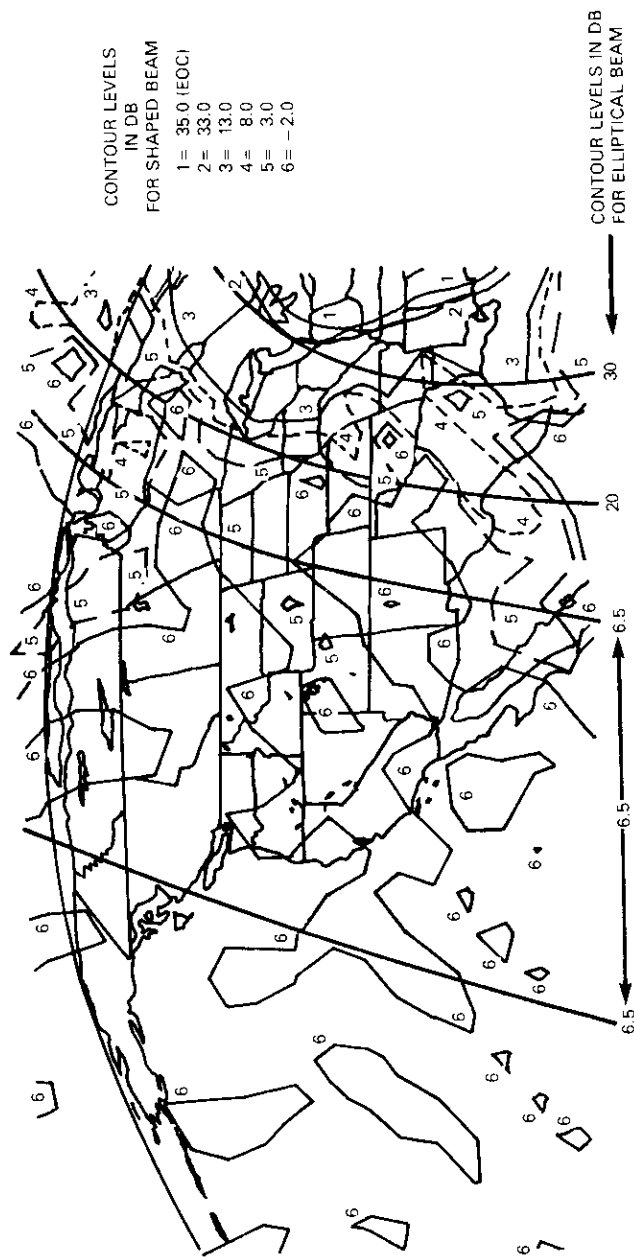


Figure A1. ESA-Shaped Beam and Elliptical Beam Gain Contours Over Canada and Central/Western U.S.

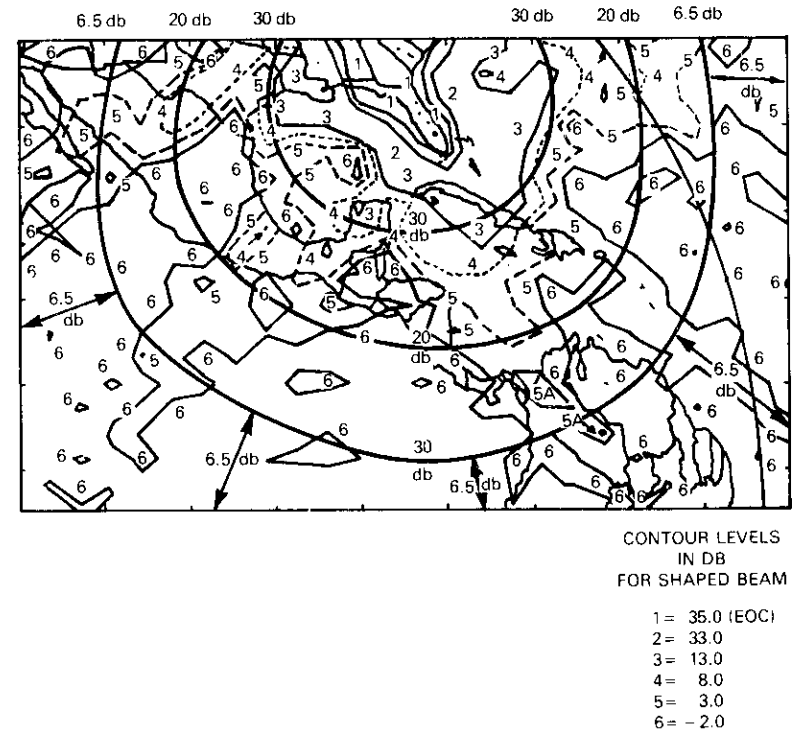


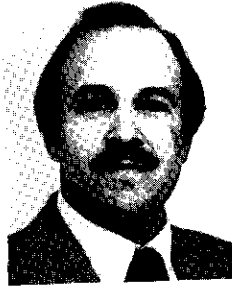
Figure A2. ESA-Shaped Beam and Elliptical Beam Gain Contours Over Territories South of the United States

TABLE
SAT

CHARA

Antenna I
Individual
Commu
Reference
Minimum
Elevatio
Power Flux
(dBW/m²)
(Edge of c
(99% of w
Individual
Community
Maximum
between
edge of s
(dB)
Maximum C
Satellite I
(dB)
Satellite anten
Transmit Re
Pattern
Half-Power
(deg)
Shape
Gain (a and
and minor
power bea
respective
Pointing Acc
Angular Rota
Elliptical E
(deg)
Satellite Spacin
Stationkeeping
(deg)

*Refer to the

used by mo:
bandwidths i
two types of

Ernesto R. Martin received a B.S. in mechanical engineering from the University of Florida and an M.S. in engineering from the California Institute of Technology. He is currently the Director of Systems Engineering, Satellite Television Corporation. Mr. Martin joined COMSAT Laboratories in 1968. He was the principal investigator on a research program that led to design changes in the INTELSAT IV spacecraft. From 1973 to 1975 he was Senior Spacecraft Engineer on COMSAT General's MARISAT program. In 1975 he became Manager, Spacecraft Division on the AEROSAT program, spending a year and a half in Holland where he directed a group of COMSAT General and European Space Agency personnel. His most recent position prior to joining Satellite Television Corporation was Manager, Systems Engineering, in the Advanced Systems Development Office of COMSAT General. He belongs to various professional organizations and is a member of AIAA's Space Systems Technical Committee.

Home equipment terminal characteristics

D. L. DURAND

Individual residence

The individual reception home equipment will consist of three basic elements: a receiving antenna with a supporting mount, an outdoor microwave unit, and an indoor unit (IDU) as shown in Figure 1. The receiving antenna, its universal mount, and the microwave unit constitute the outdoor unit (ODU). The indoor and outdoor units are connected by a cable. The ODU mounting will vary depending on home architecture and the foliage or structural blockages in the direction of the satellite.

The 12-GHz signals received by the home antenna are down-converted and amplified appropriately for transmission to the IDU. This unit, which is located in proximity to the subscriber's TV receiver, further amplifies the received signals, allows channel selection, and processes the selected audio and video signals to a form that can be accepted by the subscriber's unmodified TV receiver. Input to the TV set is at the receive antenna terminals. Figure 2 is an overall block diagram of one possible form of the individual reception home equipment.

OUTDOOR UNIT

STC's baseline ODU employs an antenna diameter of 0.75 m. Antennas of 0.6- and 0.9-m diameter may also be used. The antenna and microwave unit are basically broadband devices which may be operated across the full BSS operating frequency band and would be suitable for operation with any 12-GHz BSS system implementation in the United States. The microwave unit will contain the necessary amplifiers, mixers, filters, and oscillators to down-convert the received 12-GHz signal to an intermediate frequency, nominally in the 800- to 1300-MHz range. Nominal overall ODU performance characteristics are shown in Table 1. Final specifications will be determined after further studies and detailed discussions with hardware suppliers.

Abbreviations and acronyms used in this series of papers are defined on Page 265.

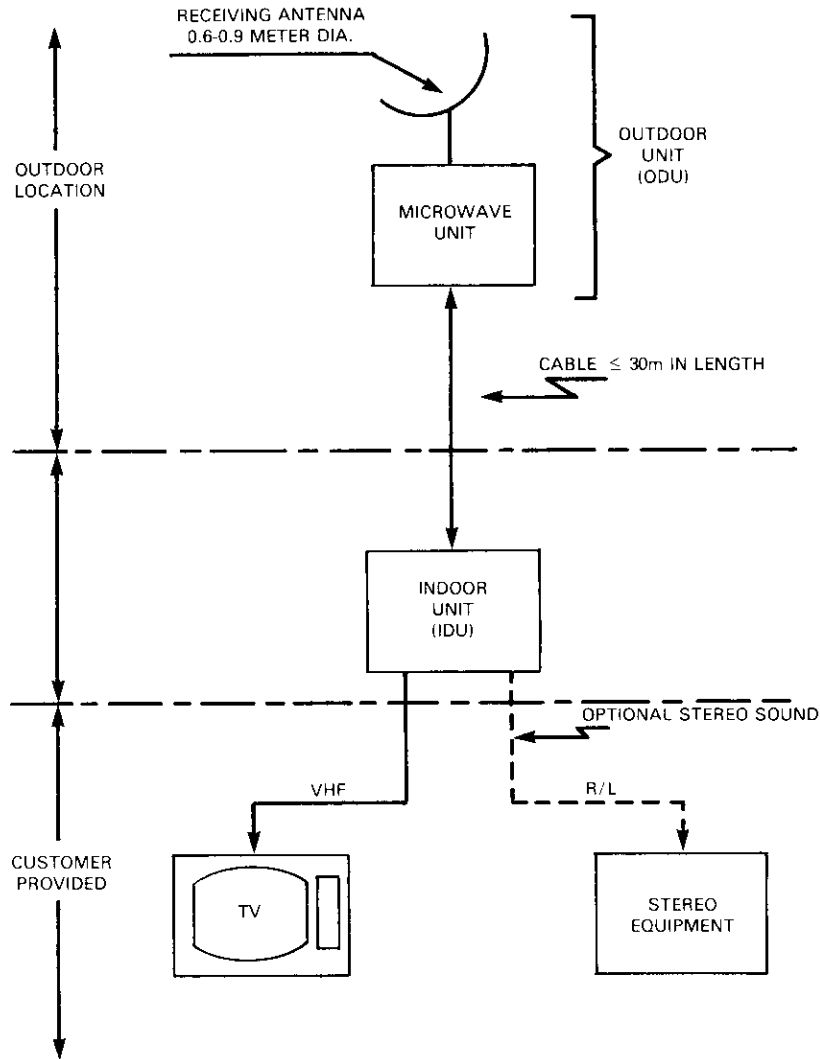


Figure 1. Individual Reception Equipment (Basic Elements)

INDOOR UNIT

The IDU will contain the necessary electronics and controls to allow subscriber channel selection, FM demodulation, descrambling, and AM remodulation. Normal channel reception is expected to be on either

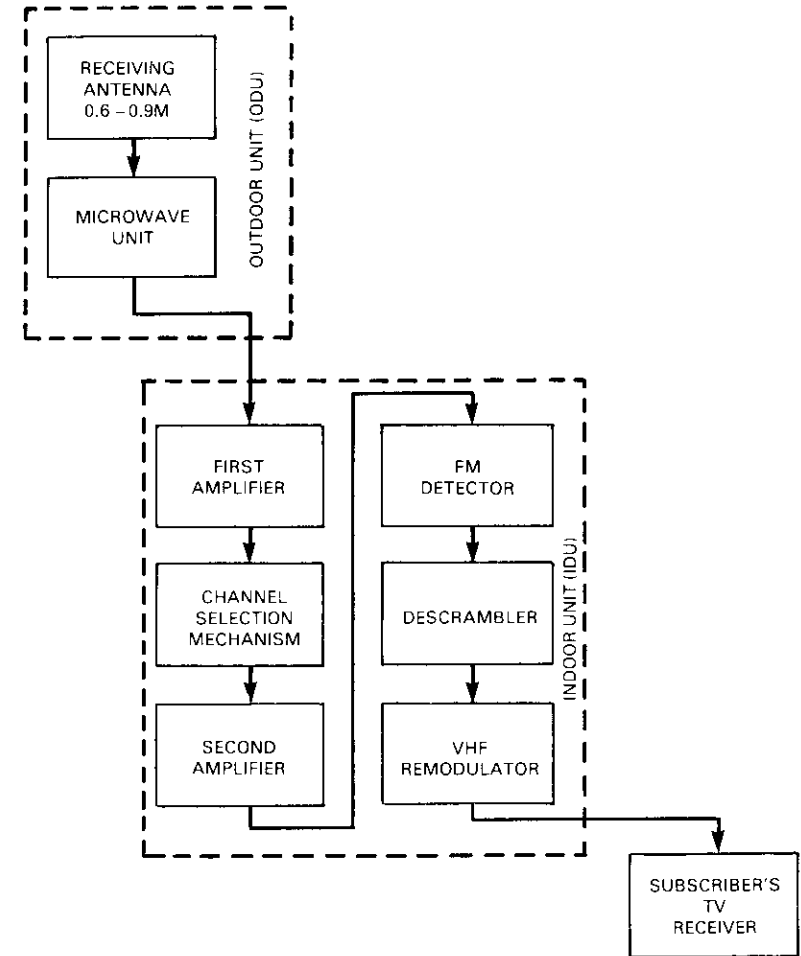


Figure 2. Home Equipment Block Diagram (Typical)

VHF channel 3 or 4. The IDU provides a standard NTSC formatted signal with the usual adjustments of color, hue, volume, and tone retained in the viewer's TV receiver.

When second language transmissions are programmed, a switch on the IDU permits their reception using the viewer's TV audio channel. Low-level stereo output jacks will also allow the IDU to be connected to subscriber-owned stereo equipment suitably located for reception

TABLE 1. OUTDOOR UNIT PERFORMANCE (NOMINAL)

Antenna/Mount	
Frequency Range	12.2–12.7 GHz maximum
Antenna Diameter (m)	0.6, 0.75, 0.9
Gain (dB) at 12.5 GHz	34.9, 36.8, 38.4
Polarization	Circular, selectable at installation
Adjustment	10° – 80° elevation ± 70° Azimuth
Wind Survival	120 km/hr (75 mph)
Mounting	Universal
Weight	Approximately 26 kg
Microwave Unit	
Noise Figure	≤4.5 dB
Bandwidth IF	Same as frequency range above
Frequency IF	In 800- to 1300-MHz range
Stability	± 1.0° × 10 ⁻⁵
Temperature Range	- 20 to + 38° C

of stereo broadcast transmissions. The subscriber would lower the sound on the TV receiver when stereo transmissions are broadcast.

Each IDU will be uniquely addressable to allow control of individual subscriber service over the air from Las Vegas (e.g., special program subscriptions, access to bilingual transmissions and stereo service, and captioning and teletext services). Table 2 lists the presently planned performance characteristics of the IDU.

TABLE 2. IDU PERFORMANCE CHARACTERISTICS

Nominal Input Frequency	800 to 1300 MHz
Number of Selectable Channels	3 (expandable with module change)
Input Level	- 75 dBm + 15 dBm
Second IF Bandwidth	16 MHz
Output	
Frequency	VHF channel 3 or 4 60–72 MHz
Signal Level	7 dBmV ± 3 into 75Ω
Video-Audio Ratio	Approximately + 12 dB
Connector	F type
Audio (Stereo)	1 V rms/channel unbalanced

Community reception

Multiple dwelling units (e.g., apartments and condominiums) will be provided with service similar to that of the individual residences through use of a slightly different outdoor unit and distribution system as shown in Figure 3.

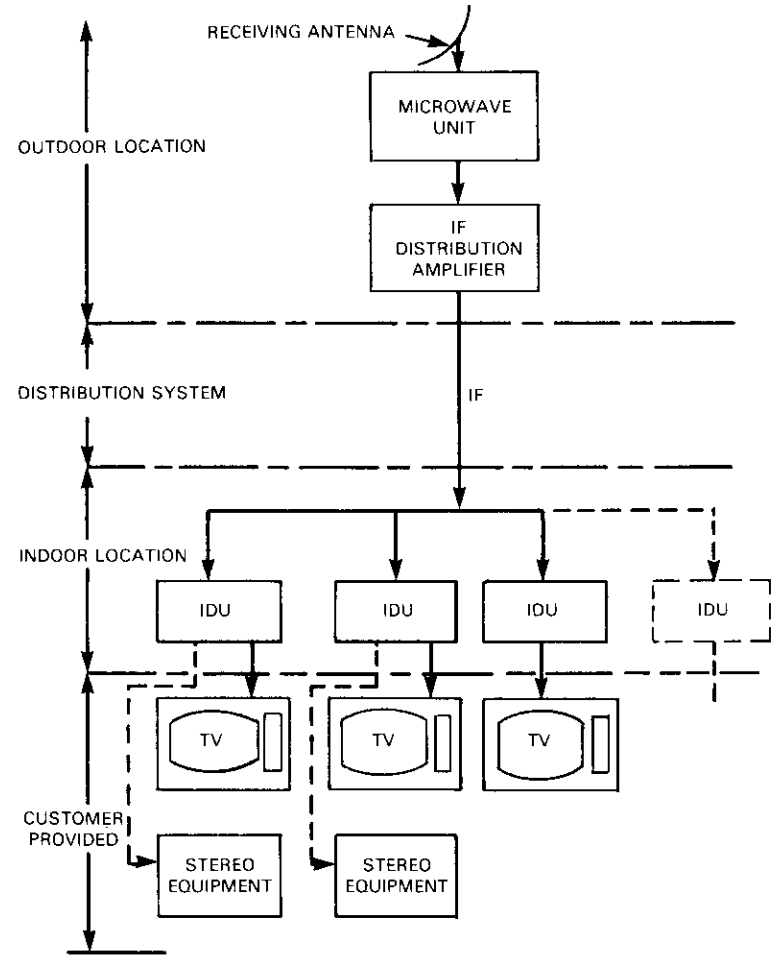


Figure 3. Multiple Dwelling Unit Receiving Equipment (Basic Elements)

This configuration will provide scrambled service to each dwelling resident and use IDUs at each set location similar to those required for individual residence reception. A larger receive antenna and high-gain IF distribution amplifier are envisioned for multiple dwelling unit installations.

Service to cable system operators is also contemplated. High-quality link performance can be achieved at cable head ends with a larger receiving equipment antenna than the 0.75-m baseline individual reception equipment. Head end receiving equipment would down-convert, demodulate, and descramble all channels simultaneously. Channelizers and regenerators would then condition the signals for transmission over the cable system using the local cable security system to protect the service.

Teletext

Broadcast teletext transmissions are envisaged which will deliver selected textual and graphical information to the subscriber. This information will be transmitted during the normal TV broadcast periods with a special digital code embedded in the vertical blanking interval, and will be cyclically repeated. Through operation of a simple key pad, the subscriber's special (optional) teletext decoder will select the page of interest and store it for local viewing.

Teletext standards have not been fully developed in the United States. Extensive experiments are planned and standards should be established before the introduction of STC's service.

Set-top versions of existing teletext decoding equipment interface with the TV receiver at its antenna terminals. However, full display potential of the TV tube is not achieved with this equipment because the video text generated is impaired by passage through the tuner, IF detector, and video circuits. Future television receivers with built-in teletext reception capability will allow direct drive of the picture tube's red, green and blue electron guns; consequently, color saturation and sharpness limited only by the tube itself will be realized. Effects which may be present with set-top units (*e.g.*, subcarrier dot crawl, receiver noise, misregistration of chrominance and luminance, and ghosting) should no longer be present, and an extraordinarily good display of text will be possible. When broadcast in this ancillary manner, teletext may provide access to hundreds of pages of information.

Captioning for the hearing-impaired

Captioning is a process by which the audio portion of a TV program

is translated successively into subtitles that appear on the viewer's screen. A closed captioning process can only be viewed on a TV set equipped with a special (optional) decoding unit. Because of the distractive nature of captions to the general viewer, closed captioning provides maximum enjoyment to both general viewers and the hearing-impaired.

Special encoders and decoders have been developed under the auspices of the United States Department of Health and Human Services to allow transmission of audio captions on line 21 of the standard TV signal in the vertical blanking interval. At the TV receiver, a special decoder extracts the coded information from line 21 and processes it, controlling character generators and attribute logic to produce the visible caption.

To prepare for a captioned broadcast, video tapes of the planned programs will be provided to one of the established National Captioning Institute centers, where editors arrange the audio dialogue into captions that are recorded on a magnetic disk. The captions are then digitally inserted on line 21 of the TV picture during program transmission, so that it is received along with the regular picture and sound program.

Special decoder units are presently available for closed captioning under the product name "Telecaption." Two versions are available: an adapter which easily attaches to an ordinary TV set, and a 19-inch color portable set with built-in decoding circuitry.

Up-link and ground control facilities

D. L. DURAND

The ground facilities portion of the system will include a centralized Broadcast Center and System Control Facility (SCF) near Las Vegas, Nevada, and backup transmission and monitoring facilities at Santa Paula, California, and Washington, D.C., respectively. The home receiving equipment in its various configurations was described previously.

Construction is to be completed at facilities near Las Vegas, and in Santa Paula and Washington 1 year prior to the first spacecraft launch, and full operational status is expected 6 months later.

Las Vegas complex

The Las Vegas complex will be the major ground communications, operational and control facility of STC's system. The Broadcast Center will perform program and RF operations, and other specialized data processing functions. The SCF provides system control, including satellite TT&C. Figure 1 shows a typical layout of the Las Vegas complex.

PROGRAM OPERATIONS

The Broadcast Center program operations area will control all aspects of program production, scheduling, editing, reproduction, evaluation, control, and airing. To accomplish these functions, the facility will contain a comprehensive array of television broadcast equipment capable of providing up to nine channels of continuous programming for dissemination to the satellite transmission system.

The output channels and media playback equipment will be directly controlled by a computerized automated program system, capable of supervising on-the-air playback without operator assistance. Facilities for program editing, monitoring, switching, processing, and review will maintain the highest possible program quality, and a central video console will provide final production direction, distribution, cueing,

Abbreviations and acronyms used in this series of papers are defined on Page 265.

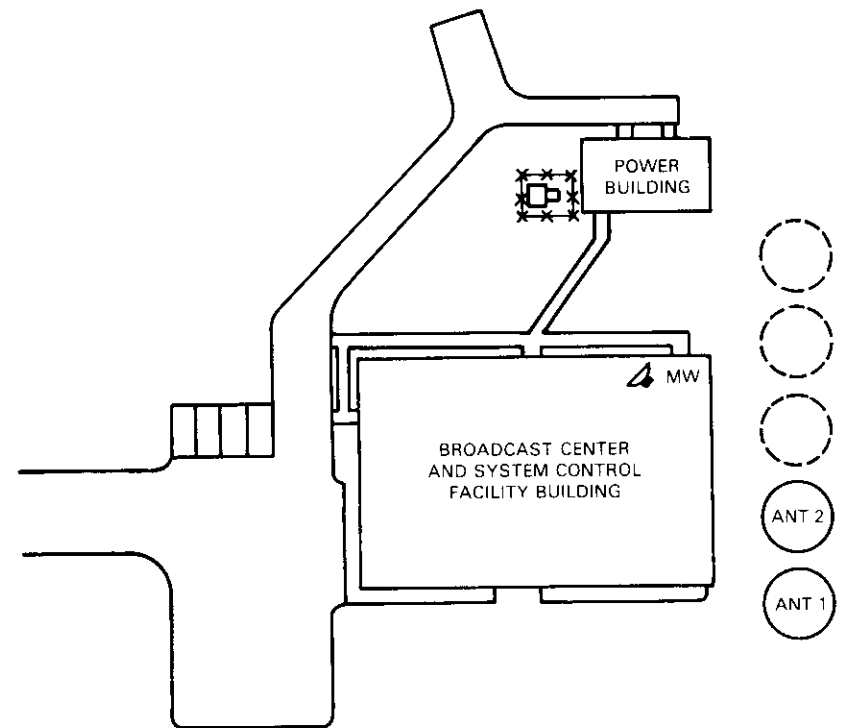


Figure 1. Las Vegas Ground Facility

and control of up-link video. All up-link channels will be monitored and controlled in this area.

Equipment will be provided for program recording and reproduction by a variety of media including video tape, film, disc, and other broadcast quality reproduction formats. Real-time material may also be used for broadcast and will be obtained via a terrestrial microwave link.

A modest studio facility with appropriate switching, audio control, lighting, production cameras, scenery, and furniture will be available at the Broadcast Center to accommodate local program production.

RF OPERATIONS

The baseband, intermediate frequency, and radio frequency equipment necessary to channelize, scramble, modulate, up-convert, and process video signals for transmission to the satellites will be located

in the RF operations facility of the Broadcast Center. Under normal conditions, all up-link video transmissions will originate at the Broadcast Center. Satellite down-link transmissions will be monitored for service continuity and tests. Transmissions to the PSA and MSA will be received directly; transmissions to the CSA and ESA normally will be monitored at the engineering support facility in Washington, D.C., but may be patched back to Las Vegas in the event of transmission anomalies to expedite any necessary corrective action.

Five 11-meter antennas operating in the 12/17-GHz BSS bands are planned at Las Vegas. One will be equipped with auto track, program track, and manual positioning capability. The other four antennas will have limited motion for transmission to the satellites in service. Table 1 lists the planned antenna characteristics, and Figure 2 shows a representative RF configuration.

The equipment in Las Vegas is designed so that normal TV programming and TT&C operations can occur simultaneously without impairment or interruption of either function.

DATA PROCESSING OPERATIONS

Certain service information (*e.g.*, request to bring new subscribers on line), special program subscription, billing data, and home equipment inventory status or needs will be generated and processed at various regional locations throughout the country. These data will be formatted and transmitted to the Las Vegas complex for disposition. Certain information will require development of appropriate transmissions for broadcast on the video data subcarrier.

SYSTEM CONTROL FACILITY

The SCF is depicted in Figure 3. Spare and adjacent operating satellites will be controlled by a single antenna. The SCF can handle all facets of satellite housekeeping on a stand-alone basis.

The SCF monitors and controls the performance of all satellites. It continuously processes and limit-checks all satellite telemetry data, generates commands, coordinates ranging and angle tracking of satellites for orbit determination, and performs other coordinating functions related to launch and transfer orbit operations, and in-orbit testing. Major components of the SCF include the operator console, minicomputers, display panels, and telemetry and command processing equipment. Considerable redundancy will be provided for all control center functions.

TABLE 1. ANTENNA CHARACTERISTICS

Electrical	
Operating Frequency Range	
Transmit	17.3–18.1 GHz
Receive	12.2–12.7 GHz
Antenna Gain	
Transmit	63.5 dBi at 17.5 GHz
Receive	60.5 dBi at 12.5 GHz
Half-Power Beamwidth	
Transmit	0.11°
Receive	0.15°
VSWR	1.3 to 1
Polarization	RHCP/LHCP selectable
	Receive—orthogonal to transmit
Axial Ratio	1.4 to 1 V
Noise Temperature at 30° Elevation	20 K
Mechanical	
Antenna Size	11 m
Mount Type	Elevation over azimuth
Antenna Point Range (limited motion)	Azimuth, 110° Elevation, 15° to 60°
Pointing Accuracy	0.015° rms in 48 km/hr winds gusting to 72 km/hr 0.11° rms in 96 km/hr winds gusting to 136 km/hr
Survival Wind Loads	200 km/hr any direction
Steering Modes	
Full Performance	Auto Track Program Track Manual Slew Manual Position
Limited Motion	Auto Track Manual Slew Manual Position

Transmitter amplifiers dedicated to command functions are sized so that satisfactory link performance will exist for at least 99.995 percent of the time. Other TT&C-dedicated units include telemetry receivers, up/down-converters, and RF filters; adequate redundancy will be provided for all equipment.

The SCF includes equipment which, in conjunction with additional equipment located at other field sites, can test the satellites' initial performance in orbit. Periodic in-orbit testing, as required, will be managed from Las Vegas.

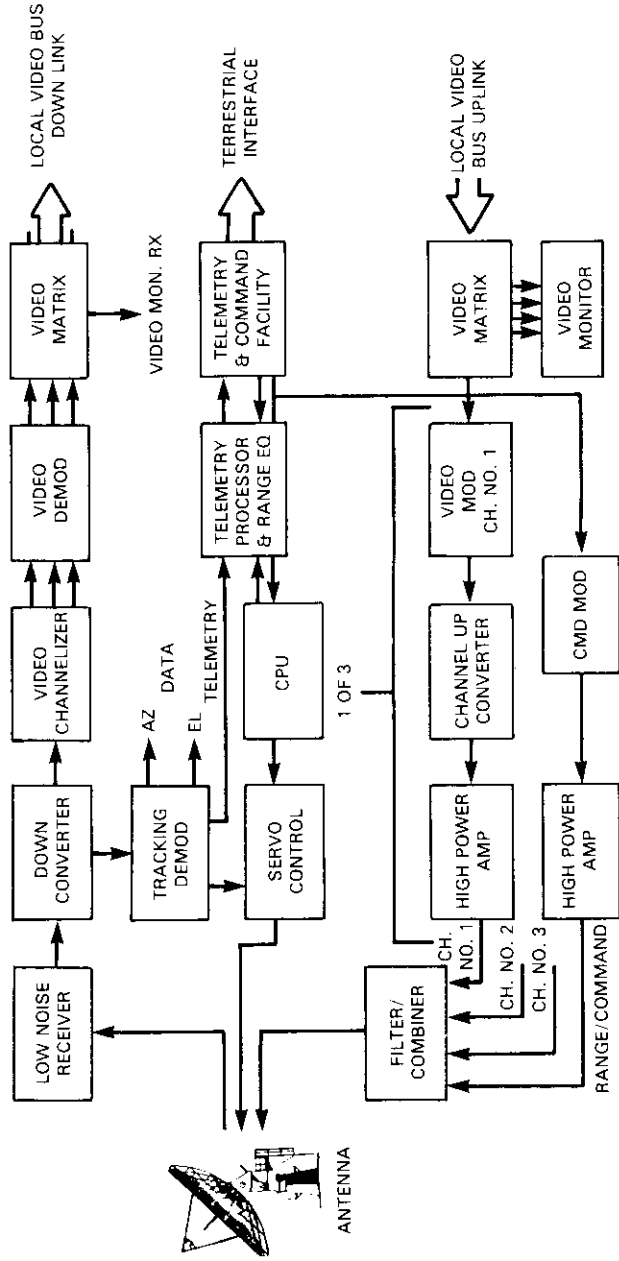


Figure 2. Representative RF Configuration (Las Vegas)

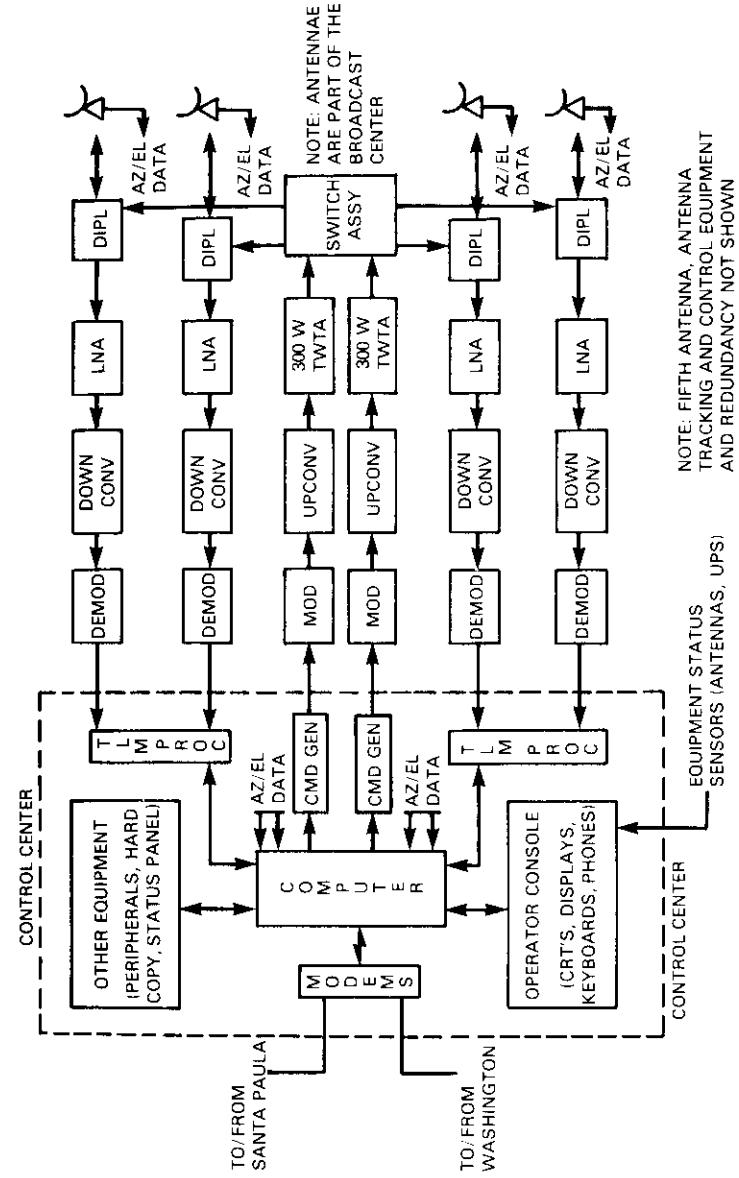


Figure 3. System Control Facility

Engineering support facility

STC's engineering operations will be supported by an existing facility in Washington, D.C., where personnel will provide overview support for satellite system technical operations (including monitoring ESA and CSA transmissions), perform orbital mechanics computations, handle specialized data reduction and analysis, provide advice on engineering decisions (*e.g.*, satellite battery management), and aid SCF personnel in the event of satellite anomalies. The facility, which will require some equipment augmentation, will be interconnected with the SCF via terrestrial voice and data links, and will be equipped with computers, telemetry processors, display panels, and related equipment.

Santa Paula facility

An existing COMSAT GENERAL earth station site at Santa Paula, California, will be augmented with one 11-meter antenna and appropriate equipment in the initial phase of implementation to provide full backup of all satellite control functions. This station will also be equipped with facilities for limited video program up-linking and customer advisory services in the event of a major failure at Las Vegas. The Santa Paula facility will be linked with the Las Vegas complex and the engineering support facility in Washington, D.C., by both full-period and dial-up terrestrial data/voice circuits.



David L. Durand received a B.S. in electrical engineering from Indiana Institute of Technology. He is currently Director of Equipment Engineering, Satellite Television Corporation. He joined COMSAT in 1965 as a member of the technical staff. From 1969 to 1974, he was Chief Engineer at the Andover Earth Station, Andover, Maine, and from 1974 to 1977, Manager of the COMSAT General Earth Station, Southbury, Connecticut. Prior to joining COMSAT, Mr. Durand was with the National Radio Astronomy Observatory at Greenbank, West Virginia, and the Atlantic Missile Range, Cape Canaveral, Florida.

DBS/FS frequency sharing

J. E. WHITWORTH

The 12-GHz frequency band allocated to the BSS at WARC-79 is presently used domestically by the Private Operational Fixed Service, which has approximately 1,600 licensed transmitters. As the name of this service implies, most users of the band are private organizations. (Approximately 64 percent are in the business/industrial category; the remainder are educational institutions; city, state, and local governments; emergency/medical; and religious organizations.)

Some of the characteristics of this service that will affect sharing possibilities are:

- a. The FCC has designated paired 20-MHz channels 260 MHz apart, and paired 10-MHz channels interleaved between the 20-MHz channels, which are 240 MHz apart.
- b. A high percentage (65 to 70 percent) of the systems are video or wideband digital with 20-MHz bandwidth assignments.
- c. Typically, pathlengths are quite short (24 percent of the paths are less than or equal to 1.6 km) and antennas are small (0.6 to 1.8 m). Transmitter powers typically range from 20 mW to 1 W.
- d. A high percentage of users are presently located in a few major metropolitan areas, such as Los Angeles and New York, creating serious frequency congestion in these cities.

The potential for interference from the Fixed Service into DBS home receivers has been analyzed [1] and found to be a significant problem that must be resolved before introducing DBS in the United States. Basically, three possible sharing alternatives exist: co-channel sharing, adjacent channel sharing (interleaving), and band segmentation.

STC has evaluated all three possibilities through predictive modeling of interference levels and a field measurements program. The measurements program was conducted to accomplish the following:

- a. determine the extent and magnitude of potential interference

Abbreviations and acronyms used in this series of papers are defined on Page 265.

in several of the major metropolitan areas where frequency congestion in the 12.2- to 12.7-GHz band is significant;

- b. provide a basis for comparing predicted and measured interference levels to develop a more realistic prediction model; and
- c. evaluate the possibility of implementing either co-channel or adjacent channel frequency sharing.

Measurements were made at 16 different sites in Boston, New York City, Philadelphia, and Cleveland. The data obtained indicated that the level of interference that would be experienced by DBS home receivers is significantly less than that predicted by commonly used computer models. Figure 1 shows the cumulative distribution of the difference between measured and predicted values. As the figure indicates, 85 percent of the measured values were more than 10 dB below computer-predicted values. The difference results from the fact that computer-predicted values typically do not consider terrain, foliage, and structure shielding of the small DBS antenna, or fine grain pattern variations of the FS antenna.

Although typical levels of interference were significantly below predicted values, measured interference levels were high enough to lead STC to conclude that co-channel interference would be a serious problem. (Values corresponding to a $C/I = -2$ dB at the input to a typical DBS receiver were measured.)

The actual spectrum occupancy of the FS systems in the band was in many cases less than that allowed by the assigned bandwidths. On the other hand, there were cases of digital modulation in which the FS spectrum occupied the total 20-MHz bandwidth, and if DBS systems were interleaved (*i.e.*, operating +10 MHz from these FS systems), unacceptable interference would be experienced.

The results of the measurements program were used as an input in the development of a more realistic computer model, which could then be used to predict the number of households that would experience unacceptable interference from FS systems. The analytic model culled a data base of current FS systems to determine their frequency, transmitted power, antenna pattern, and location, and used these data to compute interference intensity contours. These contours were then used to compute the number of households that would likely experience unacceptable interference in six major metropolitan areas: Los Angeles, New York City, Cleveland, Philadelphia, Dallas, and Boston.

The interference intensity contours were prepared on 15 arc minute width maps that were subdivided into 7½ arc minute quadrants. Figure 2 shows the complexity of these contours in and around Boston (each

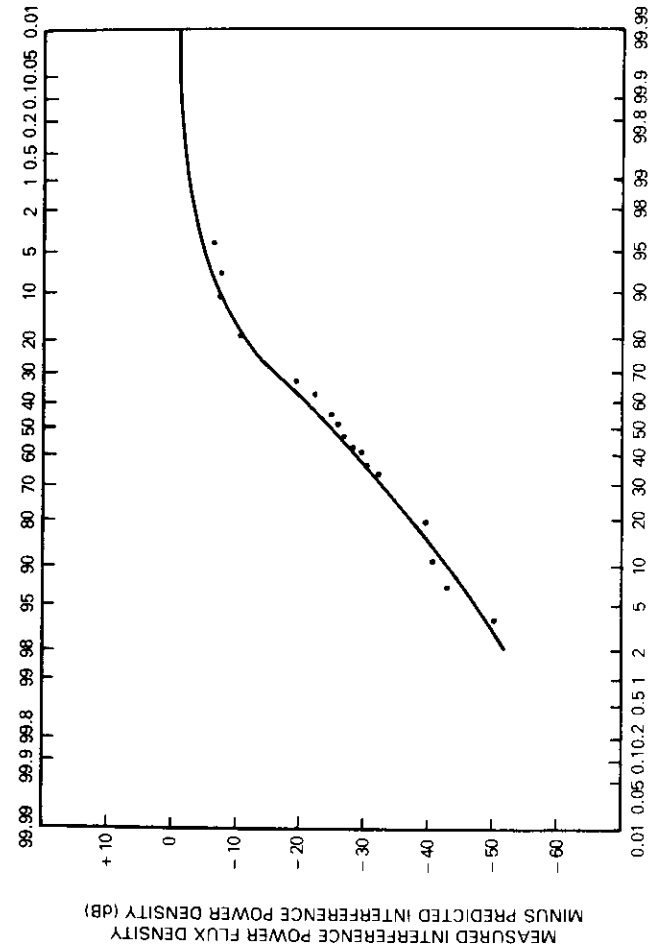


Figure 1. Percent of Data Points < Ordinate

(ADJACENT CHANNEL INTERFERENCE CALCULATION)

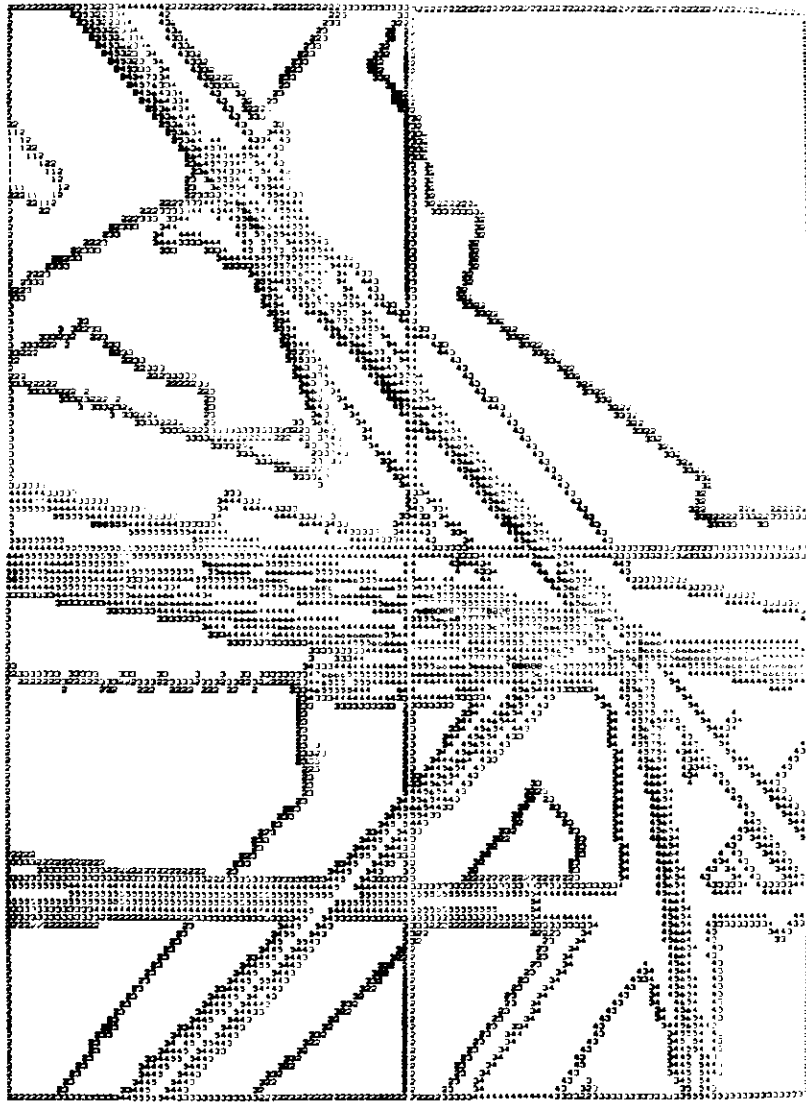


Figure 2. Interference Intensity Contours for the Boston Area (12280/12420/12660 MHz Composite)

numerical value in the figure represents a different interference level). These maps were used to calculate the percentage of the area that contained interference levels corresponding to a C/I value of less than 35 dB.

As indicated, actual FS installations, with their individual characteristics, and realistic DBS antenna patterns were used for these calculations. In addition, the propagation model used for the calculations assumed an extra 10 dB of attenuation based on field measurements. It was also assumed that the DBS home terminal antenna would provide 47-dB discrimination (relative to the main beam) against FS interference.

Demographic data from the 1970 U.S. census (updated to 1979 on the basis of such information as birth rate and construction permits) were used to calculate the number of households in each of the 7½ arc minute quadrants. These demographic data were available for 1-minute by 1-minute grids throughout the United States. The percentage of the area of each 7½ arc minute quadrant with predicted interference of C/I less than 35 dB was multiplied by the number of households in each quadrant, and the numbers of households with such interference in each quadrant were added to arrive at the results in Tables 1 and 2.

As shown in Table 1, approximately 6.4 million households in the six metropolitan areas, or approximately 51 percent, would experience unacceptable interference with co-channel sharing.

TABLE 1. CO-CHANNEL SHARING: NUMBER OF HOUSEHOLDS IN MAJOR METROPOLITAN AREAS THAT MIGHT EXPERIENCE SIGNIFICANT FS INTERFERENCE

MAJOR METROPOLITAN AREAS (MMAs) ^a	NOMINAL CASE ^b (THOUSANDS)	+ 10 dB (THOUSANDS)
Los Angeles	3,018.3	3,949.8
New York (ESA)	2,588.6	4,451.2
Boston (ESA)	344.7	797.3
Philadelphia (ESA)	248.4	577.7
Dallas	135.3	362.3
Cleveland (ESA)	84.1	223.5
Total National MMAs	6,419.4 ^c	10,361.8
Total Eastern Service Area MMAs	3,265.8	6,049.7

^aCities located in STC's proposed Eastern Service Area (ESA) are identified.

^bNumber of households that would have a C/I less than 35 dB on one or more of the 12,270 MHz, 12,410 MHz, and 12,650 MHz frequencies.

^cApproximately 51 percent of the total households in these MMAs.

To provide a basis for sensitivity analysis, a second case labeled "+10 dB" is shown. This would be the predicted number if, for example, the DBS antenna provided 10 dB less isolation than assumed for the nominal cases. As shown, in the +10 dB case, the number of households experiencing unacceptable co-channel interference would increase to 10.4 million.

Table 2 shows the estimated number of households in the six major metropolitan areas that would experience interference if adjacent channel sharing were attempted. The nominal case in the table assumes a DBS receiver filter selectivity providing 30-dB isolation against the adjacent channel FS signals. Even with this assumption (which would require very sharp filter skirts in the home terminal), approximately 930,000 households in the six major metropolitan areas would still experience unacceptable interference. A +10-dB case is again shown, representing the situation if either the DBS antenna did not provide the assumed sidelobe discrimination, or the filter selectivity provided only 20-dB instead of 30-dB isolation against adjacent channel interference. The number of households experiencing interference increases to approximately 2.6 million in this case.

TABLE 2. ADJACENT CHANNEL SHARING: NUMBER OF HOUSEHOLDS IN MAJOR METROPOLITAN AREAS THAT MIGHT EXPERIENCE SIGNIFICANT FS INTERFERENCE

MAJOR METROPOLITAN AREAS (MMAs) ^a	NOMINAL CASE ^b (THOUSANDS)	+ 10 dB (THOUSANDS)
Los Angeles	634.3	1,661.2
New York (ESA)	224.2	714.6
Boston (ESA)	32.3	101.0
Philadelphia (ESA)	10.8	35.7
Dallas	13.4	62.3
Cleveland (ESA)	15.1	46.3
Total National MMAs	930.1 ^c	2,621.1
Total Eastern Service Area MMAs	282.4	897.6

^aCities located in STC's proposed Eastern Service Area (ESA) are identified.

^bNumber of households that would have a C/I less than 35 dB on one or more of the 12,280 MHz, 12,420 MHz, and 12,660 MHz frequencies.

^cApproximately 7 percent of the total households in these MMAs.

These results show that the number of households that potentially would suffer interference is significant, despite the fact that realistic assumptions were incorporated in the modeling (e.g., the 30-dB filter

isolation factor used in the adjacent channel case and the extra 10-dB attenuation over free space used in both the co-channel and adjacent channel cases to account for shielding effects).

Note that even though the number of households experiencing interference in the adjacent channel case is significantly less than in the co-channel case, the former still is not a good solution. It would not be possible to predict beforehand which households actually would experience interference without conducting a site survey for each customer. Therefore, not only would adjacent channel sharing require excellent filtering in DBS receivers but, in addition, it could create serious operational and installation problems.

In summary, it was concluded that co-channel sharing is not feasible because of the unacceptably large number of households that would be affected. There does not appear to be any practical way of locating DBS home receivers so that interference could be avoided. A second conclusion was that adjacent channel sharing, although not as problematic as co-channel sharing, would still result in a significant number of households (7 percent) that might be subject to interference. It could also create serious operation problems and necessitate a difficult and costly receiver design.

The third sharing alternative that has been investigated is band segmentation, for which several approaches have been considered. All the preferred approaches recognize the basic characteristics of FS users, and are designed to minimize impact on existing FS users. For example, the band could be segmented with a single boundary. From the viewpoint of spectrum efficiency, this is an optimum approach, and also has the advantage of limiting the RF bandwidth of the DBS home terminals, which could reduce costs and lower the receiver noise figure somewhat. The FS frequency plan presently in use in the band, however, provides predominantly for paired (20-MHz) assignments separated by 260 MHz. Therefore, to minimize the impact on FS users, two bands separated by 260 MHz could be cleared for DBS systems. This would continue to provide FS systems with the same frequency separation for their paired frequencies, and would result in only one FS frequency being displaced for each BSS frequency assigned.

Recently, strategies for band segmentation that would lead to efficient band sharing have been examined. Based on an analysis of the Los Angeles area, it has been determined that the existing FS systems in that area, which now span the entire 12.2- to 12.7-GHz band, could be compacted into approximately half this bandwidth if the following actions were taken:

a. Some systems presently assigned 20-MHz channels with capacity requirements of less than 300 telephony channels are reassigned to 10 MHz.

b. A new optimized frequency assignment plan is developed for FS making maximum use of the present paired frequencies.

c. All systems with 0.6-, 1.2-, and 1.8-m antennas are required to upgrade to 1.8-m high-performance antennas, and all 2.4-m antennas are upgraded to 2.4-m high-performance antennas, to reduce intrasystem interference and allow more frequency reuse within a given geographical area.

d. Two "star" type networks (one with 17 radial paths, the other with 15 radial paths) plus approximately 16 additional paths are reassigned outside the 12.2- to 12.7-GHz band.

Since Los Angeles is by far the most congested area of the country in terms of FS use, the same amount of compacting could be accomplished nationally with relative ease.

The overall cost of clearing a given part of the band for DBS is reduced if frequency compacting is used in conjunction with moving some FS systems to other bands. Since there is considerable unused spectrum allocated and available to the terrestrial fixed service in the 18- and 22-GHz bands, there should be no barriers to FS operation in these bands.

Some classes of FS systems are better suited than others to move to higher bands. In general, short-haul, single-hop systems could move up easily at minimal cost and with no significant degradation of service. Figure 3 shows the distribution of path lengths of systems presently using the 12.2- to 12.7-GHz band. As shown in the figure, 55 percent of the paths are less than or equal to 8 km. These types of systems should be first considered for reassignment to the higher bands. In addition, approximately 10 percent of the currently operating FS systems are providing less than 300 channels of telephony. Recently, equipment for operation in the 18-GHz band for these types of telephony systems has become available.

Some types of FS systems could not move to higher bands quite so easily. Long-haul, multihop systems are one such type, along with systems that have very high reliability requirements. In such cases, movement out of the band, while still possible, could be expensive. Therefore, to the extent that movement out of the 12-GHz band is necessary to accommodate DBS, systems that happen to be on the frequencies assigned to DBS should not simply move out; rather, the

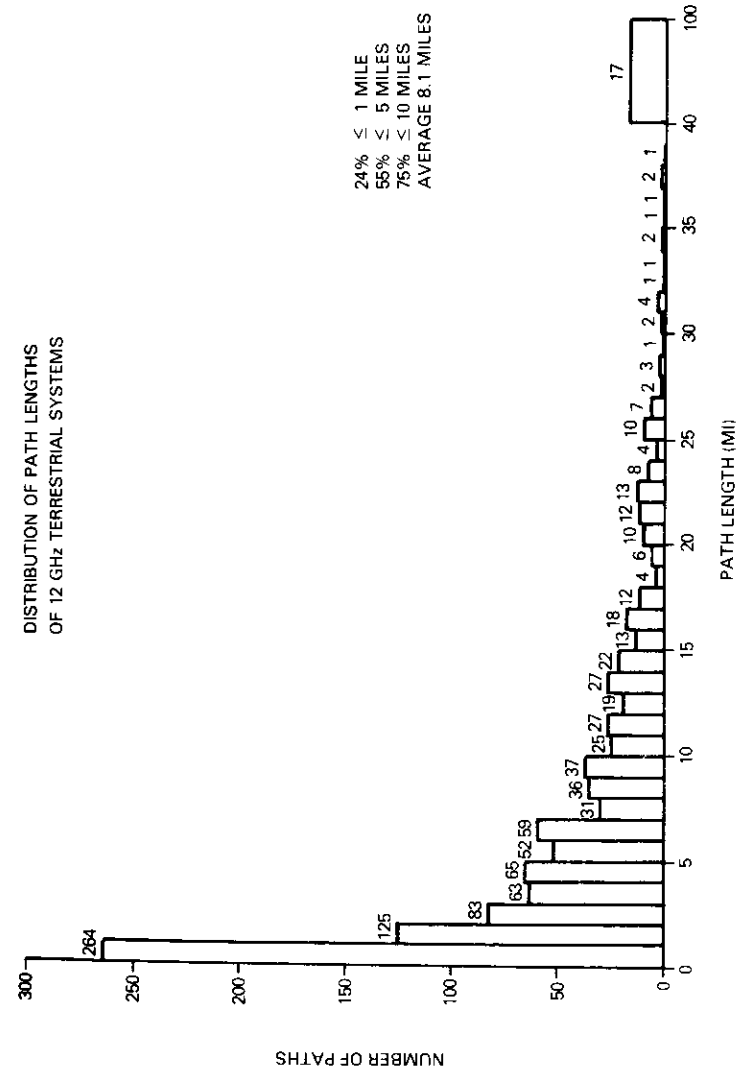


Figure 3. Distribution of Path Lengths of 12-GHz Terrestrial Systems

efficiency of present FS band use should be examined, and a sequence of moves planned that takes into account inefficiencies in present FS assignments, as well as the compatibility of individual FS system characteristics with operation at the higher frequencies.

Acknowledgements

The measurements program reported herein was performed by COMSAT General's Spectrum Engineering Department. COMPU-COM, Inc. of Dallas, Texas, provided the data base characterizing current FS users and computed the interference intensity contours used in the calculations to determine interference into DBS receivers. COMPUCOM also performed the analysis of compacting Los Angeles FS systems into approximately half the current bandwidth.

References

- [1] H. Akima, "Sharing of the Band 12.2-12.7 GHz Between the Broadcasting Satellite and Fixed Services," NTIA Report 80-32, January 1980.



James E. Whitworth received a B.S.E.E. from the University of Tennessee in 1961 and an M.S.E.E. from George Washington University in 1967. He is presently Director of Telecommunications at Satellite Television Corporation, responsible for all telecommunications activities which define and support the characteristics of the STC communications system. Before joining STC in 1980, Mr. Whitworth was Deputy Program Manager of COMSAT General's ARABSAT program. Prior to joining COMSAT General in 1974, he held positions with Fairchild Space and Electronics, National Scientific Laboratories, IBM Corporation, and Atlantic Research Corporation.

Abbreviations and Acronyms

AKM	Apogee Kick Motor
BSS	Broadcasting Satellite Service
CCIR	International Radio Consultative Committee of the ITU
CONUS	Contiguous United States
CSA	Central Service Area
DBS	Direct Broadcast Satellite
ESA	Eastern Service Area
FCC	Federal Communications Commission
FS	Fixed Service
FSS	Fixed Satellite Service
HDTV	High Definition Television
IDU	Indoor Unit
ITU	International Telecommunications Union
MSA	Mountain Service Area
NTSC	National Television System Committee
ODU	Outdoor Unit
PAM-D	Payload Assist Module—Type D
PSA	Pacific Service Area
RARC-83	1983 Regional Administrative Radio Conference
SCF	System Control Facility
STC	Satellite Television Corporation
STS	Space Transportation System
TASO	Television Allocation Study Organization
TT&C	Tracking, Telemetry, and Command
TWT	Traveling-Wave Tube
TWTA	Traveling-Wave Tube Amplifier
WARC-ST	1971 World Administrative Radio Conference for Space Telecommunication
WARC-77	1977 World Administrative Radio Conference
WARC-79	1979 World Administrative Radio Conference

SBS system evolution

W. H. CURRY, JR.

(Manuscript received July 18, 1981)

Abstract

In early 1981, Satellite Business Systems (SBS) initiated customer services consisting of private, switched networks for integrated voice, digital, and image transmission using satellite links among earth stations located on customer premises.

SBS plans to evolve system capabilities to allow the introduction of shared services for customers with more modest transmission needs and to accommodate growth in large networks.

The paper relates the essential engineering features to the resulting operational capabilities, and describes currently planned system evolution. Segments discussed include the satellite, earth station, and telemetry, tracking and command (TT&C) and control configuration, as well as the time-division multiple-access (TDMA) burst architecture.

System and service overview

SBS offers large-capacity telecommunications services to business and government organizations via communications satellites providing connectivity throughout the contiguous 48 states. Customer services consist of private line, switched communications networks for integrated voice, data, and image transmission among dispersed customer locations. In addition, Communications Network Service, Series A (CNS-A) provides advanced services, such as video teleconferencing and other high-data-rate transmissions, which are economically sup-

ported through earth stations located on customer premises.

The transmission capacity of the customer's network is allocated among network earth stations as needed. Optional transmission capacity can be provided on demand to a network during peak traffic periods. Other CNS-A features, such as voice activity compression, further improve transmission efficiency and thereby reduce the cost of quality service.

SBS earth stations can interconnect with customer-provided PBXs, data terminals, and other communications terminal equipment, as well as with other common carrier communications services and facilities. Customer equipment collocated with an SBS earth station can be interconnected with conventional on-site facilities. Customer terminal locations remote from the earth station can be interconnected by communications facilities or by services acquired either by the customer or by SBS on the customer's behalf from other common carriers. Complete interconnectivity of all services specified by the customer is provided by the system switching and transmission design. The principal operating features of CNS-A and the technical features that make them possible are summarized in Table 1.

TABLE 1. SBS SERVICE/TECHNICAL FEATURES

CNS-A FEATURES	GOVERNING TECHNOLOGY
Integrated Voice, Data, and Image Transmission	Time Division Multiple Access
Private Networks	All-Digital Transmission
Bulk Transmission Encryption* (optional)	RF Transmission at 12/14 GHz
Unattended Earth Stations*	5- or 7-Meter-Diameter (nominal) Parabolic Antennas
Centralized Network Management	
Dynamic Allocation of Network Capacity	
Port Activity Compression for Increased Transmission Efficiency	
Temporary Assignment on Demand of Pooled Transmission Capacity (optional)	

* Evolutionary.

Because of the wide range of alternatives and the great flexibility offered by the SBS design, there is no "typical" CNS-A network. A network can consist of as few as 3 or as many as 100 earth stations,

each serving as a switching node for as many as 365 voice circuits (or the equivalent capacity in data transmission), to an aggregate of about 12 Mbit/s per satellite communications controller (SCC). The earth station configuration is shown in Figure 1.

Users perceive little significant difference between SBS service and the service and procedures characteristic of local public telephone companies and private networks. For example, call dialing procedures, audible call processing signals (dial tone, ringing, busy), and the speed of completing connections are similar. An advantage of CNS-A is that it extends these reliable services to high-rate data and image transmission. Moreover, network transmission capacity may be used interchangeably for voice or data and dynamically assigned among network nodes as needed.

SBS plans to introduce additional services late in 1981 to economically serve customers with smaller traffic volume by sharing network resources. Communications Network Service, Series B (CNS-B), will permit two or more private networks to share an earth station. Message Service Type I (MS-I) will permit low-cost long-distance telephone service. Access to MS-I earth stations will be via dedicated lines furnished by SBS. Later, SBS plans to introduce MS-II, which will connect users to earth stations via the public telephone system.

The SBS design features which allow the flexible evolution of these services include stored program controlled switching and processing at earth stations, and time-division multiple-access of the satellite transponder. The details of that design and the planned evolution of the services are addressed in the sections that follow.

Major system segments

The major system segments are the ground, space, and control segments, whose interrelationship is depicted in Figure 1. The TT&C system and the network control center (NCC) provide satellite and network control for all customer networks. Individual customer networks consist of three or more earth stations communicating through a transponder. A key component of each earth station is the SCC, which performs a variety of functions summarized in Table 2.

One earth station in each transponder provides the TDMA timing reference and dynamic capacity allocation for all networks operating in the transponder. This station, called the reference station, performs

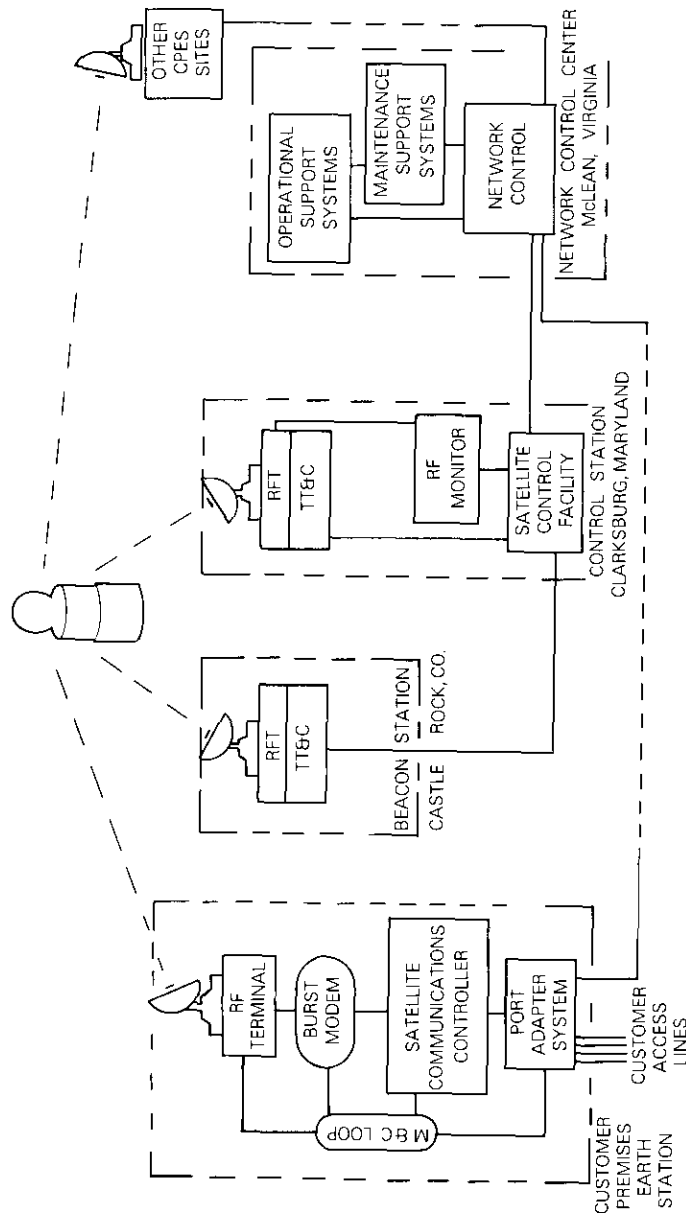


Figure 1. Major System Components

TABLE 2. FUNCTIONS OF MAJOR EARTH STATION COMPONENTS

COMPONENT	FUNCTION
Port Adapter System (PAS)	Provides signal level conversion, supervisory signaling, and 48-VDC signaling power.
Satellite Communications Controller (SCC)	Performs call processing (port-to-port), analog/digital conversions (voice/data), error control (FEC), activity compression, time-division multiplexing/demultiplexing of data streams, and synchronization of transmit/receive bursts. Controls burst modem and M&C system. Provides traffic activity status to the reference station, call records to the NCC, and system health information to the NCC.
Monitor and Command (M&C) System	Collects and reports status and alarms from all major earth station components.
Burst Modem (BM)	
Transmit	Modulates the two channels (I&Q) of data from the SCC into a QPSK IF signal and provides it to the RFT in bursts.
Receive	Demodulates the QPSK IF data stream from the RFT and provides it in two I&Q channels to the SCC.
Radio Frequency Terminal (RFT)	
Transmit	Translates the 70-MHz IF burst provided by the BM to 14 GHz, amplifies and transmits it to the satellite transponder.
Receive	Receives the satellite transponder data stream (including own station) at 12 GHz, amplifies and translates it to 70-MHz IF for demodulation by the BM.

this function through software contained in the SCC. Any SCC can be configured as the reference. A second earth station is similarly configured as a backup. The reference station function can be transferred automatically under specified conditions, or manually under direction of the network control center.

Ground segment

The ground segment consists of all the customer-premises earth stations. As indicated in Figure 1, the main components of an earth station are the port adapter system (PAS), the SCC, the burst modem (BM), the radio frequency terminal (RFT), and the monitor and command (M&C) system. The functions of these components are summarized in

Table 2. The significant earth station RF characteristics are summarized in Table 3.

TABLE 3. EARTH STATION CHARACTERISTICS

Antenna Diameter	5	7
Nominal (m)		
e.i.r.p. (dBW)	79.8	82.7
G/T (dB/K)	30.4	33.3
Gain (dB)		
Receive	53.8	56.7
Transmit	55.3	58.2
Beamwidth		
3-dB Points (deg)		
Receive	0.37	0.27
Transmit	0.31	0.22
Polarization		
Receive	Horizontal	Horizontal
Transmit	Vertical	Vertical
Tracking	Stepped	Stepped
	Command	Command

Other earth station components now under development include the data aggregator (DAG) and the specialized carrier switch (SCS). The DAG will allow networks to operate across more than one transponder, thus increasing the overall network capacity. The SCS expands the voice-band switching and call processing capacity of the system. These capabilities, needed to allow for system growth in CNS-A, CNS-B, and Message Services, are described in more detail in the section entitled *System Evolution*.

Earth stations are configured with an RF shelter and antenna which are co-located on the customer premises, as shown in Figure 2. The shelter houses the transmitting and receiving RF chains (amplifiers and frequency converters) necessary to couple the up-link (14-GHz) and down-link (12-GHz) from/to the 70-MHz intermediate frequency of the burst modem.

The antenna diameter normally used is approximately five meters. A larger antenna (nominal 7-meter diameter) is available at SBS discretion to ensure acceptable performance in some geographic areas. Five-meter antennas are intended to be roof or ground mounted, whereas seven-meter antennas are normally ground mounted. A low-noise amplifier (LNA) is mounted on the antenna structure for improved receiving (G/T) performance.



Figure 2. 5.5-Meter-Diameter SBS Antenna and RF Shelter Installed on Customer's Rooftop in Chicago, Illinois

The remaining earth station components (burst modem, satellite communications controller, and port adapter system) are located on-site convenient to interconnections to the customer's communications plant and terminals. These components are connected to the RF shelter and antenna via a 70-MHz interfacility link (IFL). The M&C loop,

connecting the earth station components to the network control center through the satellite communications controller, is designed to allow unattended operation of the earth station.

SBS intends to have more than 50 earth stations installed by year-end 1981 and approximately 200 by year-end 1983. Some of these installations will be required to support services that exceed the capacity of a single SCC and some must be able to operate in more than one transponder. These variations are discussed in more detail in the section entitled *System Evolution*.

Space segment

The SBS space segment includes the satellites, the TT&C earth stations, and the satellite control facility (SCF).

Satellites

Each satellite carries 10 active and 6 redundant traveling wave tube amplifiers (TWTAs), each of nominal 43-MHz bandwidth, plus 1 active and 3 redundant receivers. One receiver serves all TWTAs. (A receiver/TWTA combination is referred to as a transponder.) The satellite communications subsystems are shown schematically in Figure 3. Figure 4 is a photograph of the SBS (Hughes Aircraft Company type 376) spacecraft undergoing tests.

The satellite orbit is precisely maintained to minimize satellite drift and thereby eliminate the cost of accurate earth station antenna tracking. The satellite antenna coverage, shown in Figure 5, has been shaped to provide weighted coverage of the contiguous U.S., favoring the areas of high earth station density.

Using a Delta vehicle, SBS launched its first satellite into geostationary orbit at 100°W longitude on November 15, 1980. A second Delta vehicle launch to 97°W longitude is scheduled for fall 1981 and a Space Shuttle launch to 94°W longitude is scheduled for 1982.

Telemetry, tracking, and command (TT&C) Earth Stations

Space segment operational support is provided by a complex consisting of a beacon station, a control station, and a satellite control facility. For a spacecraft launch, additional tracking and command facilities to provide worldwide coverage are leased.

SBS uses two geographically separated TT&C stations for receiving telemetry from the satellites, for tracking to determine the orbital parameters, and for issuing commands to the satellite. Each station is

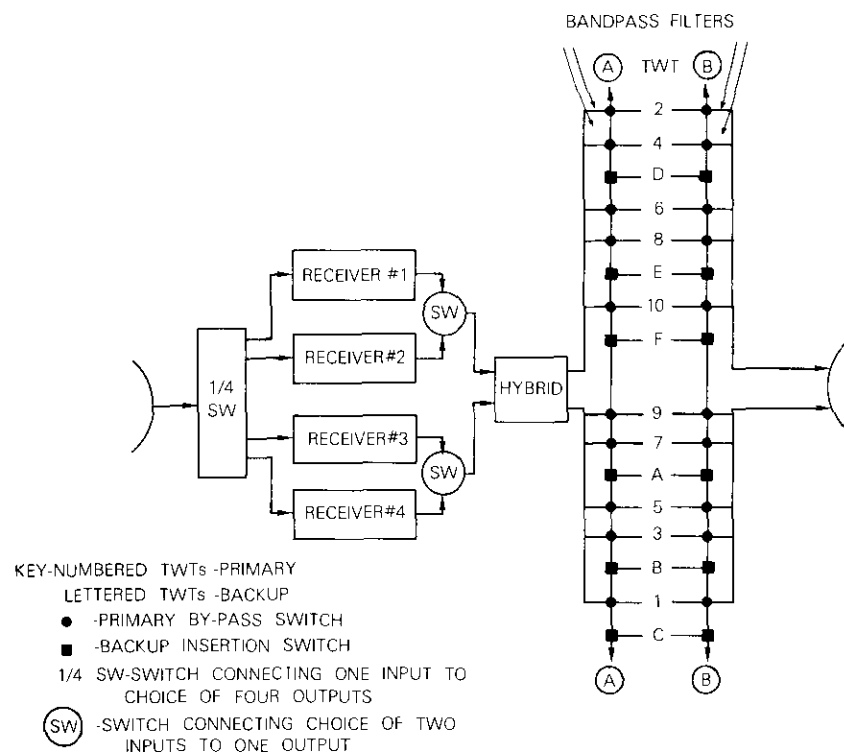


Figure 3. *Simplified Satellite Communications Subsystem Configuration*

now equipped with antennas and associated equipment that will enable simultaneous processing of TT&C signals and beacon transmissions. The satellite uses the beacon RF carrier as a reference for antenna pointing. The TT&C signals are transmitted to each satellite as modulation of the beacon RF carrier.

One TT&C earth station located at Castle Rock, Colorado, is designated as the primary beacon station. Figure 6 is an architect's rendering of this station. The other TT&C station is combined with the satellite control facility at Clarksburg, Maryland, and is designated as the primary control station. Figure 7 is an architect's rendering of the Clarksburg TT&C site.



Figure 4. SBS-1 (Hughes type 376) Spacecraft Undergoing Tests

BEACON STATION

The beacon station currently consists of a fully steerable antenna and RF terminal equipment, two limited motion RF terminals, and tracking, telemetry, and command processing facilities. The beacon station provides the following functions for the SBS system:

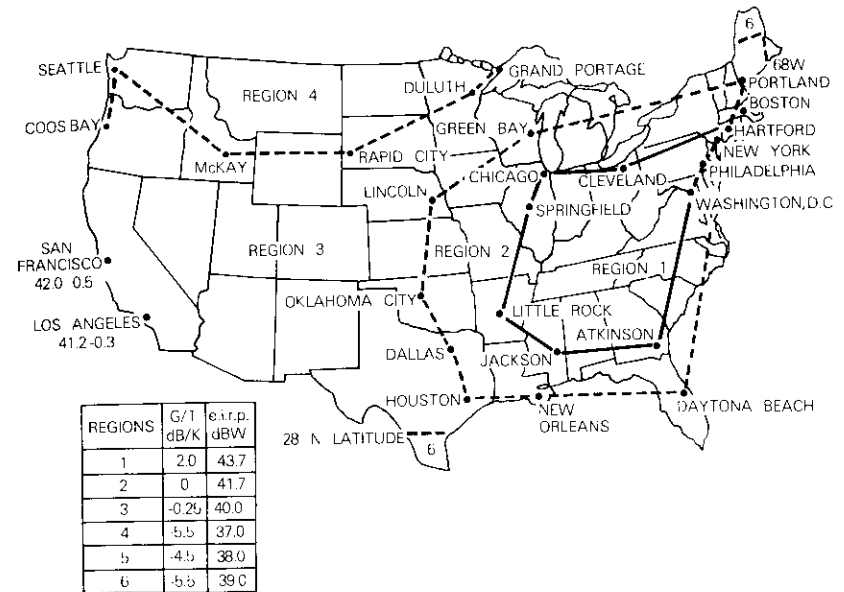


Figure 5. Satellite Antenna Coverage Specification



Figure 6. Castle Rock, Colorado, TT&C Facility

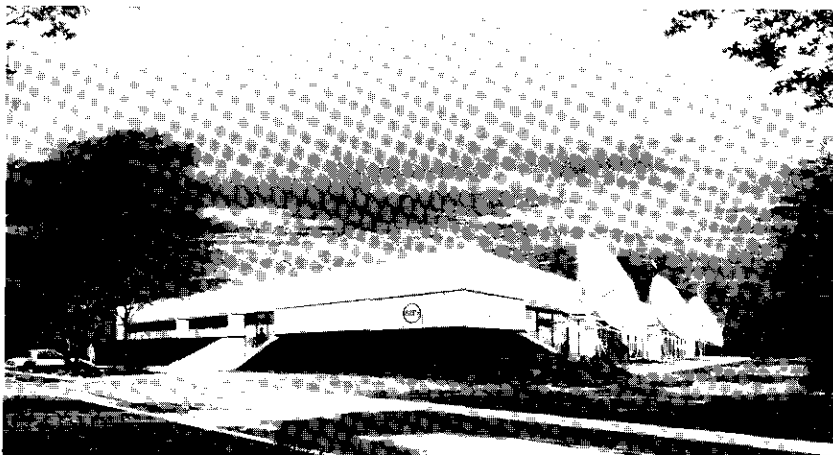


Figure 7. Clarksburg, Maryland, TT&C Facility

- a. primary tracking beacon for satellite antenna pointing,
- b. primary satellite commanding (modulating the tracking beacon),
- c. in-orbit testing,
- d. drift orbit monitoring,
- e. secondary telemetry processing,
- f. tone ranging.

Each of the limited motion antennas is dedicated to a specific geostationary satellite and provides beacon and command capability and secondary telemetry processing. The fully steerable antenna supports the drift orbit monitor/control and in-orbit testing and ranging, as required, and provides backup to the limited motion antennas and RF transmitting and receiving functions.

CONTROL STATION

The control station currently consists of two limited motion antennas and RF systems, and the associated TT&C processing facilities. It serves the following functions in the SBS system:

- a. primary telemetry processing,
- b. secondary spacecraft commanding and beacon transmission,
- c. RF system monitoring,
- d. tone ranging.

The control station also has a prototype customer-premises earth station RF terminal to support system testing.

Satellite control facility

The satellite control facility—the nerve center of the TT&C system—is responsible for control of satellite operation. Satellite commands are formulated in the satellite control facility and forwarded to the proper TT&C earth station for formatting and transmission. In addition to general monitoring of the satellite status, this facility is used to perform the following specific functions:

- a. to generate, validate, and transmit commands;
- b. to evaluate telemetry information;
- c. to relay attitude and ranging data to the orbit determination computer at COMSAT;
- d. to receive attitude and orbit correction parameters from COMSAT computers and generate proper correction commands;
- e. to evaluate inputs from the RF system monitor;
- f. to exchange appropriate information with the network control center.

RF system monitor

The RF system monitor (RFSM) is a key component of the satellite control facility used to analyze transmissions from all SBS satellite transponders for their RF characteristics. It has receive and display equipment that is tunable over the entire satellite down-link frequency band. It is collocated with and shares an RF terminal with the satellite control facility.

Current system operation

The SBS system supports private customer networks providing both advanced and conventional communications services. The advanced services involve high transmission rates and connectivity not otherwise available. The conventional services are those that customers accept as standard from common carriers, but that can be flexibly integrated with more advanced customer requirements.

A CNS-A Network consists of all the earth stations serving a particular customer, the access lines, and a satellite transponder. Customer-premises earth stations (CPES) communicate among one another via TDMA bursts in the transponder. More than one network may operate in any given transponder.

SBS designates one earth station in each transponder as the reference station. The reference station provides the accurate time reference needed for TDMA and controls the allocation of network capacity.

CNS-B Network operation is similar except that some customers may share the resources of specific earth stations. The resulting CNS features are described in the following sections.

Full connectivity

All earth stations in a network can communicate directly with all other earth stations in the same network. Likewise, any switched station on a customer's network (*e.g.*, telephone or data terminal) can be connected on a dial-up basis to any other compatible station.

Dynamic network capacity allocation

Because earth station transmissions and satellite access are accurately controlled in time, network and satellite transponder capacity can be flexibly and efficiently assigned to meet dynamically changing customer traffic requirements. In a CNS network, as opposed to networks using fixed-capacity trunk routes, changing the relative transmission time allocated to earth stations in a given network permits the network capacity to be dynamically allocated to match the demand.

Five levels of capacity allocation control operate in conjunction to provide demand assignment of network capacity:

- a. assignment of full-time transmission units (FTUS) to the network for basic services (tariffed feature);
- b. dynamic assignment of demand transmission units (DTUS) to/from a network as network loading changes (optional tariffed feature);
- c. fully variable/demand assignment (FV/DA), a standard CNS feature;
- d. variable destination/demand assignment (VD/DA), a standard CNS feature;
- e. voice activity compression (VAC), a standard CNS feature.

FULL-TIME TRANSMISSION UNITS

An FTU is a full-time assignment of 224 kbit/s of simplex transmission capacity to a CNS network. The minimum tariffed CNS network configuration is one FTU per earth station and three earth stations per network (minimum of three FTUS per network). Since the number of FTUS required to support a network is a function of the network configuration, changes to the FTUS in a specific network would normally

be made commensurate with major network reconfigurations.

The FTUS are assigned to a network rather than to individual earth stations. The transponder reference station can automatically allocate capacity to specific earth stations on demand within the network capacity boundaries established by the number of network FTUS (and DTUS) authorized by the customer.

DEMAND TRANSMISSION UNITS

A portion of each transponder's capacity (time assignment) is available in a pool for assignment on demand to customer networks that have selected this tariffed option. A DTU is 224 kbit/s of transponder capacity assigned from a common pool (subject to availability) to a customer's network. Upon request, the reference station increases or decreases network capacity from/to the DTU pool in minimum increments of 224 kbit/s. The maximum augmentation available to a network is limited to the number of DTUS authorized by the customer. DTU capacity changes are implemented over TDMA superframe burst boundaries, which occur several times per second.

FULLY VARIABLE/DEMAND ASSIGNMENT

The reference station normally allocates available network capacity by assigning the burst length (capacity) of each network earth station determined by the total network leased capacity (FTUS and DTUS). This capacity allocation is based upon the current traffic, which is reported by each SCC to the reference station several times per second. Total network capacity is thereby efficiently reallocated among network nodes (earth stations) as nodal traffic requirements change.

VARIABLE DESTINATION/DEMAND ASSIGNMENT

To enable a call at an originating earth station to be directed to a specific address served by a destination earth station, the TDMA frame structure provides a destination address for each traffic channel in an earth station transmission burst. Therefore, the transmit SCC can flexibly load its assigned burst capacity with traffic without regard to the traffic destination. Further, the reference station need not be concerned with the assignment of received capacity to individual earth stations, since the destination SCC can screen the aggregate network traffic as received and strip off for processing and delivery those traffic channels with local addresses. Variable destination/demand assignment—a standard feature of CNS TDMA—thereby simplifies the process

of adding new calls and deleting old calls from the burst traffic channels at each earth station and facilitates efficient utilization of transmission burst capacity.

VOICE ACTIVITY COMPRESSION

Typical periods of port inactivity substantially exceed the earth station burst repetition interval of one burst every 15 ms (66 $\frac{2}{3}$ bursts per second). Voice activity compression—another standard feature of CNS TDMA—reduces channel loading by recognizing temporarily inactive voice ports and excluding their data from traffic channels in the TDMA burst.

Voice activity compression is implemented by sampling the content of voice-band transmit buffers and filling assigned burst capacity according to a priority system that excludes information from inactive ports. Since telephone conversations are marked by frequent pauses and listening periods that substantially exceed the 15-ms transmission burst repetition rate, there is frequently no need to assign a traffic channel in every burst to every port carrying a conversation in progress. If no new voice information is received, destination receive buffers insert normal idle channel “noise” to the talker’s receive circuit so that a normal telephone conversation ensues.

The network capacity assignment features discussed in the previous paragraphs result in a significant reduction in the transmission capacity that would otherwise be necessary to support a given function and network, and thereby provide significant cost savings to the users.

Time-division multiple-access (TDMA) architecture

Many of the CNS advanced features are possible because access to the satellite transponder is controlled in the time domain. This process is called time-division multiple-access (TDMA). The SBS TDMA burst architecture is designed to allocate transmission capacity among earth stations of a network according to total network activity. This is achieved by assigning each earth station in the network an exclusive periodic time interval during which only signals from that satellite communications controller appear in the transponder. The duration of this exclusive time assignment is dynamically varied (shortened or lengthened) in response to changes in traffic activity among the SCCs of a network. Specific SCC transmit burst time boundaries (capacity) are assigned by the transponder reference station as a result of periodic capacity status messages from each SCC operating in the transponder. Changes to SCC capacity assignments are implemented within seconds.

Figure 8 is a diagram of the SBS TDMA frame structure showing the frame, the control field, the traffic field, and a traffic channel. The frame is exactly 15 ms in duration, including the unassigned portion. A superframe is 300 ms in duration, and consists of 4 groups of 5 frames, or 20 frames total. The superframe represents a complete SCC

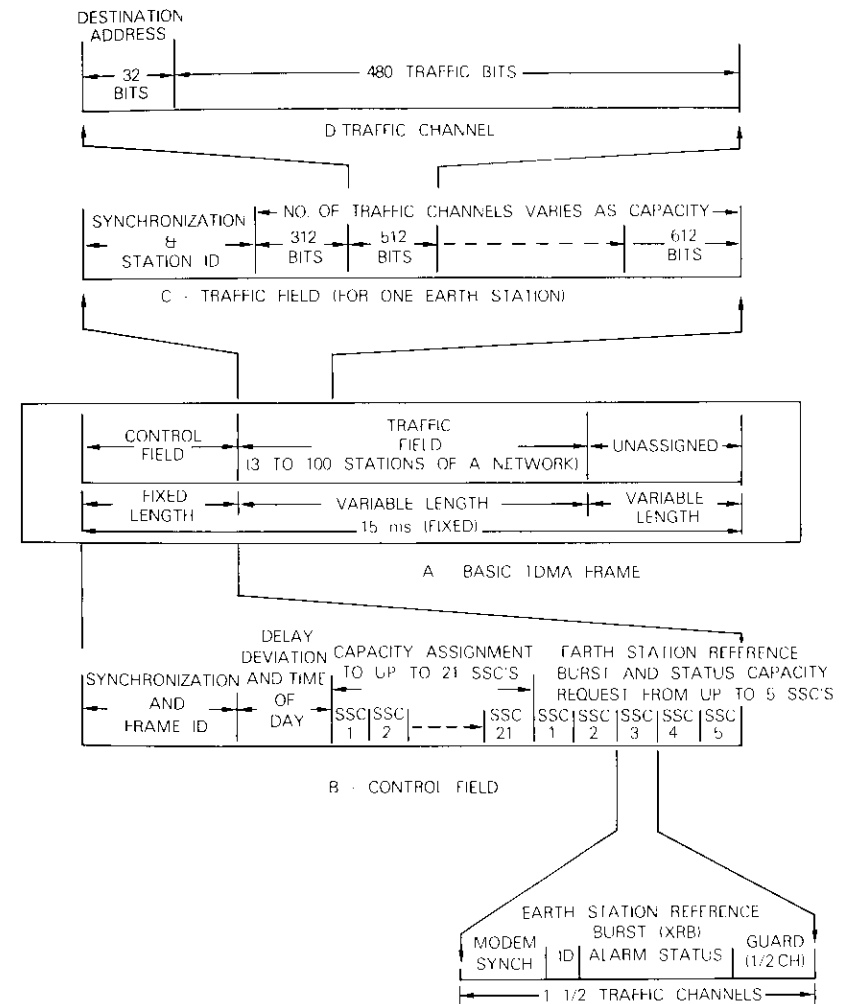


Figure 8. SBS TDMA Frame Structure

status reporting and capacity assignment cycle for a transponder. Changes in the capacity allocation among the transponder SCCs can occur only at superframe boundaries.

The frame (Figure 8a) is the basic repetitive unit of the TDMA structure. The frame duration is controlled by a primary frequency standard (atomic clock) at the reference station with an accuracy of one part in 10^9 or better. (This basic repetition rate is subdivided as necessary to drive all of the clock circuits in the SCC, including the digital data port clocks.)

The control field (Figure 8b), identified by a synchronizing burst from the reference station SCC, marks the beginning of each frame. It has a duration of 10.5 channels. (A channel, consisting of 512 bits, is the basic capacity measure of the TDMA burst hierarchy.) The control field is used by the reference station to transmit burst time boundaries (capacity assignments) and other control information such as any deviation from the nominal satellite range (propagation delay).

The control field also contains the transmit reference burst (XRB) sent by each SCC in the transponder once per superframe. The XRB is used to report traffic activity and earth station status and alarms, and to confirm the accuracy of the transmitting station's synchronization with the reference station.

The traffic field (Figure 8c) contains the individual traffic bursts from each SCC utilizing the transponder. Each SCC's traffic burst is separated from the previous SCC's burst by several symbol periods of guard time, followed by the synchronization preamble identifying the next SCC traffic burst. The preamble is then followed by the number of active traffic channels at the SCC, which is constrained by the current SCC burst length assignment by the reference station.

Each traffic channel consists of an address portion (16 bits plus an additional 16 bits for forward error control of the address portion), followed by 480 bits of traffic data. A channel represents 480 bits per frame and 32 kbit/s, which is the equivalent voice delta modulation bit rate.

In the case of data transmission, the channel represents the next 480 data bits. For data rates less than 32 kbit/s, data accumulate at a rate less than one channel per 15 ms and therefore need not be included in each burst. On the other hand, for data rates exceeding 32 kbit/s, the data accumulate at a rate greater than one channel per 15 ms and therefore multiple channels per burst must be allocated. The SCC stored program generates the proper channel transmission patterns to efficiently load each SCC burst. For example, the burst pattern for a data port operating at 9.6 kbit/s is three channels per ten bursts. The pattern

for a data port operating at 224 kbit/s is seven channels per burst.

If the capacity allocated to an SCC exceeds the number of active channels during a frame, the SCC fills out its burst with null channels. Should traffic activity exceed the assigned capacity, then one or more ports (usually a voice port) will not be allocated a channel in the next burst. This condition is referred to as "freezeout." Because of the redundancy of speech, an occasional 15-ms freezeout of a voice port will not impair a conversation in progress.

If the 15-ms frame capacity is not fully used by the (one or more) subscribing networks operating within a transponder, the reference station will assign the unused capacity to itself so that the entire frame will be filled. This unused capacity represents a pool of transmission capacity that is available to be assigned to one of the customer networks as demand transmission units (DTUs).

System evolution

SBS currently has under development a series of system enhancements planned to extend the range of services that can be competitively offered. These evolutionary capabilities will allow service extension to both larger and smaller volume users. The planned system components, configurations, and services are described briefly in the following paragraphs.

Data Aggregator

Some large private and shared networks (CNS-B, Message Service) will outgrow in a few years the capacity and connectivity afforded by a single transponder. The data aggregator, currently under development, will allow a network to operate through two or more transponders. An earth station will be configured to transmit into one transponder (one up-link transmission) and receive data streams from two or more transponders (multiple down-link reception). The two or more down-link data streams will be screened for addresses and those destined to local users will be collected into a standard 15-ms frame for processing by the SCC. Earth station up-link transponder assignments will be made to balance the network traffic load. Figure 9 shows such a configuration using the data aggregator to receive from four transponders simultaneously. Since all stations can monitor the data streams of the four transponders, full network connectivity is preserved although stations can transmit on only one transponder.

Some earth stations (with or without data aggregators) may be

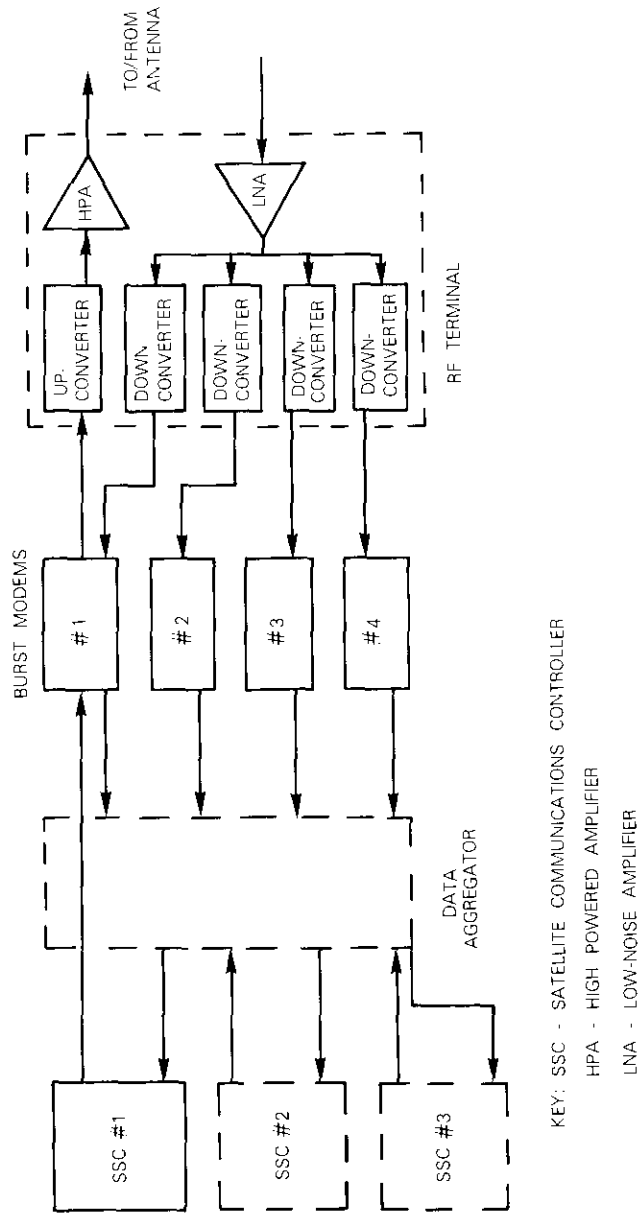


Figure 9. Earth Station Configuration with Data Aggregator

required to support more than one RF transmit chain sharing a single antenna. The data aggregator design allows it to support as many as three SCCs (Figure 9.) Without a data aggregator, two SCCs can be installed at an earth station by using separate RF terminals and a single antenna, as shown in Figure 10. The necessary additional component is the hybrid coupler to allow both RF terminals to operate with the single antenna.

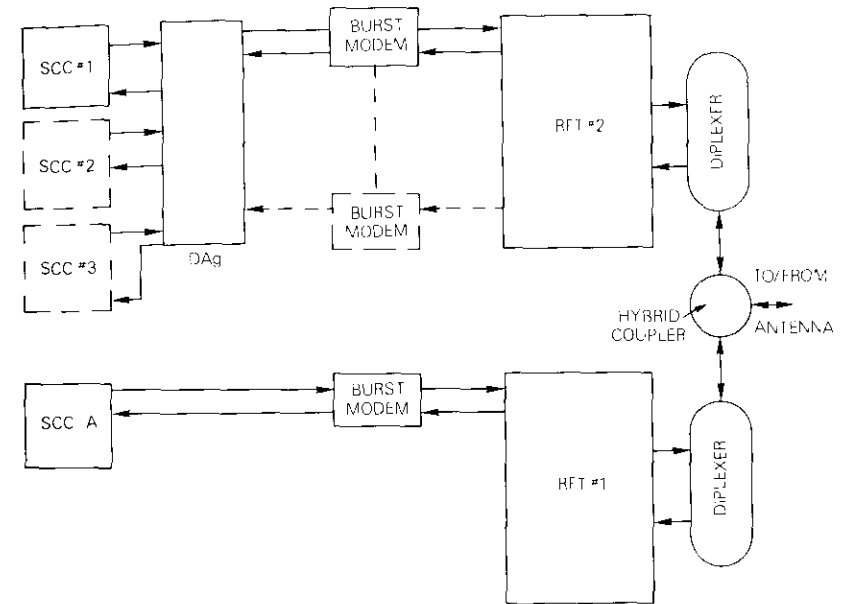


Figure 10. Earth Station Configuration Using Two RF Terminals and One Antenna

Specialized carrier switch

SBS is procuring a digital switch and call processor to provide voice-band services for small volume (Message Service) users. For such applications, customers will be charged by call activity, as opposed to CNS-A and B services, in which the charges are based on full-time lease of the service without regard to usage (with the exception of DTUs). The specialized carrier switch will concentrate small volume demands and route calls using either satellite or terrestrial transmission paths as appropriate.

A typical earth station configuration employing a specialized carrier switch is shown in Figure 11. The specialized carrier switch may or may not be collocated with the earth station. As mentioned earlier, use of separate RF chains will permit a single antenna to be used at an earth station to serve CNS-B and Exchange Services.

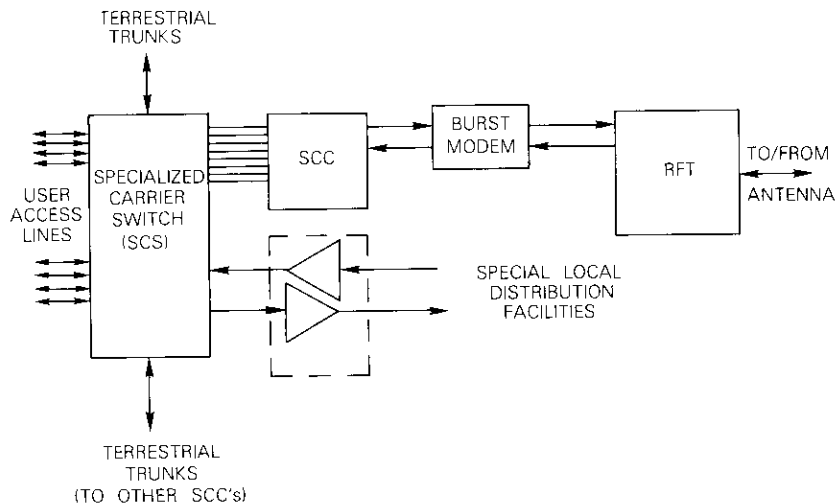


Figure 11. Earth Station Configuration with Specialized Carrier Switch (used for Message Services)

Local data distribution

A current impediment to the expansion of high-data-rate (>9.6-kbit/s) communications applications is the lack of the local (within a 30- to 50-mile radius of the application) distribution facilities that are pervasive for voice-band (≤ 3 -kHz) services. To demonstrate the technology for providing such services, SBS is currently providing the earth stations and the satellite link between local data distribution networks in New York City and San Francisco. This demonstration uses cellular radios operating in the recently authorized 10-GHz band and coaxial cable to connect high-data-rate terminals with the SBS earth stations. Figure 12 shows the concept, which is planned to demonstrate operational capabilities starting in the third quarter of 1981.

Bulk encryption

SBS has under development a bulk encryption feature that will

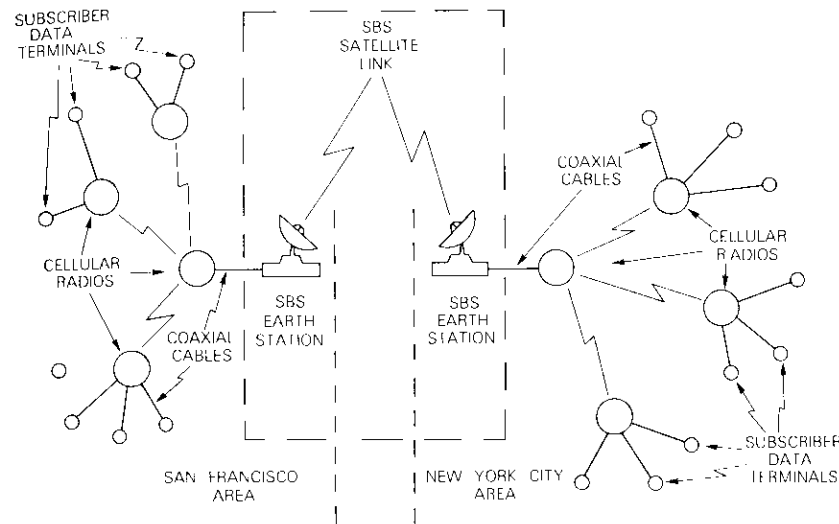


Figure 12. Example of Local Data Distribution Configuration Using 10-GHz-Band Cellular Radios

protect all the information channels of a network. This feature, which is planned to be available in the second half of 1983, will use the federally approved Data Encryption Standard (DES) algorithm.

Encryption/decryption will be implemented as a modular option for either single- or multiple-transponder CNS-A Networks.

Teleconferencing

The use of coordinated video, facsimile, and audio technology to allow meetings among groups dispersed across the contiguous United States promises to significantly improve business productivity. Over the past several years, SBS has conducted demonstrations and participated in the development of specialized equipment to make video teleconferencing an economical and effective business tool. These efforts have led several SBS customers to plan for the implementation of teleconferencing service in late 1981 and early 1982.

SBS offers consulting services for design and implementation of teleconferencing facilities, and, of course, provides the transmission links among customer premises.

Dynamic assignment of network capacity, discussed earlier, is a

significant factor in making teleconferencing (and other high-data-rate services) cost effective.

Conclusion

The SBS system is now involved in revenue operations, and customer installations are proceeding rapidly. As of late summer 1981, 21 customers had subscribed to the initial private network service (CNS). The first satellite was launched to 100°W longitude on November 15, 1980, and the second satellite is scheduled for launch to 97°W longitude in late September 1981. The number of installed earth stations will exceed 50 by year-end 1981 and 200 by year-end 1983.

The system design allows for a variety of earth station configurations to support a wide range of competitive services. The system evolution is proceeding to extend economical service to both larger and smaller volume users.

The operational experience gained by SBS in evolving expanded service capabilities is also being applied to the second generation system planning. Over the next decade, SBS intends to continue to assume a leading role in implementing technological and engineering innovation to enhance business productivity.

Acknowledgments

Many SBS employees have contributed material or valuable constructive suggestions to this manuscript. Among them, the author would like to recognize A. Balgrove, C. Kittiver, G. Pendleton, and W. Schmidt.

References

- [1] *Application of Satellite Business Systems for a Domestic Communications Satellite System*, Vol. II, *System Description*, filed with the Federal Communications Commission, Washington, D.C., December 1975 (amended April 1976).
- [2] C. Kittiver and F. R. Fitzman, "The SBS System—An Innovative Domestic Satellite System for Private Line Networks," AIAA/CASI Sixth Communication Satellite System Conference, Montreal, Canada, April 1976.
- [3] H. A. Rosen, "The SBS Communication Satellite—An Integrated Design," *IEEE EASCON '78 Record*, September 1978.
- [4] B. Goode, "Demand Assignment as Part of the SBS TDMA Communications System," *IEEE EASCON '78 Record*, September 1978.

- [5] W. H. Curry, Jr., "SBS System Description," *Proceedings of the Eighteenth Space Congress*, Cocoa Beach, Florida, April 1981.

William H. Curry is a graduate of the U.S. Naval Academy (Naval Science, 1957), the Naval Postgraduate School (Communication Engineering, 1967), and Southern Illinois University (MBA, 1977). He served as Assistant Professor of Naval Science at the Massachusetts Institute of Technology (1961–62), and as a surface line officer, mostly in destroyers. As the Seventh Fleet communications officer (1970–72), he was responsible for the early introduction of satellite communications to fleet operations. He spent a one-year sabbatical at COMSAT in 1973, studying advanced satellite communication engineering. He commanded a naval communication station (1976–77) and then left active naval duty, joining Satellite Business Systems, where he was responsible for planning and coordinating system evolution. He is currently Manager of Satellite Operations for Southern Pacific Communications, SPACENET Division.



4/6-GHz ionospheric scintillation measurements during the peak of sunspot cycle 21

D. J. FANG AND M. S. PONTES

(Manuscript received July 29, 1981)

Abstract

Since 1970, COMSAT Laboratories has been conducting C-band ionospheric scintillation measurements using INTELSAT earth stations around the world. Early data established the existence of 4- and 6-GHz ionospheric scintillations and gross features, such as dependence on local sunset conditions, diurnal and seasonal patterns, geomagnetic boundaries, and magnitude of frequency (f) dependence. Analyses of power spectral density confirm an f^{-3} dependence for weak scintillations, which can be explained by the conventional weak scattering theory for a thick screen with a power law electron density fluctuation spectrum of $p = 4$. Data collected from 1977 to 1980 at the Hong Kong Earth Station provide further insight into 4- and 6-GHz scintillations during maximum solar activity. Characteristics such as occurrence frequencies, durations, global scales, and spectral roll-off slopes are unique in that they had not been observed in previous years. Peak-to-peak fluctuations of up to 14-dB magnitude were observed for which the f^{-3} power spectrum dependence is no longer valid. In terms of cumulative statistics, a model of scintillation increase as a function of solar activities was developed for engineering applications.

Introduction

Studies of electromagnetic wave propagation in the ionosphere date back half a century, with T. L. Eckersley's (1930) among the earliest

[1]. However, not until World War II and later did engineers and scientists engage in large-scale research on this subject. Lovell and Clegg present a good summary of work done before 1950 [2].

In the 1960s and 1970s, scattering mechanisms became the focus of studies of ionospheric wave propagation studies. Practical scatter communications systems were implemented at UHF, and the theory was used to develop probing techniques and diagnostic methodologies for the upper atmosphere [3]–[6]. Among these, scintillation analyses of forward- and backward-scattered radio waves determined characteristics of ionospheric inhomogeneities, *i.e.*, the irregular fluctuations of dielectric constant. Such analyses are essential in establishing cumulative statistics for fading and/or scintillation, which are needed to evaluate the reliability of communications links. Since the mean fluctuation of the dielectric constant, $\langle \epsilon - \epsilon_0 \rangle$, is inversely proportional to the square of the frequency, the level of electromagnetic wave interaction with ionospheric plasma decreases with frequency. Before 1970, therefore, it was assumed that no ionospheric scintillation would occur at gigahertz frequencies.

Since 1970, COMSAT Laboratories has been measuring 4/6-GHz ionospheric scintillations through INTELSAT earth stations and satellites. These measurements produced a significant finding that was confirmed by other researchers: even at gigahertz frequencies, ionospheric scintillations of appreciable magnitude do exist [7], [8]. Intense signal fluctuations often erupt suddenly without a noticeable precursor and can last for hours with intermittent changes in magnitude and time rate [9]–[16].

The gross features of 4/6-GHz ionospheric scintillations can be summarized as follows:

a. Scintillations occur in the geomagnetic equatorial region, mainly between 30° GMN and 30° GMS and expand and contract as solar activities increase and decrease, respectively.

b. The frequency of occurrence of scintillation events has strong diurnal peaks. The probability of occurrence is greatest about one hour after local ionospheric sunset, and scintillations may last for hours until midnight.

c. The frequency of occurrence varies by season, with peak activity around vernal equinox and high activity at autumnal equinox.

d. An f^{-s} relationship with s between 1.5 to 2.0 exists between the 4- and 6-GHz scintillation amplitudes.

e. The power spectral densities of the scintillation generally exhibit a power law frequency dependence for spectral frequencies greater than the Fresnel frequency. An f^{-3} asymptotic frequency dependence can be considered reasonable for most weak scintillation events.

All these features have annual variations related to the 11-year sunspot cycles.

This paper analyzes ionospheric scintillation data collected at the Hong Kong Earth Station from March 1977 to October 1978 and from November 1978 to June 1980, as the solar activities increased toward the peak of the current sunspot cycle 21 as shown in Figure 1. The data provide further details of ionospheric scintillations which are unique in solar maximum years.

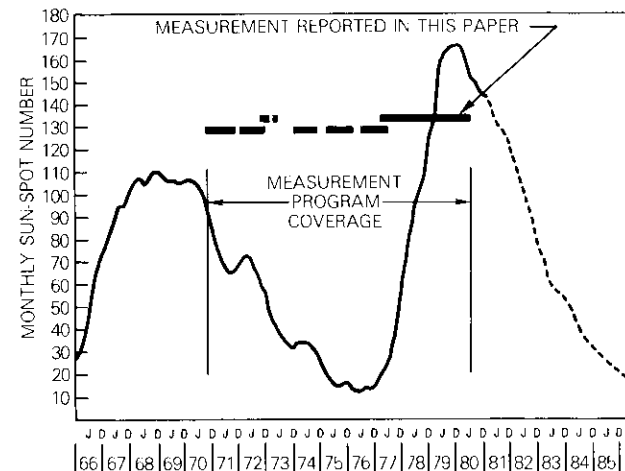


Figure 1. Monthly Sunspot Numbers From 1966 to 1985 and INTELSAT Ionospheric Scintillation Measurement Program From 1970 to Present

Experimental configurations

Two geostationary satellites, five earth stations, and eight up/down-link signals were involved in the experiment. The two satellites, INTELSAT IV F8 Pacific Ocean Region (POR) and INTELSAT IV-A F1 Indian Ocean Region (IOR), were at 174°E and 63°E, respectively. The five earth stations were Stanley, Hong Kong; Sentosa, Singapore; Si Racha, Thailand; Paumalu, Hawaii; and Padukka, Sri Lanka. Detailed

information is given in Table 1. Only the Hong Kong Earth Station (HK) was used for data collection. The separation between the IOR-HK and POR-HK links in the ionosphere at an altitude of 300 km is about 2,000 km, or about 1 hour geographical local time. Two beacons and six communications carrier signals were monitored at the Hong Kong Earth Station, as illustrated in Table 2. The lowest transmission path, from Si Racha to POR, has an elevation angle of approximately 8°. The elevation angles for all the other paths are more than 10°, which is well above the angle (~5°) at which tropospheric and multipath effects may degrade microwave signals [17]–[19].

After more than 10 years of continuous measurements at selected INTELSAT earth stations, the method of monitoring carriers and data analysis for ionospheric scintillation studies have been standardized [15]. For each carrier or beacon signal, a buffered output proportional to the automatic gain control (AGC) voltage is fed to a strip chart and an FM magnetic tape recorder for data collection. The input to each IF amplifier includes an attenuator, which is normally set at 5 dB; the amplifier gain is then adjusted to accommodate the attenuation. The data can thus be calibrated by changing the attenuation in 1-dB steps to provide a ±5-dB range for a scintillation experiment within ±0.5-dB accuracy. This accuracy limit is established because even under clear sky conditions, the buffered IF output has small noise-induced variations.

Data analyses for strip chart data follow the 15-minute P_{\max} and P_{\min} method of Whitney, Aarons, and Malik [20]. The scintillation index, SI , is then defined as

$$SI = \frac{P_{\max} - P_{\min}}{P_{\max} + P_{\min}} \times 100\%$$

SI is used for the evaluation of cumulative statistics for a year and for a worst month, which are essential for system applications. Magnetic tape data are analyzed for a detailed study of severe scintillation events for research purposes.

General patterns of signal fluctuations observed at an earth station

To identify ionospheric scintillation, it is first necessary to recognize the general patterns of signal fluctuations observed at 4 GHz in a standard INTELSAT 30-m antenna receive system. Figures 2–4 give patterns observed at the Taipei Earth Station during 1977 [15].

TABLE 1. EARTH STATION INFORMATION

EARTH STATION	GEOGRAPHIC LOCATION		GEOGRAPHIC LATITUDE	ANTENNA (SATELLITE)	ELEVATION ANGLE (DEG)	MEASUREMENT PERIOD
	LONGITUDE	LATITUDE				
Stanley, Hong Kong	114°13'E	22°12'N	10.52°N	HK1(POR) HK2(IOR)	19.59 27.76	1977–1980
Sentosa, Singapore	103°50'E	01°15'N	10.36°S	SN1(IOR) SN2(POR)	42.78 11.31	1979–1980
Si Racha, Thailand	100°56'E	13°06'N	1.57°N	SR1(POR) SR2(IOR)	7.87 43.94	1977–1980
Paumotu, Hawaii	158°02'W	21°40'N	21.40°N	PA(POR)	49.05	1977–1978
Padukka, Sri Lanka	80°06'E	07°11'N	2.88°S	PD(IOR)	67.12	1977–1978

TABLE 2. SIGNALS MONITORED AT HONG KONG EARTH STATION (HK)

PATH	FREQUENCY (MHz)		NATURE
	UP-LINK	DOWN-LINK	
POR → HK1	None	3950 ± 2.5	POR Beacon
SN2 → POR → HK1	5977.5	3752.5	Communications Carrier
SR1 → POR → HK1	6227.5	4002.5	Communications Carrier
IOR → HK2	None	3950 ± 2.5	IOR Beacon
SN1 → IOR → HK2	6190.0	3965.0	Communications Carrier
SR2 → IOR → HK1	6103.75	3878.75	Communications Carrier
PA → POR → HK1	5940.0	3715.0	Communications Carrier
PD → IOR → HK2	6097.5	3872.5	Communications Carrier

Figure 2 reveals a typical pattern in which mild (less than 4 dB), but clearly noticeable scintillations occurred mostly along the IOR link. These events started suddenly, and reached maximum peak-to-peak fluctuation in a few minutes. Major scintillations lasted less than 2 hours, but mild fluctuations did not taper off until past local midnight.

Figure 5 shows the spectra of the six 10-minute records given in Figure 2. Spectra A and F (before and after the intense signal fluctuations, respectively) are typical of weak scintillations. The mean square fluctuations of amplitude increase with frequency at the low frequency end until they reach the maximum near the Fresnel frequency. Beyond this point, the spectra roll off in a Gaussian form. However, during signal fluctuations (B, C, D, and E), the characteristics of roll-off change from Gaussian to a power law form. For the four records (B, C, D, and E), the roll-off slope remains approximately the same, yielding an f^{-3} dependence. Theoretically, the f^{-3} dependence is consistent with the conventional weak scattering theory, with a power law electron density fluctuation index of $p = 4$ [4], [10], [11], [15], [16].

Figure 3 is a signal fluctuation pattern resulting from atmospheric turbulence and local wind. Strong signal fluctuations were observable from beacon and tracking channels at both IOR and POR antenna receive systems. The fluctuations are caused not only by effects such as turbulent refraction, lower atmospheric gradient, and local terrain multipath, but also by the angle-of-arrival change resulting from the dynamic response of the earth station automatic tracking systems [16]. For earth stations, such as Taipei and Hong Kong, those fluctuations occur predominantly in the early morning or early afternoon.

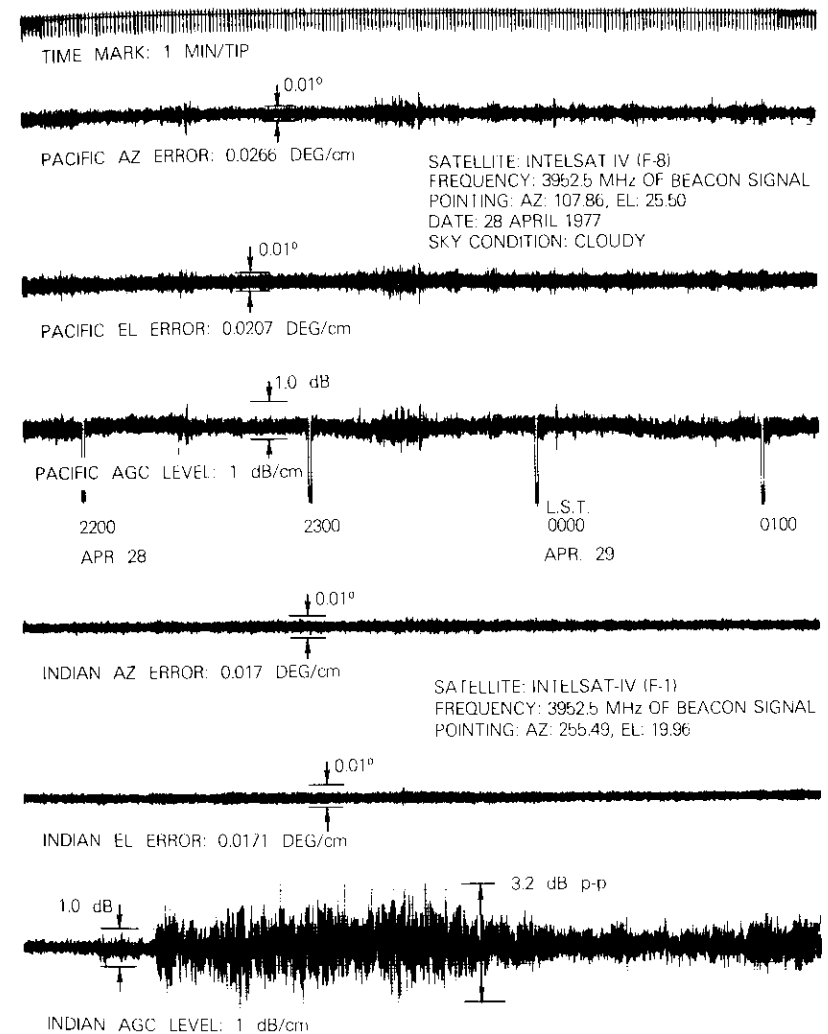


Figure 2. General Patterns of Signal Fluctuations Observed From an Earth Station Antenna Receive System—Ionospheric Scintillation

Figure 4 shows a typical pattern for earth stations during precipitation. Absorption of water vapor and raindrops attenuates electromagnetic waves. The attenuation is not apparent in the figure because at 4 GHz the value of attenuation coefficients is very small [21]. Signal

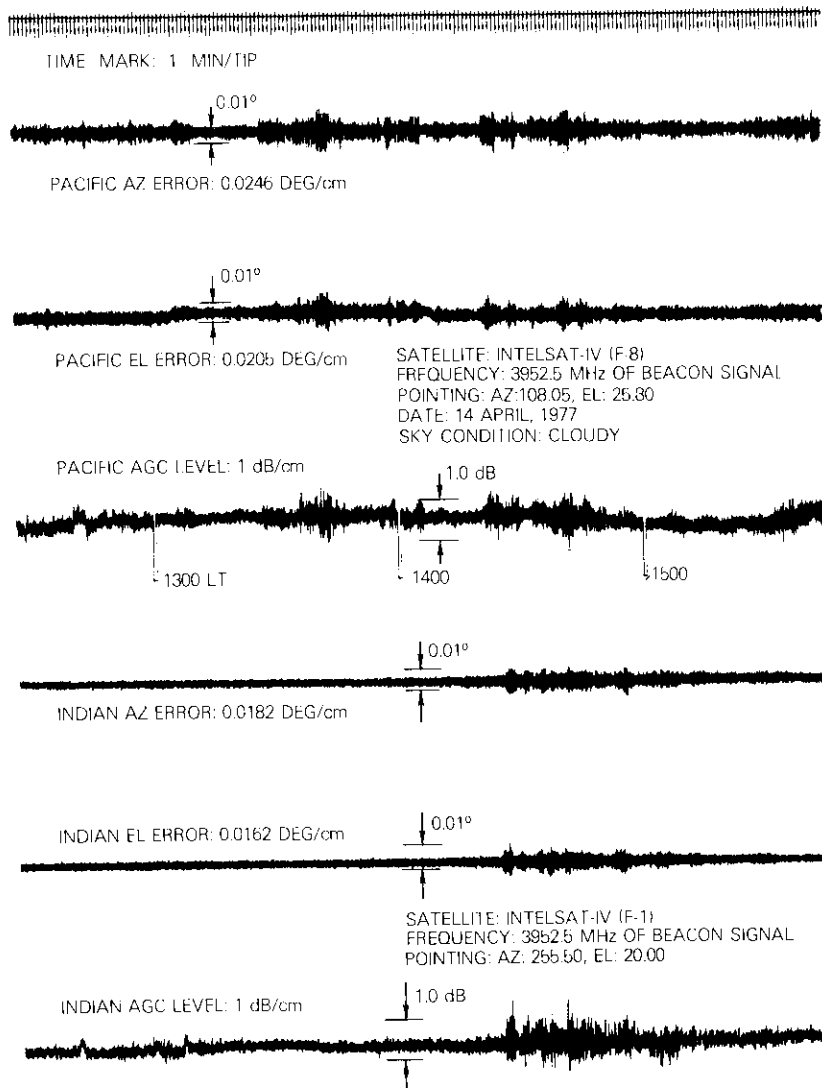


Figure 3. General Patterns of Signal Fluctuations Observed from an Earth Station Antenna Receive System—Tropospheric Scintillation

fluctuation is evident in beacon channels but not in tracking channels because, during absorption, no significant amount of phase or wave-

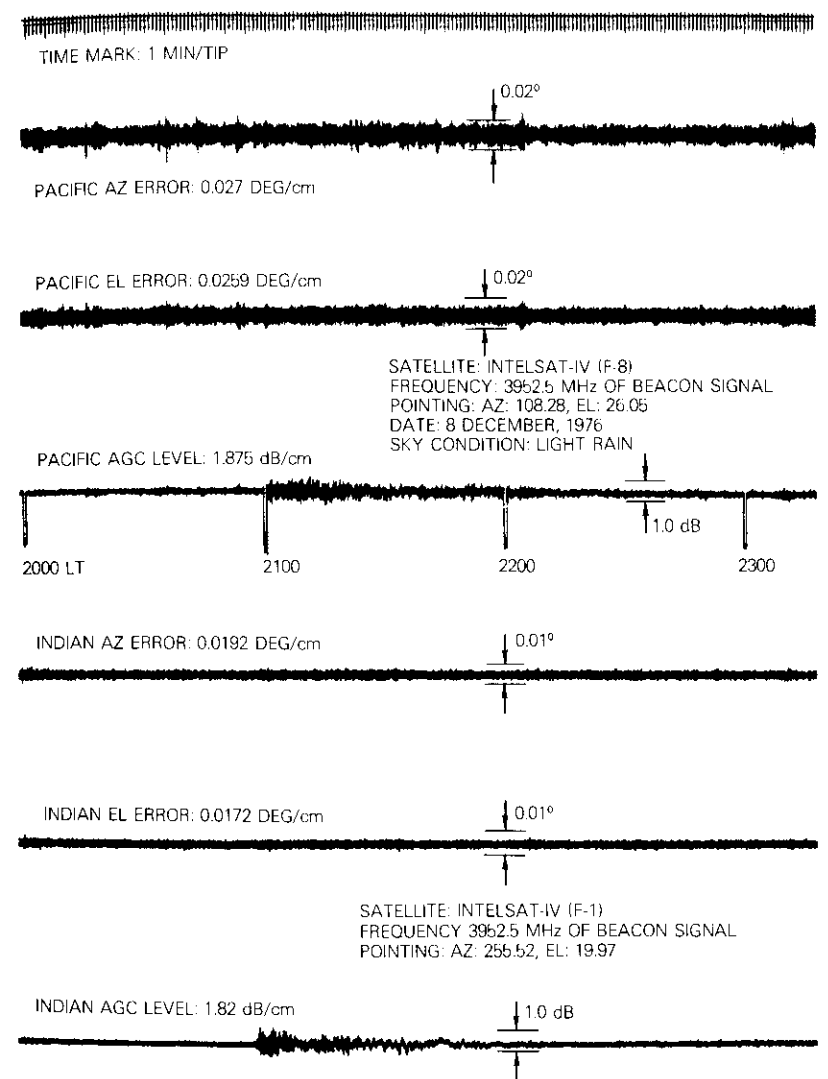


Figure 4. General Patterns of Signal Fluctuations Observed from an Earth Station Antenna Receive System—Precipitation

front distortion will occur. The beacon fluctuations are attributed to the volatility of water vapors, and characteristics of raindrops such as

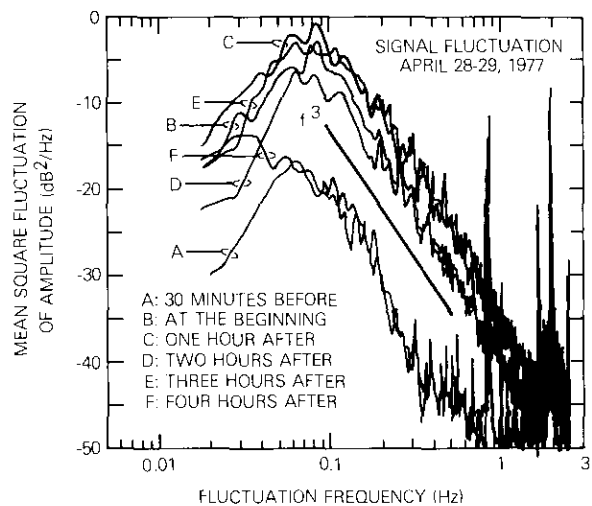


Figure 5. Power Spectral Density for Six 10-Minute Sample Periods During the Ionospheric Scintillation Event Shown in Figure 2

particle size, shape, drop-size distribution, and terminal velocity [21]. Fluctuations of tropospheric origins shown in Figures 3 and 4 can be further differentiated from the ionospheric scintillations in Figure 2 by studying the power spectral densities in terms of factors such as Fresnel frequencies and roll-off slopes. The turbulence structures in the lower atmosphere have scale sizes, elongations, and refractive index correlation spectra that are distinctively different from those in the ionosphere [11], [12], [15], [16].

Outstanding features of ionospheric scintillations in the solar maximum year

From March 1979 to March 1980, ionospheric scintillations of over 1.0-dB peak-to-peak fluctuations at either IOR or POR links were observed at the Hong Kong Earth Station for about 100 evenings. In March 1980, scintillations occurred almost every evening, as shown in Figure 6. The frequency of occurrence (20 evenings in April 1979 and 10 evenings in September 1979) confirms the theory that scintillations have seasonal variations, with peaks at vernal and autumnal equinoxes.

Except for the evening of March 21, 1980, when only the IOR link scintillated, the monthly glance clearly suggests that scintillations

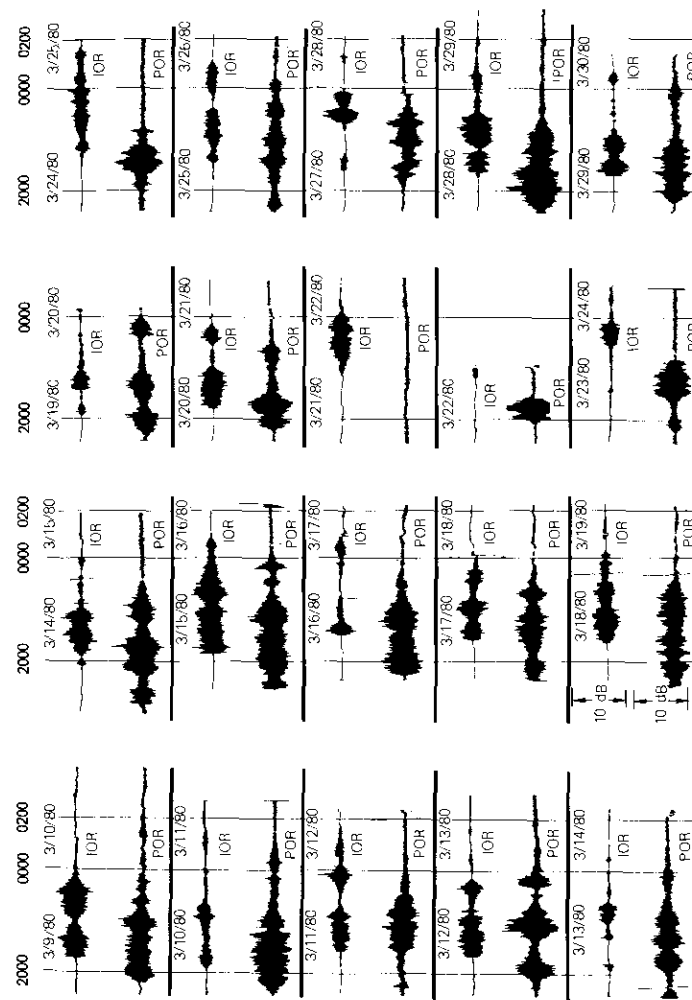


Figure 6. Monthly Glance at Ionospheric Scintillations in March 1979

usually occurred on both links and lasted from 3 to 5 hours in at least one link. This behavior had not been observed in earlier years when sunspot numbers were much lower. For example, in Figure 2, only the IOR link indicated fluctuations for about 2 hours, although residual fluctuations remained. Obviously, ionospheric disturbances responsible for gigahertz scintillations are stronger, larger, faster, and of longer duration during years of high solar activity than during years of low to medium solar activity. A similar conclusion has been reached by researchers studying various types of ionospheric disturbances, some of which are related to gigahertz scintillations, such as equatorial spread-F and gravity waves.

Figures 7, 8, and 9 provide records of three ionospheric scintillation events in March 1979. In all three figures, the fluctuation patterns of the two carrier signals from the IOR satellite are well correlated, irrespective of the up-link paths (*i.e.*, whether the signals are from Singapore or from Thailand). This is also true for the fluctuation patterns of the two POR satellite signals. This correlation has proved valid for data collected over the year, suggesting that ionospheric scintillations observed from an earth station are predominantly down-link phenomena.

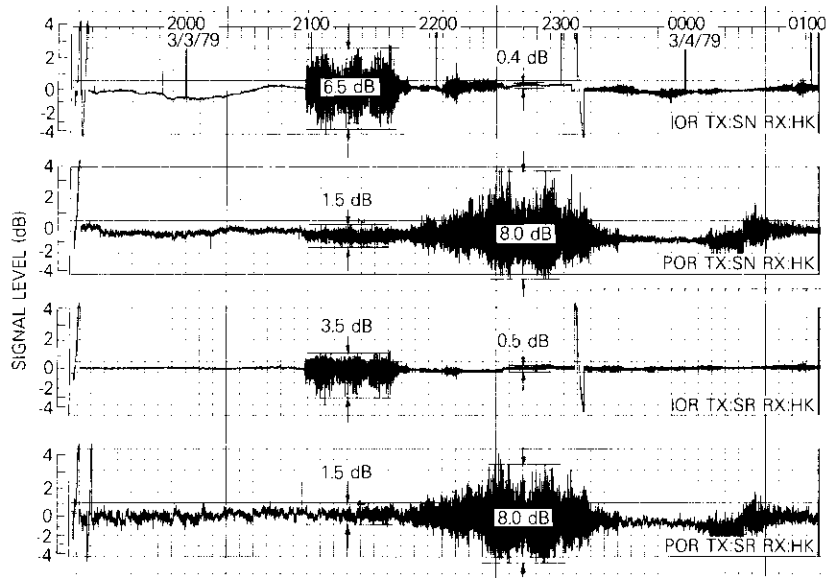


Figure 7. Records of Ionospheric Scintillation on March 3-4, 1979

Figure 7 shows that the IOR link scintillated before the POR link, which is rare for a year of maximum solar activities. Before 2200 hours local time, significant scintillation occurred in the IOR link, while the POR link had only low-level fluctuations. Furthermore, the IOR scintillation started suddenly without any precursor. These features are typical for years of low solar activities, as illustrated in Figure 2. IOR scintillation lasted almost an hour and then faded quickly. A separate and obviously uncorrelated scintillation event occurred along the POR link at about 2200 hours. The signal fluctuation enhanced itself gradually until it reached a magnitude of about 8 dB peak-to-peak. The event lasted slightly more than an hour and was followed by another minor event with peak-to-peak fluctuations of 3 dB.

Figures 8 and 9 represent the majority of events with the following typical characteristics:

- a. Scintillations occurred on both links. Although the onset times of the two links were not simultaneous (they differed from a few minutes to 2 hours), the scintillations nevertheless overlapped for a significant length of time (from 20 minutes to several hours). That the two links are separated at an F-max height (300 km) of

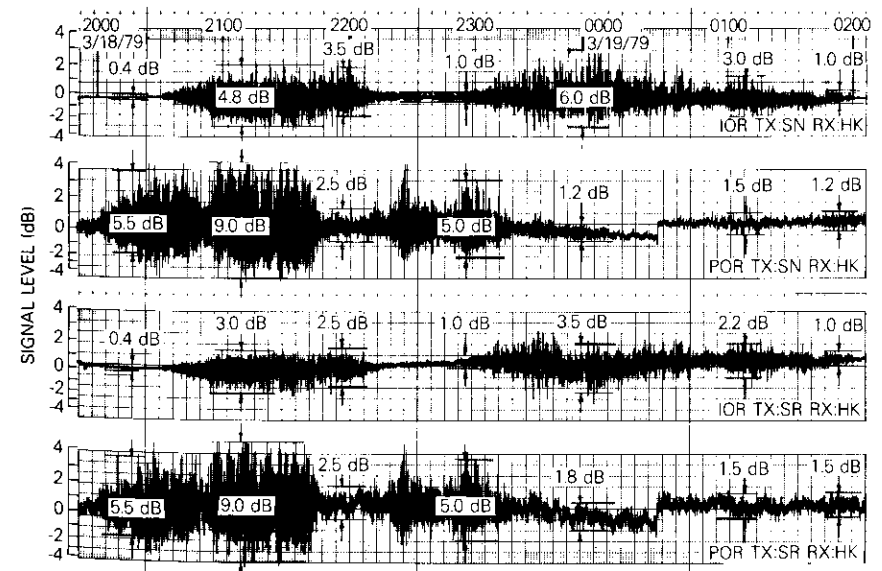


Figure 8. Records of Ionospheric Scintillation on March 18-19, 1979

about 2,000 km suggests that ionospheric disturbances, which created irregularities causing ionospheric scintillations, may have scales on the order of at least 2,000 km.

b. Most scintillations did not erupt suddenly, but with a noticeable gradual increment of fluctuations as precursors. Frequently, the scintillations were intermittent for an entire evening; they were not confined to 2 to 3 hours as those observed in previous years. Individual fluctuation events lasting more than 2 hours along at least one link were common.

c. Because of the precursor, it is difficult to identify the exact onset time of a scintillation event. However, the figures clearly show that the POR link scintillated much earlier than the IOR link, and the time delays of scintillations between the two links were on the order of 30 minutes to 2 hours. This indicates that gigahertz scintillation is an ionospheric sunset phenomenon, and the time delays are associated with the ionospheric sunset times at altitudes of 200 to 400 km where F-region irregularities are known to be present under disturbed ionospheric conditions.

d. An extensive effort was made to correlate the scintillation

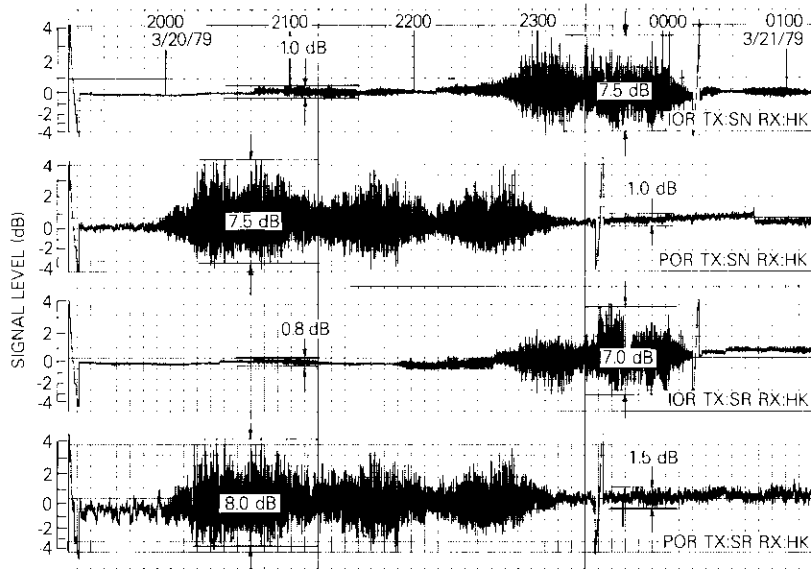


Figure 9. Records of Ionospheric Scintillation on March 20-21, 1979

patterns between the two links with a proper shift of time scale to accommodate the time delays. Detailed correlations between the links could not be established; hence, it was concluded that the scintillations along the two links were independent events. Recent observations [22], [23] suggest that, although the disturbances may have a spatial scale as large as 2,000 km and a time scale of several hours, and travel with the ionosphere from east to west in line with the local sunset, the specific irregularities responsible for scintillations nevertheless exhibit much smaller spatial scales and are relatively short-lived.

Further details on ionospheric scintillations can be obtained by examining the signal fluctuation patterns in the frequency domain. Since data collected at Hong Kong involved AGC voltages corresponding to the intensities of the waves incident on the antenna, only power spectral densities can be analyzed.

Power spectral density curves for the event on March 18, 1979 are plotted in Figure 10 for three separate 10-minute segments of data starting at 2100, 2300, and 0000 hours local time. As expected, the mean square fluctuation first increases with frequency until it reaches a maximum at the Fresnel frequency, beyond which it starts to roll off with a power law slope. Note that the roll-off slope no longer follows an f^{-n} law with n equal to approximately 3, as observed in scintillation studies for previous years [4], [11], [13], [15], [16]. The slope and the Fresnel frequency change significantly as a function of time, as does the peak-to-peak fluctuation. To illustrate this point, the Fresnel frequencies and roll-off slopes for the three representative events given earlier are tabulated in Table 3.

The differences between scintillations on the POR link and on the IOR link can be clearly seen from Table 3. During the sunset hours in Hong Kong, the IOR link penetrates the ionosphere westward in the direction of the sun. The IOR scintillation events have Fresnel frequencies generally less than 0.100 Hz and f^{-n} roll-offs with $n < 3.0$. On the other hand, along the eastward POR link, which penetrates the dark ionosphere, scintillation events show a spectral broadening effect, with Fresnel frequencies consistently greater than 0.10 Hz. The broadening effect is caused by multiple scatterings, which are more likely to occur along the eastward than along the westward link. Furthermore, the roll-off slopes along POR are significantly steeper than those of IOR since the value n exceeds 3.0 all the time. Ionospheric irregularities along the IOR and POR links are obviously not identical. They differ in physical parameters such as height, size, moving velocities, and

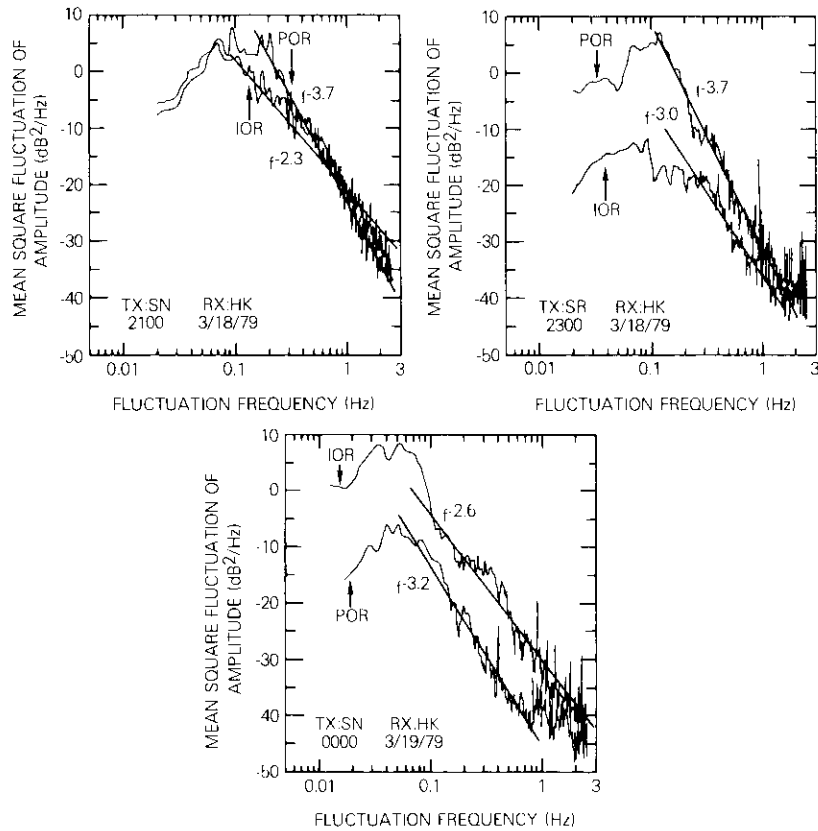


Figure 10. Power Spectral Density for Three 10-Minute Sample Periods During the Ionospheric Scintillation Event Shown in Figure 8

random refractive index spectra, which dictate the Fresnel frequencies and roll-off slopes.

Annual statistics of scintillation and their solar cycle dependence

For communications applications, the cumulative statistics (*i.e.*, the percentage of time in a year, and in a worst month, that ionospheric scintillations exceed a given level) are crucial for link design. These statistics are needed to establish the system margins that ensure the desired quality of a link. Annual statistics of ionospheric scintillations

TABLE 3. FRESNEL FREQUENCY AND ROLL-OFF SLOPE OF SCINTILLATION EVENTS GIVEN IN FIGURES 7, 8, AND 9

DATE AND TIME (hr)	UP-LINK CARRIER	POR LINK				IOR LINK			
		P-P FLUCTUATION (dB)	SCINTILLATION INDEX (%)	FRESNEL FREQUENCY (Hz)	f^{-n} ROLL OFF n	P-P FLUCTUATION (dB)	SCINTILLATION INDEX (%)	FRESNEL FREQUENCY (Hz)	f^{-n} ROLL OFF n
March 3, 1979	SN	1.5	18	0.200	3.2	4.0	43	0.100	2.8
	SR	0.6	—	—	—	2.2	25	0.120	2.9
	SN	6.0	60	0.160	3.8	0.3	—	—	—
	SR	6.5	63	0.180	3.9	0.3	—	—	—
March 18-19, 1979	SN	7.0	66	0.160	3.5	0.3	—	—	—
	SR	7.0	66	0.180	3.7	0.3	—	—	—
	SN	8.0	72	0.190	3.7	3.0	33	0.090	2.3
	SR	9.0	77	0.180	3.7	3.0	33	0.15	2.9
	SN	1.8	20	0.160	3.7	3.0	33	0.065	2.5
	SR	2.0	22	0.155	3.7	1.8	20	0.074	3.3
	SN	1.2	14	0.115	4.0	1.2	14	0.032	2.0
	SR	5.0	52	0.115	3.7	1.2	14	0.230	3.0
	SN	4.0	42	0.070	3.2	4.0	43	0.052	2.6
	SR	1.5	18	0.072	3.4	2.5	28	0.058	3.0
March 20, 1979	SN	1.8	20	0.105	4.5	3.0	33	0.058	3.6
	SR	1.5	18	0.120	3.7	2.5	28	0.060	3.0
	SN	1.0	11	0.115	4.5	0.3	—	—	—
	SR	1.5	18	0.100	3.7	0.3	—	—	—
March 20, 1979	SN	6.5	63	0.160	3.5	0.3	—	—	—
	SR	6.5	63	0.175	3.5	0.3	—	—	—
	SN	1.5	18	0.118	4.6	6.0	60	0.084	3.4
SR	1.8	21	0.128	3.8	4.5	48	0.088	3.6	

are provided in Figure 11, where POR and IOR beacon signals are shown in solid and dashed lines, respectively. Besides the four sets of annual statistics covering March 1977–March 1978, October 1977–October 1978, November 1978–November 1979, and June 1979–June 1980, the figure also includes statistics collected in two earlier measurements: March 1975–March 1976 as measured in Hong Kong, and June 1976–June 1977 as measured in Taipei. Recalling the surge of monthly sunspot numbers from 1975 to 1980, shown in Figure 1, one can readily conclude that ionospheric scintillations are closely correlated with solar activities.

To examine this correlation further, the occurrence of scintillations was evaluated in terms of the percentage of time in a year during which peak-to-peak signal fluctuations exceeded 1.0 dB, as a function of the monthly averaged Zürich sunspot numbers for past and present INTELSAT ionospheric scintillation programs. For each program, upper and lower bounds of occurrence are established based on the maximum and minimum percentages of occurrence monitored in the multiple carrier channels. The bounds of the abscissa are the maximum and minimum monthly sunspot numbers observed. Figure 12, which gives a summary plot, suggests a log-linear dependence of the scintillation occurrence on sunspot numbers for the years in which the maximum sunspot number is less than 70. A gradual saturation appears as the sunspot number exceeds 70.

Cumulative statistics for communications carriers at the Hong Kong Earth Station are similar to those for the beacons because the 4-GHz down-link path is always dominant for signal fluctuations observable at the receiving station. The effects of the up-link path and of the satellite on carrier fluctuations observed at down-link are complicated and involve such phenomena as up-link scintillations, rain attenuations and depolarization, transponder nonlinearity, interchannel and co-channel interferences, antenna pointing errors, signal angle-of-arrival variations, and sky brightness temperature changes. Most of these phenomena can be regarded as attenuation in the time domain and dispersion in the frequency domain, which tend to have a smoothing effect on scintillations. The smoothing effect is evident in Figure 13, which compares cumulative statistics for carriers and beacon signals. Statistics for carrier signals are consistently lower than those for beacons. For the POR/SR link, which involves a low elevation angle up-link path with a considerable amount of up-link tropospheric scintillations over a year, the difference of statistics can be 2 to 4 dB for a fixed percentage of exceedance time. Beacon statistics mark the upper

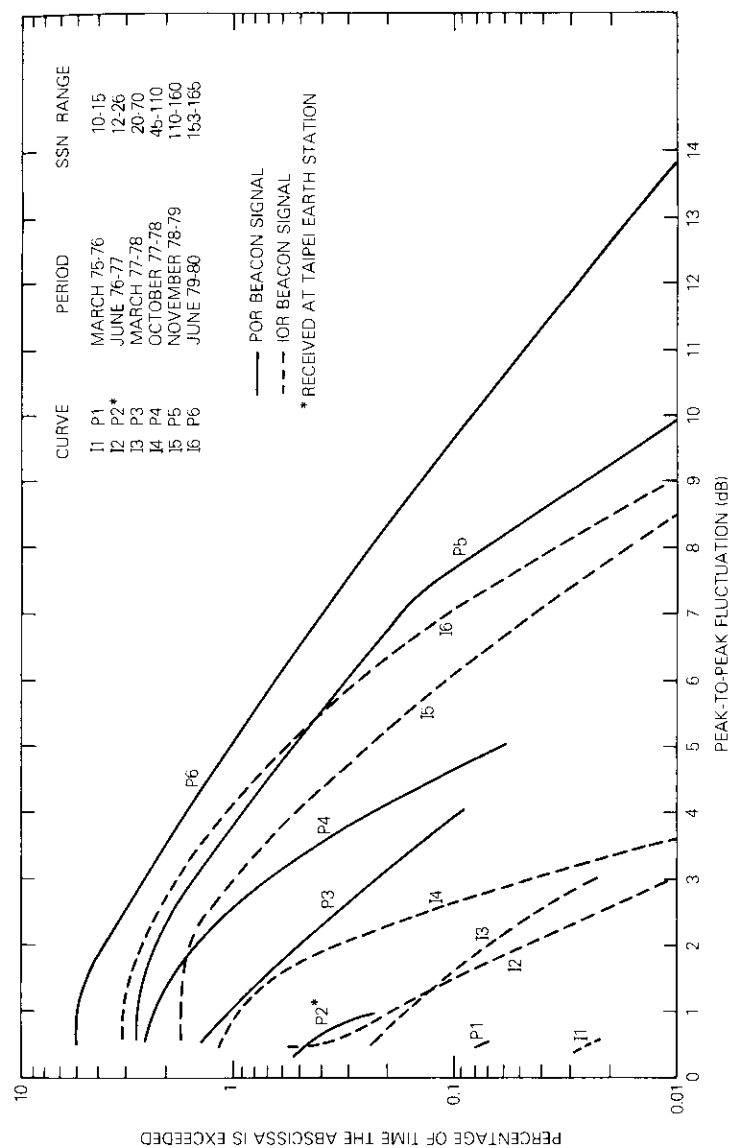


Figure 11. Annual Statistics of Ionospheric Scintillations at Hong Kong Earth Station

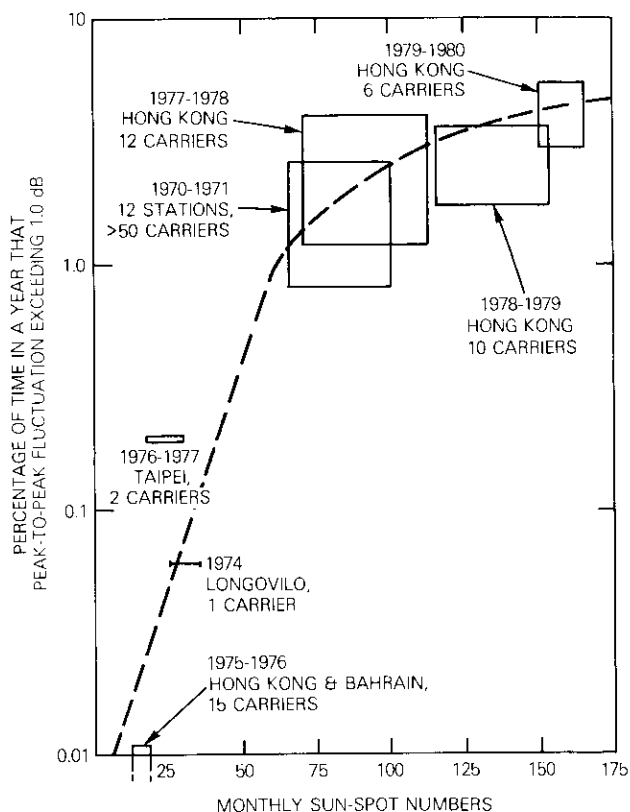


Figure 12. *Dependence of 4-GHz Equatorial Ionospheric Scintillations on Monthly Averaged Zürich Sunspot Numbers*

limit of signal fluctuations for all carriers in communications systems applications.

Worst-month statistics

In digital communications systems, outages from loss of synchronization and the time required to restore it are critical. To establish an outage condition, a typical CCIR criterion is that the mean 1-minute value of the bit-error rate should not be worse than 10^{-4} for more than 0.3 percent time in any month [14], [15]. Consequently, in addition to

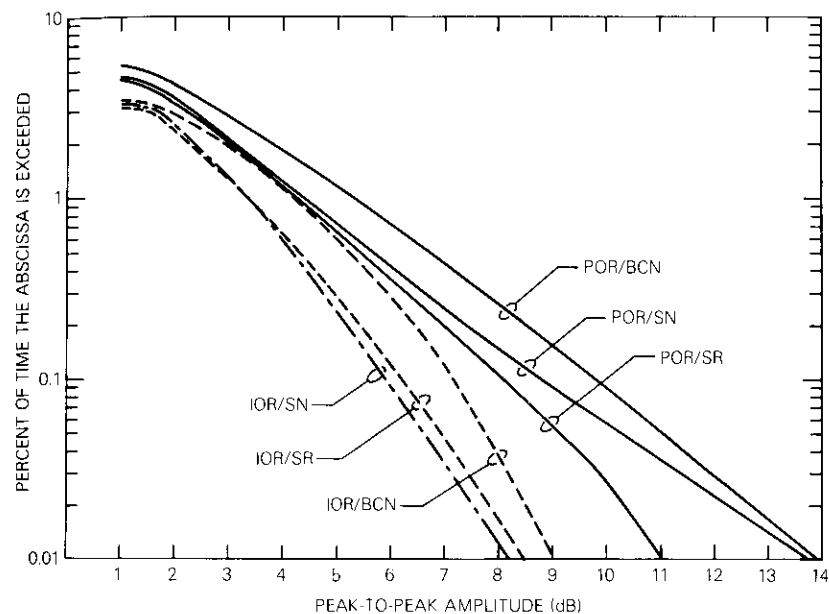


Figure 13. *Comparison Between Cumulative Statistics of Beacon Signals and Carriers*

annual statistics for ionospheric scintillations, worst-month occurrence statistics are also essential.

The worst month can be defined either as the worst calendar month or as the worst 30 days. The worst calendar month is a month in which the maximum minutes of peak-to-peak signal fluctuations are equal to or greater than 0.5 dB, the minimum detectable level of ionospheric scintillation. The worst 30 days is a continuous 30-day period covering major scintillation events with the highest magnitude of peak-to-peak fluctuations in the entire year. For years of low and medium solar activity when the scintillation level is low to moderate, worst-month statistics for both definitions differ substantially, which would yield substantial differences in assessing the impact on a digital communications system [14], [15]. In solar maximum years, such discrepancy does not exist. For either definition, March is the worst month for 1979 and for 1980. In both months, ionospheric scintillations occurred almost every evening and maximum peak-to-peak fluctuations were

registered. The worst-month statistics for March 1980 are shown in Figure 14 along with annual statistics and "4.4/1 conversion" statistics for comparison. The 4.4/1 conversion is an engineering rule, used when worst-month statistics are not available to convert annual statistics into monthly statistics, or vice versa [14]. According to this rule, the annual percentage exceedance for a given scintillation level is multiplied by 4.4 to derive the worst monthly percentage exceedance for the same scintillation level. The figure shows that this rule generally underestimates scintillation by approximately 1 dB of the actual worst-month statistics.

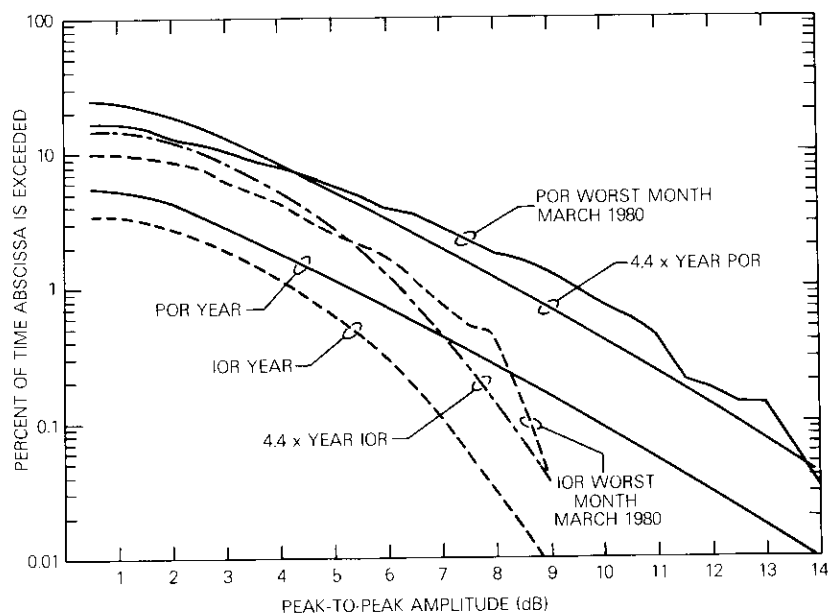


Figure 14. Worst-Month Statistics and 4.4/1 Conversion Statistics at Hong Kong Earth Station

The diurnal variation of ionospheric scintillation is shown in Figure 15, which clearly indicates that ionospheric scintillations occur after local sunset. For the POR link, activity starts around 1800 hours local time, increases drastically with time, and peaks between 2000 to 2200 hours. Activity decreases gradually through midnight, then drops off quickly in the early morning after 0200 hours. The pattern for the IOR link is similar but has a time lag of approximately 1 hour.

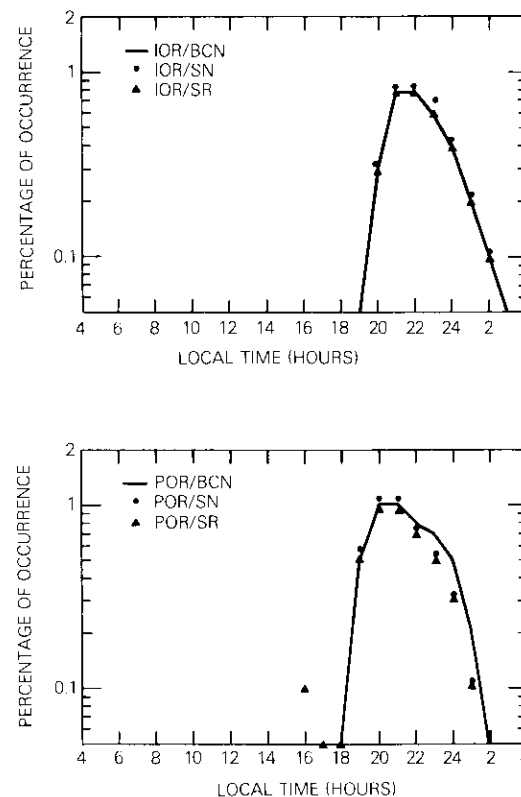


Figure 15. Diurnal Variations of Ionospheric Scintillations at Hong Kong Earth Station

Monthly scintillation variations are shown in Figure 16. The two peak activity periods are March and September. Compared with earlier results [7], [8], [13], it is evident that during solar maximum years, scintillation activities spread considerably around the equinoxes. However, the pattern is not necessarily universal. Recent AFGL ionospheric scintillation measurements at Ascension Island, in which COMSAT Laboratories also participated, indicated that January is the worst month and March is a quiet month in that location. It is suggested that the monthly variation pattern is geometrically dependent on the propagation path relative to the location of intense ionization patches in the ionosphere known as the Appleton Anomalies [22], [23].

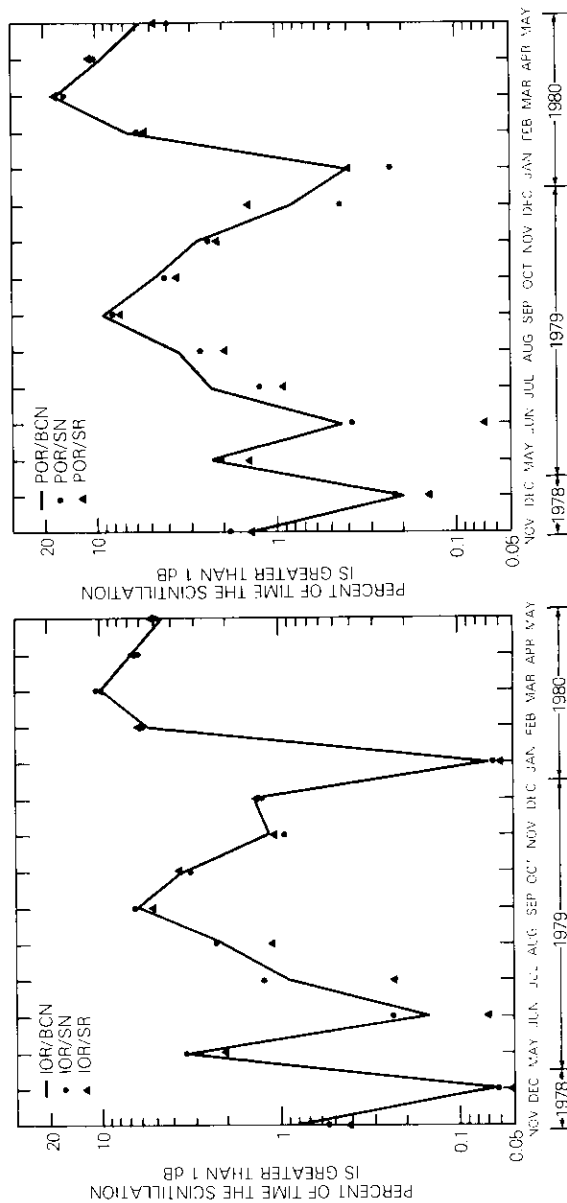


Figure 16. Monthly Variations of Ionospheric Scintillations at Hong Kong Earth Station

Conclusions

Ionospheric scintillation measurements at Hong Kong from 1977 to 1980 coincided with the solar maximum period of the current solar cycle 21. During 1979 and 1980, scintillations were observed for approximately 100 evenings, a much longer time than in previous years. Additional data have provided a new view of the phenomena: many scintillations appear unique compared with those of previous years. Satellite beacon signals with maximum peak-to-peak fluctuations of 14 dB were observed. Furthermore, simultaneous observations of signals from the POR and IOR satellites provided a rare opportunity to examine ionospheric scintillation on a global scale. Scintillations frequently occurred on both links with POR usually starting fluctuation first. The onset time delays varied from a few minutes to 2 hours. Power spectra revealed that the f^{-3} dependence is no longer valid. Scintillations in evening hours at Hong Kong, as observed from the eastward link pointing to the dark zone of the ionosphere, do not correlate with those observed from the westward link pointing to sunlit areas of the ionosphere. Solar cycle dependence is evident when cumulative statistics are compared for six consecutive 1-year periods. Worst-month statistics provide correction criteria for the empirical 4.4/1 conversion rule used for system engineering applications.

Acknowledgment

This work was sponsored by the International Telecommunications Satellite Organization (INTELSAT) as well as by an internal corporate R&D program. Views expressed in this paper are not necessarily those of the sponsors. Sincere thanks are expressed to Cable and Wireless, Ltd. for undertaking the measurements, and to the engineers at Hong Kong Earth Station who were responsible for the tedious daily collection of data for three years.

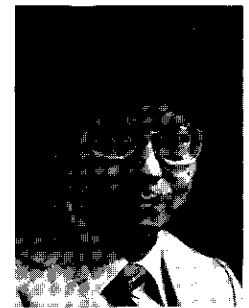
References

- [1] T. L. Eckersley, "An Investigation of Short Waves," *Journal of the Institution of Electronics and Telecommunication Engineers*, Vol. 67, 1929, pp. 992-1032.
- [2] A. C. B. Lovell and J. A. Clegg, *Radio Astronomy*, London: Chapman and Hall, 1952.

- [3] H. G. Booker and W. E. Gordon, "A Theory of Radio Scattering in the Troposphere," *Proceedings of the Institute of Radio Engineers*, Vol. 38, 1950, pp. 401-412.
- [4] C. L. Rufenach, "A Power-Law Wavenumber Spectrum Deduced from Ionospheric Scintillation Observations," *Journal of Geophysical Research* Vol. 77, 1972, pp. 4761-4772.
- [5] D. J. Fang, "The Formation of High-Latitude Plasma Irregularities by Wind-Shear Action in the Upper Atmosphere," *Journal of the Atmospheric Sciences*, Vol. 27, 1970, pp. 316-321.
- [6] E. J. Fremouw and D. J. Fang, "An All-Sky-Camera Format for Radar Auroral Studies," *Radio Science*, Vol. 10, 1975, pp. 891-904.
- [7] R. R. Taur, "Ionospheric Scintillations at 4 and 6 GHz," *COMSAT Technical Review*, Vol. 3, No. 1, Spring 1973, pp. 145-163.
- [8] R. R. Taur, "Ionospheric Scintillation at Frequencies Above 1 GHz," *COMSAT Technical Review*, Vol. 4, No. 2, Fall 1974, pp. 461-476.
- [9] J. Aarons, H. E. Whitney, and R. S. Allen, "Global Morphology of Ionospheric Scintillations," *Proceedings of the IEEE*, Vol. 59, 1971, pp. 159-172.
- [10] C. L. Rufenach, "Ionospheric Scintillation by a Random Phase Screen-Spatial Approach," *Radio Science*, Vol. 10, 1975, pp. 155-165.
- [11] R. K. Crane, "Spectra of Ionospheric Scintillation," *Journal of Geophysical Research*, Vol. 81, 1976, pp. 2041-2050.
- [12] E. J. Fremouw, R. C. Livingston, and D. A. Miller, "On the Statistics of Scintillating Signals," *Journal of Atmospheric and Terrestrial Physics*, Vol. 42, 1980, pp. 717-731.
- [13] R. R. Taur, "Simultaneous 1.5- and 4-GHz Ionospheric Scintillation Measurements," *Radio Science*, Vol. 11, 1976, pp. 1029-1036.
- [14] D. J. Fang, D. J. Kennedy, and C. Devieux, "Ionospheric Scintillations at 4/6 GHz and Their System Impact," EASCON-78 paper, IEEE Pub. No. CH1352-4/78/0000-0385, 1978.
- [15] D. J. Fang, "4/6 GHz Ionospheric Scintillation Measurements," AGARD Conference Proceedings No. 284, *Propagation Effects in Space/Earth Paths*, 1980, pp. 33-1-33-12.
- [16] D. J. Fang, "C-Band Ionospheric Scintillation Measurements at Hong Kong Earth Station During the Peak of Solar Activities in Sunspot Cycle 21," *Proceedings of III Ionospheric Effect Symposium*, 1981, Paper 3A-2, pp. 1-12.
- [17] D. J. Fang, "Scattering from a Perfectly Conducting Sinusoidal Surface," *IEEE Transactions on Antennas and Propagation*, Vol. AP-20, 1972, pp. 388-390.
- [18] D. J. Fang and J. M. Harris, "Precipitation Attenuation Studies Based on Measurements on ATS-6 20/30 GHz Beacon Signals at Clarksburg, Maryland," *IEEE Transactions on Antennas and Propagation*, Vol. AP-27, January 1979, pp. 1-11.

- [19] D. J. Fang, F. T. Tseng, and T. O. Calvit, "A Low Elevation Angle Propagation Measurement of 1.5 GHz Satellite Signals in the Gulf of Mexico," *IEEE Transactions on Antennas and Propagation*, Vol. AP-30, January 1982, (to be published).
- [20] H. E. Whitney, J. Aarons, and C. Malik, "A Proposed Index for Measuring Ionospheric Scintillations," *Planetary Space Science*, Vol. 17, 1969, pp. 1069-1073.
- [21] D. J. Fang and J. Jih, "A Model for Microwave Propagation Along an Earth-Satellite Path," *COMSAT Technical Review*, Vol. 6, No. 2, Fall 1976, pp. 379-411.
- [22] J. Aarons, J. P. Mullen, and H. E. Whitney, "The Dynamics of Equatorial Irregularity Patch Formation, Motion and Decay," *Journal of Geophysical Research*, Vol. 85, 1980, pp. 139-149.
- [23] J. Aarons, H. E. Whitney, and Eileen MacKenzie, "Microwave Equatorial Scintillation Intensity During the Current Solar Maximum," *Radio Science*, 1981, (to be published).

Dickson J. Fang received his B.S.E.E. in 1962 from Taiwan University, Taipei, China, and his M.S.E.E. and Ph.D. from Stanford University in 1964 and 1967. From 1967 to 1974, he was a radio physicist at Stanford Research Institute, studying electromagnetic wave propagations, radio auroras, and ionospheric irregularities. While on leave from Stanford (1969-1970), he was a visiting professor at Taiwan University, where he published a graduate textbook on electromagnetic theory and five articles on the college education system.



Dr. Fang joined the Propagation Studies Department, COMSAT Laboratories, in 1974 and became Manager in 1980. He is involved in studies of ionospheric scintillations, microwave precipitation, and atmospheric optical transmission characterizations. As Manager, he plans and supervises research on microwave propagation for satellite-earth communications applications. He is the author or co-author of more than 50 technical papers and reports. As a member of U.S. delegations to CCIR and URSI, Dr. Fang is actively involved in drafting documents for establishing international standards.



Marlene S. Pontes received a B.S.E.E. from the University of Juiz de Fora, Brazil, in 1969, and an M.S. from the Catholic University of Rio de Janeiro, Brazil, in 1971. She is with the Catholic University as an Assistant Professor at CETUC (Center of Studies in Telecommunications) where she is engaged in teaching and microwave propagation research. Ms. Pontes is an INTELSAT nominee from Brazil. Since 1979 she has worked in the Propagation Studies Department at COMSAT, where she has been actively involved in ionospheric and tropospheric scintillation studies.

Index: filter, elliptic function, bandpass

Generalized dielectric resonator filters*

A. E. ATIA AND R. R. BONETTI

(Manuscript received July 7, 1981)

Abstract

Methods of designing and realizing generalized dielectric resonator filters in a microwave integrated circuit structure are presented. These methods permit realization of the most general transfer function characteristics of narrow bandpass filters, including real, imaginary, and/or complex transmission zeros. Design and test results on an elliptic function bandpass filter show close agreement between the theoretical response and the experimental data.

Introduction

Microwave integrated circuit (MIC) technology offers numerous advantages in the realization of various components for satellite transponders. Advances in MIC technology and requirements of high reliability, performance, mechanical and thermal integrity, light weight, ease of tuning and testing, and reproducibility led to the development of integrated MIC receivers [1] for satellite transponders. In addition, the introduction of solid-state microwave power amplifiers in the transmitters will contribute to the integration of portions of the transponders. However, high-quality microwave bandpass filters required in the channelizing input and output multiplexers need high Q resonators for their realizations. Waveguide cavities that cannot be

* This paper is based on work performed at COMSAT Laboratories under the sponsorship of the International Telecommunications Satellite Organization (INTELSAT).

reduced to MIC form are currently used for such filters. For the multiplexers to meet required electrical performance specifications under environmental conditions, the waveguide cavities must be made of a highly temperature-stable material. Invar is the most commonly used material for this application, although recently lighter graphite fiber-reinforced plastics (GFRP) have also been used in the construction of flight-qualified filters. Therefore, integration of the channelizing input multiplexers in an MIC structure is a very desirable development in transponder and filter technology.

Since high Q resonators are necessary in the realization of these filters, the conventional edge-type coupled resonators in microstrip or strip lines are not suitable. High dielectric constant low-loss materials present an attractive medium for realization of the narrowband filters.

A dielectric body having free-space boundaries can resonate in various modes [2]–[4]. If the dielectric constant of the material constituting the body is high, the electric and magnetic fields of a given resonant mode will be confined within and near the resonator and will attenuate to negligible values at a distance that is small compared to the free-space wavelength. Therefore, radiation loss is usually very small, and the unloaded Q of the resonator is limited mainly by losses inside the dielectric body. In most materials, the magnetic permeability is unity, and no magnetic losses exist. Electric field losses occur because of the nonzero loss tangent of the dielectric material. If all the electric energy of the resonant mode is stored inside the dielectric resonator, and if no losses occur because of external fields, then the unloaded Q will be given by $Q_u = 1/\tan \delta$. In practice, the relative dielectric constant (ϵ_r) of the material is large, but finite, and external losses always result because of radiation or dissipation in the surrounding metal shield. These losses tend to reduce Q_u , whereas external electric-stored energy tends to increase Q_u . For a relative dielectric constant of 30 or higher, these effects are small, and $Q_u \approx 1/\tan \delta$ is a good approximation. Typical $\tan \delta$ values for materials of interest are about 0.0001 to 0.0002; therefore, Q_u values of 5,000 or more may be expected.

For the fundamental mode resonance, the dimension of a dielectric resonator is one-half wavelength in the dielectric material. Since $\lambda_d = \lambda/\sqrt{\epsilon_r}$, where λ_d is the wavelength in dielectric and λ the wavelength in air, the resonator dimensions will be small compared to λ if ϵ_r is large. Because the dimensions of an air-filled waveguide cavity are of the order of the free-space wavelength λ , a dielectric resonator can be made much smaller than a waveguide cavity resonator.

Much work was performed about 10 years ago on dielectric resonator filters with materials such as TiO_2 that possess a relative dielectric constant of about 100 at room temperature [5]–[7]. This material, used in filter applications, has a disadvantage: its dielectric constant variations with temperature amount to about 1,000 ppm/°C, compared to Invar cavities which register 1 ppm/°C. This fact greatly limits the use of dielectric resonator filters in most applications. Recent developments in low-loss, high relative dielectric constant and low temperature coefficient materials [8]–[9] have revived interest in the subject. With the newly developed materials, the unloaded Q 's of metallic cavities and the stability of Invar can be approximated. Though several designs of dielectric resonator filters in coaxial and waveguide realizations have been developed [10]–[11], no elliptic function filter realization using dielectric resonators has been reported. Realization of generalized transfer functions of bandpass filters with finite transmission zeros (*i.e.*, elliptic function and group-delay-equalized filters) using dielectric resonators should be valuable in achieving smaller and lighter filters and multiplexers for easy integration.

This paper describes new configurations of dielectric resonator filters that realize the most general transfer functions suitable for MIC structures and that are potentially useful for satellite applications. Since the estimated loss in these filters is higher than that of corresponding waveguide filters, their use may be attractive in input multiplexers where losses are tolerable. Filter configurations given are of the canonical form [12], where the "series" couplings between resonators are provided by either the evanescent fields outside the resonators or by microstrip lines; the "shunt" or "cross" couplings are produced by microstrip lines of appropriate electrical lengths.

Since, in the realizations presented here, the dielectric resonators are embedded in the inhomogeneous medium of the microstrip substrates and various metallic boundaries, their resonant frequencies are considerably different from those of isolated resonators; therefore, an iterative analytical method for computing resonant frequencies of dielectric cylindrical resonators in inhomogeneous media was developed [13] and is summarized in the next section.

The main steps in computing the coupling between a dielectric resonator and a microstrip transmission line are also presented. Measurements on several test cases show good agreement between theory and experimental data.

The new configurations for the generalized bandpass filters using dielectric resonators and microstrip lines are exemplified in the design

of a representative filter that verifies the basic principle of realizations of finite transmission zeros. Measured response of this filter, which was constructed and experimentally tested, agrees well with the theoretical model.

Dimensioning the resonator

Several approximate methods have been developed [4], [7], [11] for determining the resonant frequency of a dielectric cylinder in the presence of either one or two conductor planes perpendicular to its axis. When a resonator is used in a microwave circuit employing a microstrip transmission medium, the microstrip substrate, as well as other dielectric supports and metallic boundaries, can significantly alter the resonant frequency predicted by the idealized conditions usually assumed.

This section summarizes the results of a method for computing the resonant frequency of a high dielectric constant cylinder inside a metallic cylindrical cavity [13], which includes a microstrip dielectric support and several options for supporting the resonator (Figure 1).

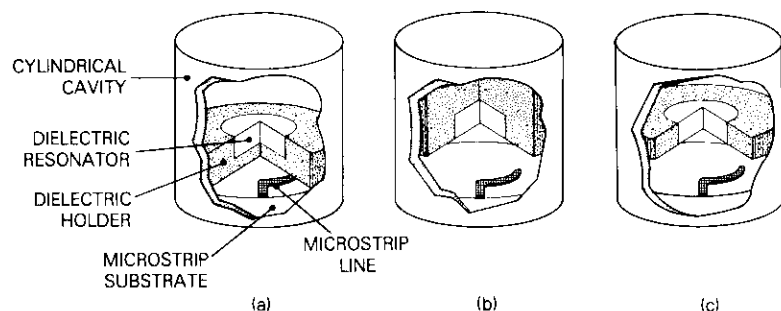


Figure 1. Three Possible Ways for Supporting a Dielectric Resonator Coupled to a Microstrip Line (a) from below; (b) from above; (c) from the side edge

The basic assumptions are as follows:

- All dielectric materials involved are isotropic and lossless.
- The metallic boundaries are perfectly conducting.
- The electromagnetic field distribution is that of the dominant TE_{018} mode.

Figure 2, which shows the configuration analyzed, consists of a

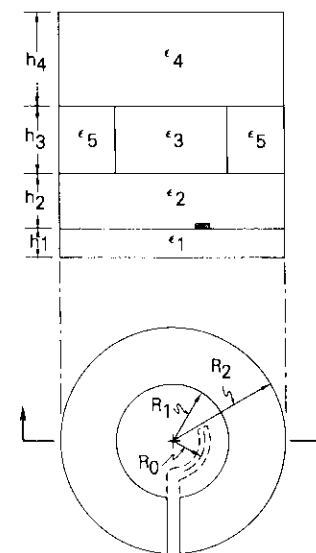


Figure 2. Cross Section of Cavity Under Analysis

cylindrical, high dielectric constant material (region 3), positioned within three layers of different dielectrics (regions 1, 2, and 4). Reference 13 describes the method for obtaining the resonant frequency of the dominant mode in this structure.

Examples of the results for the resonant frequency as a function of both physical and geometrical parameters are given in normalized form in Figures 3 to 5. Several important conclusions can be drawn from these data. First, the metallic boundaries strongly affect the free-space resonance by shifting it up to 25 percent. Second, variations of the dielectric constant of the microstrip substrate will produce a perturbation of less than 1 percent if its nominal value is not greater than half the resonator dielectric constant and its thickness is not larger than one-fourth of the resonator thickness. Also, the side walls effect can be neglected if they are farther than one resonator radius away. The theoretical results extracted from Reference 13 were compared to several experimental data sets obtained with different size resonators placed inside different boundaries; it was concluded that the accuracy of the method is better than 1 percent, and a sample of these results is provided in Figure 6.

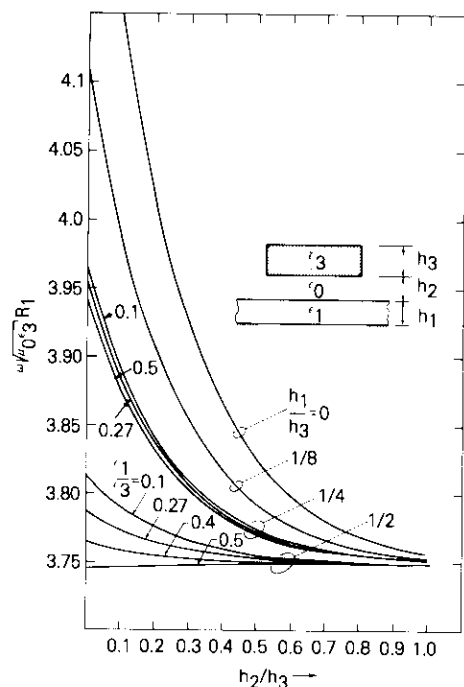


Figure 3. Normalized Resonant Frequency of a Dielectric Disk in the Presence of a Dielectric Coated Conductor Plane

Computation of coupling between dielectric resonators and microstrip

Since the filter realizations considered use dielectric resonators coupled to microstrip transmission lines, accurate determination of physical dimensions and properties of the coupling structure is essential for successful filter designs. This section presents the basis for theoretically computing the external *Q* of a dielectric resonator coupled to a microstrip transmission line. The following basic assumptions are made in the analysis:

- a. The width of the microstrip line is small enough so that the field distribution in the resonator is not significantly disturbed from the field configuration of the dominant TE₀₁₈ mode.
- b. The coupling line length of the microstrip within the resonator is smaller than a quarter wavelength in the substrate.

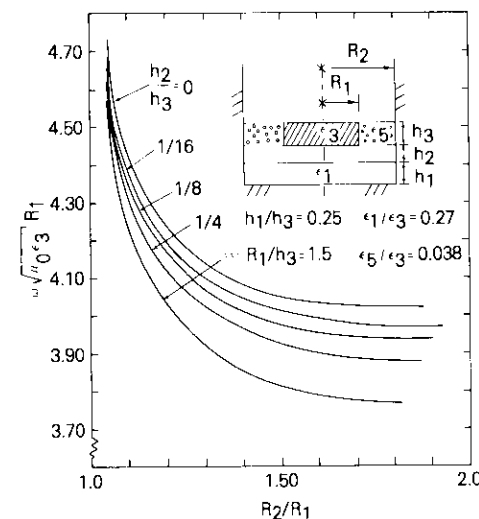


Figure 4. Normalized Resonant Frequency as Affected by the Sidewalls

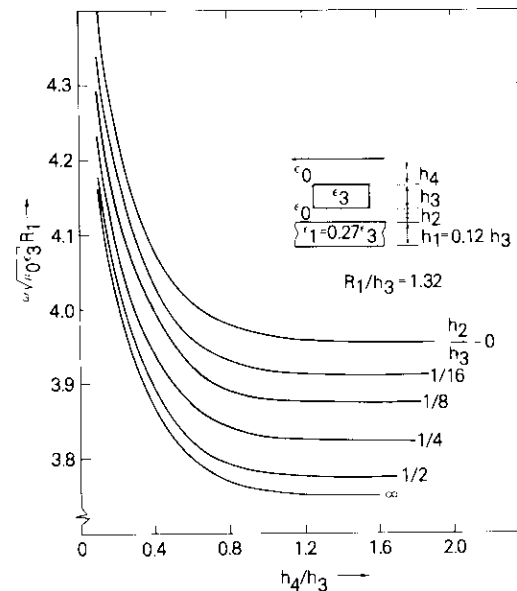


Figure 5. Normalized Resonant Frequency Dependence on the Proximity of Two Conductor Planes (one supporting a microstrip substrate)

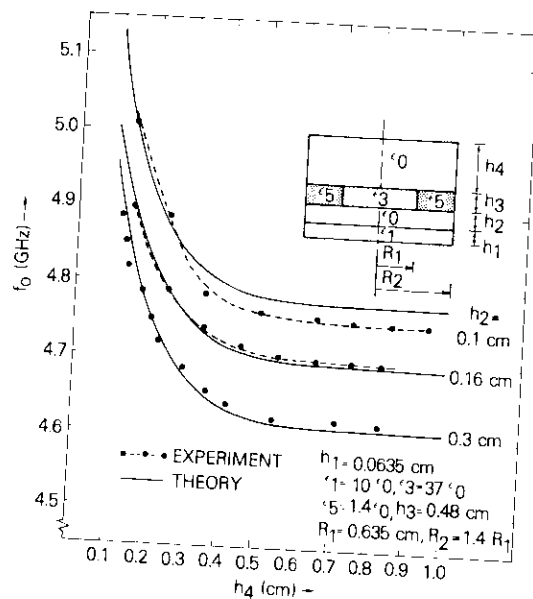


Figure 6. Theoretical and Experimental Results for a Prototype Cavity as Depicted in the Insert

c. The dielectric constant of the resonator is much larger than that of the microstrip line substrate and the surrounding supporting structure.

Circuit model and analysis

The structure under consideration consists of a dielectric cylindrical resonator placed above the substrate of a microstrip transmission line as shown in Figure 2. This coupling configuration is similar to the one described in Reference 10, except that in the coupling region, the microstrip line consists of a circular arc of radius R_0 with the center coinciding with the cylindrical resonator's axis, and subtends an angle ψ . With a proper choice of R_0 , this coupling scheme allows the peak magnetic fields of the resonator to coincide with the magnetic fields of the current on the arc of the microstrip line. The magnitude of the coupling can be controlled by either the angle ψ or the height h of the resonator above the substrate, or both.

Couplings among dielectric resonators are achieved by one of two

means. In the first configuration, the resonators are placed inside a rectangular metal box, which is also the microstrip housing. The dimensions of the housing must be those of a waveguide below cutoff for the frequency band used to avoid spurious modes.

The second configuration for generalized filters provides indirect coupling between resonators by first coupling the energy from the resonator to a microstrip transmission line, and then coupling the energy back from the microstrip line to the second dielectric resonator. The two housings have a common metallic wall; the microstrip line passes near the bottom of the common wall as shown in Figure 7. The

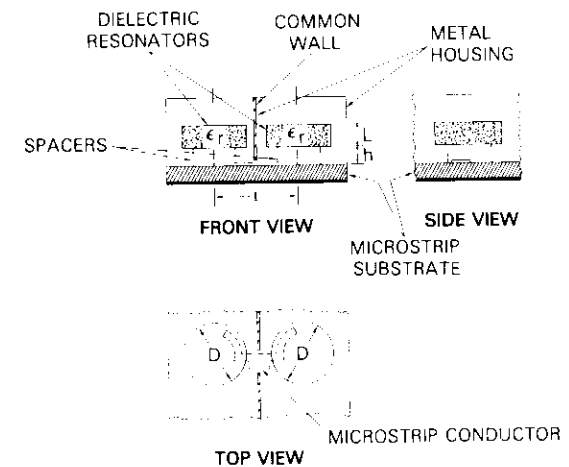


Figure 7. Coupled Dielectric Resonators by Means of a Microstrip Transmission Line

amount of coupling between the two resonators is controlled by the height h of the resonator above the microstrip substrate, while the sign of the coupling is controlled by line length l . This new means of coupling enables the realization of arbitrary sign and the most general transfer function characteristics of bandpass filters, as described later.

Quantitative determination of the coupling coefficient between resonators, mounted as shown in Figure 7, can be deduced from knowledge of coupling resonators to microstrip as shown in Figure 2 and the equivalent circuit of the line length connecting the resonators. If the coupling coefficient between the resonator and the microstrip is

known, the equivalent circuit of two resonators coupled as in Figure 7 appears as shown in Figure 8a. The coupling coefficient M between the two microstrip-coupled cavities can be obtained by calculating the

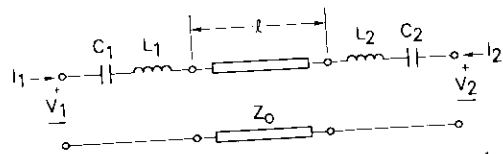


Figure 8a. Equivalent Circuit of Microstrip Coupled Dielectric Resonators

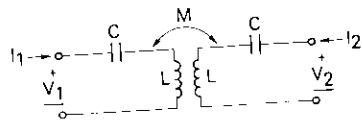


Figure 8b. Direct-Coupled Cavity Equivalent Circuit

open-circuit impedance parameters of the two circuits in Figures 8a and 8b and identifying the corresponding elements. The condition for equivalence between the two circuits can be easily determined to be

$$\cot \beta \ell = 0 \quad \text{i.e.,} \quad \ell = \frac{(2k + 1)\lambda}{4}, \quad k = 0, 1, 2, \dots \quad (1)$$

where λ is the wavelength in the dielectric substrate. For the values of ℓ given by equation (1), the coupling between the two cavities is

$$M = \frac{1}{\sqrt{Q_{c1} Q_{c2}}} (-1)^k \quad (2)$$

when Q_{c1}, Q_{c2} are the external Q 's of the resonators. Thus, for a positive coupling coefficient, the line length ℓ must be a quarter wavelength, and for a negative coupling, it must be a three-quarter wavelength. Either sign coupling is realizable by proper choice of line length or configuration, while the magnitude of the coupling is controlled by the height h of the dielectric resonator above the microstrip substrate, the arc radius R_0 , the angle ψ (see Figure 2), and the line's characteristic impedance Z_0 .

To determine the external Q 's in equation (2), the lumped element equivalent circuit (Figure 9) of the structure shown in Figure 2 is

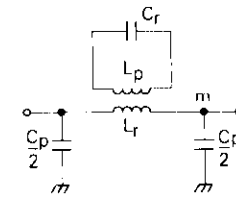


Figure 9. A Lumped Element Equivalent Circuit of the Coupling Region Between Dielectric Resonator and Microstrip Line

considered. The series resonant circuit represents the resonant properties of the dielectric resonator, while the pi-circuit is an approximation of the equivalent circuit of the microstrip line short section. It is assumed that energy coupling between the two circuits occurs only through the mutual coupling m of the inductors; the coupling is primarily inductive due to the magnetic fields of the microstrip and those in the resonator. The values of L_p and C_p are the total inductance and capacitance of the microstrip line section, respectively. These values are assumed to include any effects or perturbations introduced to the line from the presence of the resonator.

The input impedance of the circuit in Figure 9 at the reference plane is [14]

$$Z_{in} = j \frac{1 + \omega L_p \frac{2}{\omega C_p} \frac{2\omega_r L_r \Delta}{\omega^2 m^2}}{\frac{4\omega_r L_r \Delta}{\omega^2 m^2} + \frac{\omega C_p}{2} - \frac{\omega_r L_r \Delta}{m^2} L_p C_p} \quad (3)$$

where

$$\omega_r = (L_r C_r)^{-1/2}$$

and

$$\Delta = (\omega - \omega_r)/\omega_r$$

The external Q of this circuit, defined by

$$Q_c = \frac{2\pi (\text{Stored Energy})}{(\text{Energy Exchanged per Cycle})} \quad (4)$$

can be computed from the input impedance as

$$Q_e = \frac{\omega_r}{2Z_0} \left. \frac{\partial X_{in}}{\partial \omega} \right|_{\omega = \omega_r} \quad (5)$$

After algebraic manipulation, substituting equation (3) into equation (5) yields

$$Q_e = \frac{4Z_p^2}{Z_0 Z_c} + \frac{Z_p}{Z_0} \quad (6)$$

where

$$Z_p = \frac{1}{\omega_r C_p} \quad (7)$$

$$Z_c = \frac{\omega_r m^2}{L_p} \quad (8)$$

The impedance Z_c is conveniently defined as the coupling impedance since it characterizes the tightness or looseness of the coupling proportionately to its value. Note that even for large values of Z_c , the external Q cannot be made arbitrarily small since it has a lower bound which is (Z_p/Z_0) .

Computation of coupling impedance

The self-inductance of the dielectric resonator can be computed from

$$L_r = \frac{2\bar{W}_m}{I_r^2} \quad (9)$$

where \bar{W}_m is the average magnetic energy stored. At resonance, this value can be computed from the energy stored in the electric field

$$W_e = \frac{1}{2} \iiint_V \epsilon E^2 dv \quad (10)$$

In the above expression, W_e is the maximum value of the energy and relates to \bar{W}_m by

$$\bar{W}_m = \frac{1}{2} W_e \quad (11)$$

An incremental voltage induced in the microstrip due only to a current in the resonator loop can be computed via

$$\Delta V = j\omega m I_r \quad (12)$$

and also from the magnetic flux in the loop ABCD in Figure 10:

$$\Delta V = j\omega \mu_0 \iint_{S_1} \underline{H} \cdot d\underline{S}_1 \quad (13)$$

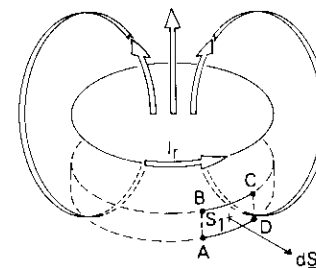


Figure 10. Magnetic Flux Linkage of the Resonator Field into an Increment of the Microstrip Line

Combining equations (9) through (13) and substituting in equation (8) yields the coupling impedance:

$$Z_c = \frac{\omega_r \mu_0^2 \left[\iint_{S_1} \underline{H} \cdot d\underline{S}_1 \right]^2}{\frac{1}{2} \iiint_V \epsilon E^2 dV} \quad (14)$$

Explicit expressions of electric and magnetic field components E and H can be found in Reference 13.

Experimental and numerical results

Measurements performed with several microstrip circuits of different lengths and radii are compared to theoretical computations (when

C
r
a
d
n
c
ψ
n
tl
c
r

applicable). Figure 11 shows the dependence of the external and unloaded Q 's on the position of the microstrip coupling arc. The results of external Q were normalized with respect to the minimum value (which occurs around $R_0/R_1 \approx 0.65$), since the purpose of this plot is to verify experimental results with theory where this minimum occurs.

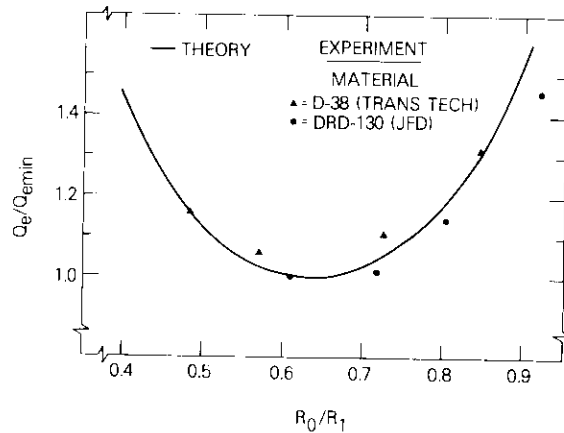


Figure 11. Measured and Computed External Q 's of Dielectric Resonators as a Function of R_0/R_1

Figure 12 shows theoretical computations based on equation (6) for three different values of the line capacitance C_p , as affected by the presence of the resonator, normalized with respect to its unperturbed value (C_0).

The experimental data slope fits well with the theoretical one for small values of the normalized line length ($\psi R/\lambda_g$) as expected, since only one section of lumped elements was used to characterize the transmission line. The dielectric resonator increased microstrip capacitance by 20 to 35 percent from its unperturbed nominal value.

Filter realization

The most general (narrow) bandpass transfer function characteristics can be realized by the canonical form of coupled cavities described in Reference 12. For an even number ($2n$) of cavities, this canonical form is symmetrical and consists of two identical halves. Each half contains n direct coupled cavities with series couplings of the same sign. Each

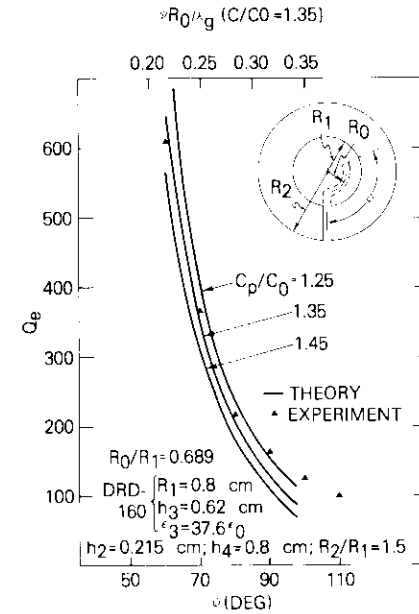
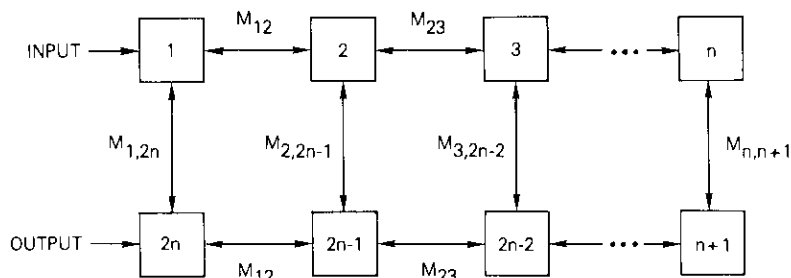


Figure 12. Measured and Computed External Q 's of Dielectric Resonator as a Function of Microstrip Coupling Angle ψ_0 (dielectric resonator material DRD-160)

cavity in one half is coupled to the corresponding cavity in the other half by a shunt coupling. For the realizations of the most general transfer functions, the filter structure should be capable of providing the shunt couplings with prescribed signs; that is, certain shunt couplings must be positive while others must be negative, depending on the filter transfer function. Figure 13 is a schematic diagram of the canonical form filter, which may be realized in two ways using dielectric resonators and microstrip lines and the coupling configurations discussed above.

The first configuration uses all microstrip couplings for both the series and shunt couplings of the canonical forms, as shown in Figure 14. Input/output coaxial-to-microstrip launchers provide the filter terminals. All series couplings are realized by means of $\lambda/4$ lines. Shunt couplings of positive sign are also realized by $\lambda/4$ lines, while those of negative sign are realized by $3\lambda/4$ lines. Since most of the shunt couplings are small compared to the series couplings, the angular



'SERIES' COUPLINGS $M_{12}, M_{23}, \dots, M_{n,n+1}$ ALL HAVE SAME SIGN (POSITIVE)

'SHUNT' COUPLINGS $M_{1,2n}, M_{2,2n-1}, \dots, M_{n-1,n+2}$ MUST BE EITHER POSITIVE OR NEGATIVE FOR ARBITRARY REALIZATION

Figure 13. Canonical Form of a $2n$ Cavity Filter-Series Couplings All Having Same Sign (positive); Shunt Couplings Must be Either Positive or Negative for Arbitrary Realization

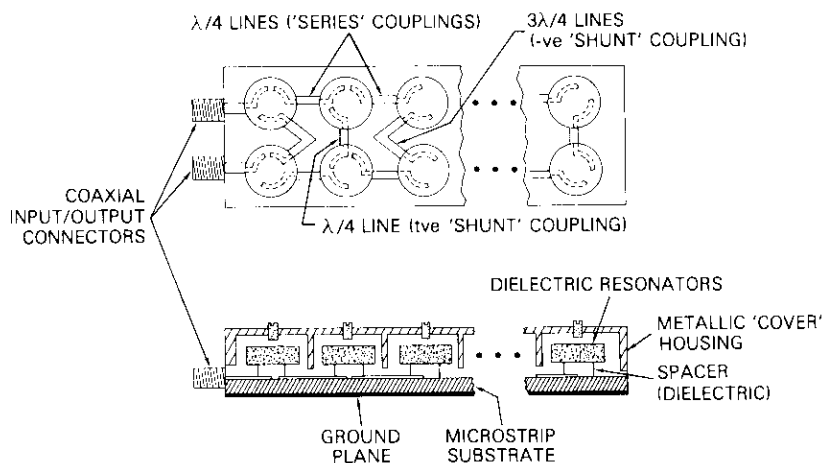


Figure 14. Possible Realization of a General Dielectric Resonator Filter

extent ψ_0 of the shunt lines can be made small to provide the required coupling values. Also, the lines for the small couplings can be made of a lower characteristic impedance to further reduce the couplings.

The direct evanescent fields of the resonators are prevented from producing couplings by the metallic housing. This housing can be made in the cover by cylindrically shaped grooves surrounding each of the dielectric resonators as shown in Figure 14. Tuning screws can be added to fine tune the resonator center frequency. In this configuration, all couplings are realized in the microstrip and are therefore controllable to a high degree of accuracy by the line's characteristic impedances. However, losses increase because of added housing surrounding the resonators and the conductor losses in the microstrip.

The second configuration is similar to the first, except that the series couplings are realized by the evanescent fields inside a waveguide beyond cutoff. Shunt couplings are still realized by the microstrip lines. In this case, the filter housing consists of two rectangular boxes with a common wall open at the bottom allowing for the shunt microstrip couplings between the corresponding resonators. Because this configuration is a lower loss structure, due to series couplings realized through the cutoff waveguide fields, conductor losses of the microstrip are avoided. However, spacings between resonators must be precisely controlled to provide the appropriate couplings.

Design of a representative filter

This section describes a representative generalized dielectric resonator filter and provides an experimental verification of the realization and coupling computations explained earlier. A 4-pole filter provides the basic unit for experimental verification.

4-Pole Filter Design

A 4-pole elliptic function filter with a center frequency f_0 of 4.75 GHz and an equal ripple bandwidth W of 30 MHz was chosen for the verification. The passband ripple of the filter is 0.05 dB and the minimum out-of-band rejection is 25 dB. The synthesis procedure described in Reference 12 can be applied to obtain the following normalized element values of the prototype circuit shown in Figure 15:

$$R = 1.2052 \quad M_{12} = 0.884$$

$$M_{23} = 0.8236 \quad M_{14} = -0.2565$$

For a configuration in which the microstrip lines coupling any two

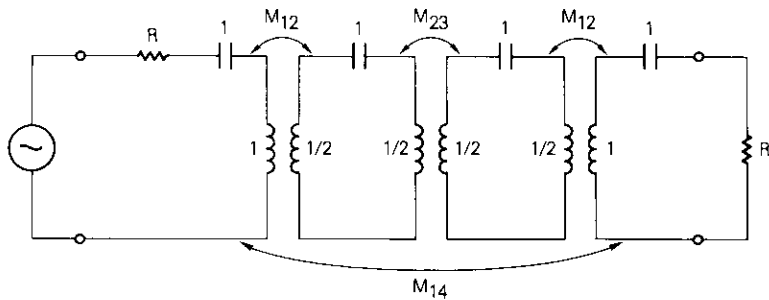


Figure 15. Equivalent Circuit of 4-Pole Filter

resonators are identical, the external Q's of each resonator are determined as

$$Q_{e1} = \frac{1}{R} \frac{f_o}{W} = 131.4 \quad Q_{e2} = \frac{1}{M_{12}} \frac{f_o}{W} = 179.1$$

$$Q_{e21} = \frac{1}{M_{23}} \frac{f_o}{W} = 192.2 \quad Q_{e14} = \frac{-1}{M_{14}} \frac{f_o}{W} = 617.3$$

The microstrip line was etched on RT-Duroid substrate 0.025 in. thick. A 0.059-in. (1.5 mm) spacing was used for the distance between the resonator and substrate. The corresponding coupling angles were subsequently determined as

$$\psi_{11} = 100^\circ \quad \psi_{12} = 90^\circ$$

$$\psi_{23} = 87.8^\circ \quad \psi_{14} = 61.64^\circ$$

Figures 16 to 18 contain the measured responses of the experimental filter. Figure 16 shows the insertion and return loss. The insertion loss response contains the two zeros of transmission characterizing the elliptic function response, with the average minimum out-of-band rejection of 21.5 dB, which is slightly lower than the 25-dB designed rejection. This discrepancy is primarily due to a realized M_{14} coupling slightly larger than the design value. Figure 17 is an enlarged insertion loss response. The 1.7-dB mid-band loss, when corrected for the launcher and microstrip line losses of 0.25 and 0.35 dB, respectively, corresponds to average unloaded resonator Q's of approximately 3,500; these agree closely with the manufacturer's quoted value. The center frequency of this filter is within 0.1 percent and the bandwidth is within

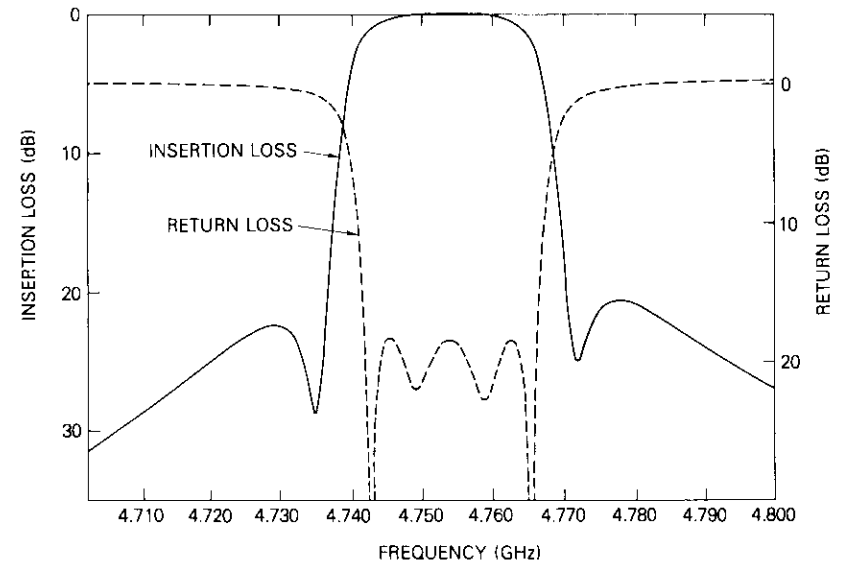


Figure 16. Measured Insertion and Return Loss Response of 4-Pole Dielectric Resonator Elliptic Function Filter

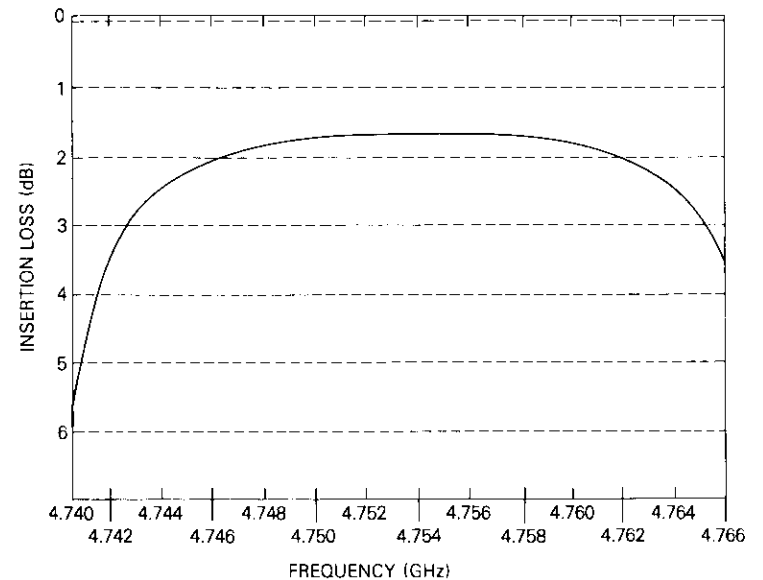


Figure 17. Enlarged In-Band Insertion Loss

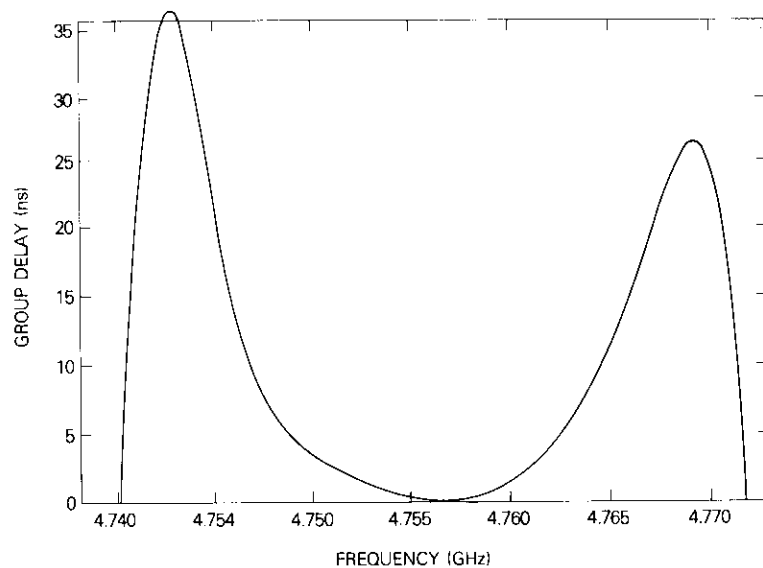


Figure 18. *Group-Delay Response*

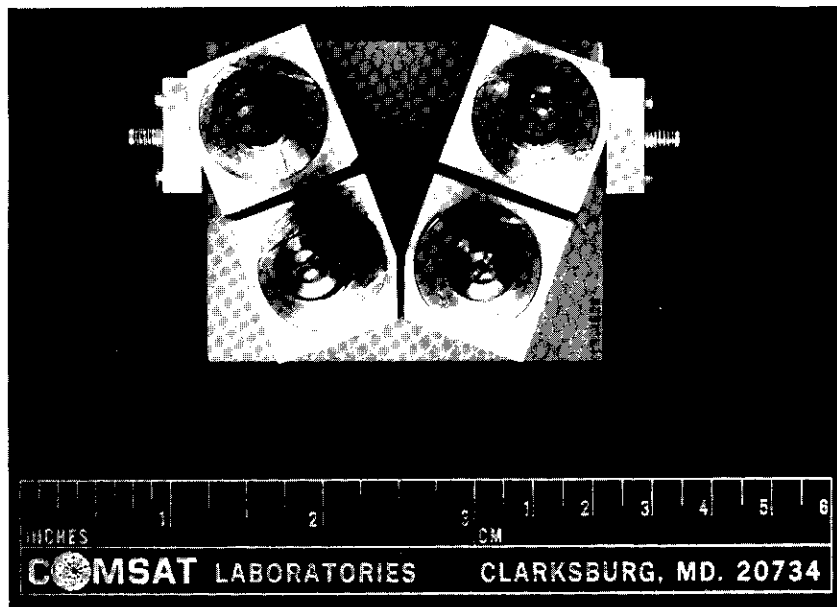


Figure 19. *Experimental 4-Pole Filter*

0.2 percent of the design value. Figure 18 shows the measured group-delay filter response, and Figure 19 is a photograph of the experimental filter.

Conclusions

This paper has discussed advances in realizing generalized narrow-band microwave filters using high dielectric constant resonators. Theoretical computations of both the resonant frequency and coupling-to-microstrip lines as a function of the resonator's properties were reviewed with excellent experimental verification. New filter structure configurations realizing the most general filter transfer functions were introduced and the concept was experimentally verified. These structures are fully compatible with MIC technology and represent a significant advance toward realizing an MIC input multiplexer for satellite transponders.

Acknowledgments

The authors wish to thank Ronald R. Kessler for constructing the test fixtures, Wayne H. Chang for etching the microstrip circuits, William J. Getsinger for providing many helpful suggestions, and Arnold Berman and Pier L. Bargellini for offering the encouragement and support that led to this publication.

References

- [1] H. Ozaki, M. Eick, and M. Silence, "Communications Satellite Receiver Design," *Satellite Communications*, Edited by Harry L. Van Trees, IEEE Press, New York, 1979, pp. 484-497.
- [2] R. D. Richtmeyer, "Dielectric Resonators," *Journal of Applied Physics*, Vol. 10, June 1939, p. 391.
- [3] H. Y. Yee, "Natural Resonant Frequencies of Microwave Dielectric Resonators," *IEEE Transactions on Microwave Theory and Techniques*, Vol. MTT-13, March 1965, p. 256.
- [4] J. C. Sethares and S. J. Maumann, "Design of Microwave Dielectric Resonators," *IEEE Transactions on Microwave Theory and Techniques*, Vol. MTT-14, January 1966, pp. 2-7.
- [5] W. H. Harrison, "A Miniature High-Q Bandpass Filter Employing Dielectric Resonators," *IEEE Transactions on Microwave Theory and Techniques*, Vol. MTT-16, April 1968, pp. 210-218.

- [6] S. B. Cohen, "Microwave Bandpass Filters Containing High-Q Dielectric Resonators," *IEEE Transactions on Microwave Theory and Techniques*, Vol. MTT-16, April 1968, pp. 218-227.
- [7] A. Karp, H. J. Shaw, and D. K. Winslow, "Circuit Properties of Microwave Dielectric Resonators," *IEEE Transactions on Microwave Theory and Techniques*, Vol. MTT-16, October 1968, pp. 818-829.
- [8] J. K. Plourde et al., " $Ba_2Ti_9O_{20}$ as a Microwave Dielectric Resonator," *Journal of American Ceramic Society*, 58 (9-10), 1975, pp. 418-420.
- [9] W. Wakino et al., "Microwave Bandpass Filters Containing Dielectric Resonators with Improved Temperature Stability and Spurious Response," *IEEE-MTT Symposium Digest*, May 1975, pp. 63-65.
- [10] J. K. Plourde and D. F. Linn, "Microwave Dielectric Resonator Filters Utilizing $Ba_2Ti_9O_{20}$ Ceramics," *IEEE-MTT Symposium Digest*, June 1977, pp. 290-293.
- [11] M. W. Pospieszalski, "Cylindrical Dielectric Resonators and Their Applications in TEM Line Microwave Circuits," *IEEE Transactions on Microwave Theory and Techniques*, Vol. MTT-27, March 1979, pp. 233-238.
- [12] A. E. Atia, A. E. Williams, and R. W. Newcomb, "Narrow-Band Multiple-Coupled Cavity Synthesis," *IEEE Transactions on Circuits and Systems*, Vol. CAS-21, No. 5, September 1974, pp. 649-655.
- [13] R. R. Bonetti and A. E. Atia, "Design of Cylindrical Dielectric Resonators in Inhomogeneous Media," *IEEE Transactions on Microwave Theory and Techniques*, Vol. MTT-29, No. 4, April 1981, pp. 323-326.
- [14] R. R. Bonetti and A. E. Atia, "Coupling of Cylindrical Dielectric Resonators to Microstrip Lines," *IEEE/MTT-S International Microwave Symposium Digest*, June 1981, pp. 167-169.



Ali E. Atia received a B.S.E.E. from Ain Shams University (Cairo, Egypt), and an M.S.E.E. and a Ph.D. from the University of California at Berkeley. Prior to joining COMSAT in 1969, Dr. Atia held different research and teaching positions at both previously attended universities. As a Senior Scientist in the Microwave Laboratory at COMSAT Laboratories, he made significant contributions to several satellite programs including INTELSAT, ARABSAT, and AUSTRALIASAT. He was also responsible for implementing flight hardware on

COMSAT's NASA ATS-F Propagation Experiment and the COMSTAR Beacon Experiment. He is presently a Senior Director of Satellite System Design for INTELSAT Technical Services responsible for directing the system design analysis and evaluation activities of current and future satellite systems for use by INTELSAT. He is a Senior Member of IEEE.

René R. Bonetti received a B.S. in electrical engineering from Maua Institute of Technology (Sao Paulo, Brazil), an M.S. from the Institute for Space Research (INPE), and a Ph.D. from the Technological Institute of Aeronautics (both in electrical engineering). Prior to joining COMSAT Laboratories in 1981, he worked on microwave integrated circuit design and development at INPE from 1972 to 1979. From 1979 to 1981, he worked for INTELSAT at the Microwave Circuits Department of COMSAT Laboratories. He is presently a Staff Scientist in the Advanced Microwave Techniques Department of COMSAT Laboratories, where he is involved in the development of dielectric resonator filters, multiplexers, and oscillators.



Analysis of throughput efficiency and delay in ARQ systems

D. M. CHITRE

(Manuscript received June 26, 1981)

Abstract

The concept of user-related delay associated with automatic-repeat-request (ARQ) protocols is defined. An exact analytical expression for delay is obtained for the selective-repeat ARQ system with infinite buffer. The ARQ scheme which is a hybrid mixture of go-back- N and selective-repeat is examined. Analytical expressions for throughput efficiency and delay are derived for this hybrid system as well as for go-back- N and the selective-repeat ARQ system with finite buffer size. The performance of each technique is compared for various bit error rates, block sizes, and channel capacities.

Introduction

Error control systems for reliable digital data transmission can be broadly divided into two categories: (1) forward error correction (FEC) systems using error-correcting codes, and (2) ARQ systems using error-detecting codes and error correction by retransmission. In the current state of technology, error protection provided by the ARQ systems is orders of magnitude better than that obtained with FEC systems. Thus, ARQ is the most commonly used scheme for error control in a data communications system whenever a feedback channel is available.

There are three basic types of ARQ systems: stop-and-wait, go-back- N , and selective-repeat. In the first, the transmitter sends a data block,

encoded for error detection, to the receiver and waits for an acknowledgment before sending the next block or retransmitting the same block. This system is inherently inefficient because of the idle time spent waiting for an acknowledgment for each transmitted data block. It gives very low throughput for data communications via satellite. In go-back- N ARQ, data blocks are transmitted in an interleaved manner. When a data block is negatively acknowledged, the transmitter backs up to the data block and resends that block and succeeding blocks. Go-back- N ARQ and its variations are more efficient than stop-and-wait ARQ [1]–[5]; however, they require relatively low bit error rates. Performance becomes degraded at higher bit error rates for channels with high data rates or large round-trip delays as in satellite channels. The throughput efficiency drops rapidly as the channel error rate increases. For example, in go-back- N ARQ, the efficiency is less than 10 percent for channel capacities greater than 1 Mbit/s and for bit error rates higher than 10^{-5} . This inefficiency, which is caused by the rejection of possible error-free data blocks by the receiver and their transmission following an erroneous data block, can be overcome to a varying degree in the selective-repeat system.

In an idealistic infinite buffered selective-repeat ARQ, the transmitter resends only those data blocks that are negatively acknowledged. Then throughput efficiency is given by $1 - B$, where B is the block error probability. However, with finite buffers, successfully transmitted blocks can be lost because of receive buffer saturation; in this case, an implementable selective-repeat ARQ is required. The net consequence is that some redundancy can occur, which lowers the performance from the idealized infinite buffer case. With a finite buffer and any ARQ scheme involving either selective reception or transmission, the probability of successful transmission and reception of a data block depends upon the past history of that data block and those preceding it.

Recent work by Easton [6] analyzing selective-repeat ARQ assumes that a retransmitted data block always arrives error-free at the receiver. This is not consistent with the random distribution of channel errors. In Yu and Lin's analysis [7], an artificial inferior system is constructed which operates with help from a "genie." The transmitter resends the erroneous data blocks before the negative acknowledgments arrive, since the genie knows which data blocks were originally transmitted erroneously. The approach taken here is to focus on a randomly chosen data block and trace its history to find the average number of transmissions needed for successful transmission and reception. The

assumptions used here are explicitly related to the past history, and as a result, the bounds obtained for throughput and delay can be readily improved.

This paper develops a realistic model for selective-repeat protocol which considers the implication of finite buffering. The modifications to selective-repeat ARQ introduced to avoid buffer overflow are feasible to implement. First, a hybrid ARQ scheme is considered which consists of go-back- N transmission and selective reception. This system is designed for buffers of size N and improves the performance given by go-back- N ARQ without the full complexity of selective-repeat ARQ implementation logic. Next, selective-repeat ARQ is analyzed with both infinite and finite buffering. Throughput efficiency and delay are computed for each of the ARQ schemes. The concept of delay is closely tied to the user and is defined as the total delay incurred in delivering the data block to the user after it leaves the transmitter. This delay consists of D_0 , the transmission and propagation time for a data block, and D_1 , the possible delay resulting from retransmission of that data block and those preceding it. The delay, D_1 , will be referred to as the ARQ delay. In selective-repeat ARQ, it occurs first because of retransmission of an erroneous block, and second, because the data blocks must be delivered to the user in sequential order. Thus, a data block, even after arriving error-free at the receiver, will be held up in the buffer until all preceding data blocks are received error-free.

In go-back- N ARQ, the delay is directly related to the number of retransmissions and hence to the throughput. If B is the block error probability, and $N - 1$ data blocks are sent during the time interval between the transmission of a data block and the receipt of its acknowledgment, then the average number of times a block must be retransmitted before delivery to the user is known [1] to be $NB/(1 - B)$, and the throughput efficiency, η , is

$$\eta = \frac{1}{1 + NB/(1 - B)} \quad (1)$$

In go-back- N ARQ, if a block is retransmitted k times, then

$$D_1 = kd$$

where d is the time interval between two consecutive transmissions of the same block. (It is essentially the round-trip time needed to receive the acknowledgment.) Thus, the average delay, D , is

$$D = D_0 + \frac{NB}{1 - B} d \quad (2)$$

In deriving equation (1), it was assumed that a data block is found to be in error at the time of its expected arrival at the receiver. This would not always be the case, since the loss of a data block would not be detected until the next data block arrives. The expression for throughput in that case has been computed by Kaul [2], and differs slightly from equation (1).

Go-back-N transmission and selective reception

In the conventional go-back-N ARQ system, the $N - 1$ received data blocks following an erroneously received block are discarded regardless of whether they are received successfully. This results in a significant reduction in throughput efficiency and increased delay as the channel error rate increases. This paper considers an ARQ scheme in which the transmission is still go-back-N, and hence simple to implement, but the reception of data blocks is selective. Thus, more complex logic is required at the receiver buffer, which is activated whenever an erroneous block is detected; and a negative acknowledgment (NACK) is sent to the transmitter. In this scheme, however, the $N - 1$ succeeding blocks are checked for errors and the successful ones are stored in the buffer. After receiving a NACK, the transmitter backs up to the negatively acknowledged data block and retransmits it and $N - 1$ succeeding blocks. The data blocks are sent to the user in sequential order as soon as one or more contiguous error-free blocks are found without any missing blocks.

The following analysis assumes that the transmitter always has a data block to send, and that it transmits a block every t seconds. If d is the round-trip time (time to receive the acknowledgment), then N and d are related by the following expression:

$$(N - 1)t \leq d < Nt$$

Consider a data block "X," which is being transmitted for the first time at time T seconds. Suppose that l_1 out of N data blocks sent at the times $T - (N - 1)t, T - (N - 2)t, \dots, T - t, T$, have not been received successfully at the receiver (see Figure 1). The probability of that event is

$${}^N C_{l_1} \cdot B^{l_1} \cdot S^{N - l_1} \quad (3)$$

where $S = 1 - B$. The above expression does not consider the past history of the $N - 1$ data blocks sent in the current cycle at times $T - (N - 1)t, T - (N - 2)t, \dots, T - 2t, T - t$. Since some of these blocks could have been sent successfully prior to $T - (N - 1)t$, equation (3) will produce a lower bound for the throughput of the system and an upper bound for the delay.

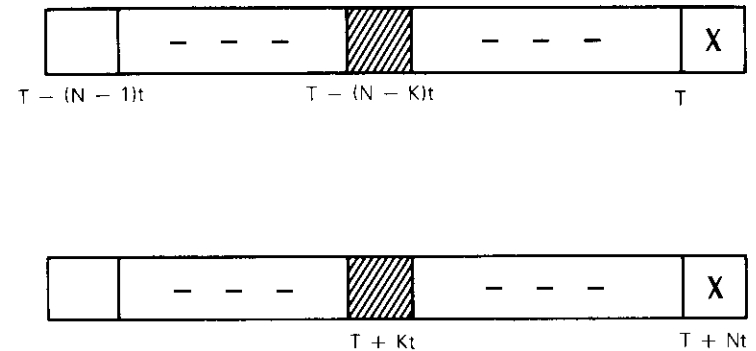


Figure 1. Retransmission of Data Block X because of an Error in a Preceding Block in the Hybrid ARQ System

The data block X is sent only once if $l_1 = 0$. The probability of that event is then given by

$$P(1) = S^N \quad (4)$$

It is sent twice if l_1 is nonzero, and during the next cycle where data blocks are sent at $T + t, T + 2t, \dots, T + (N - 1)t, T + Nt$; the unsuccessful blocks from the previous cycle are sent error-free (see Figure 1). Thus, the probability that the data block X is sent twice is

$$P(2) = \sum_{l_1=1}^N {}^N C_{l_1} \cdot B^{l_1} \cdot S^{N - l_1} \cdot S^{l_1} = S^N [(1 + B)^N - 1] \quad (5)$$

The data block X will be sent n times if $n - 1$ retransmissions are

required to clear the l_i errors. The probability of this condition will be given by

$$\begin{aligned}
 P(n) &= \sum_{l_1=1}^N \sum_{l_2=1}^{l_1} \cdots \sum_{l_{n-1}=1}^{l_{n-2}} {}^N C_{l_1} B^{l_1} S^{N-l_1} \\
 &\quad \cdot {}^{l_1} C_{l_2} B^{l_2} S^{l_1-l_2} \cdots {}^{l_{n-2}} C_{l_{n-1}} B^{l_{n-1}} \\
 &\quad \cdot S^{l_{n-2}-l_{n-1}} \cdot S^{l_{n-1}} \\
 &= S^N [(1 + B + B^2 + \cdots + B^{n-1})^N \\
 &\quad - (1 + B + B^2 + \cdots + B^{n-2})^N] \tag{6}
 \end{aligned}$$

for $n \geq 2$. Thus, the average number of times the data block X is sent is

$$\begin{aligned}
 \bar{n} &= S^N \left\{ 1 + \sum_{n=2}^{\infty} n \left[\left(\frac{1 - B^n}{1 - B} \right)^N - \left(\frac{1 - B^{n-1}}{1 - B} \right)^N \right] \right\} \\
 &= \sum_{K=1}^N (-1)^{K+1} \frac{{}^N C_K}{1 - B^K} \tag{7}
 \end{aligned}$$

As in the go-back- N case, throughput efficiency, η , and delay, D , are then computed from \bar{n} as

$$\eta = \frac{1}{\bar{n}} \tag{8}$$

$$D = D_0 + (\bar{n} - 1)d \tag{9}$$

Selective-repeat

The conventional go-back- N ARQ system or its variations are inadequate for high channel error rate. The advantages of the scheme discussed in the previous section are that it is simple to implement on the transmission side, it needs a buffer of size N blocks at the receiver, and there is no buffer overflow. The simplicity, however, has been achieved at the expense of resending data blocks which may have already been sent successfully. The only way to avoid this problem is by the selective-repeat scheme with an infinite buffer available to store successfully transmitted blocks. The throughput of this system is

simply given by S , since the average number of times a block needs to be transmitted before it reaches the receiver is $1/S$. However, in contrast with the go-back- N transmission scheme, the delay experienced by the data block is not directly related to the average number of times a data block is transmitted. The delay arises because the receiver outputs the data blocks only in sequential order.

Selective-repeat ARQ with unlimited buffer

Consider a data block X transmitted for the first time at time T . The time interval from $T - (N - 1)t$ to T (including both end points) is defined as the first cycle. All data blocks transmitted during this cycle would sequentially precede X . If these blocks are received error-free, then the delay for the data block is D_0 , and the probability of that event is S^N . Now, suppose the K th data block sent at time $T - (N - K)t$ is received in error; then it will be retransmitted at $T + Kt$. Thus, the data block X will be delayed by $D_0 + Kt$, if the block retransmitted at $T + Kt$ is received error-free and, prior to this, all other data blocks sent during the first cycle have been received successfully. Notice that if l_1 blocks out of the first $K - 1$ blocks sent during the first cycle contain errors and if those blocks and the K th block are sent successfully in the first retransmission during the second cycle, the block X will still be delayed by $D_0 + Kt$. Thus, when the probabilities of all these events are included, the probability that the delay is $D_0 + Kt$ is given by

$$\begin{aligned}
 P(D_0 + Kt) &= \sum_{l_1=0}^{K-1} {}^{K-1} C_{l_1} B^{l_1+1} \cdot S^{N-l_1+D} \cdot S^{l_1+1} \\
 &= S^N \cdot B \cdot (1 + B)^{K-1} \tag{10}
 \end{aligned}$$

with $1 \leq K \leq N$.

Suppose that all the erroneous data blocks sent during the first cycle are not cleared in the transmission of the second cycle, but later during the third cycle. Let the last block to be cleared be transmitted at $T + Kt + Nt$ (see Figure 2). If l_1 blocks out of the first $K - 1$ blocks sent during the first cycle were in error, and if l_2 of them are still in error after retransmission during the second cycle, these l_2 blocks and the K th block (the shaded block in Figure 2) are sent successfully during the third cycle. Also, out of $N - K$ blocks sent during the first cycle after the K th block, m_1 blocks could be in error. These m_1 blocks would be sent successfully during the second cycle because the K th

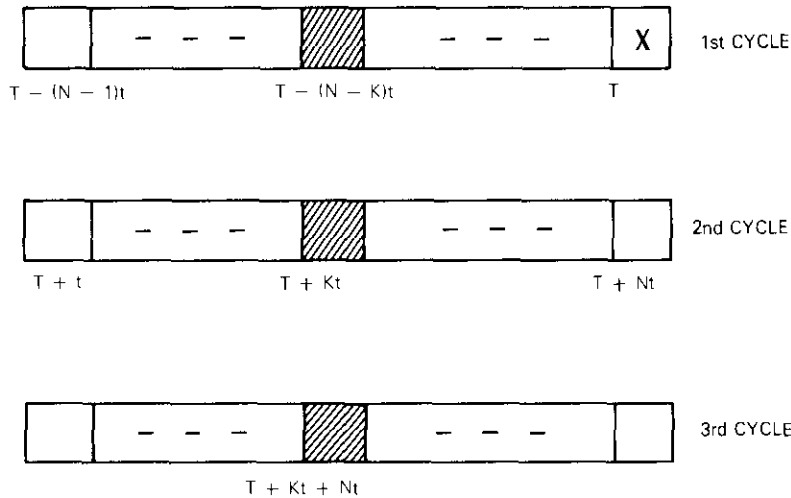


Figure 2. Repeated Errors in the Transmission of a Data Block Preceding Data Block X in the ARQ Scheme of Selective-Repeat with Infinite Buffer

block is the last one to be cleared during the third cycle. With the probabilities of all these events included, the probability that the delay is $D_0 + Nt + Kt$ is given by

$$\begin{aligned}
 P(D_0 + Nt + Kt) &= \sum_{l_1=0}^{K-1} \sum_{m_1=0}^{N-K} \sum_{l_2=0}^{l_1} {}^{K-l_1}C_{l_1} B^{l_1+1} \cdot {}^{N-K-m_1}C_{m_1} B^{m_1} \\
 &\quad \cdot S^{N-l_1-1-m_1} \cdot {}^{l_1}C_{l_2} B^{l_2+1} \cdot S^{l_1-l_2} \cdot S^{m_1} \cdot S^{l_2} \cdot 1 \\
 &= S^N \cdot B^2(1+B)^{N-K} \cdot (1+B+B^2)^{K-1} \quad (11)
 \end{aligned}$$

Equations (10) and (11) can be generalized to find the probability that the delay is $D_0 + nNt + KT$, which requires $n + 1$ retransmissions, and the K th block is cleared last during the $(n + 2)$ th cycle. The final expression can be derived in the same manner as equation (11), and is given by

$$\begin{aligned}
 P(D_0 + nNt + Kt) &= S^N \cdot B^{n+1} \cdot (1+B+\dots+B^n)^{N-K} \\
 &\quad \cdot (1+B+\dots+B^{n+1})^{K-1} \\
 &= S \cdot B^{n-1} \cdot (1-B^{n+1})^{N-K} (1-B^{n+2})^{K-1} \quad (12)
 \end{aligned}$$

where $1 \leq K \leq N$ and $n = 0, 1, 2, \dots$. The average delay is thus given by

$$\begin{aligned}
 D &= D_0 \cdot S^N + \sum_{n=0}^{\infty} \sum_{K=1}^N (D_0 + nNt + Kt) P(D_0 + nNt + Kt) \\
 &= D_0 + D_1
 \end{aligned}$$

where D_1 is the average delay associated with the selective-repeat ARQ system and is given as

$$\begin{aligned}
 D_1 &= \sum_{n=0}^{\infty} \sum_{K=1}^N (nNt + Kt) \cdot S \cdot B^{n+1} (1-B^{n+1})^{N-K} (1-B^{n+2})^{K-1} \\
 &= t \sum_{l=1}^N (-1)^l {}^N C_l \frac{B^{2l}}{1-B^l} \\
 &\quad + \frac{(N+1)t}{(1-B)} \sum_{l=1}^N (-1)^{l+1} \frac{{}^N C_l}{l+1} \cdot \frac{B^l(1-B^{l+1})}{1-B^l} \quad (13)
 \end{aligned}$$

Equation (13) is an exact expression for delay in a selective-repeat ARQ scheme with the availability of unlimited buffer. This "ideal" delay may be compared with average delays computed in the previous section for the go-back- N transmission/selective-reception system, and in the next section for selective-repeat with a finite buffer.

Selective-repeat ARQ with finite buffer

In reality, buffers are always finite; thus, in a selective-repeat ARQ scheme whenever a data block needs to be retransmitted a few times, buffer overflow occurs. Since the erroneous block is selectively retransmitted, the data blocks following it are transmitted sequentially and the successful data blocks among them must be stored until the erroneous block is received successfully. Therefore, with a finite size of the buffer at the receiver, there is a finite probability that some data blocks will be received successfully at the receiver and must be discarded for lack of buffer space. To compute the throughput efficiency and delay, the discard probability must be considered. However, the ARQ scheme could be modified so that no data blocks are discarded. Thus, if the available buffer size is greater than or equal to nN , but less than $(n + 1)N$, the selective transmission is changed so that any time a data block needs to be retransmitted for the n th time, it adopts

go-back- N transmission and selective reception. The data block and those following it which were transmitted in the previous cycle will be re-sent until the transmitter receives an ACK for that data block. Selective-repeat ARQ will be used as long as no block needs to be retransmitted more than $n - 1$ times. Note that the ARQ scheme has been adapted to eliminate any buffer overflow. As an example, the throughput efficiency and delay will be computed when a buffer of size $2N$ data blocks is available. The extension of this analysis for a larger size buffer is quite straightforward.

THROUGHPUT EFFICIENCY

Consider a data block X that is being sent for the first time at time T . This block is sent only once if it is not in error and none of the $N - 1$ blocks sent before X (during the first cycle as shown in Figure 3) need to be retransmitted for the second time (otherwise, the data block X will be re-sent during the second cycle). Thus, if l_1 blocks out

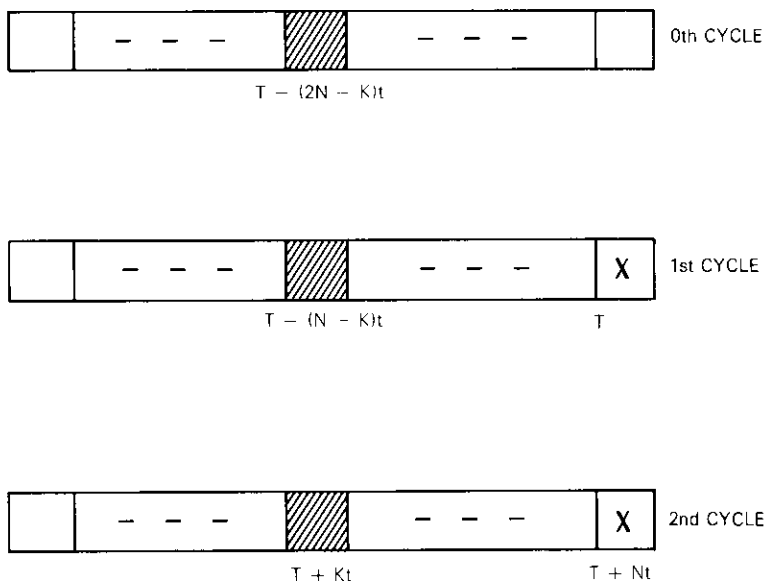


Figure 3. Retransmission of Data Block X Because of Two Retransmissions of a Data Block in the ARQ Scheme of Selective-Repeat with Finite Buffer

of these $N - 1$ blocks sent during the first cycle are in error, these must not be the repeat errors of blocks transmitted during the previous cycle (referred to as the 0 th cycle in Figure 3). For example, if the data block sent at $T - (N - K)t$ is erroneous, the corresponding block sent at $T - (2N - K)t$ during the previous cycle should be error-free; otherwise, this block must be retransmitted for the second time at $T + Kt$ during the second cycle. The probability of the above event is then given as

$$\sum_{l_1=0}^{N-1} {}^{N-1}C_{l_1} S^{l_1} \cdot B^{l_1} S^{N-l_1} = S^N(1 + B)^{N-1} \quad (14)$$

As in the previous section, the past history of the $N - 1$ blocks sent before the data block X is not considered. Since some of these blocks could have previously been sent successfully, the throughput efficiency will be a lower bound and the delay calculated with the same assumption will be an upper bound.

The data block X could be transmitted twice in two distinct ways: (1) if it is in error in the first transmission, and if l_1 out of $N - 1$ blocks transmitted before X during the first cycle are in error, and none of them is being retransmitted for the second time; and (2) if some of the l_1 blocks are repeat errors and hence during the second cycle, X will be retransmitted whether or not it was transmitted successfully during the first cycle. In both cases, all the blocks sent erroneously during the first cycle are transmitted successfully during the second cycle. Thus, the probability that block X is sent twice is given by

$$\begin{aligned} P(2) &= \sum_{l_1=0}^{N-1} {}^{N-1}C_{l_1} S^{l_1} \cdot B^{l_1} \cdot B \cdot S^{N-1-l_1} \cdot S^{l_1-1} \\ &+ \sum_{l_1=1}^{N-1} \sum_{l_0=0}^{l_1} l_1 C_{l_0} B^{l_0} S^{l_1-l_0} {}^{N-1}C_{l_1} B^{l_1} S^{N-1-l_1} \\ &\cdot S(1 + B) \cdot S^{l_1} \\ &= S^N[(1 + B)^N - (1 + BS)^{N-1}] \quad (15) \end{aligned}$$

By a similar argument, X is transmitted n times in two distinct ways: (1) if it is in error in the first transmission with no repeat errors occurring in the other $N - 1$ blocks, and the erroneous blocks in the first cycle get successfully sent in the next $n - 1$ cycles; and (2) if

some of the blocks sent during the first cycle are repeat errors and these blocks and block X are cleared during the next $n - 1$ cycles. The probability of this event can be calculated in the same manner as equation (15), and is given by

$$P(n) = S^N \{ (1 + B + \dots + B^{n-1})^N - (1 + B + \dots + B^{n-2})^N + [1 + BS(1 + B + \dots + B^{n-3})]^{N-1} - [1 + BS(1 + B + \dots + B^{n-2})]^{N-1} \}, \quad n \geq 3 \quad (16)$$

When the average number of transmissions is written as \bar{n} ,

$$\begin{aligned} \bar{n} &= \sum_{n=1}^{\infty} nP(n) \\ &= S^N [(1+B)^{N-1} - B^{N-1}] \\ &\quad + \sum_{k=1}^N {}^N C_k \frac{(-1)^{k+1}}{1-B^k} \\ &\quad + S^N (1+B)^{N-1} \sum_{k=1}^{N-1} {}^{N-1} C_k \frac{(-1)^k}{(1+B)^k (1-B^k)} \end{aligned} \quad (17)$$

and the throughput efficiency is given as

$$\eta = \frac{1}{\bar{n}}$$

DELAY

If all the data blocks sent during the first cycle from $T - (N-1)t$ to T seconds are received error-free, then the delay for block X is the delay, D_0 , and the probability of that event is S^N . Suppose that the K th data block transmitted at $T - (N-K)t$ is received in error and that this is not a repeat error, i.e., the data block sent at $T - (2N-K)t$ was sent successfully. The delay for block X will be $D_0 + Kt$, provided that none of the erroneous blocks sent during the first cycle before the K th block is a retransmitted block and all of them are sent successfully during the second cycle. Thus, the probability that the delay is $D_0 + Kt$ is given by

$$\begin{aligned} P(D_0 + Kt) &= \sum_{l_1=0}^{K-1} {}^{K-1} C_{l_1} \cdot S^{l_1+1} \cdot B^{l_1} \cdot S^{K-1-l_1} \\ &\quad \cdot B \cdot S^{N-K} \cdot S^{l_1+1} \\ &= S^N BS(1+BS)^{K-1}, \quad 1 \leq K \leq N-1 \end{aligned} \quad (18)$$

The delay would be $D_0 + Kt + Nt$, if some l_2 of the l_1 blocks and the K th block are in error in the second cycle, and are sent successfully in the third cycle. There is also the possibility that some m_1 blocks out of $N - 1 - K$ blocks sent after the K th block during the first cycle contained errors which were cleared in the second cycle. The probability that the delay is $D_0 + Nt + Kt$ is then given by

$$\begin{aligned} &P(D_0 + Nt + Kt) \\ &= \sum_{m_1=0}^{N-1-K} \sum_{l_1=0}^{K-1} {}^{N-1-K} C_{m_1} {}^{K-1} C_{l_1} S^{l_1+m_1+1} B^{l_1} \cdot B \cdot B^{m_1} \\ &\quad \cdot S^{K-(l_1+1)} \cdot S^{N-K-m_1} \\ &\quad \cdot \sum_{l_2=0}^{l_1} l_1 C_{l_2} B^{l_2} \cdot B \cdot S^{l_1-l_2} \cdot S^{m_1} \cdot S^{l_2+1} \\ &= S^{N+1} B^2 (1+BS)^{N-1-K} [1+BS(1+B)]^{K-1} \end{aligned} \quad (19)$$

The factor of $S^{l_1+m_1+1}$ guarantees that none of the errors in the blocks sent during the first cycle is a repeat error from the 0 th cycle.

When the above expression is generalized, the probability that the delay is $D_0 + nNt + Kt$ is given by

$$\begin{aligned} &P(D_0 + nNt + Kt) \\ &= S^{N+1} B^{n+1} [1+BS(1+B+\dots+B^{n-1})]^{N-1-K} \\ &\quad \cdot [1+BS(1+B+\dots+B^n)] \\ &= S^{N+1} B^{n+1} [1+B(1-B^n)]^{N-1-K} \\ &\quad \cdot [1+B(1-B^{n+1})]^{K-1} \end{aligned} \quad (20)$$

with $1 \leq K \leq N - 1$ and $n = 0, 1, 2, \dots$

For the above delays, the data block X is sent only once. Whenever the block X is sent twice or more, the delay involved will be $D_0 + nNt$, where n is the number of retransmissions. Thus, the probability of delay being $D_0 + Nt$ will be given by equation (15) and the probability of the delay being $D_0 + nNt$ will be given by $P(n + 1)$ from equation (16) for $n \geq 2$. Therefore, the average delay will be

$$\bar{D} = D_0 + D_1$$

where

$$\begin{aligned}
 D_1 &= \sum_{n=0}^{\infty} \sum_{k=1}^{N-1} (nNt + Kt) P(D_0 + nNt + Kt) \\
 &+ \sum_{n=1}^{\infty} (nNt) P(n+1) \\
 &= Nt(\bar{n} - 1) + \sum_{k=1}^{N-1} F(B, N, t, K) \quad (21)
 \end{aligned}$$

where \bar{n} is the average number of times the data block X is sent, and

$$F = Nt(1 - B^2)^{N-1} \frac{(-1)^{k+1} N^{-1} C_k B^k (1 - B^{k+1})}{(K + 1)(1 + B)^k (1 - B^k)} \quad (22)$$

Numerical results

The finite expressions given in the previous sections for throughput and delay were numerically evaluated for data block sizes of 1 and 2 kbits. The round-trip delay, d , is assumed to be 600 ms. The number of 1-kbit data blocks (N) sent during one round-trip delay is given by 39, 154, and 927, which correspond to satellite channel capacity of 64 kbit/s, 256 kbit/s, and 1.544 Mbit/s, respectively.

Figures 4 to 7 show throughput efficiency as a function of bit error rate for the two block sizes and for increasing satellite channel capacity. The three curves in each figure are for go-back- N , the hybrid scheme of selective-reception and go-back- N transmission, and selective-repeat with finite buffer size. The fourth curve represents the hypothetical case of selective-repeat with an infinite buffer. Note that the hybrid scheme significantly outperforms go-back- N ARQ. The throughput for selective-repeat with a finite buffer approaches the throughput for selective-repeat with an infinite buffer for bit error rates less than 10^{-6} .

Figures 8 to 11 present the corresponding curves for the ARQ delay. Even in the selective-repeat with an infinite buffer case, the delay is very significant, of the order of several seconds for bit error rates greater than 10^{-4} . Again, the hybrid system produces considerably less delay than the go-back- N scheme for all ranges of bit error rates; and the delay for selective-repeat with a finite buffer case approaches the delay for selective repeat with an infinite buffer for bit error rates less

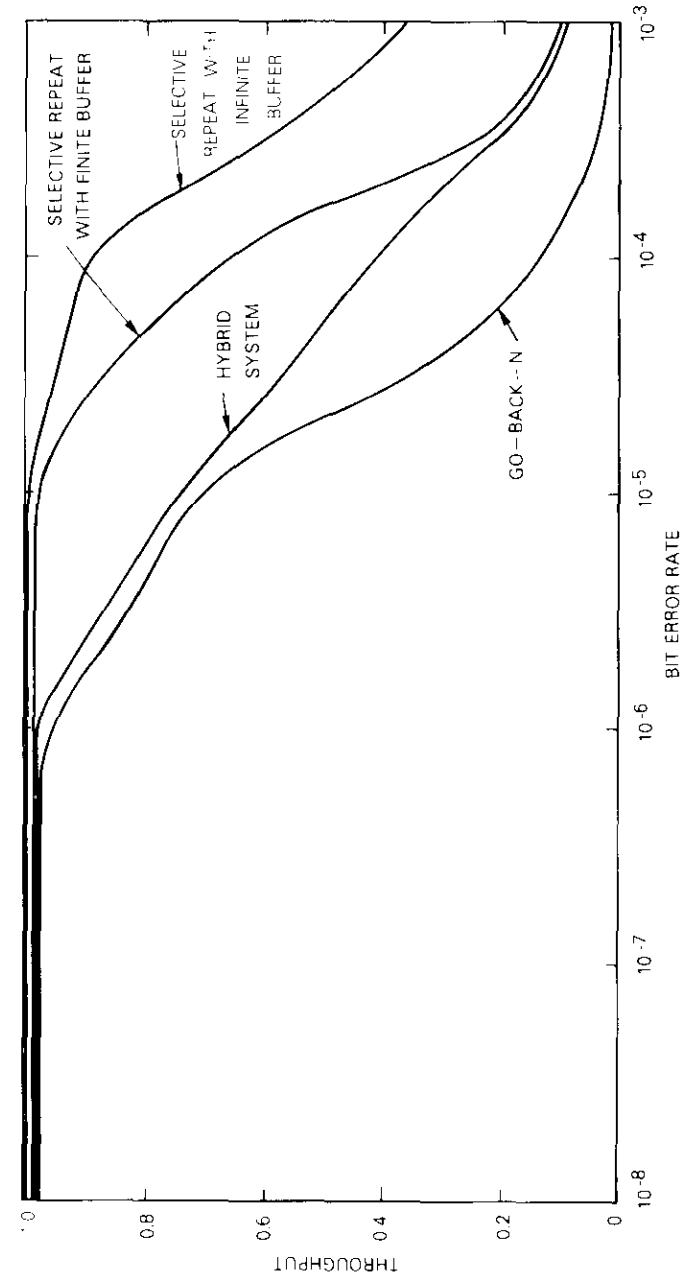


Figure 4. Throughput Efficiency with 1-kbit Block Size and 64-kbit/s Channel Capacity

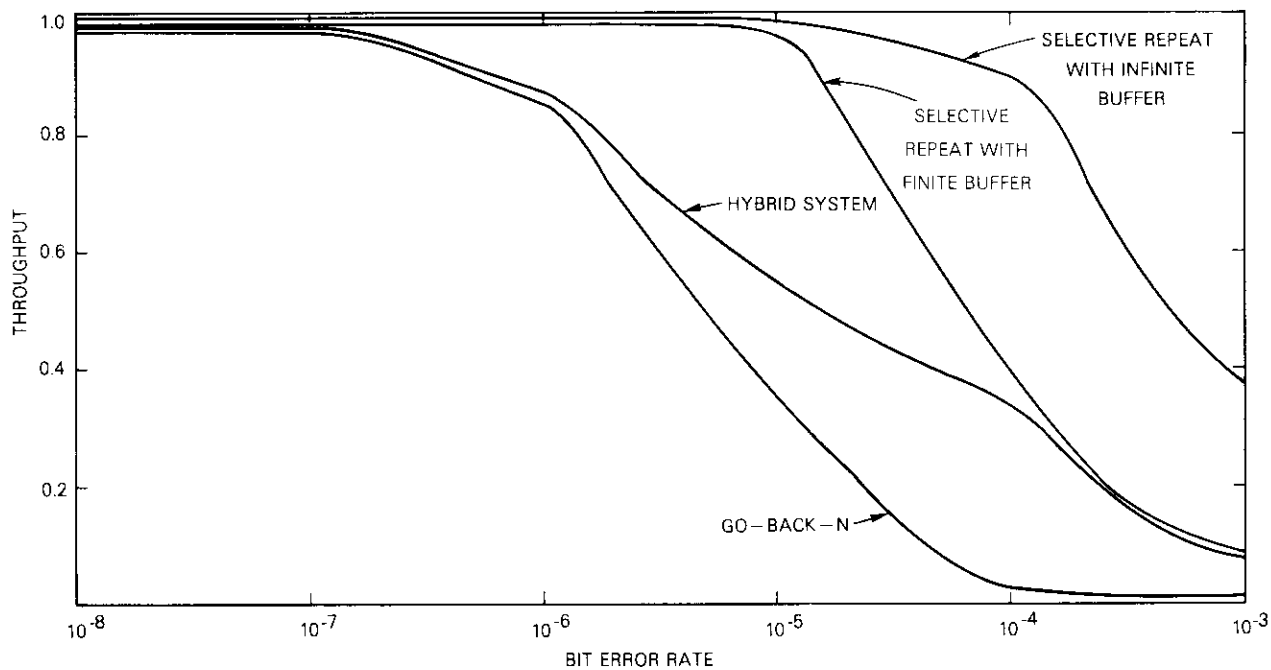


Figure 5. Throughput Efficiency with 1-kbit Block Size and 256-kbit/s Channel Capacity

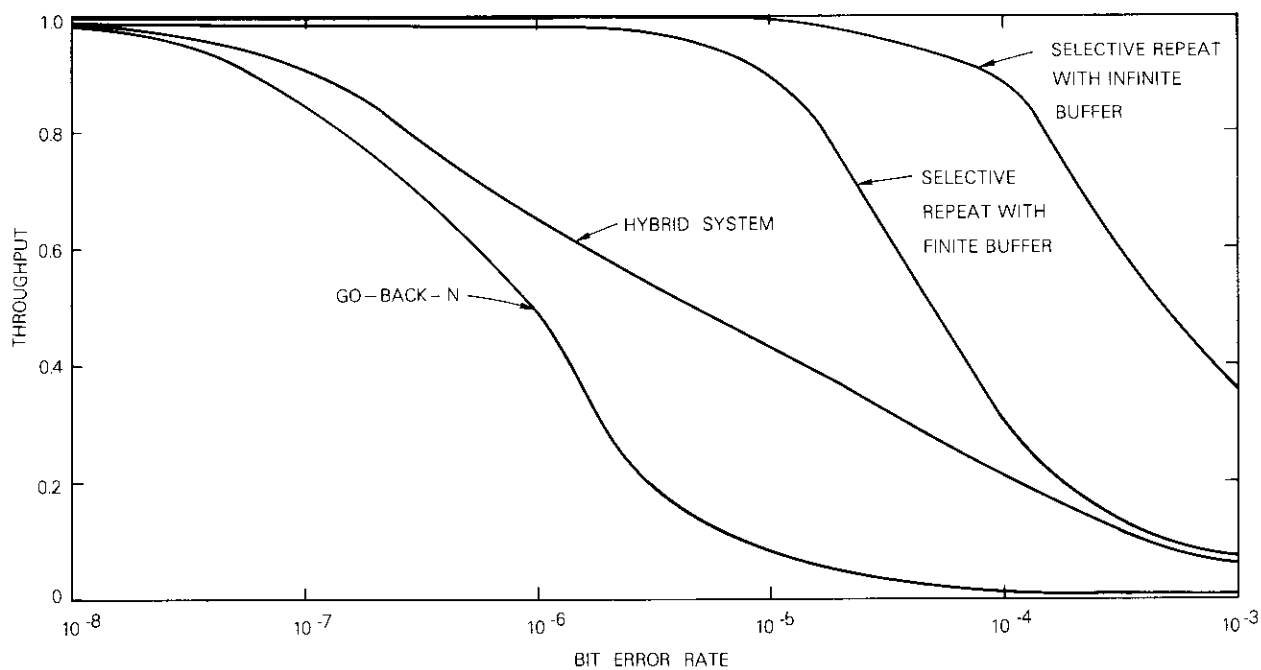


Figure 6. Throughput Efficiency with 1-kbit Block Size and 1.544-Mbit/s Channel Capacity

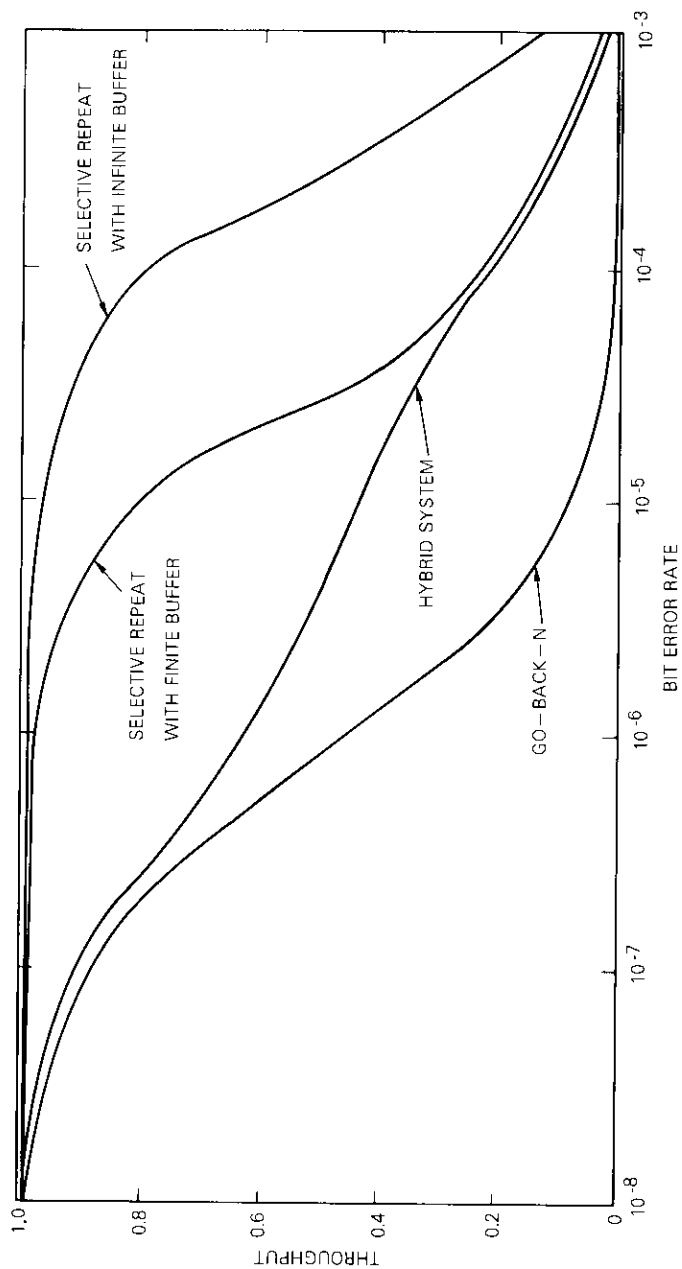


Figure 7. Throughput Efficiency with 2-kbit Block Size and 1.544-Mbit/s Channel Capacity

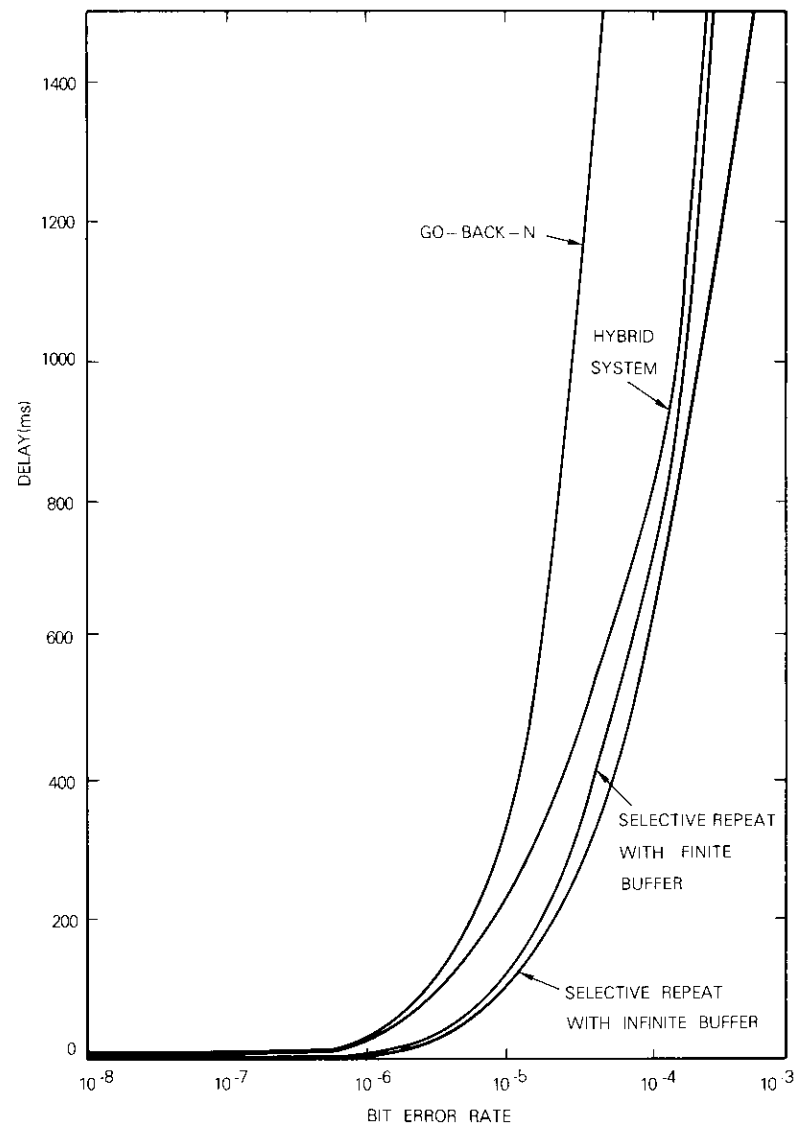


Figure 8. ARQ Delay with 1-kbit Block Size and 64-kbit/s Channel Capacity

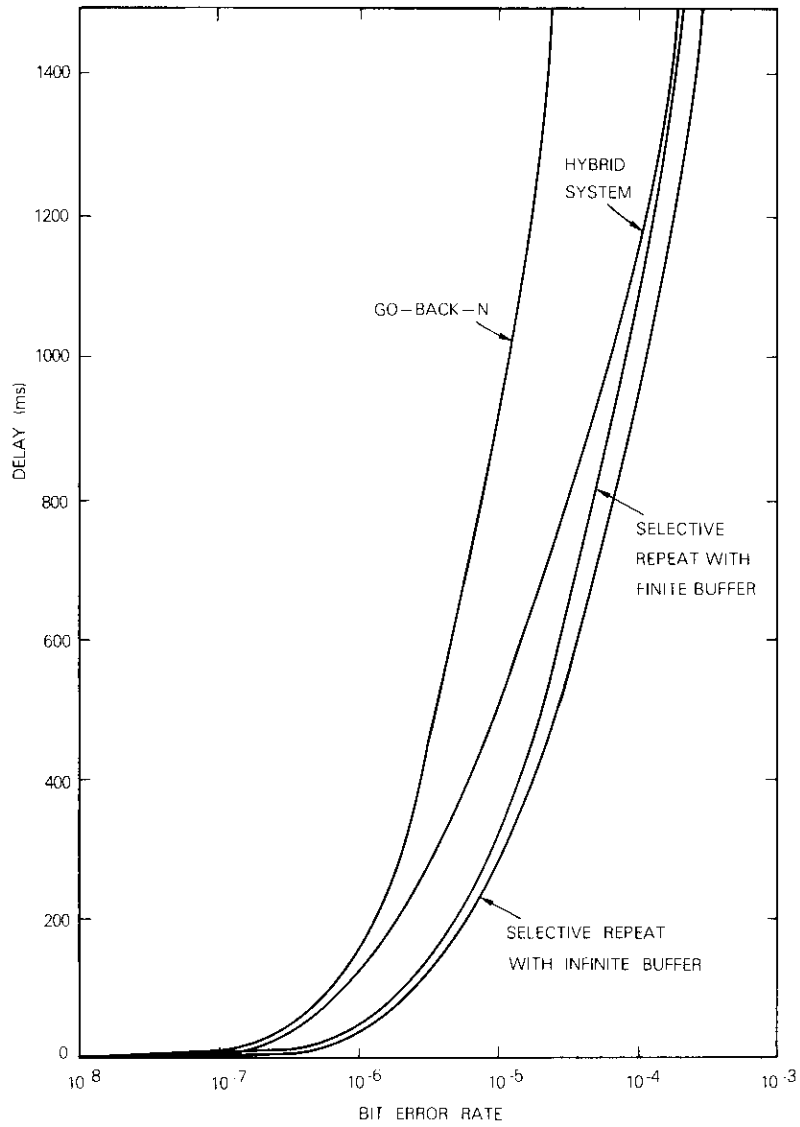


Figure 9. ARQ Delay with 1-kbit Block Size and 256-kbit/s Channel Capacity

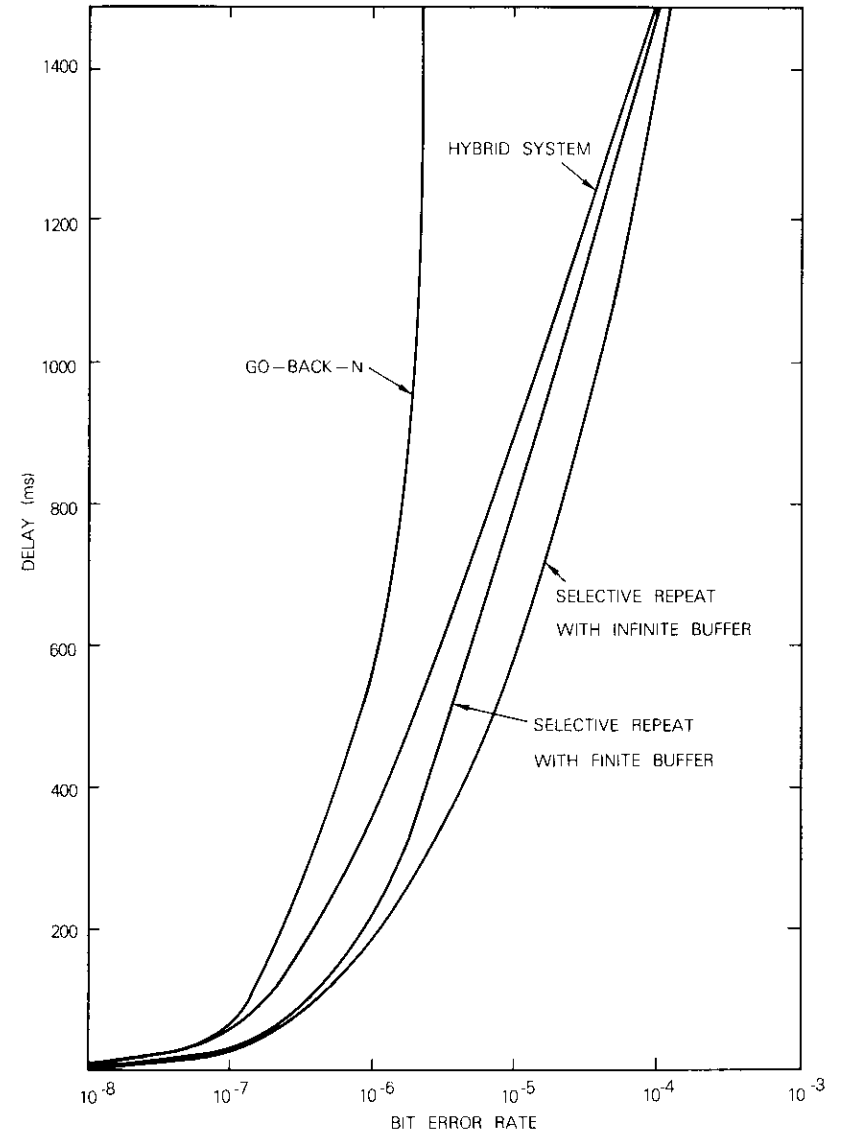


Figure 10. ARQ Delay with 1-kbit Block Size and 1.544-Mbit/s Channel Capacity

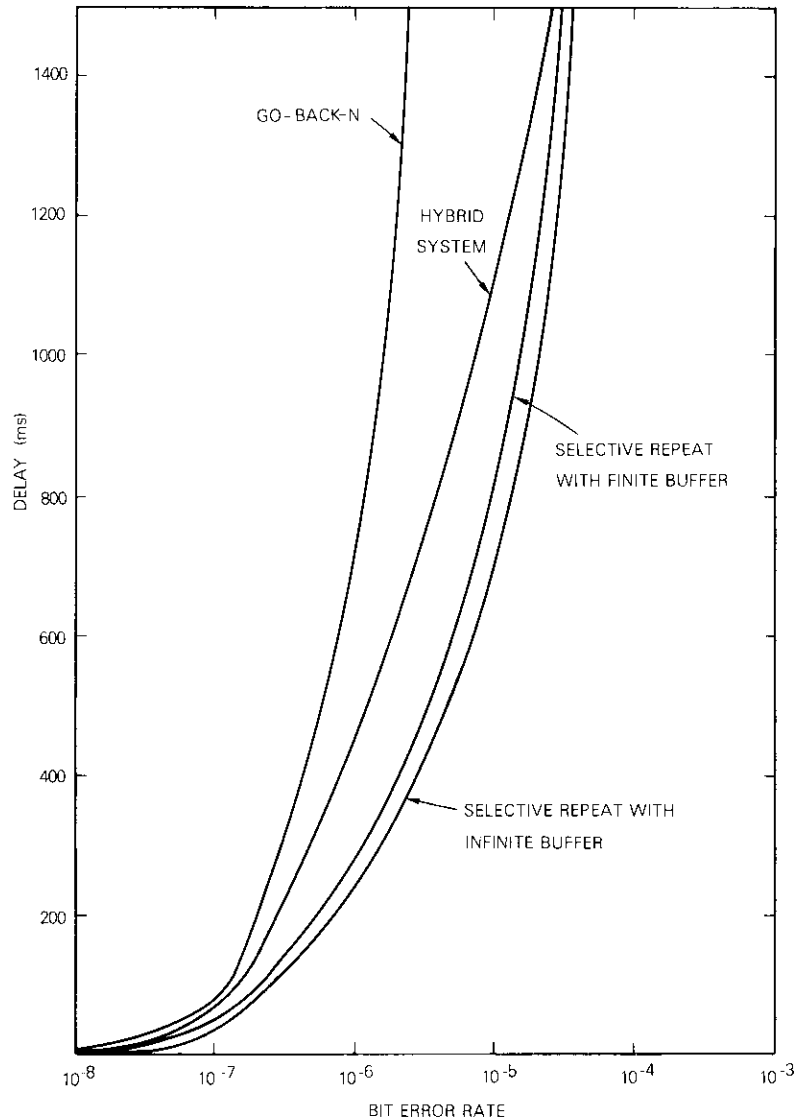


Figure 11. ARQ Delay with 2-kbit Block Size and 1.544-Mbit/s Channel Capacity

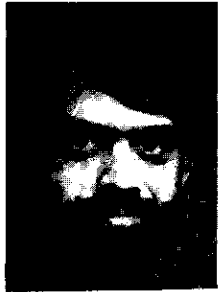
than 10^{-5} . Since a particular ARQ scheme would be selected based on the grade-of-service requirement for both the throughput efficiency and the ARQ delay, and the complexity of the implementation, Figures 4 to 11 would facilitate this choice.

Acknowledgments

The author is indebted to Dr. A. K. Kaul and Dr. W. L. Cook for numerous helpful discussions and to Mr. S. J. Donnelly of the Computer Center for his assistance.

References

- [1] H. O. Burton and D. D. Sullivan, "Errors and Error Control," *Proc. IEEE*, Vol. 60, November 1972, pp. 1293-1301.
- [2] A. K. Kaul, "Performance of HDLC in Satellite Communications," *COMSAT Technical Review*, Vol. 8, No. 1, 1978.
- [3] A. R. K. Sastry, "Improving Automatic Repeat-Request (ARQ) Performance on Satellite Channels Under High Error Rate Conditions," *IEEE Transactions on Communications*, Vol. COM-23, April 1975, pp. 436-439.
- [4] J. M. Morris, "On Another Go-Back-N ARQ High Error Rate Conditions," *IEEE Transactions on Communications*, Vol. COM-26, January 1978, pp. 187-189.
- [5] S. Lin and P. S. Yu, "An Effective Error Control Scheme for Satellite Communications," *IEEE Transactions on Communications*, Vol. COM-28, March 1980, pp. 395-401.
- [6] M. C. Easton, "Batch Throughput Efficiency of ADCCP/HDLC/SDLC Selective Reject Protocols," *IEEE Transactions on Communications*, Vol. COM-29, February 1980, pp. 187-195.
- [7] P. S. Yu and S. Lin, "An Efficient Selective-Repeat ARQ Scheme for Satellite Channels and Its Throughput Analysis," *IEEE Transactions on Communications*, Vol. COM-29, March 1981, pp. 353-363.



Dattakumar M. Chitre received a B.Sc. in mathematics from the University of Bombay, India, an M.A. in mathematics from Cambridge University, U.K., and a Ph.D. in physics from the University of Maryland. Dr. Chitre joined COMSAT Laboratories in 1980 as a member of the technical staff in the Transmission Systems Laboratory, and is currently involved in investigations of packet communications in the Systems Technology Division. He is a member of the International Astronomical Union.

Index: computer, communications, satellite networks, synchronization, small earth terminals

Frequency and time coordination via satellite

L. VEENSTRA, J. KAISER, C. COSTAIN,
W. KLEPCZYNSKI, AND D. ALLAN

(Manuscript received January 22, 1981)

Abstract

During 1978 and 1979, COMSAT Laboratories participated in an experiment of frequency and time synchronization via satellite. This paper describes COMSAT's efforts to assist with time synchronization experiments conducted by the United States Naval Observatory (USNO), Washington, D.C.; the National Bureau of Standards (NBS), Boulder, Colorado; and the National Research Council of Canada (NRC). The experiments were performed via the Communications Technology Satellite (CTS), using two small 2.4-m earth terminals operating in the 12/14-GHz bands. These terminals were colocated with the master time scales at USNO and NBS. This paper also describes a new application of PSK data transmission to the problem of standard synchronization.

To synchronize the master time scales (primary time standards) so that uncertainties are less than 5 ns, transmission speeds of 1 Mbit/s BPSK have been demonstrated to be practical. For the coordination of less demanding frequency and time standards, such as commercial atomic clocks, potentially useful results have been demonstrated with PSK transmission data rates of 50 and even 25 kbit/s. Additional work is indicated to improve the methods and equipment for clock synchronization, and for comparison of time and frequency standards, as well as for spacecraft ranging.

Introduction

COMSAT's participation in an experiment of frequency and time synchronization using the Communications Technology Satellite (CTS)

[1] was intended to demonstrate the advantages of employing small (2.4-m) satellite earth terminals operating at 12/14 GHz at the site of the master time scales. Prior to COMSAT's participation, the experimenters transported clocks from the master time scale locations to larger fixed earth terminals for the duration of the experiment. These clocks were then returned for recomparison to determine their drift. This process introduced inaccuracies that were unacceptable, and the cost of transporting the clocks was relatively high.

In addition to providing small earth terminals at the master time scale sites, COMSAT introduced a digital transmission format to replace the FM analog video format used at the larger earth terminals. This application of digital communications techniques and theory to the time and frequency coordination problem may enable development of a commercially viable frequency coordination and time synchronization system via satellite.

The experiments described in this paper were primarily applicable to the synchronization of master time scales with frequency uncertainties of one or two parts in 10^{14} . COMSAT's long-term goal is to develop time and frequency synchronization methods that can also satisfy less demanding satellite communications applications for which frequency standard uncertainties of one to two parts in 10^{12} are acceptable; the cost of the system must also be economical in terms of satellite resources and earth terminal equipment.*

The use of the time transfer process to synchronize frequency standards that are typically used for communications (one part in 10^{12} accuracy) must provide uncertainties of no more than 50 ns. Such frequency uncertainty between standards would produce a possible drift of their dependent time scales of 10^{-12} s/s \times 86,400 s/day = 86 ns/day. Therefore, a daily time transfer to 50-ns uncertainty would allow frequency coordination to the specified accuracy.

Currently available one-way satellite broadcast methods for clock synchronization can achieve uncertainties of about 1 ms. For these systems, uncertainties are limited by the inaccuracy of onboard satellite oscillators, the bandwidth of the broadcast circuit, and the uncertainty in the satellite-to-user path length.

The term "time transfer" refers to the process of measuring the difference between the indicated time of day of a distant clock and a

*An immediate economy can be realized in the equipment if the requirement is only to coordinate frequency and not absolute time between sites.

master time scale [2]. One classic method of time transfer is to physically carry a portable clock between the two locations. This clock is synchronized with the primary time scale prior to its departure, and then serves as the master clock against which the distant clock is compared. The transportable clock is resynchronized on its return to determine the drift and to compute the probable error at the time that the distant clock was synchronized. A frequency coordination can be made with two or more time transfers between standards by measuring the relative drift rate of the time scales, that is, their frequency difference.

Background

A master time scale typically consists of an ensemble of Hewlett Packard 5060 series cesium standards. The frequency uncertainty in such a standard is about four parts in 10^{13} . The ensemble frequency uncertainty can be as low as one or two parts in 10^{14} , which corresponds to time drift rates of approximately 1 ns/hr for individual clocks and 5-6 ns/day for the ensemble. Loran C may be used to maintain synchronization of widely separated clocks to within 1 μ s. It is possible to compare clocks by carrying a portable clock between sites, which may result in uncertainties as low as 0.2 μ s. Two-way satellite synchronization has already demonstrated a significant improvement over these standard techniques.

Two-way satellite time transfer

Two-way time transfer is a cooperative exchange of local time of day (TOD) to determine any difference between the TOD generated by two clocks. The offset, T , is defined by the difference in the local TOD at two stations (A and B):

$$T = TOD_A - TOD_B \quad (1)$$

If the oscillator frequencies on which the local time scales are based are not exactly the same, then successive measurements of T will show a change in T with respect to the time of observation. The time of observation will be designated by X (in seconds) and will start at some convenient time of day (*i.e.*, $X = 0$). The relative drift rate of two time

scales is defined by the dimensionless quantity ϵ such that at times 1 and 2

$$\epsilon = \frac{T_1 - T_2}{X_1 - X_2} \quad (2)$$

The value ϵ is equal to the inverse of the relative frequency offset of the frequencies on which the two time scales are based and will indicate the drift rate between the two scales. It will be assumed that ϵ is constant over the range of X being used. Therefore, the measurement $T(X)$ can be expressed as a linear function in X . Thus,

$$T(X) = T_0 + \epsilon X \quad (3)$$

can be used to determine T , the time offset, at any time after the reference start time of day (when $X = 0$). The offset at this time is T_0 . If the two clocks under test are colocated, T can be measured directly with just a time interval counter. The counter is started with the first clock's 1-pulse per second (1-pps) output and stopped with the second clock's 1-pps output. It is assumed the two clocks differ by less than 1 s, since this is the largest difference that can be measured using 1 pps. The accuracy of this direct measurement of T is limited by the resolution of the time interval counter, the repeatability of the trigger level settings of the interval counter, and the short-term phase noise of the oscillators controlling the two time scales.

Noise-free satellite link

If the two clocks are not colocated, the time interval counter must be connected between the clocks via a communications channel, and the stop trigger pulse originating at the distant clock must travel over this channel. The propagation delay will appear as an additional time offset if the measurement is attempted directly as described above. To avoid this problem, a two-way symmetric link via satellite can be used. Each earth station typically has an atomic (cesium) clock generating a pulse sequence of 1- μ pulses at a rate of 1 pps. At both stations, each pulse starts a time interval counter and is then sent through the satellite transmission channel (full-duplex operation between stations) to the opposite station. The received pulses are used to stop the time interval counters at each station. The time interval Y recorded by the two stations (A and B) will be

$$Y_A = T + ET_B + U_B + SC_A + D_A + ER_A \quad (4)$$

$$Y_B = -T + ET_A + U_A + SC_B + D_B + ER_B \quad (5)$$

where ET = equipment transmit time delay (the time required for a signal to travel from the time interval counter start input to the station antenna)
 ER = equipment receive time delay (the time required for a signal to travel from the station antenna to the stop input of the time interval counter)
 U, D = up-link and down-link propagation times, which are a function of the satellite range with respect to the particular station and the frequency used
 SC = internal propagation time of the satellite transponder at the frequency used.

The observed value of Y for two stations can be used to determine the offset, T , between the station time scales under the following conditions:

a. The total signal propagation time in both directions between the two stations must be equal:

$$U_B + SC_A + D_A \cong U_A + SC_B + D_B \quad (6)$$

b. The ground equipment delays should be known so that a constant (K) can be directly predicted, yielding

$$(ET_B + ER_A) - (ET_A + ER_B) = K \quad (7)$$

To satisfy condition (a), any inequality in equation (6) should be less than the uncertainties in the expected measurement made using the link. Based on equations (4) and (5), these conditions yield

$$T = \frac{Y_A - Y_B - K}{2} \quad (8)$$

Figure 1 shows a diagram of this process. If K is not known (*i.e.*, the terminal delays have not been measured), the absolute time offset cannot be measured. In this case, the frequency offset can be determined by repeated measurement of Y_A, Y_B if it can be assumed that the

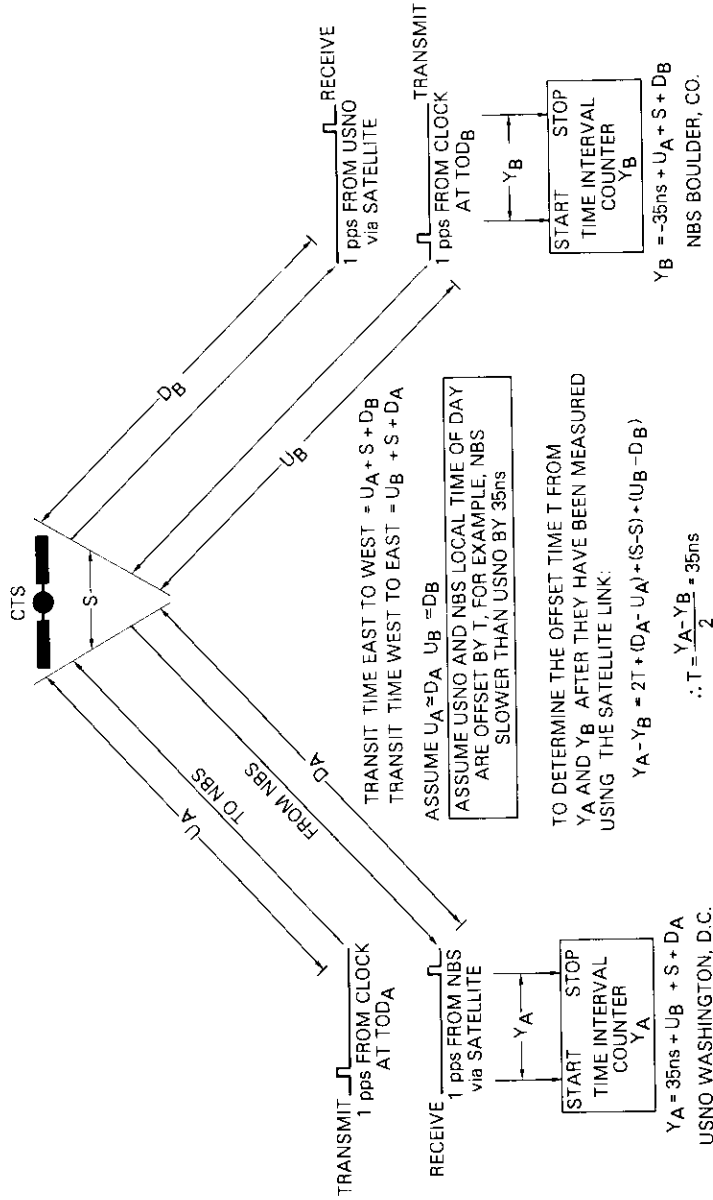


Figure 1. Time Transfer via Satellite

unknown value of K does not change between measurements. Thus, from equation (2),

$$\epsilon = \frac{(Y_{A1} - Y_{B1} - K) - (Y_{A2} - Y_{B2} - K)}{2(X_1 - X_2)} \quad (9)$$

$$\epsilon = \frac{(Y_{A1} - Y_{B1}) - (Y_{A2} - Y_{B2})}{2(X_1 - X_2)} \quad (10)$$

The frequency offset ($1/\epsilon$) can be determined by two measurements of Y_A, Y_B at different times. In most applications, it is not necessary to know the actual time offset between two sites that require a frequency coordination, which eliminates the need to measure K . Consequently, earth station instrumentation can be simplified significantly since the individual transmit and receive time delays are difficult to measure with nanosecond resolution.

Noisy satellite link

The previous methods must be modified when a single measurement of Y for each path is not sufficient to measure the absolute time offset with the desired accuracy. With a noisy communications channel, it is necessary to make repeated measurements of Y at each station to form a good statistical estimate. The process is complicated since the spacecraft is not perfectly stationary with respect to the earth stations. Thus, the observed time interval Y is a function of the time of observation. For relatively short periods of observation (500–1,000 s), $Y(X)$ can be modeled by a third-order power series [3]. The coefficients of this power series can be experimentally found by fitting a third-order curve to the result of repeated measurements of Y over a short period. The factors contributing to these coefficients can be analyzed by collecting the terms of equation (4) into three groups—the time base factors, the spacecraft and propagation delay, and the ground terminal delay:

$$Y(X) = T(X) + P(X) + E(X) \quad (11)$$

The time base term $T(X)$ has the components

$$T(X) = T_0 + \epsilon X \quad (12a)$$

The propagation and spacecraft transmission time delay can be approximated by a third-order power series:

$$P(X) = P_0 + P_1X + P_2X^2 + P_3X^3 \quad (12b)$$

Since the earth station equipment delays are fixed:

$$E(X) = ET + ER = A \quad (12c)$$

If the three factors are substituted in equations (12a)–(12c) and collected

$$Y(X) = (A + T_0 + P_0) + (P_1 + \epsilon)X + P_2X^2 + P_3X^3 \quad (13)$$

Typical frequency standard offsets (ϵ) are 10^{-13} , while typical range rates (P_1) are greater than 10^{-8} seconds per second (s/s) or about 3 m/s. Since $P_1 \gg \epsilon$, equation (13) reduces to

$$Y(X) = (A + T_0 + P_0) + P_1X + P_2X^2 + P_3X^3 \quad (14)$$

The sign of T_0 at the A and B stations will be different. The fundamental assumption in two-way time transfer is that $P(X)$ will appear the same to both stations. Therefore, the A and B expressions of $Y(X)$ can be subtracted, as in equation (8), producing an expression for the time offset between the two station clocks in terms of the curves $Y(X)$ developed at each station from the observed data:

$$T_0 = \frac{Y_A(X) - Y_B(X) - K}{2} \quad (15)$$

where K is the difference in the terminal delays $A_A - A_B$, as in equation (7). If the fundamental assumption is valid, $T_0(X)$ will not contain significant terms X^N with $N > 1$. This will not be the case if the A and B transponder paths have significantly different time delays or if the relative spacecraft motion with respect to the ground stations cannot be accurately modeled by $Y(X)$ of the order used.

High-speed data collection

In a typical time transfer situation, the relative time between two standard clocks is known to better than 500 ns. This knowledge can be used to increase the rate of data collection beyond the one data point per second obtained using 1 pps without introducing ambiguity due to the path length. If the period between pulses is less than the

propagation time over the satellite link ($\cong 250$ ms), an uncertainty as to the true path length is introduced, since the received pulse used to stop the time interval counter will not have originated at the same time as the starting pulse to the counter. For example, assume that a 1-MHz square wave is transmitted instead of the 1 pps and that the time interval counter is started on the rising transition of the transmitted signal and stopped on the next rising transition received from the second station. The path time measured will be less than actual path time (measured using 1 pps) by some integer number of microseconds, since the time interval counter will never wait more than $1 \mu\text{s}$ for a stop transition. Since the true clock offset is known to within $0.5 \mu\text{s}$, no ambiguity is introduced by measuring the path time modulo by the transmission rate.

The advantages of high-speed data collection are apparent if the process is considered in terms of the standard deviation for each second of data.

If N independent samples (X) are made of a random population with a mean of μ , a variance of σ^2 , and a normal probability distribution, the sample mean and sample variance will be approximately μ and σ^2 , respectively; this is the case provided that N is sufficiently large, typically greater than 30. However, as demonstrated in Reference 4, if each N sample set is averaged to form a single new statistic \bar{X} such that

$$\bar{X} = \frac{X_1 + X_2 + \cdots + X_N}{N}$$

the mean $\mu_{\bar{X}}$ will be equal to μ and the new sample variance will be

$$\sigma_{\bar{X}}^2 = \frac{1}{N^2} (\sigma_{x_1}^2 + \cdots + \sigma_{x_N}^2) = \frac{\sigma^2}{N}$$

Therefore, the standard deviation of a large number of such N averaged samples will be σ/\sqrt{N} . The sample standard deviation is a useful measure of the quality of a particular link for time transfer service.

For example, if a particular link transmitting 1 pps has a 15-ns standard deviation, increasing the rate to 1,000 pps (without otherwise changing the character of the link) and averaging 1,000 samples to generate one statistic per second will result in a 0.47-ns standard

deviation. The gain can be even greater if the individual samples are not strictly independent but are drawn from a source containing periodic as well as random noise.

Data reduction technique

In an actual satellite time transfer, the observed Y is recorded along with the time of day at which the interval counter was started. Typically, one point per second is recorded during the observation period. Later, the observed values of Y (Y_i where $i = 1$ to N , the total number of observations) and the time of day are processed as an estimate of the path length by fitting a polynomial of X (the time of day in seconds) to the data set by the method of least squares. The accuracy of the resulting polynomial is measured by calculating the standard deviation, sigma (σ), from the difference of the observed points (Y_i) and the fitted curve $Y(X)$, or the "goodness of fit":

$$\sigma = \frac{\left(\sum_{i=0}^N [Y_i - Y(X)]^2 \right)^{1/2}}{N - 1} \quad (16)$$

The data are filtered by discarding improbable values, those more than $\pm m\sigma$ from the fitted curve. If $m = 3$, there is a probability of less than 0.26 percent that a valid point is rejected. After the improbable data points have been removed, the coefficients of $Y(X)$ are recomputed from the remaining points and the test and discard process is repeated. The series of operations is iterated until no points are left outside the ($m\sigma$) window, as flowcharted in Figure 2. The quality for time transfer of the link under evaluation is measured by the value of sigma resulting from this process.

† If the errors observed on a link corrupted by white noise have the expected Gaussian distribution, filtering to a 3- σ bound would not have a significant effect on the uncertainty of the time transfer since the number of points removed would be low. However, for some types of links, mechanisms can produce bursts of errors lying outside a Gaussian distribution. Two examples have been observed in time transfer work: Threshold operation of an FM system, and PSK systems operating at low energy per bit to noise power density ratios. Under these conditions, the filtering can be used to include only the data points produced

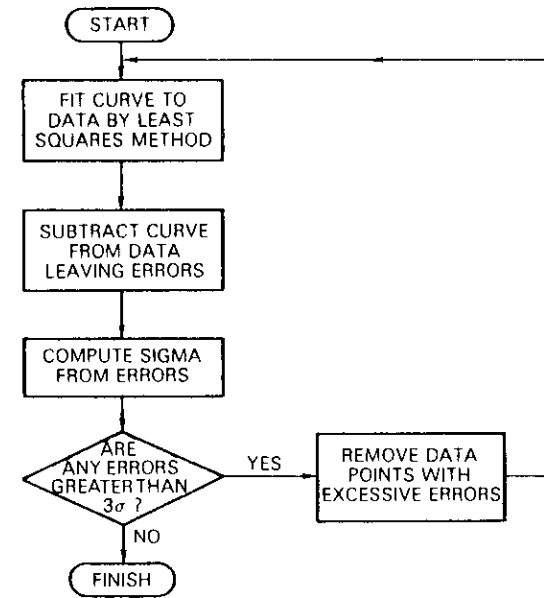


Figure 2. Data Reduction Algorithm

when the transmission system is well behaved, that is, producing errors with a Gaussian or normal distribution, allowing operation with a marginal link.

Ideally, the scatter of errors [$Y_i - Y(X)$] in the observed data will be random with a normal distribution. Plots of the scatter with respect to time can reveal any periodicity in the errors or other nonrandom effects in the system. In a well-designed time transfer system, the observed errors will be only random.

Wideband FM transmissions for time transfer tests using CTS (Hermes) and Symphonic satellites

Tests were conducted in a 3-station configuration between USNO, NBS, and NRC/CRC using the CTS (HERMES) satellite. The SYMPHONIE satellite was used for tests between Ottawa and Paris, France. Initially, a 1-pps signal was exchanged between pairs of participants. The transmission format was limited by the video modem equipment

available at the Canadian earth station which required that wideband FM be used with a transmission signal containing video sync pulses. The actual 1- μ s pulse was added to the synchronization signal to form a composite video signal for transmission. During some of the CTS experiments and in the continuing SYMPHONIE trials, the 1-pps signal was replaced with a 1-MHz signal. The format of the video is shown in Figure 3. The video baseband was limited to 4.2 MHz and the system RF bandwidth was typically 20 to 30 MHz. This system required an overall link budget of 87-dB Hz carrier-to-noise spectral density or a C/T of -141.6 dBW/K to remain above the FM threshold (13 dB) of the demodulators used for this experiment.

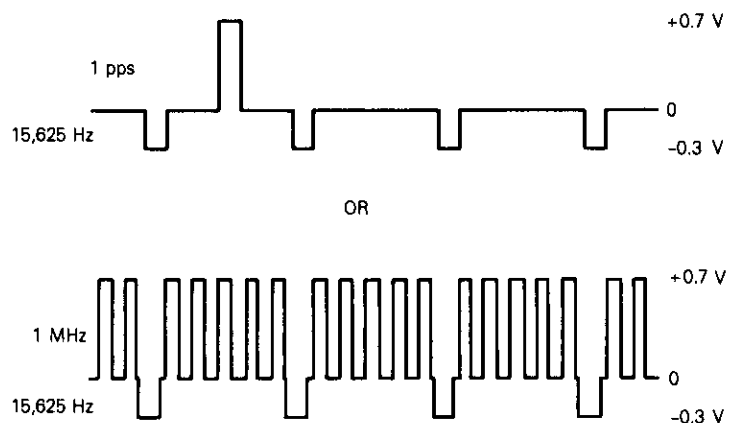


Figure 3. Modulation into the TV Video Satellite Terminal

A detailed report on the FM results and COMSAT's participation is contained in References 3 and 5. Typical results produced uncertainties in the 1-s measurements between 1.5 and 16 ns depending on the earth stations used. The 1-MHz signal combined with the use of a phase lock loop (PLL) tracking filter at the receiver has shown random errors (scatter) with less than 0.2-ns standard deviation. However, these accuracies are achieved at the expense of considerable satellite and earth station resources.

Use of PSK transmission for time and frequency transfer

The actual time transfer experiments conducted between American, Canadian, and French standard laboratories have used experimental

satellites which were made available without charge to the participants [CTS(HERMES) and SYMPHONIE]. The experiments required essentially full transponder service with a carrier-to-noise density ratio (C/N_0) of better than 87 dB Hz. A commercially viable time transfer system demands a more efficient transmission method. The use of PSK in this discussion does not refer to a spread spectrum system in which system timing is recovered by correlation techniques. Considerable work has been performed using spread spectrum for time transfer work, but this technique was not employed for the experiments reported in this paper. These experiments were conducted to evaluate the use of a communications type of PSK transmission, that is, using signals with an E_b/N_0 greater than zero at the "chip" or data clock rate, as compared to spread spectrum signals where the E_b/N_0 is typically less than zero at the chip rate [6].

Typical BPSK modem

The simplified diagram of a typical BPSK modem (Figure 4) shows the essential operations that relate to its use for time transfer. The clock from the data source generates a PN sequence which is modulo 2 added to the input data. The result is applied to the IF port of a double-balanced mixer. The mixer output is a phase-modulated ($\pm 90^\circ$) signal suitable for satellite transmission. The receiver coherently detects the BPSK signal to recover the randomized data stream. A PLL bit synchronizer recovers the original clock frequency. The presence of the PN sequence ensures that this circuit has sufficient transitions to function irrespective of the type of data being sent. The regenerated clock is used to produce an identical PN sequence that is synchronized to the one used in the transmitter. The sequence is again modulo 2 added to the data stream, and the original data are recovered, as shown in Figure 5. The PSK modem can be directly substituted for the video channel used in the wideband FM experiments to transmit 1 pps between participating stations. This can be done as described above using the 1 MHz from the cesium standard as a clock and the 1 pps as data to the modem. In a typical commercial PSK modem, the regenerated clock is used to gate out the received data. A user extracting time information may apply either the edge of the data or its associated clock pulse as a reference. This allows the use of high data collection rates by starting and stopping the time interval counters on the modem clock rather than the data signal. This method would permit simultaneous use of the link to provide time and data transfer for different customers.

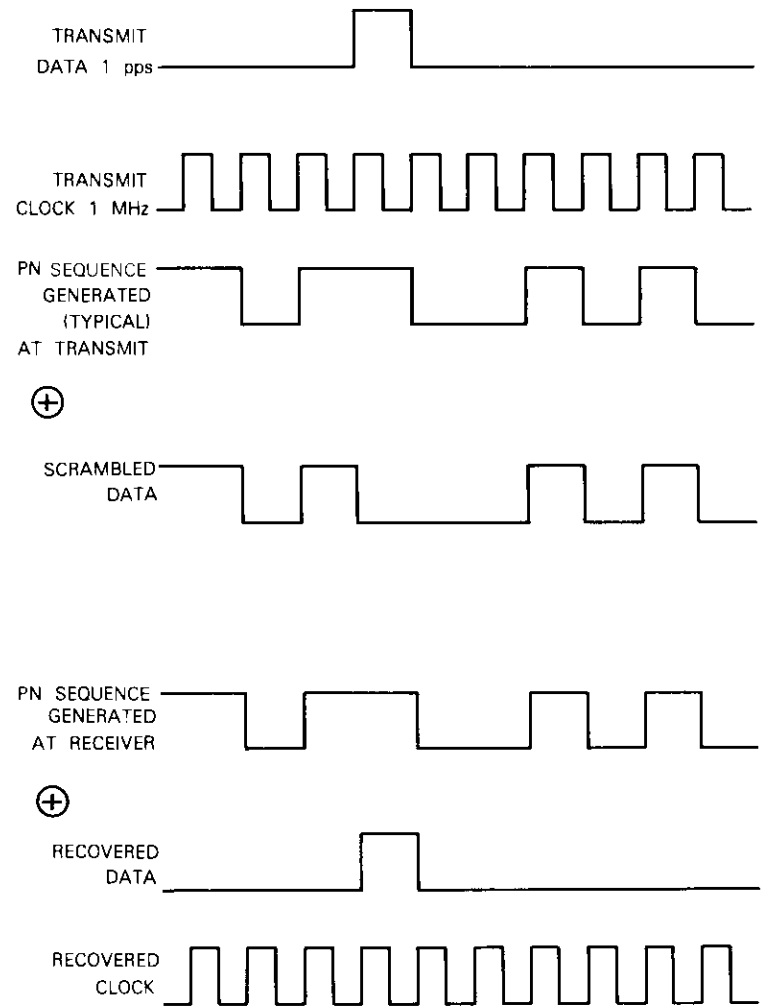
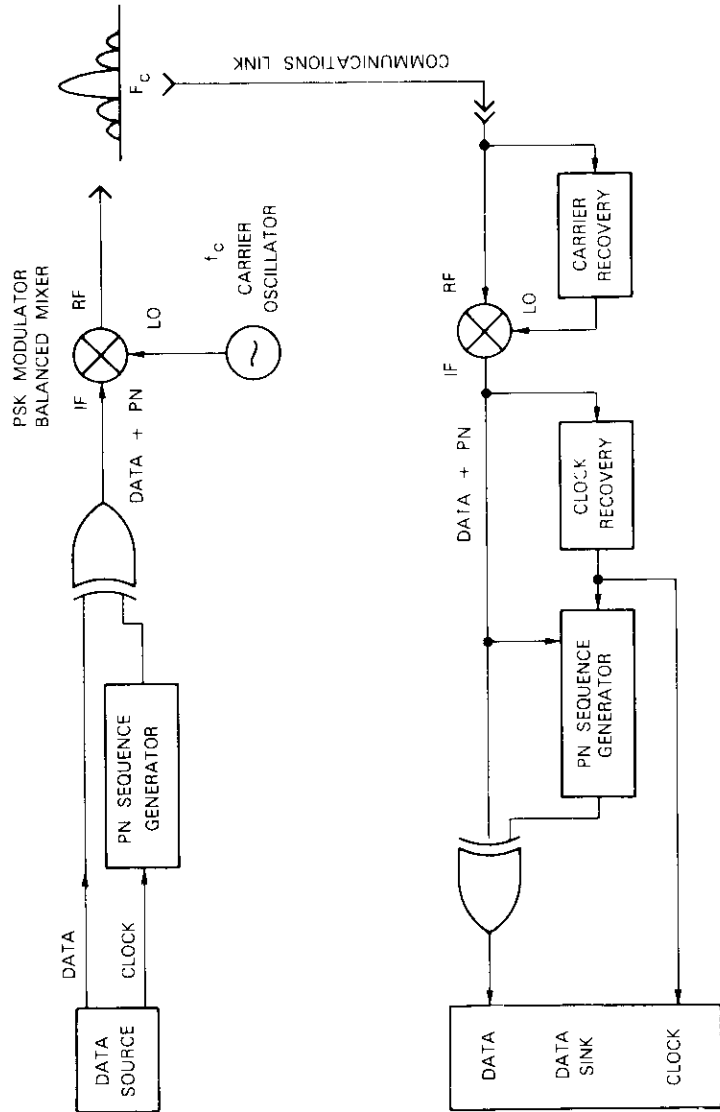


Figure 5. PSK Time Transfer Data Patterns

Description of tests conducted

During May 1979, a series of tests was made with Harris PSK modems located at USNO and NBS to demonstrate the feasibility of using PSK in

time transfer work. The tests evaluated only the system's random error performance for a limited set of data rate and C/N_0 configurations. No attempt was made to calibrate the terminal delays.

For these tests, an interface was designed and built at COMSAT Laboratories. Figure 6 is a block diagram of this interface which allowed the modem to be driven with a data clock rate between 1 MHz and 10 kHz. The actual data input to the modem from the interface could be any signal from 1 to 1,000 pps. All clock and data signals were derived from the cesium standard's 1-MHz output with the dividers reset by the cesium 1-pps signal.

For the results presented in this paper, the data signal was always 1,000 pps. The HP9825A time interval counter was set up to internally average 1,000 time interval values measured at the 1,000-pps rate, and to output the average value. This resulted in a nominal 1 point per second to be recorded by the HP9825A calculator-controller. The HP9825 also recorded the time of day from the HP59309 clock with each data point. The HP59309 has a resolution of 1 s. Therefore, the data points recorded were logged as having occurred at the last integer second; their actual time of occurrence could have been up to just under 1 s later.

$$T_{\text{RECORDED}} \leq T_{\text{ACTUAL}} < T_{\text{RECORDED}} + 1 \quad (17)$$

This uncertainty in the actual time caused problems in the data reduction.

A possible error of up to 1 s in the recorded time can have a significant effect when it occurs in the presence of satellite motion. For example, if the observed range rate ($\Delta Y/\Delta T$) is 50 ns/s, and a measurement of Y is made at 125.8 s but recorded at 125.0 s, the error in Y would be $0.8 \text{ s} \cdot 50 \text{ ns/s}$ or 40 ns. This type of error is peculiar to the experimental configuration used in these tests and would not be observed in a properly designed PSK time transfer system.

COMSAT-conducted PSK experiments

COMSAT conducted a series of tests in cooperation with the NBS Boulder, Colorado, facility to evaluate the performance of a satellite link using PSK modulation of time transfer signals. A small 12/14-GHz terminal was supplied by COMSAT at the Boulder site. The performance

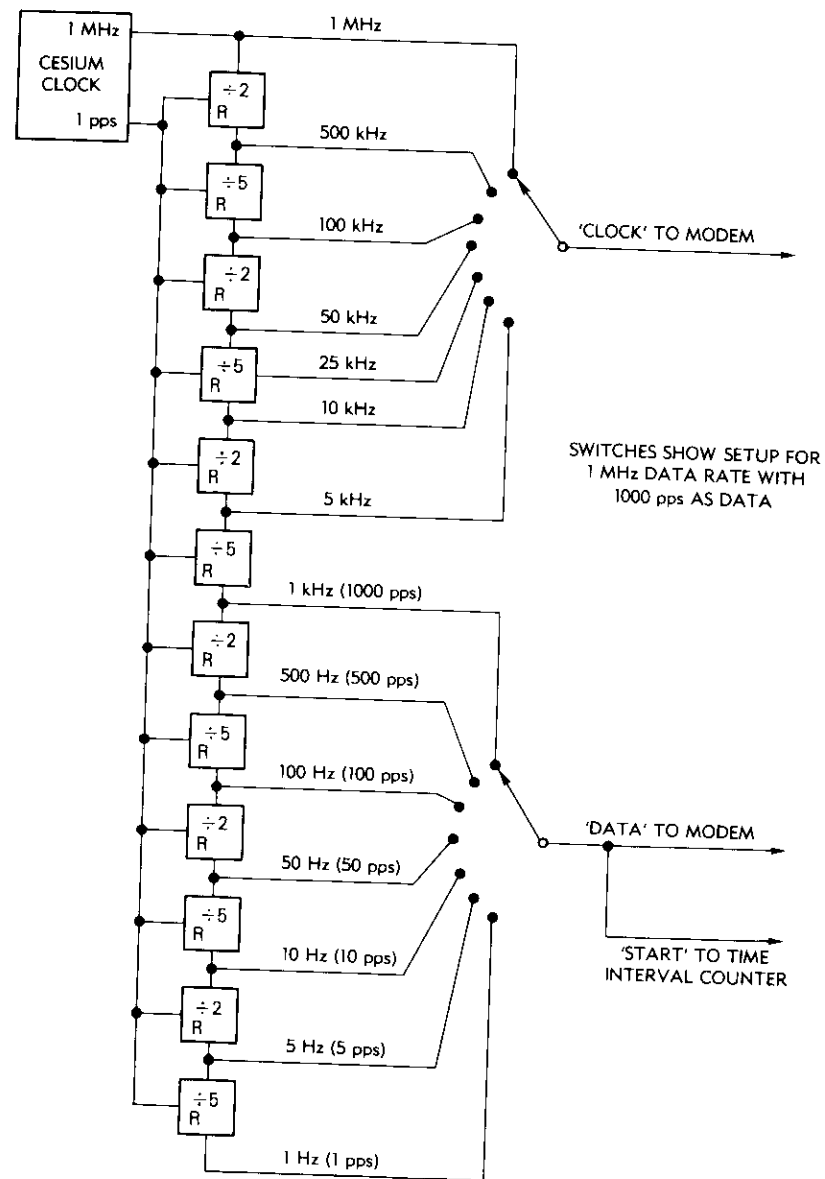


Figure 6. Simplified Block Diagram of Clock/Modem Interface

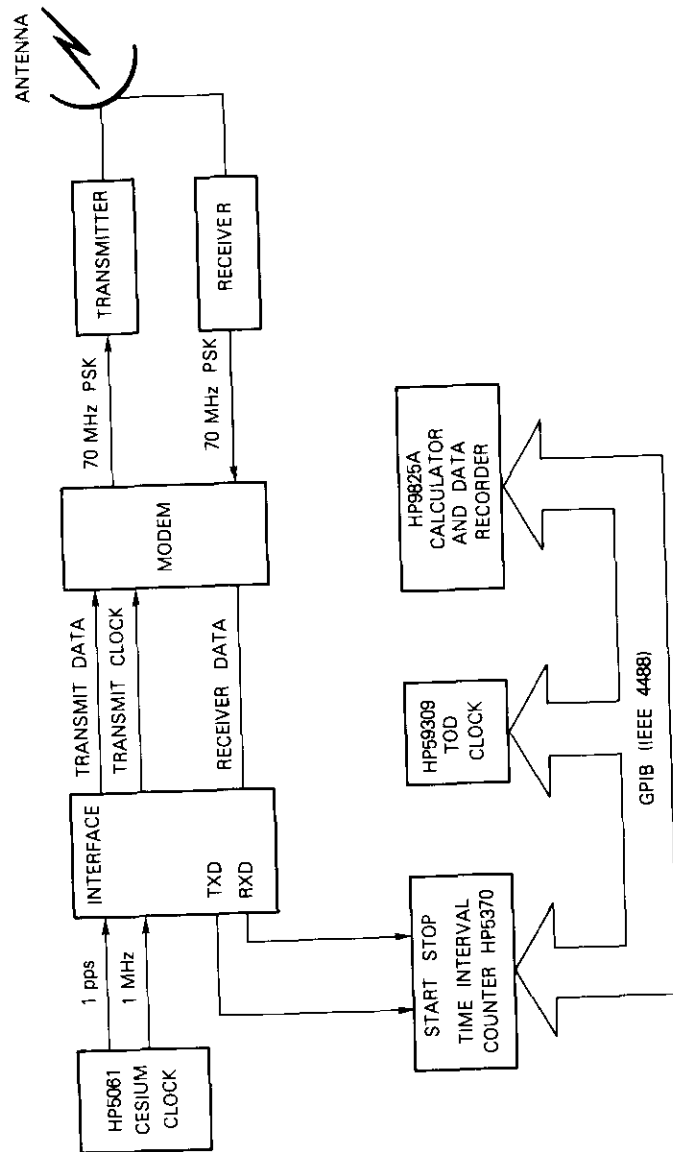


Figure 7. Time Transfer for Terminal Setup

was measured by computing the size of the random error performance of each trial circuit and by analyzing error scatter diagrams for the presence of any nonrandom errors.

Bench test

Prior to the satellite transmission tests, one of the Harris modems was connected in a 70-MHz IF loopback configuration. Data were collected in the same manner as in the satellite trials, and the standard deviation calculated as previously described. These results (Table 1) represent the ultimate performance that can be expected from these modems. No bench tests were conducted with controlled noise levels injected at the IF because equipment was unavailable.

TABLE 1. MODEM PERFORMANCE OF 70-MHz LOOPBACK WITHOUT NOISE

CLOCK RATE (kHz) (ALL DATA = 1,000 pps)	STANDARD DEVIATION SIGMA (ns)
1,000	0.27
500	0.36
100	0.51
50	1.5
25	2.9
10	9.0

Satellite trials

Two 12/14-GHz transportable earth terminals were used for this experiment, one at USNO and another at NBS. Each has 2.4-m antennas, FET receivers, and 20-W TWT transmitters. Reference 1 contains a detailed report on these terminals. Tests of the PSK modem for time transfer were conducted using a satellite loopback of signals from the NBS Boulder terminal. Thus, the results represent a spacecraft ranging experiment rather than a true time transfer. However, the random errors observed are the same as those that would be experienced in a two-station transfer experiment. Trials using CTS transponder 1 (200-W) were run with 10 W of terminal transmit power. Trials in the second transponder (spacecraft power of 20 W) used the full 20 W of terminal power to start, and lower transmitter power as required to achieve the indicated C/N_0 . Tables 2 and 3 contain link budgets for

TABLE 2. LINK POWER BUDGET FOR TIME TRANSFER PSK TESTS (2.4-m TERMINALS, TRANSPONDER 1)

UP-LINK	
Transmitted Power (dBW)	10
Gain (2.4-m antenna)(dB)	48.5
e.i.r.p. (dBW)	58.5
Path Loss (dB)	-207.3
Spacecraft G/T (dB/K)	6.4
C/T up (dBW/K)	-142.4
DOWN-LINK (SPACECRAFT ATTENUATOR = 5 dB)	
Spacecraft e.i.r.p. (dBW)	52
Path Loss (dB)	-206.3
G/T (2.4-m antenna)(dB/K)	21.4
C/T down (dBW/K)	-132.9
C/T overall (dBW/K)	-142.8
C/N ₀ (dB Hz)	85.7

TABLE 3. LINK POWER BUDGET FOR TRANSFER PSK TESTS (2.4-m TERMINALS, TRANSPONDER 2)

UP-LINK	
Transmitted Power (dBW)	13
Gain (2.4-m antenna)(dB)	48.5
e.i.r.p. (dBW)	61.5
Path Loss (dB)	-207.3
Spacecraft G/T (dB/K)	6.4
C/T up (dBW/K)	-139.4
DOWN-LINK (SPACECRAFT ATTENUATOR = 4 dB)	
Spacecraft e.i.r.p. (dBW)	39
Path Loss (dB)	-206.3
G/T (2.4-m antenna)(dB/K)	21.4
C/T down (dBW/K)	-145.9
C/T overall (dBW/K)	-146.8
C/N ₀ overall (dB Hz)	81.8

both configurations at full power. All tests used BPSK. Time data transmitted at 1,000 pps and internal averaging by the time interval counter produced one data point per second for recording. This production of raw data at 1 pps is consistent with the methods used

in the wideband FM work reported in References 3 and 5.

Time base errors

Initial results showed surprisingly high values of sigma (≈16 ns). Examination of the error scatter diagrams revealed an obvious periodic error in the form of a sawtooth waveform of about 50-ns amplitude and 14-s period. The scatter diagram for file 15501 is shown in Figure 8 as an example. For this data file, the initial fitted curve was

$$Y(X) = 3.57 \times 10^{-4} - 5.78 \times 10^{-8}X - 5.17 \times 10^{-14}X^2 - 9.64 \times 10^{-17}X^3 \quad (18)$$

The value of X is given in seconds, starting at X = 0 for the first data point; Y is the range in seconds. Since the data signal used was 1,000 pps, the maximum value of any Y data point is 1 × 10⁻³ s. The range rate or change in path length at the time of this data file was about 58 ns/s. The source of the periodic error is the discrepancy between the recorded and actual time of the data, as described in equation (17). If the data were collected at a rate of 1.077 s/point, rather than 1 point/s after 12 points, the recorded time would be in error by 1 s. At a range rate of 58 ns/s, the resulting error is 53 ns. To reduce these data, the time scale of the raw data was computed with even-sized increments starting at X = 0 and an increment DT:

$$DT = \frac{\text{Last TOD} - \text{First TOD}}{\text{Number of Points} - 1} \quad (19)$$

This assumes that the data points were generated at even increments. An operational system would require a more precise clock in the data logging system since system error is limited by clock quantization and the range rate.

Results

Table 4 gives the error performance of the links measured, which represents the use of a ±3σ window in the reduction process.

DETAILS OF TYPICAL FILES

These results were computed with a corrected time base, equation (19), to remove the sawtooth error pattern. Even with this correction,

TABLE 4. PSK MODEM RESULTS

FILE NUMBER	CTS TRANSPONDER	DATA CLOCK RATE	C/N ₀ (dB Hz)	E _s /N ₀ (dB)	SIGMA (ns)	MODEM LIMIT (NO NOISE)	CLOCK RECOVERY SIGMA/SYMBOL LENGTH(%)
15501	1	1 MHz	86	26	0.39	0.27	0.04
15502	1	1 MHz	86	26	0.36	0.27	0.04
15503	1	1 MHz	86	26	0.75	0.27	0.08
15504	1	1 MHz	86	26	0.63	0.27	0.06
15505	2	1 MHz	82	22	0.50	0.27	0.05
15506	2	1 MHz	67	7	5.6*	0.27	0.56
15606	2	1 MHz	67	7	2.9	0.27	0.29
15507	2	100 kHz	62	12	10	0.51	0.10
15508	2	50 kHz	57	10	15*	1.5	0.07
15608	2	50 kHz	57	10	7.5	1.5	0.04
15509	2	50 kHz	51	4	11	1.5	0.06
15510	2	25 kHz	57	13	18	2.9	0.05
15511	2	25 kHz	52	8	180	2.9	0.45

*Excessive error was observed as a result of time base inaccuracy. All results use 1000 points averaged per recorded point with a nominal 1-point/s recording rate.

periodic errors still occur in many of the scatter diagrams. Figures 9a and 9b show the scatter diagram of file 15505 with and without time base correction. Although the standard deviation (sigma) of the error scatter is low, 0.5 ns, the true random error may be even lower and masked by a periodic error. To analyze this periodic effect, the scatter data sets for both the original and the corrected time base calculations were passed through a discrete Fourier transform to measure the frequency components. Figures 10a and 10b plot the results of the process. The Y axis (in nanoseconds) represents the amplitude of the spectral component at the particular frequency indicated on the X axis.* Figure 10a, the transform of the uncorrected data set, displays

*To compute the FFT, the error data set was interpolated to form a new data set sampled at a 1-Hz rate. The new data set was processed 128 points at a time, providing a frequency resolution at the output of 1/128 or about 7.8×10^{-3} Hz. The amplitude present at each point is the magnitude of the complex result at each point. Each data set was subdivided into as many whole 128-point blocks as possible, and the FFT was calculated for each block. The results of all the blocks are averaged to form the transform of the entire data set. For example, data set 15505 (350 s long) was processed in two blocks, consisting of times 0 to 127 s and 128 to 256 s. The points of time 257 to 350 s were not used.

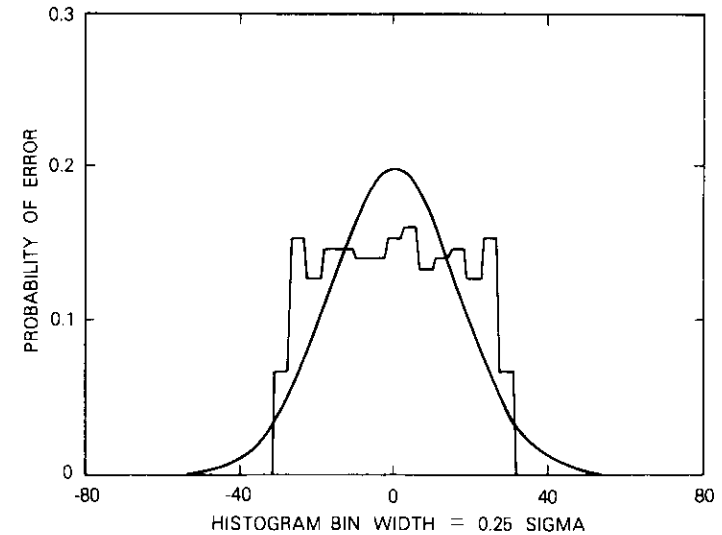
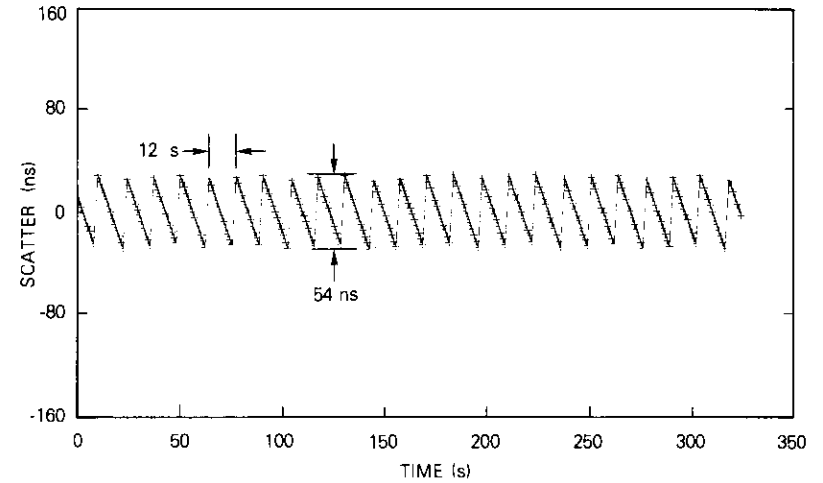


Figure 8. Errors Caused by Inaccurate Time Record

the characteristic decaying ($1, \frac{1}{2}, \frac{1}{3}, \frac{1}{4}, \frac{1}{5}, \dots$) power series of a triangular waveform. The actual amplitude of the first spectral component is related to the peak-to-peak amplitude of a sawtooth by a

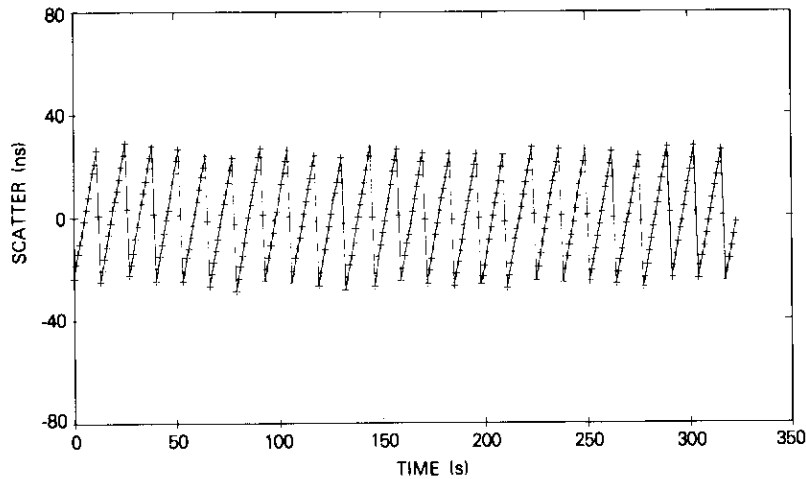


Figure 9a. File Number 15505 Original Time Base

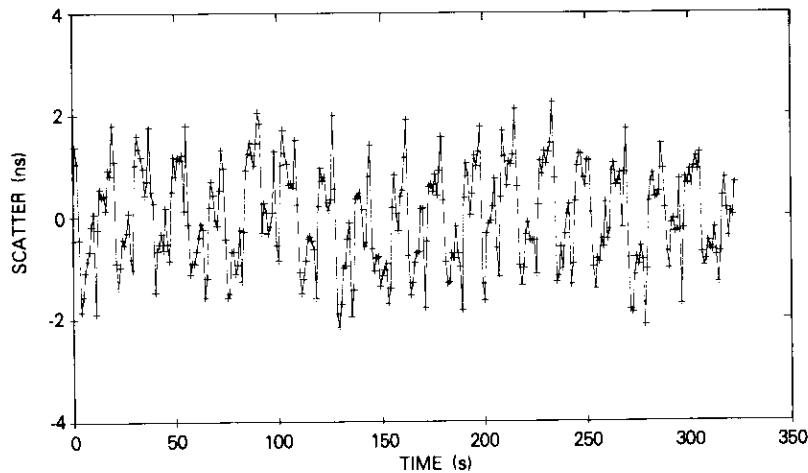


Figure 9b. File Number 15505 Corrected Time Base

factor of $1/\pi$. The rms amplitude, corresponding to the standard deviation, is equal to $1/\sqrt{12}$ times the peak-to-peak amplitude. Both of these factors are approximately equal to 0.3 times the peak-to-peak amplitude. Thus, the 53-ns peak-to-peak sawtooth of the uncorrected data has its first component at 0.085 Hz with a 16-ns amplitude. When

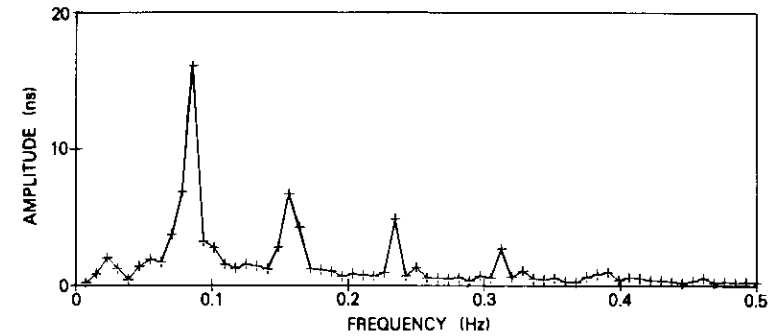


Figure 10a. FFT of File 15505 Original Errors

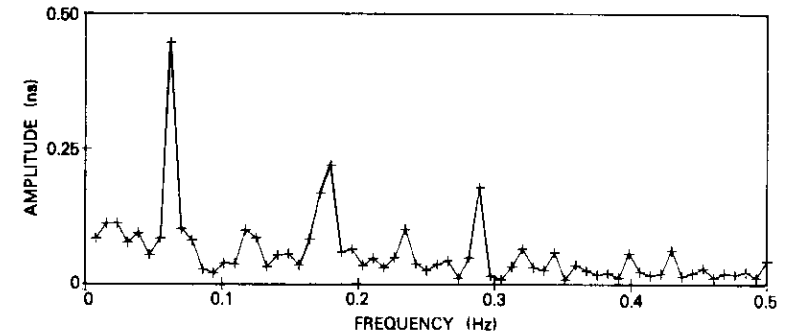


Figure 10b. FFT of File 15505 Corrected Errors

compared with Figure 10b, the FFT of the corrected time base error data set show the same spectral components are reduced in amplitude. The first peak of 0.45 ns corresponds to a sawtooth amplitude of about 1.5 ns. The sawtooth signal remaining in these data is a significant part of the computed sigma, 0.5 ns.

Many of the data sets show evidence of slower periodic errors, which are also believed to be related to the required time base correction. The algorithm used assumed that the original data were sampled at a uniform rate. The slow variations observed, for example, in file 15506 (Figure 11), are probably due to changes in the sample rate as the original data were recorded. File 15606 (Figure 12) was created from the first 160 s of file 15506 in an attempt to measure the sigma for a relatively less disturbed section. The sigma of the new data

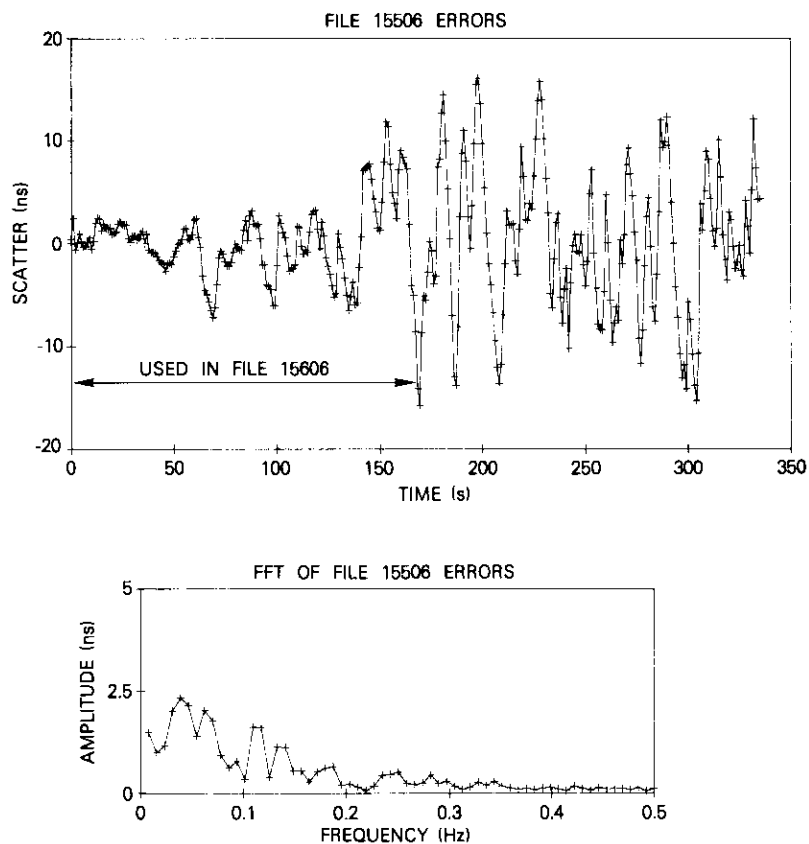


Figure 11. Data File 15506

set (3 ns) still contains significant periodic noise in the 0- to 0.1-Hz region.

In a data set in which the errors are from a Gaussian source and thus have a normal distribution, less than 0.26 percent can be expected to fall outside a 3- σ filter window. For a typical raw data set of 300 points, less than one point can be expected to be excluded. Figure 13, the scatter diagram of data set 15509 before filtering, shows the advantage of using this type of filtering on data containing some points well outside a normal distribution. These raw data had a sigma of 141 ns before filtering with a 3- σ window. The filtered data had a final sigma of 11 ns with a distribution of errors that is approximately Gaussian.

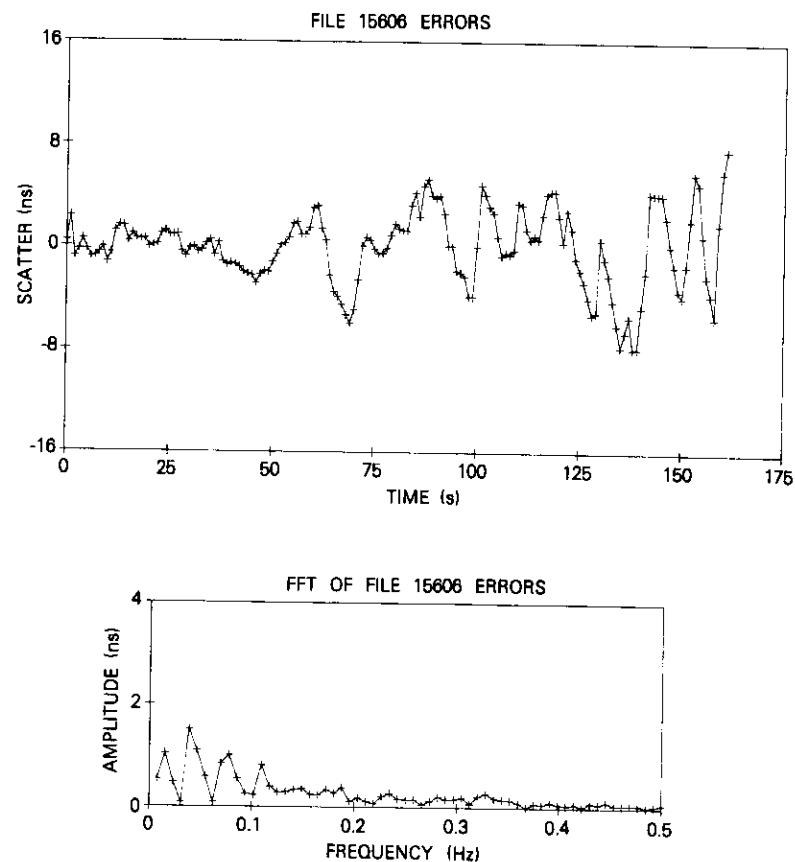


Figure 12. Data File 15606

Figure 14 shows the error distribution before and after filtering. This error pattern is typical of the performance of a phase-locked loop operating at a low E_b/N_0 . The outside points are produced when the loop has lost phase lock and are distinctive from the Gaussian behavior of the locked loop.

In much of the data obtained by these trials, the observed link performance was limited by the systematic error made in recording the time of day. An operational system would have to be designed to collect data at as high a rate as possible and to log it with accurate timing. The ultimate rate of data collection will be limited by factors such as the time interval counter's reset time and internal averaging

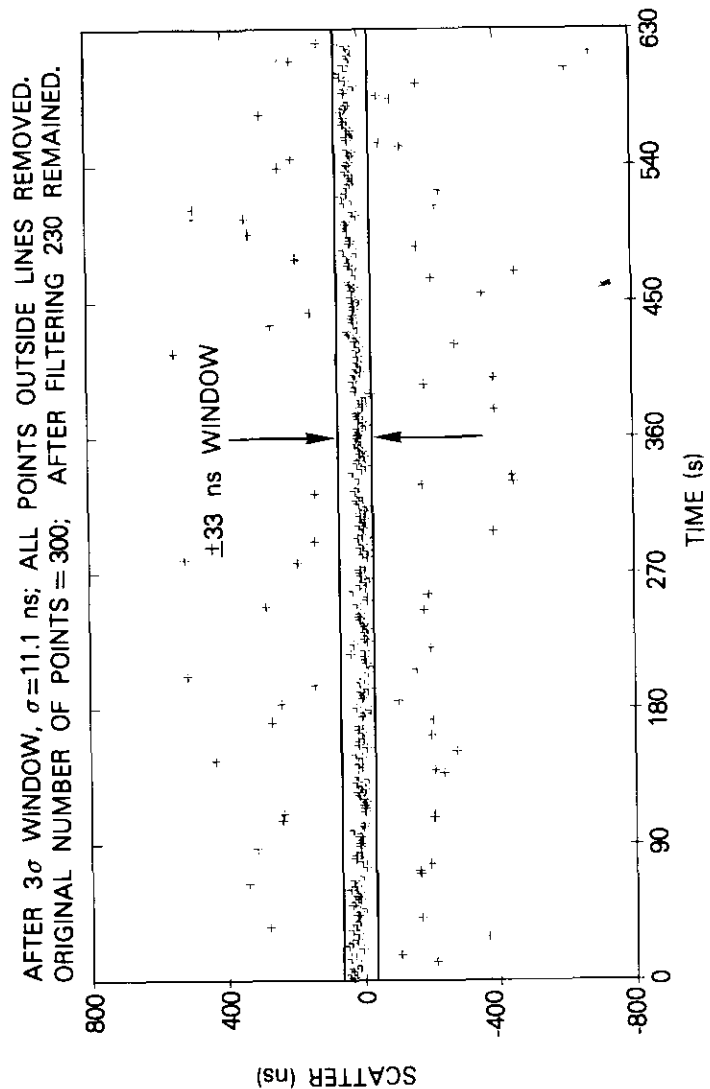
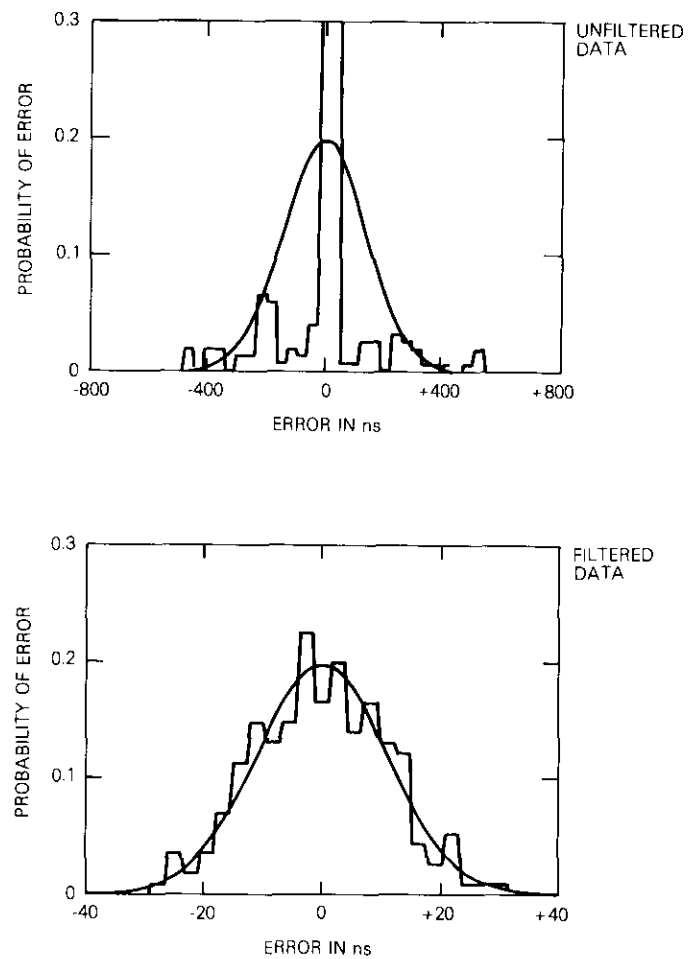


Figure 13. Scatter Diagram Unfiltered Data Set 15509



NOTE:
HISTOGRAM BEAM WIDTH = 0.25 SIGMA.
THE SMOOTH CURVE IS A NORMAL
DISTRIBUTION WITH THE SAME MEAN
AND VARIANCE AS THE ERROR DATA SET.

Figure 14. Error Distribution Data Set 15509

speed, the data transfer and storage speed, and ultimately the observed time interval zero crossings caused by the satellite range rate. Despite the systematic errors, it has been demonstrated that the system used for these tests can provide an efficient, usable time transfer communications link. The low data rates of 25 and 50 kbit/s are particularly suitable for frequency coordination of local crystal and rubidium standards.

Areas requiring additional work

Laboratory simulation of link performance

Work involving the use of satellites for two-way time transfer has been primarily "on the air" tests. Controlled tests are necessary at the baseband and IF levels to evaluate the performance of existing and proposed systems. The relatively inefficient video FM time transfer method, which consumes large power bandwidth, is still being used via SYMPHONIE between Ottawa and Paris.

The PSK system will require additional work to characterize time transfer performance as a function of C/N_0 , data rate and clock recovery methods. Existing commercial modems must be evaluated to determine their suitability for this type of service. These measurements should be made using the standard tools of the time transfer field, the cesium clock source and precise time interval counters, and the existing system simulation equipment such as modems, up/down-converters, and noise generators.

"Free" time transfer

Evaluation of techniques for free time transfer over existing PSK full-duplex data circuits such as spade and TDMA is needed. Time transfer does not require any information transfer in the usual sense. The transfer can be made by tracking the phase relationship of the receive and transmit clocks associated with a digital transmission. If necessary, a one-time transmission of the time of day by each station can resolve any bit-to-bit timing ambiguity. The link can then support time transfer and data transfer for separate customers at practically no increase in link budget or reduction in data throughput.

TDMA Environment

The high data rate associated with the specified INTELSAT full-transponder TDMA system is particularly attractive for high accuracy

time and frequency comparisons between network stations. For example, a 120-Mbit/s service would have a QPSK symbol length of approximately 17 ns. With a clock recovery circuit able to yield sigma-to-symbol length ratio of 1 percent, link performance of .17 ns is better than the other limitations to time transfer accuracy and exceeds the requirements of most potential users. This technique would not require participants to receive their own down-links, and only needs a duplex connection between pairs of time transfer stations. In addition to providing time transfer service, network operation may also benefit from the ability to accurately synchronize station clocks.

Earth terminal equipment delay calibrations

The precision of the time transfer results achieved by previous work (uncertainty in each 1 s worth of samples) has reached the point (<5 ns) that the limit to system accuracy is the uncertainties in different earth terminal equipment delays. One approach to the problem is to minimize the delay differences with identical earth stations at each end. Even this method would not be sufficient for the sub-nanosecond resolution that can be expected in the field. A more universally attractive solution would be to directly measure the transmit delay with a phase detector by probing the radiated signal. The receiver delay can then be measured with a mixer and local oscillator to simulate the satellite signal. Theoretically, this can be accomplished; additional work is required, however, to make such a system operational and to determine the accuracy obtainable for both C and K_u -band terminals; this will require on-the-air tests.

Applications to ranging

The mechanics of time transfer are similar to the satellite ranging problem. The ability to resolve round-trip time delays to within nanoseconds (feet) should be useful operationally. Furthermore, the use of "piggy back" ranging on data transmissions may be attractive to commercial systems.

Low-cost modem for time transfer

A complex high-performance communications PSK modem may not be necessary for time transfer work, particularly when time transfer only is to be accomplished. A modified COMSAT universal modem reduced to a 70-MHz modulator and carrier recovery demodulator,

without the data randomizer, could be used to transmit timing information in BPSK.

Systematic errors

The work completed so far has assumed that the *A-to-B* and *B-to-A* path lengths used were approximately equal. Analysis of the magnitudes of relativistic effects and the effect of ionospheric propagation velocity changes is needed to determine when these effects become significant.

Conclusions

The fundamental problems associated with two-way satellite frequency and time transfer have been discussed. The work performed under COMSAT Laboratories' Small Terminal Project to assist experiments of USNO, NBS, and NRC in the field has been described and the results of an innovative application of PSK to the problem have been presented. For comparison of the primary time standards where uncertainties of less than 5 ns are desired, 1-MHz BPSK has been demonstrated to be practical. For comparison of less demanding standards such as isolated commercial atomic and secondary standards, potentially useful results have been demonstrated for data rates of 50 and even 25 kbit/s. Additional work is needed to confirm and improve the demonstration experiments reported in this paper.

References

- [1] J. Kaiser, L. Veenstra, E. Ackerman, and F. Seidel, "Small Earth Terminals at 12/14 GHz," *COMSAT Technical Review*, Vol. 9, No. 2, Fall 1979, pp. 549-601.
- [2] R. S. Cooper and A. Chi, "A Review of Satellite Time Transfer Technology—Accomplishments and Future Applications," NASA Technical Memorandum 79652, Greenbelt, Maryland, November 1978.
- [3] C. C. Costain et al., "Two-Way Time Transfer via Geostationary Satellites NRC/NBS, NRC/USNO, and NBS/USNO via HERMES and MRC/LPTF (France) via Symphonie," *Proc.*, Eleventh Annual Precise Time and Time Interval Applications and Planning Meeting, November 1979, NASA Conference Publication 2129.
- [4] A. Papoulis, *Probability, Random Variables, and Stochastic Processes*, New York: McGraw-Hill, 1965, Section 8-3.

- [5] C. C. Costain et al., "Two-Way Time Transfers Between NRC/NBS and NRC/USNO via the HERMES (CTS) Satellite," 10th Annual Precise Time and Time Interval Applications and Planning Meeting, November 1978.
- [6] J. W. Schwartz, J. M. Acin, and J. Kaiser, "Modulation Techniques for Multiple Access to a Hard Limiting Satellite Repeater," *IEEE Proc.*, Vol. 54, May 1966, pp. 763-777.



Lester B. Veenstra received a B.S. in physics and a B.S. in systems science from the University of West Florida, and has pursued graduate work in electrical engineering at Northeastern University. He was with the U.S. Naval Security Group for six years prior to joining COMSAT Laboratories in 1976. Presently, he is a member of the Small Terminal Development group of the Transmission Systems Laboratory. He is a member of IEEE.

Joachim Kaiser received a B.A. and an M.A. in mathematics in 1943 and 1948, respectively, and completed additional graduate work in communications theory at the University of Michigan in 1967 and 1968. He joined COMSAT Laboratories in 1968 and is Manager of Special Projects. He has performed numerous experiments in satellite communications using small earth terminals, and was the principal investigator for COMSAT's experiment on the Communications Technology Satellite. He is a senior member of the IEEE.



Cecil C. Costain B.A. University of Saskatchewan 1941, B.A. (Honours) and M.A. from the same institution in 1947, Ph.D. Cambridge University in 1951. Served in the Royal Canadian Navy during World War II as radar officer, and retired as Lt. Commander in 1945. Dr. Costain joined the National Research Council, Ottawa, Canada, in 1951, and worked in microwave spectroscopy. In 1971 he became head of the Time and Frequency Section of the Division of Physics. He is a Fellow of the Royal Society of Canada, a Fellow of the Institute of Electrical and Electronics Engineers, and past president of the Canadian Association of Physicists.



William J. Klepczynski completed his undergraduate work in astronomy at the University of Pennsylvania in 1961, received an M.A. in astronomy from Georgetown University in 1964, and a Ph.D. from Yale University in 1969. He has been employed at the U.S. Naval Observatory since 1961. Currently, he is Chief, Scientific Operations of the Time Service Division.

David W. Allan received a B.S. in physics from Brigham Young University in 1960, and an M.S. in physics from the University of Colorado in 1965. In 1960 he joined the National Bureau of Standards, Boulder, Colorado, where he worked with ammonia beam masers and related quantum electronic devices. He is currently Chief of the Time and Frequency Coordination Group of the Time and Frequency Division in the National Bureau of Standards. Mr. Allan is a member of the Scientific Research Society of America, Sigma Xi, and the International Radio Consultative Committee (CCIR).



Index: filter, Invar, fabrication techniques

Fabrication techniques of lightweight Invar microwave filters

H. I. GERSON

(Manuscript received July 29, 1981)

Abstract

This paper discusses technological problems involved in producing a lightweight (206-g) Invar filter at 4.0-GHz center frequency. The fabrication techniques offer a less expensive method of metal filter fabrication compared to conventional methods. The temperature-stable metal filter is weight-competitive with a graphite epoxy composite (GEC) filter and does not exhibit time-dependent frequency drift that results from creep of the resin matrix.

A cylindrical waveguide filter was fabricated and tested for thermal stability before and after temperature cycling. The frequency characteristics of the lightweight filter which has 0.368-mm wall thickness are similar to those of a filter with a 0.889-mm thick wall and the same electrical design.

The equation for the coefficient of thermal expansion (CTE) of plated material is derived to evaluate the frequency shift of Invar and Super Invar microwave filters.

Introduction

A thermally stable material such as Invar must be used to minimize frequency changes in spacecraft microwave waveguide channelizing filters. Invar has a CTE of 1.6 ppm/°C and the density of steel. A 4.0-GHz, 8-pole, dual-mode round filter made with 0.889-mm wall Invar

weighs 506 g (see Figure 1). An increasing number of channelizing filters are required by high-capacity communications satellites. For example, 12 channels were used on INTELSAT IV, and 29 on INTELSAT V; even more will be employed in future INTELSAT spacecraft. The increasing filter weight stimulated the search for lighter weight filter designs [1].

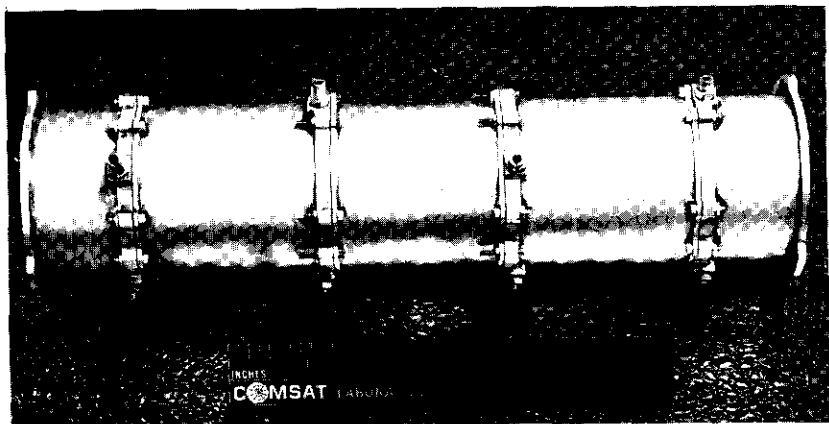


Figure 1. *Thick-wall Invar Filter*

Minimum wall and iris thicknesses of 0.889 mm and 0.508 mm, respectively, were used for the 506-g filter to ensure stable geometry over the operational temperature range. Electrical considerations also dictated other mechanical features of microwave filter design. For example, the filter sections usually span the cavity midpoints so that joint discontinuity occurs at the zero current point. Each section is machined from solid material to obtain continuity at the high current point, the cavity wall-iris interface. Bosses and flanges are also integrally machined, with screws fastening the sections together. Figure 2 shows a thick-wall (> 0.8 -mm) filter construction. The filter is costly to produce because of the extensive machining and dimensional accuracy required.

Weight and cost could be reduced significantly by replacing complex parts with simple ones, using thin material, and replacing separable joints with molten metal joining. Brazing and soldering have been proven satisfactory for cavity-iris joints in 4.0-GHz filters.

GEC, which has a density one-fifth that of Invar, can be made with an equivalent CTE. GEC filters at 4.0 GHz weighing 180 g, with

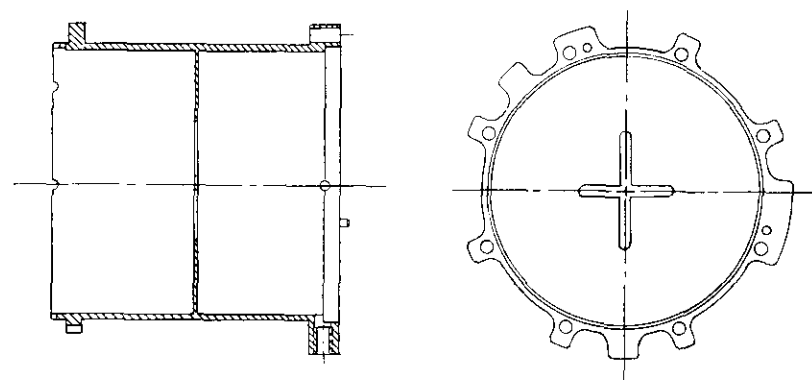


Figure 2. *Thick-wall Filter Section*

mounting bracket, have been realized; however, metallized GEC exhibits creep which results in frequency drift [2], [3]. A lightweight Invar filter weighing about 200 g would therefore be competitive with GEC and would be drift free.

This paper describes efforts to reduce Invar filter weight by using thin material, simplifying construction, improving fabrication techniques, and reducing fabrication costs. The thin walls did not buckle or distort during stability testing over a temperature range of 80°C . An equation for plated material was developed and verified to compare the frequency shift of microwave filters made of Invar and Super Invar with several different wall and plating thicknesses.

Design approach and problem areas

To achieve the weight objective of 200 g, the filter cavity wall could not exceed 0.381 mm, and the iris thickness 0.254 mm. Fabricating and joining thin parts to achieve the required geometric accuracy were major problems in producing a lightweight Invar filter. An 8-pole filter of 4.0-GHz center frequency was selected for implementation because response characteristics of a thick-wall filter were available for comparison.

The mechanical design of the lightweight filter was based on the use of four cylinders and five disks, with brazing and soldering as joining methods. Since alternate assembly sequences could be used, selection of a particular sequence determines which of the five joints are brazed and which are soldered. Because the filter interior is not accessible

after assembly, filter parts or sections must be plated beforehand.

Figure 3 shows the design selected to investigate the major problem areas. The filter consists of two similar half-sections, each with two full-length cavity cylinders brazed to an end (cruciform slot) iris. The tuning screw and connector bosses are also brazed. The half-sections

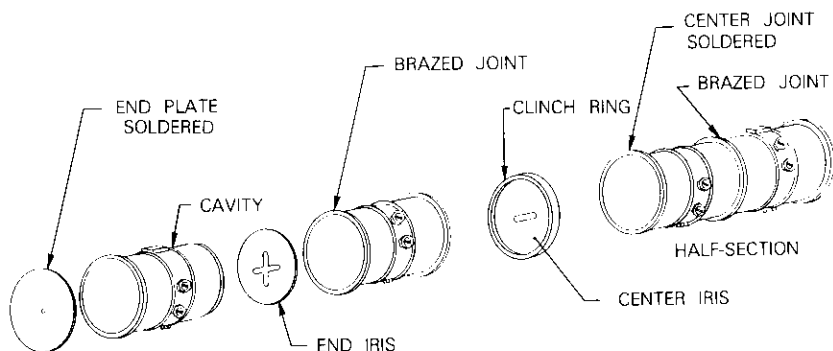


Figure 3. *Lightweight Filter Concept*

are open-ended, allowing inspection of the brazed joints and access for plating. After silver plating, the two subassemblies are soldered to the center iris. This center joint is mechanically reinforced by a clinch ring. Opposing lugs on the clinch ring, which positions the half-sections relative to each other, are swaged against the cavity flanges (see Figure 4). Finally, the end plates are soldered in place to close the filter.

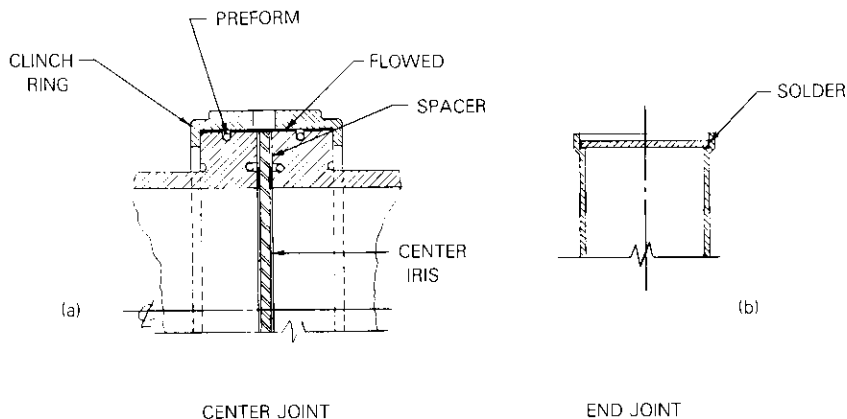


Figure 4. *Solder Joint Construction*

Figure 5 is a photograph of the completed filter, and Figure 6 shows a section through the cavity body facing an end iris.

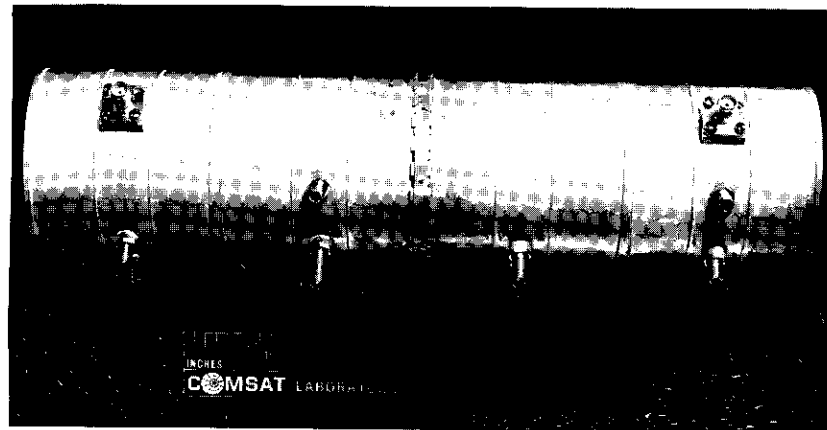


Figure 5. *Lightweight Invar Filter*

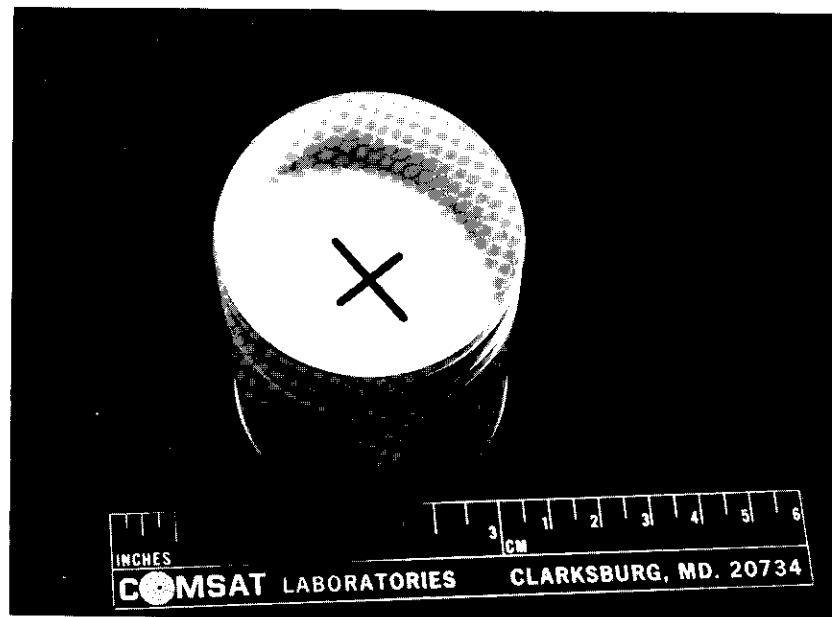


Figure 6. *Section of Lightweight Invar Filter*

Fabrication of thin Invar filters

Excellent conductivity at critical points and extremely accurate filter geometry are two requirements of microwave filters. However, tolerances for roundness and flatness, variations of which affect the as-fabricated (untuned) filter frequency, often have been based on judgment rather than testing, leading to excessively tight tolerances. Since the filter can be tuned to compensate for larger tolerances, the essential problem is to prevent distortion within the temperature range.

Cavity circularity

The cavity cylinders were machined from thick-wall tubing to eliminate the possibility that residual extrusion stresses would severely distort the finished cylinder. The finished cylinder was out-of-round over 0.102 mm.

Invar must be annealed to relieve residual stresses prior to brazing, and then heat-treated to restore its low CTE. Hot-stretch-forming concurrent with annealing improved roundness. The final cavity was round within 0.051 mm.

Initially, the holes for tuning screw and connector bosses were completed prior to annealing, but they became elliptical during stretch-forming. The holes were finished by electric discharge machining (EDM) after annealing.

Iris flatness

The iris is 0.254 mm thick, and a 152×10^{-6} -mm surface finish is specified for both sides. Since stock material was unavailable, specially rolled strip was procured. The five pieces for the irises and end plates were selected from short sections of the material that were within the required flatness tolerance.

Brazing

Several braze alloys may be used with Invar. The two selected for experiments were OFHC copper, and a 56-percent silver, 42-percent copper, 2-percent nickel alloy (Lucas-Milhaupt alloy No. 559). Either material permits fluxless furnace brazing in a reducing (hydrogen or forming gas) atmosphere. Copper was favored because it is eutectic, readily fills the joint, and allows the use of interference fits instead of fixtures. In addition, its high brazing temperature permits secondary brazing or reannealing at a lower temperature.

The novel configuration of the end iris-cavity joint was also an important consideration in braze alloy selection. Figures 7a and 7b show two conventional braze joints, each with a preform wire ring. The melted alloy flows through the gap by capillary action, forces the gas out, and fills the space without forming voids. The iris-cavity joint of the filter (Figure 7c) is a combination of the two conventional joints.

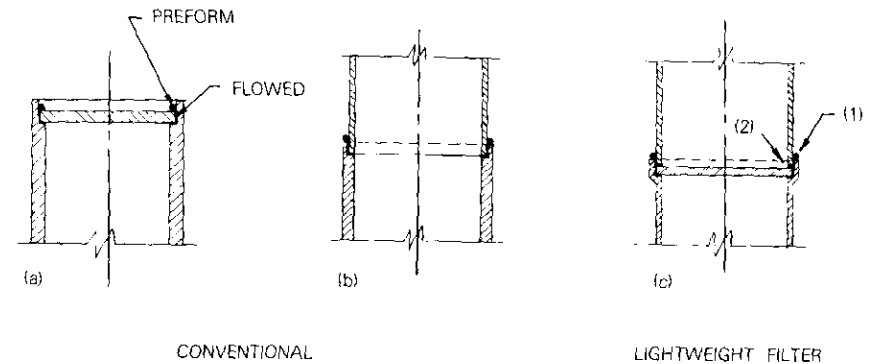


Figure 7. Braze Joint Construction

Whether the preform is placed externally at (1) or internally at (2), the gaps on both sides of the iris may not be filled completely by the molten alloy because of the dual passages. Further, gas entrapped in the joint may result in voids and reduced strength. However, satisfactory electrical performance is more important and has priority over joint strength; the joint must be filled, but its strength may be less than optimum.

Experiments with both braze alloys were performed with specimens of the iris-cavity joint configuration. With one preform located at (1) in Figure 7c, the joints were starved. Preforms were then used at (1) and (2). The No. 559 alloy was selected because the joints were almost filled; the copper joints were less satisfactory.

Optimum flow and fill of brazed joints are achieved by adjusting the brazing schedule for the individual part configuration and mass. Experiments to determine the brazing schedule were therefore performed with actual filter parts. Finally, the tuning screw and connector bosses were brazed concurrently with the filter half section. Each boss was positioned concentrically with its prefinished hole in the cavity.

Intergranular cracking and stress relieving

When Invar is brazed with silver alloys, precautions are necessary to prevent the grain boundaries of the Invar from being penetrated by silver, which produces cracking. Intergranular cracking was prevented by annealing to relieve residual stresses, heating the parts uniformly to prevent thermal stresses, and minimizing brazing temperature and time.

Center joint

Whether the filter is supported at the ends or center, the center joint is subject to maximum stress during launch. A clinch ring concentrically positions the various joint parts and is swaged and soldered to them, ensuring structural integrity (see Figure 4a). Spacers are located between the iris and each cylinder end to produce the solder joint gaps. Solder preforms are placed in the grooves on each cavity end and outside diameter. The parts are assembled between clamp-rings, and the clinch ring is swaged. The clamps are then removed and the assembly is heated in a furnace.

The center joint cannot be visually inspected after soldering. Its adequacy can be determined only by measuring cavity Q and by vibration testing. The assembly procedure was checked by assembling several specimen joints with open-ended cylinders which allowed the interior joints to be inspected visually.

The last step in assembling the filter was to solder the end plates (Figure 4b) concurrently with the center joint. Subsequently, cavity Q was measured and found to exceed 10,000.

Final geometric accuracy

After brazing the filter half-sections, cavity roundness and iris flatness were remeasured. Flatness was twice that specified; out-of-roundness was larger.

The variations of the cavity diameter, length, and circularity, and iris flatness determine the as-fabricated center frequency, which can be adjusted by tuning. Thermal stability, however, is the critical filter characteristic. Geometric stability may be the determining factor of thermal stability for a thin-wall filter. Change in iris flatness or cavity roundness, or oil-canning (buckling) either element introduced by temperature changes should not alter the frequency beyond the specified limits. Although a linear temperature-frequency relationship may be desirable, the criterion for acceptability is that the two parameters remain within their specified limits. Further testing determined whether

the large dimensional variations produced geometric instability. The filter was completed with the existing parts and found to be satisfactory.

Electrical characteristics

Test results

The filter was tuned to a center frequency of 4.075 GHz. Insertion and return loss measurements indicated good performance characteristics (see Figure 8). Thermal stability over temperatures ranging from -20°C to 60°C * in air was measured, and dry nitrogen purged moisture during the test. Response curves taken at 20°C intervals were essentially the same. The filter was geometrically stable and its characteristics did not differ from those of a heavy-wall Invar filter.

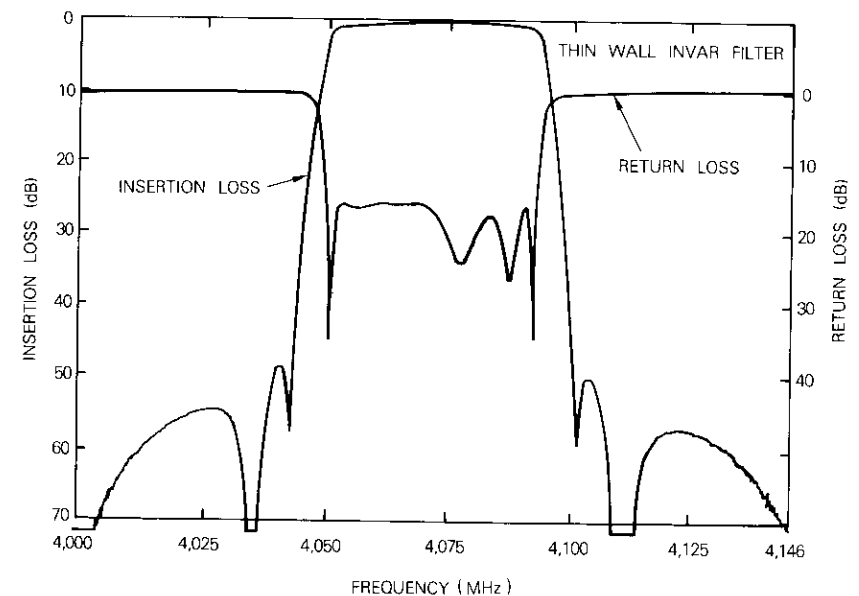


Figure 8. Response of Lightweight Invar Filter

Several thermal cycles are usually required to stabilize an Invar filter. Frequency variation was 660 kHz† for the first cycle and 700

* Temperature was measured within $\pm 1^{\circ}\text{C}$.

† Frequency was measured within ± 10 kHz.

kHz for the second. The small difference led to the conclusion that stabilization had been achieved because of the thin walls. Thus, additional cycling and measurements were not performed. Based on the theoretical CTE of Invar, the expected frequency change over the temperature range was 522 kHz rather than 700 kHz.

The filter was then thermally cycled to check joint stability, particularly of the soft-soldered joints. The exposure regime consisted of 114 cycles over the same temperature range for 6 days. The second set of frequency measurements was taken in vacuum (10^{-6} torr) to eliminate moisture effects. Three thermocouples were attached to the filter body, one at midlength and one at each end to ensure uniform temperature distribution. The frequency was measured approximately 1 hour after the temperatures at the three thermocouples were within 1 degree of each other.

A thick-wall Invar filter of the same electrical design and center frequency (3.977 GHz) was set up in the same chamber and instrumented as described previously. The thin-wall filter had coaxial connections; the thick-wall filter had waveguide connections with coax-to-waveguide transitions.

Figures 9 and 10 plot the results for the thin-wall and thick-wall filters, respectively. The temperature-frequency variation of the thick-wall filter is less linear than that of the thin-wall filter. This may be due to the thicker material sections, the mass of material at cavity joints (flanges and screws), and/or the brass coax-to-waveguide transitions at the filter ends. The thermal conductivity of Invar is low, and thermal lag will reduce the frequency shift of a filter.

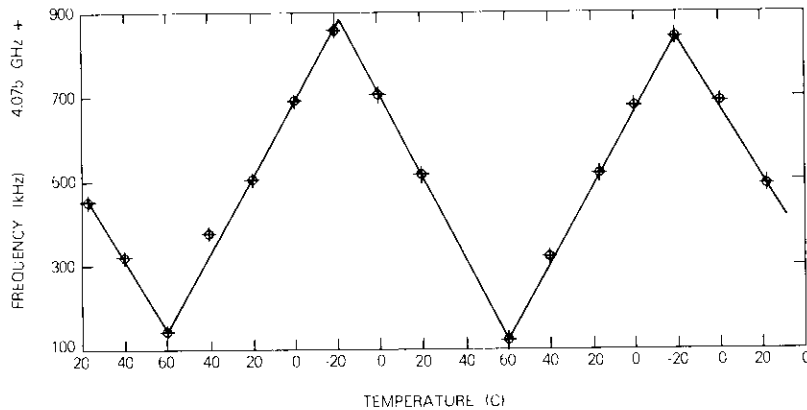


Figure 9. Frequency vs Temperature (Lightweight Invar Filter)

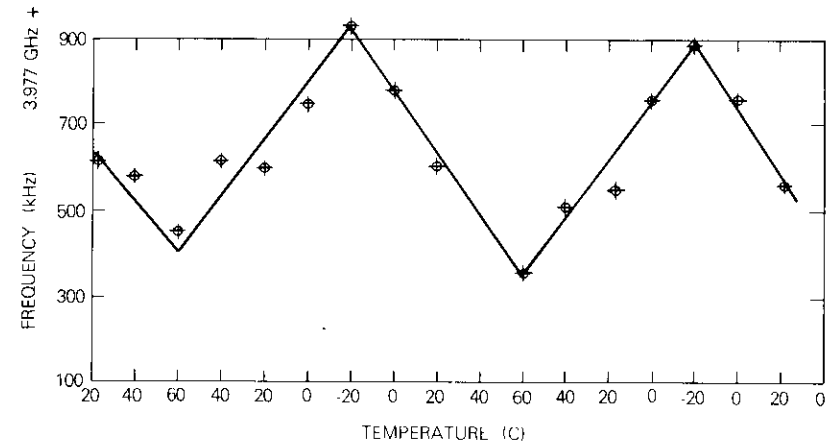


Figure 10. Frequency vs Temperature (Thick-wall Invar Filter)

The successive response curves of the thin-wall filter over the temperature range did not differ significantly from those taken initially; the differences were those which typically occur with an Invar filter. The joints and geometric stability had not deteriorated from thermal cycling.

Evaluation of Thermal Stability

Table 1 shows the total frequency shift measured for the three successive half-cycles during the thermal-vacuum test of the two filters. For the thin-wall filter, the maximum frequency shift over the 80°C range was 735 kHz, an increase from the previous 700-kHz maximum. A reasonable explanation is that repeatability had not been achieved in the first two cycles, as originally presumed. The maximum frequency excursion for the thick-wall filter was 575 kHz. The difference in frequency shift between thick- and thin-wall filters is discussed below.

TABLE 1. FREQUENCY SHIFT (kHz) for 80°C

FILTER WALL THICKNESS MM	TEMPERATURE RANGE			AVERAGE FOR 80°C
	60°C TO -20°C	-20°C TO 60°C	60°C TO -20°C	
0.889	+530	-575	+535	547
0.368	+715	-735	+710	720

Operationally, the thin-wall filter is satisfactory. On communications satellites, bandpass filters are usually located on an equipment shelf inside the spacecraft, where they are exposed to a maximum temperature variation of 60°C. For a 60°C change, the frequency shift of the thin-wall filter would be 540 kHz; that of the thick-wall filter would be 410 kHz.

Increased filter CTE

Because of the conductive plating, the measured temperature-frequency shift of an Invar filter will always be larger than that based on the theoretical CTE. Deviation from the recommended heat treatment of Invar may also increase the CTE. Water quenching from 830°C, followed by soaking at 315°C, and cooling in air is recommended [4]. This procedure was not used for the thin-wall filter because quenching may produce distortion, and reheating could promote intergranular cracking. Instead, the filter half-sections were rapidly air-cooled from the brazing temperature, which is an equally effective treatment.

The increased CTE of both filters is due to the plating with nickel and silver. Since both sides of all surfaces are plated to the same thicknesses, the resulting multilayered composite is symmetric or balanced.

CTE of flat multilayer composite

Figure 11 shows flat material consisting of five layers. If the layers are not bonded together and are exposed to a uniform temperature increase, ΔT , each will experience free expansion in the x direction shown in Figure 11 as Δl_i for material 1. The original length of each material is l_0 . If they are bonded together, the final length (l_f) of the composite and each of the five layers will be in equilibrium. Materials 1 and 2 will be compressed, and material 3 extended. Since the composite is balanced, no bending moment develops.

If flat material is exposed to a uniform temperature rise, it will experience a free longitudinal unit expansion or strain (ϵ) of

$$\epsilon = \Delta T\alpha \tag{1}$$

where α is the CTE.

If the free movement of the material is restrained or extended by another material, both will experience an additional unit strain. For a multilayer case, the final longitudinal strain (ϵ') of each sheet is the same as that of the composite:

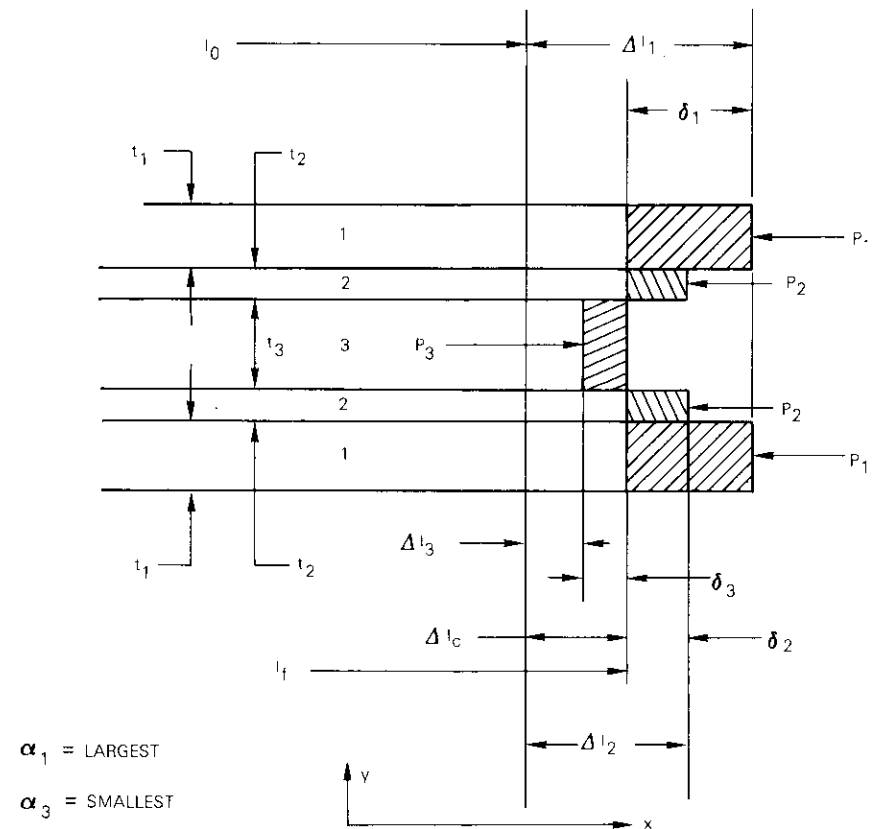


Figure 11. Flat Multilayer Balanced Composite

$$\epsilon'_i = \epsilon_c = \Delta T\alpha_i + \epsilon_i \tag{2}$$

when ϵ_i is tension, with i representing the layer number, and c the composite. The sign is negative for compression.

The described condition also exists in the material layers in the z direction, perpendicular to the longitudinal direction x . Therefore, each material layer is under a biaxial stress. For this condition, when the stress in both directions is tension, and since $\sigma_x = \sigma_z$,

$$\epsilon_x = \epsilon_z = \frac{\sigma_x}{E} (1 - \mu) \quad (3)$$

where σ is the stress, E is the elastic modulus, and μ is Poisson's ratio. Let

$$k_i = (1 - \mu_i) \quad (4)$$

Substituting equations (3) and (4) into equation (2) yields

$$\epsilon_c = \Delta T \alpha_i + \frac{\sigma_i k_i}{E_i} \quad (5)$$

Since $P = \sigma A$, for a unit width

$$P = \sigma t \quad (6)$$

where P is force, A is area, and t is layer thickness. Substituting equation (6) into equation (5) and rearranging the terms produce the following results:

$$\text{(tension)} \quad P_i = \frac{t_i E_i}{k_i} (\epsilon_c - \Delta T \alpha_i) \quad (7)$$

For equilibrium (see Figure 11),

$$2P_1 \text{ (compression)} + 2P_2 \text{ (compression)} = P_3 \text{ (tension)}. \quad (8)$$

Substituting equation (7) into equation (8) for each material and reducing to determine α_c results in

$$\alpha_c = \frac{\epsilon_c}{\Delta T} = \frac{k_2 k_3 (2t_1 E_1 \alpha_1) + k_1 k_3 (2t_2 E_2 \alpha_2) + k_1 k_2 (t_3 E_3 \alpha_3)}{k_2 k_3 (2t_1 E_1) + k_1 k_3 (2t_2 E_2) + k_1 k_2 (t_3 E_3)} \quad (9)$$

It can be similarly shown that the CTE of a cylindrical multilayer composite is also determined by equation (9).

CTE of thick- and thin-wall filters

Table 2 lists the properties and thicknesses of each material in the composite wall of both filters, and Table 3 shows α_c , and the frequency

TABLE 2. CONSTITUENT MATERIAL THERMOELASTIC PROPERTIES

MATERIAL	CTE, PPM/°C	E, GPA	μ	THICKNESS ($\times 10^{-3}$) MM	
				THICK WALL	THIN WALL
Invar	1.6	141.00	0.29	889.00	368.00
Nickel	13.3	207.00	0.30	2.54	2.54
Silver	19.6	75.80	0.37	5.08	5.08

TABLE 3. CTE AND FREQUENCY SHIFT WITH PLATED INVAR

FILTER WALL THICKNESS, MM	CENTER FREQUENCY (GHZ)	α_c (PPM/°C)	FREQUENCY SHIFT FOR 80°C (kHz)	
			WITH α_c	MEASURED
0.889	3.977	1.82	579	547
0.368	4.075	2.12	691	720

shift for 80°C. The values are based on equation (9) and Table 2. The α_c of the thin-wall filter is larger because, for a given plating thickness, the thinner walls result in a greater influence of the plating on the composite CTE. The calculated frequency shifts are within about 5 percent of the average measured values.

Related material aspects

The thinnest filter wall practical with Invar is 0.254 mm. Although α_c increases with the thinner wall, the frequency shift for 60°C would still be acceptable at 562 kHz. Table 4 shows α_c and the associated 60°C frequency shifts for filters of 4.0-GHz center frequency for three wall thicknesses made with Invar and Super Invar.

Manufacturers' specifications for Super Invar 38 (a 31-percent nickel, 7-percent cobalt, 62-percent iron alloy) indicate an average CTE as 0.69 ppm/°C from 30°C to 100°C, and 1.1 ppm/°C from 30°C to -25°C. For an operational temperature range of -10°C to 50°C, the average CTE for Super Invar 38 is 0.963 ppm/°C. This value was used in calculating the data in Tables 4 and 5.

Table 5 shows α_c and the frequency shift for the same wall thicknesses of Invar and Super Invar when used for a 12-GHz filter. In this case, the required silver plating that provides five skin depths is only 2.54

$\times 10^{-3}$ mm thick. The 2.54×10^{-3} mm nickel base coat is the minimum required to ensure that the nickel completely covers the Invar and provides a satisfactory undercoat for good adhesion of the silver plating; it cannot be reduced.

Substituting copper, which has a lower CTE (17.6 ppm/°C) and a higher modulus (110 GPa) for silver decreases the composite CTE. The α_c of the thin-wall filter, for example, would decrease from 2.12 to 1.85 ppm/°C.

TABLE 4. FREQUENCY SHIFT BETWEEN 50° C AND -10° C AT 4.0-GHZ CENTER FREQUENCY

WALL THICKNESS, ^a MM	INVAR		SUPER INVAR 38	
	α_c (PPM/°C) ^b	Δf (KHz)	α_c (PPM/°C) ^c	Δf (KHz)
0.889	1.82	437	1.19	286
0.368	2.12	509	1.51	362
0.254	2.34	562	1.74	418

^a Plating: 2.54×10^{-3} mm Ni; 5.08×10^{-3} mm Ag.

^b Rapid air cool from 925°C.

^c Annealed at 1,093°C and slow cooled. Invar average CTE for temperature range = 0.963 ppm/°C.

TABLE 5. FREQUENCY SHIFT BETWEEN 50°C, AND -10°C AT 12.0-GHZ CENTER FREQUENCY

WALL THICKNESS, ^a MM	INVAR		SUPER INVAR 38	
	α_c (PPM/°C) ^b	Δf (KHz)	α_c (PPM/°C) ^c	Δf (KHz)
0.889	1.76	1267	1.13	814
0.368	1.98	1426	1.36	979
0.254	2.14	1541	1.47	1058

^a Plating: 2.54×10^{-3} mm Ni; 2.54×10^{-3} mm (10^{-4} in.) Ag.

^b Rapid air cool from 925°C.

^c Annealed at 1,093°C and slow cooled. Invar average CTE for temperature range = 0.963 PPM/°C.

Weight and cost reduction

Weight could be reduced by shortening the tuning screws and eliminating two corners of each connector flange and boss. Thinning

the cavity wall to 0.254 mm or chemically milling the outer surfaces to a waffle pattern would result in further weight reduction.

Various cost-reduction techniques can be implemented for quantity fabrication where investment in tooling is justified. Thin extruded tubing could be used and the thicker sections of the cavities formed by swaging. Other possible methods include drawing or spinning the cylinders rather than machining them. Drawn or spun cups may be used for some sections instead of separate tubes and iris disks.

Conclusion

This paper described certain aspects of the mechanical design and fabrication techniques used to produce a thin-wall, thermally stable Invar microwave filter. These techniques will reduce filter fabrication costs below those of conventional methods regardless of wall thickness. The 206-g Invar filter is weight competitive with the GEC filter, and exhibits superior time-dependent frequency stability. Frequency characteristics of the thin-wall filter are the same as those of a heavier wall filter except for a slightly larger frequency shift. The equation developed for the CTE of plated material correlates with test results. It was used to compare the frequency shift of Invar and Super Invar filters at 4.0- and 12.0-GHz center frequency.

Acknowledgments

The author wishes to thank Mr. R. N. Carlson, who fabricated and assembled the lightweight filter, for his suggestions and assistance; Mr. R. R. Kessler for his assistance and cooperation during fabrication; Dr. A. Atia, who designed the filter electrically and performed the electrical tests; and Dr. A. E. Williams for useful discussions during the program.

References

- [1] "INTELSAT Research and Development Program—Ten Years of Progress," International Telecommunications Satellite Organization, Washington, D.C., 1980, pp. 73-81 and 145-146.
- [2] J. L. Camahort et al., "Effects of Thermal Cycling Environment on Graphite/Epoxy Composites," *Environmental Effects on Advanced Composite Materials*, ASTM STP 602, 1976.

- [3] J. Prunty, "Dimensionally Stable Graphite Composites for Spacecraft Structures," 9th National SAMPE Conference, Atlanta, Georgia, October 4, 1977.
- [4] W. S. McCain et al., "Mechanical and Physical Properties of Invar and Invar-Type Alloys," DMIC Memorandum 207, Defense Metals Information Center, Battelle Memorial Institute, Columbus, Ohio, August 31, 1965.



member of the Society of Manufacturing Engineers.

Harold I. Gerson received a Mechanical Course Certificate from the Lowell Institute School, M.I.T. Prior to joining COMSAT in 1968, he worked at Melpar, Inc., AIL, Inc., and Harvard University's Radio Research Laboratory. He is presently a member of the technical staff in the Structures/Mechanical Design Department of the Spacecraft Laboratory. His work involves the development and design of spacecraft mechanical devices, precision applications of composite materials, and mechanical design of microwave devices. He is a senior

CTR Notes

Summary of the SBS satellite communications performance specifications

G. G. CHURAN AND W. E. LEAVITT

(Manuscript received June 15, 1981)

Introduction

A contract was signed on December 31, 1977, with the Hughes Aircraft Company for the design and construction of a spacecraft to be used with the Satellite Business Systems (SBS) all-digital system. The specifications, which resulted from a tradeoff between timely delivery and communications capability, were derived after a number of iterations. This note concentrates principally on the significant parameters of the communications payload, specifically those governing the transponder and antenna. Other spacecraft features that affect communications performance are described in general.

SBS spacecraft characteristics

The SBS spacecraft is an active multichannel repeater in geosynchronous equatorial orbit. Because the antenna pattern is shaped to provide optimum coverage of the continental United States (CONUS),

William Leavitt is a Senior Engineer and Gary Churan an Advisory Engineer in Space Segment Engineering and Operations, Satellite Business Systems.

antenna beam pointing from the spacecraft must be controlled to a 3σ accuracy of 0.05° in both an east-west and a north-south direction. Beam rotation should be 0.2° or less for 7-day periods between attitude trim corrections. A beacon located in the Denver, Colorado, area permits the spacecraft to maintain the antenna pointing within these accuracies. The spacecraft position must be within $\pm 0.03^\circ$ in both the east-west and north-south direction. The original design objective allowed placement of the spacecraft between 100° and 130° west longitude without significant changes in the communications payload performance over CONUS. Actual SBS nominal assigned orbital positions of 100° , 97° , and 94° west longitude have necessitated a slight modification to the antenna system of one satellite to permit satisfactory coverage from the 94° orbital position.

The spacecraft and apogee motor with the payload assist module (PAM) are capable of injection into the nominal parking orbit trajectory when launched by the Delta 3910 launch vehicle. Launch by the Space Transportation System (STS) is to be accomplished by minimal modifications of the PAM from its Delta configuration and no change to the communications satellite. Use of the Delta launch vehicle places a weight limit of about 3,339 kg on the spacecraft, apogee motor, and PAM. The weight limit is approximately 4,355 kg for launch with the STS.

The SBS spacecraft is spin-stabilized with fuel capability to provide east-west and north-south stationkeeping for the 7-year operational life. Figure 1 shows the overall spacecraft configuration. Two solar drums provide the electrical power. During launch, the lower drum is raised above the upper drum and deployed after placement in the drift orbit; the antenna reflector is folded down.

Uninterrupted spacecraft operation for 7 years requires a battery capability that permits full operation through eclipse to at least the end of this period. Items subject to wearout and gradual degradation have a specified design life of 10 years. The probability of spacecraft survival at 7 years is specified to be in excess of 0.7 with 8 of the channels capable of continuous operation and meeting or exceeding the minimum specified channel performance.

Coverage and channelization

The SBS communications subsystem operates in the 14/12-GHz bands (14.0-14.5 GHz up-link, 11.7-12.2 GHz down-link), with 10 transponder channels available. Each channel has a 43-MHz bandwidth,

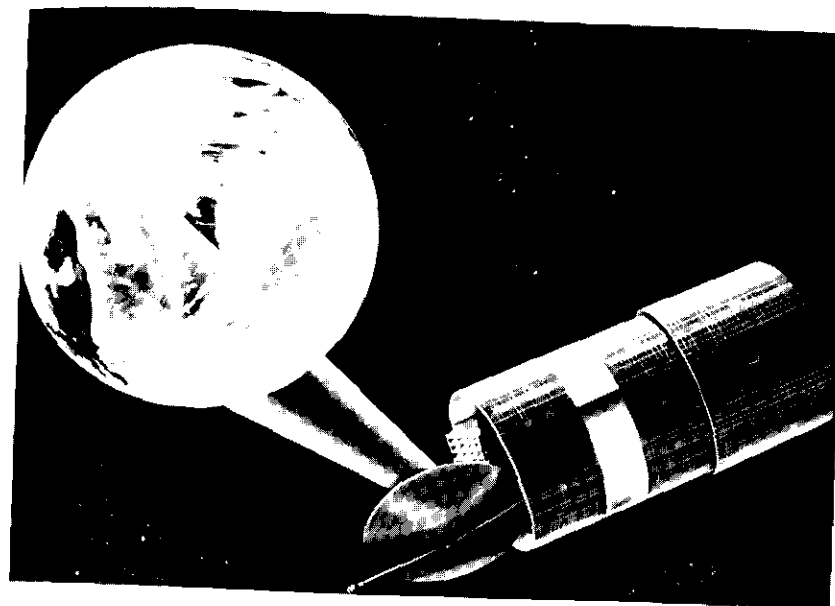


Figure 1. SBS Spacecraft Configuration

with a 6-MHz guard band between adjacent channels. The transponder frequency channelization is shown in Figure 2.

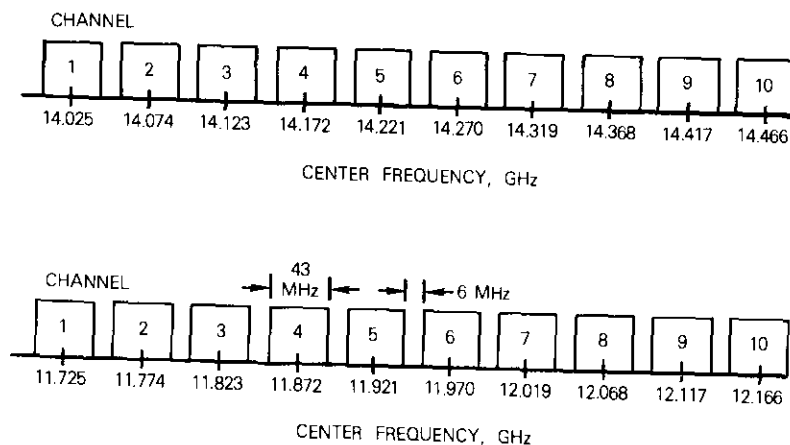


Figure 2. Spacecraft Repeater Channelization

The spacecraft antenna contains two reflectors that use orthogonal linear polarization and are mounted back to back in a single antenna structure. The received signals are vertically polarized and the transmitted signals are horizontally polarized. The cross-polarization isolation between the receive and transmit beam should be at least 15 dB. The antenna system generates shaped up-link and down-link beams for optimum coverage over CONUS. Performance specifications have been defined for six coverage regions over CONUS, as shown in Figure 3, to ensure that transmit power and receive sensitivity are concentrated in areas of greatest population. Table 1 gives the minimum specified values for saturated effective isotropically radiated power (e.i.r.p.) and receive gain-to-noise temperature ratio (G/T) for these regions.

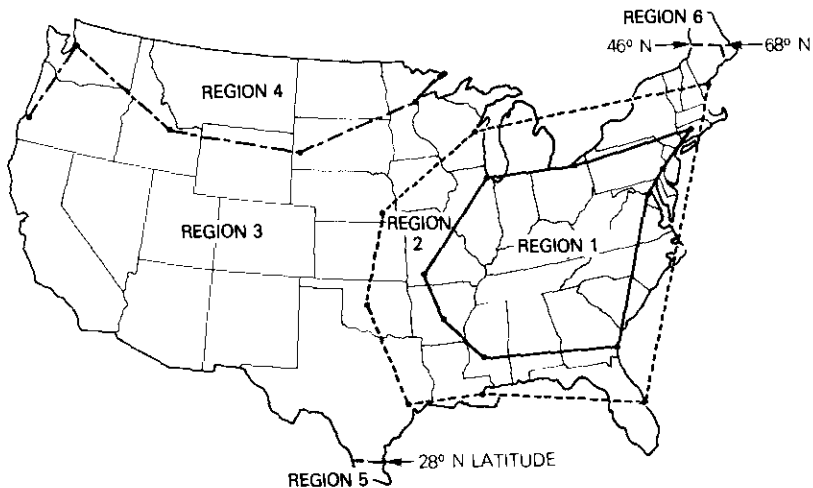


Figure 3. Antenna Coverage Regions

General transponder description

A block diagram of the transponder is shown in Figure 4. From the receive antenna-feed network, the received signal is routed to one of 4 low-noise receivers via a 1:4 redundancy switch network. Down-link frequency conversion is performed in the receiver, which also provides a single-step 6-dB signal attenuator selectable by ground command. Following amplification, the odd and even channels are separately

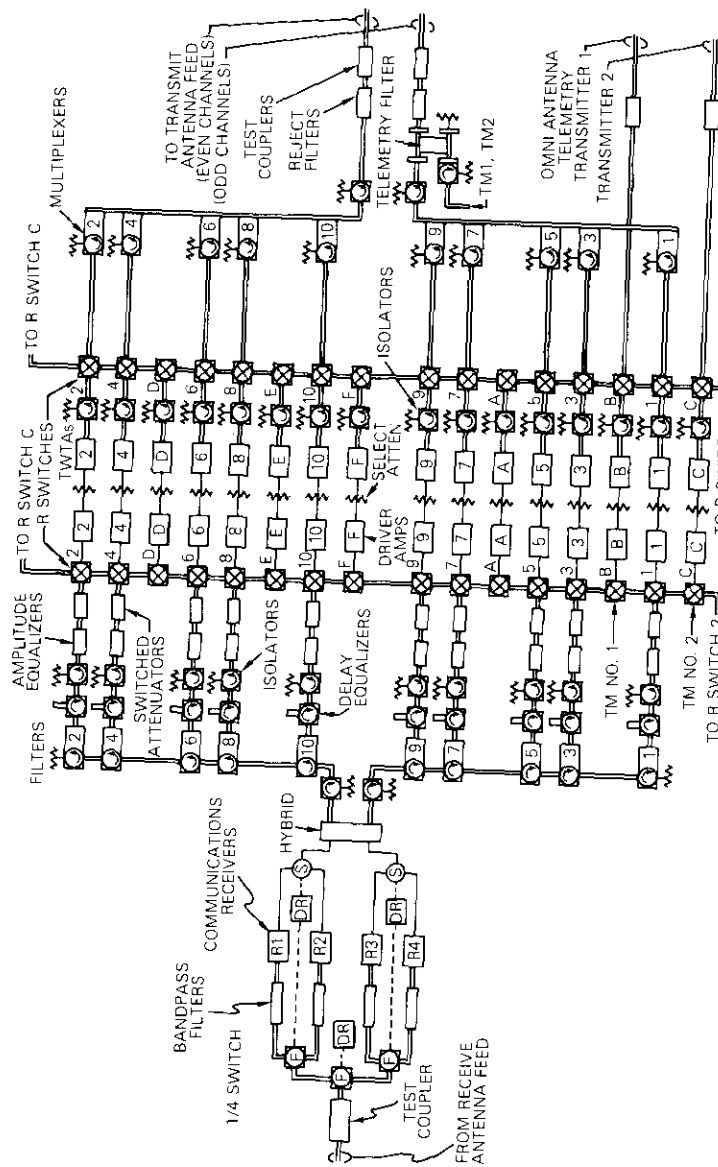


Figure 4. Transponder Block Diagram

channelized in the input multiplexer section that consists of 10 waveguide channel filters with delay and amplitude equalizers. Each channel also has a 3-dB step attenuator that is selectable by ground command.

Following the input multiplexer section, each channel signal is routed to a channel amplifier through an input redundancy switch network. This network consists of 16 mechanical waveguide switches which provide for a 16-channel amplifier redundancy for the 10 channels. The channel amplifiers contain a traveling wave tube amplifier (TWTA) preceded by a driver amplifier and a fixed attenuator that sets the overall gain of each amplifier to the same level.

The amplified channel signals from the TWTA output are routed to odd and even channel output multiplexers via an output redundancy switch network operating in tandem with the input redundancy switch network. These networks also provide the capability for routing telemetry signals through two TWTAs to the spacecraft omnidirectional telemetry antenna. The output multiplexers separately combine the odd and even channel output signals which are then transmitted by the dual-mode antenna system.

Overall communications performance specifications

The SBS transponder channel requirements are dictated primarily by the digital TDMA transmission mode. Other modes, such as FDMA/FM or FDMA/PSK, are accommodated without compromising the primary digital TDMA performance. Identical performance requirements apply to all channels; end-to-end requirements include antenna, receiver, channel filters, and output amplifiers.

LINK PERFORMANCE PARAMETERS

The change in G/T and saturated e.i.r.p. values (Table 1) in any region due to antenna beam-pointing variations should not exceed 2.5 dB over 24 hours. The flux density required for TWTA saturation from a location of minimum receive antenna gain in Region 3 is specified to be -82 ± 0.5 dBW/m² with both channel and receiver gain controls in low-gain settings.

FILTER REQUIREMENTS

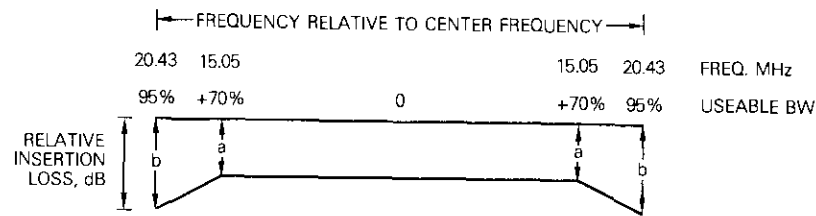
These parameters include in-band and out-of-band frequency response, gain slope, and group delay. The in-band frequency response specification is shown in Table 2.

The maximum gain slope within the usable channel bandwidth should not exceed the values given in Table 3 for signal drive levels ranging

TABLE 1. MINIMUM G/T AND SATURATED E.I.R.P. WITHIN REQUIRED REGIONS OF COVERAGE

REGION	RECEIVE G/T (dB/K)	TRANSMIT E.I.R.P. (dBW)
1	+2.0	43.7
2	0	41.7
3	-2.5	40.0
4	-5.5	37.0
5	-4.5	38.0
6	-5.5	39.0
San Francisco	+0.5	42.0
Los Angeles	-0.3	41.2

TABLE 2. IN-BAND FREQUENCY RESPONSE SPECIFICATION MASK



ILLUMINATION	ALLOWABLE VARIATIONS (dB)	
	WITHIN CENTER 70%	WITHIN CENTER 95%
From Saturation		
To Saturation +6 dB	0.5	1.4
Saturated	0.4	1.0
From Saturation to Saturation -20 dB	0.6	1.8

from 6 dB above saturation to 20 dB backed off from saturation. The total end-to-end group delay should be within the shaded areas shown in Figure 5 for all drive levels up to 6 dB above TWTA saturation. In addition, the total group-delay ripple (defined as having a period of 6 MHz or less) should not exceed 1.5 ns peak-to-peak. The channel input and output out-of-band response specifications are given in Table 4.

The input response is measured between the receiver input and the final high-power amplifier input; the output response is measured from the final amplifier input to the channel output.

TABLE 3. CHANNEL GAIN SLOPE REQUIREMENTS (dB/MHz)

FREQUENCY RANGE RELATIVE TO CHANNEL CENTER FREQUENCY	INPUT MAXIMUM GAIN SLOPE ^a	TOTAL MAXIMUM GAIN SLOPE ^b
± 15.05 MHz 70% or Less	0.10	0.20
± 17.20 MHz 80% or Less	0.20	0.35
± 19.35 MHz 90% or Less	0.35	0.55
± 21.50 MHz 100% or Less	0.8	1.3

^a Input gain slope is measured between the input to the transmission channel (including receive antenna) and the input of the final power amplifier.

^b Total gain slope is measured over the total transmission channel including the receive antenna and transmit antenna.

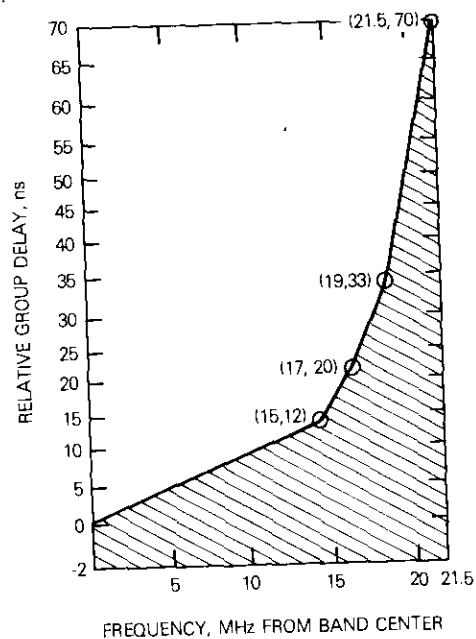


Figure 5. Total Channel Group Delay Vibration

TABLE 4. CHANNEL INPUT AND OUTPUT OUT-OF-BAND CHANNEL RESPONSE

	FREQUENCY DIFFERENCE FROM BAND CENTER ^a (MHz)	OUT-OF-BAND RESPONSE ^b (dB)
Input	± 27.7	> 15
	± 31.0	> 35
Output	± 27.5	> 10
	± 30	> 30

^a Shown in Figure 2.

^b Relative to band center.

NONLINEAR PERFORMANCE SPECIFICATIONS

Table 5 gives the limits for end-to-end channel third-order intermodulation products for the drive levels shown. The total channel phase shift must not exceed the values given in Table 6, where phase shift is the maximum shift of carrier phase when a single unmodulated carrier is varied from the specified level to no-drive. The AM-PM transfer coefficient with two carriers having an amplitude difference of up to 20 dB and the larger carrier amplitude modulated 1 dB peak-to-peak are not to exceed the values given in Table 7.

ADDITIONAL MISCELLANEOUS SPECIFICATIONS

An important consideration of a multichannel spacecraft is that the intermodulation components of the broadband receiver be sufficiently low to prevent significant spurious signals in the channel passbands. Table 8 provides these specification limits for the receiver. Additional communications parameter specifications that are important to proper operation of the satellite communications system are presented in Table 9.

Present spacecraft status

The three spacecraft presently under purchase from Hughes Aircraft Company use the Hughes HS376 bus. The first was launched on November 15, 1980, and is now operational and meeting all performance requirements. At the time of writing, the second spacecraft had been delivered to Cape Canaveral and was being readied for launch. The third is scheduled for a Space Transportation System (STS) launch in the latter half of 1982.

TABLE 5. CHANNEL CARRIER-TO-INTERMODULATION RATIOS^a

FLUX DENSITY AT THE SPACECRAFT FOR EACH OF TWO CARRIERS ^b (dB)	MAXIMUM LEVEL OF ANY THIRD-ORDER INTERMODULATION PRODUCT ^c (dB)
+3	6
0	8
-3	10
-10	15
-17	26

^a This specification will be met with any frequency separation in excess of 100 kHz, but within the passband of the transmission channel.

^b Relative to single-carrier saturation flux density.

^c Relative to each RF carrier.

TABLE 6. TOTAL TRANSMISSION CHANNEL PHASE SHIFT

FLUX DENSITY*	MAXIMUM PHASE SHIFT (deg)
+3	55
0	42
-3	30
-6	22
-9	15
-12	8

* Relative to single-carrier saturation flux density.

TABLE 7. CHANNEL AM-PM TRANSFER COEFFICIENT

TOTAL FLUX DENSITY OF TWO CARRIERS* (dB)	AM-PM TRANSFER COEFFICIENT (°/dB) (PEAK-TO-PEAK)
+3	6.0
0	6.0
-3	7.0
-6	7.0
-9	6.0
-12	4.5
-15	3.0

* Relative to single-carrier saturation density

TABLE 8. RECEIVER CARRIER-TO-INTERMODULATION RATIOS (dB)

FLUX DENSITY AT THE SPACECRAFT FOR EACH CARRIER*	CARRIER-TO-ONE INTERMODULATION PRODUCT RATIO
+17	≧ 25
+10	≧ 39
+7	≧ 45
+4	≧ 51

* Above single-carrier saturation flux density.

TABLE 9. ADDITIONAL COMMUNICATIONS PARAMETER SPECIFICATIONS

Spurious Output (in transmit band at input to transmit antenna)	
1-MHz Band	-55 dBW
4-kHz Band	-60 dBW
Long-Term Frequency Stability	
Over Lifetime, Including Initial Tolerance	± 10 parts in 10 ⁶
Over 3 mo. Including Eclipse Effects	± 2 parts in 10 ⁶
Commandable Gain Increase	
Channel	3 ± 0.25 dB
Receiver	6 ± 0.5 dB
Transponder Gain Stability (excluding attitude effects)	
Over Lifetime	3 dB peak-to-peak
Over Any Day	1 dB peak-to-peak
Over Any 10-Minute Period	0.5 dB peak-to-peak
Overdrive Capability (without subsequent degradation of lifetime performance)	9 dB above saturation

Solar absorptance degradation of an uncleaned radiator

N. L. HYMAN

(Manuscript received August 4, 1981)

Introduction

This note is an addendum to a recent paper on the measured solar absorptance (α_s) increase of the optical solar reflector (OSR) radiators on the COMSTAR satellite beacon experiment [1]. The referenced paper describes the beacon thermal and temperature telemetry characteristics, confirms constant power dissipation, and presents the theoretical basis for data reduction. Also presented are processed flight data from the first three COMSTAR satellites (D-1, D-2, and D-3); data from the fourth COMSTAR satellite (D-4) could not be included due to its much later launch (February 21, 1981).

There was confidence in the high accuracy of the α_s degradation results from the first three satellites, but two questions were not completely answered: (1) Why was the rate of α_s increase for the beacon radiators on the third COMSTAR appreciably higher than the rates for the first two satellites? (2) What were the relative contributions to degradation from inadequate prelaunch cleaning and post-launch contamination?

Prelaunch logistic priorities barred the removal of some of the D-4 OSR mirrors which would have provided an opportunity for detailed study of both the contamination accumulated during the radiator's 5-year storage and the effectiveness of subsequent cleaning. To glean useful information without perturbing satellite operations, no cleaning treatment was given to the radiator of the 28-GHz beacon package,

N. L. Hyman is a member of the technical staff in the Spacecraft Laboratory of COMSAT Laboratories.

while the 19-GHz radiator was cleaned according to the usual specifications. Non-cleaning was considered tolerable because beacon operation was to be limited to only 6 months, a time span that would not allow even a very rapid α_s degradation rate to cause excessively high temperatures. A comparison of α_s histories from these extreme radiator surface conditions was expected to offer a clue concerning the relative degradation contributions of storage and postlaunch contaminants. This Note presents the results of a comparison of α_s histories for the D-4 19-GHz cleaned and 28-GHz uncleaned radiators, as well as the 28-GHz D-1, D-2, and D-3 radiators.

Thermal model for the 19-GHz package

The referenced study concentrated on the 28-GHz beacon, comparing telemetered maximum diurnal temperatures to maximum temperature predictions based on a nodal thermal model. A technique of computing yearly fractional change in α_s from temperature data only, with no thermal model predictions, was used to confirm that the α_s vs time characteristics of adjacent 19-GHz and 28-GHz radiators (on the same satellite) matched to within 8 percent. Thus, no 19-GHz thermal model was necessary, and much labor was saved. However, since the D-4 beacon radiator surfaces are quite different, and beacon lifetime is less than one year, a 19-GHz thermal model was required for identical treatment of temperature telemetry data from both beacons. "Working curves" similar to those of Figure 2 of Reference 1 were obtained from this thermal model.

Constant dissipation and α_s calculation

The 6-month history of telemetered diurnal temperature extremes from the D-4 beacons is shown in Figure 1. The minimum temperature history of the 28-GHz package (showing a 1.5°C rise from vernal equinox to mid-April) is similar to that shown in Figure 5 of Reference 1; constant thermal dissipation in this package is thereby confirmed.

On May 19, 1981, the 19-GHz package suffered a slight power loss which caused a sudden 3°C drop in minimum temperature (equivalent to a 4-percent loss of power dissipation). This power loss is easily accommodated in calculating and presenting α_s vs time, since dissipation rates both before and after May 19 remained constant. Because change in α_s ($\Delta\alpha_s$) is of interest, the α_s vs time plot following May 19 (based on the same 34.2-W dissipation used prior to May 19) has been shifted up to match the preceding curve, with negligible loss of $\Delta\alpha_s$.

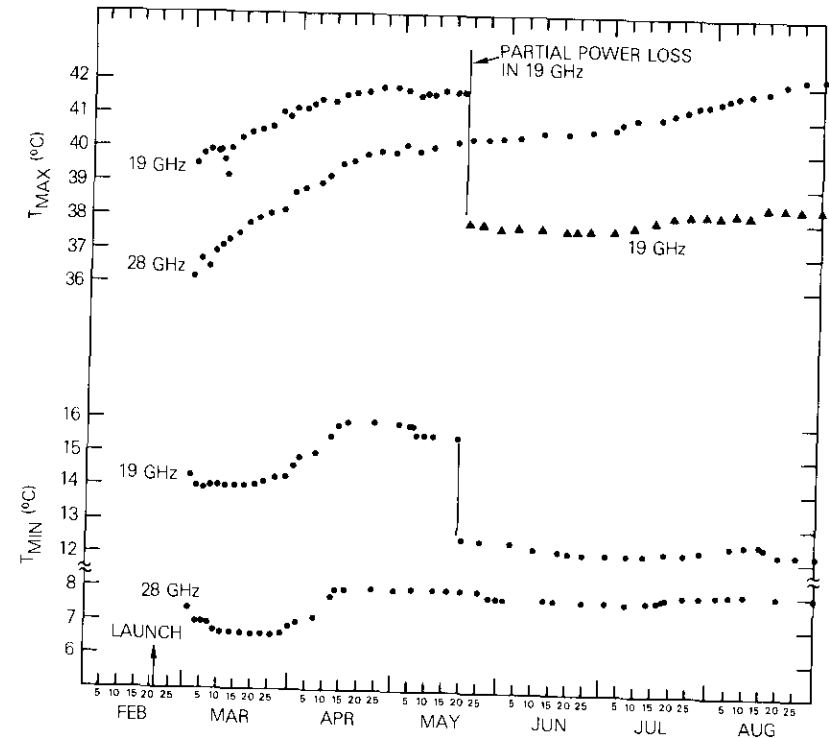


Figure 1. Diurnal Temperature Extremes from D-4 COMSTAR Beacon Telemetry

accuracy. This treatment results in a continuous curve for 19-GHz α_s vs time as shown in Figure 2, where the curve beyond May 19 has been lifted by exactly 0.02. Also shown is the α_s vs time behavior for the uncleaned 28-GHz radiator. Computations for α_s were based on the procedure described in Reference 1, using equation (4) and curves similar to Figure 2 of the reference.

Comparison with previous results

Because the data-gathering time span of the D-4 study was only 6 months, quantitative α_s vs time slopes may be subject to relatively large uncertainties. The most useful application of results is a direct comparison to the α_s vs time curves of the D-1, D-2, and D-3 COMSTAR beacon radiators over an identical time-of-year span. This approach

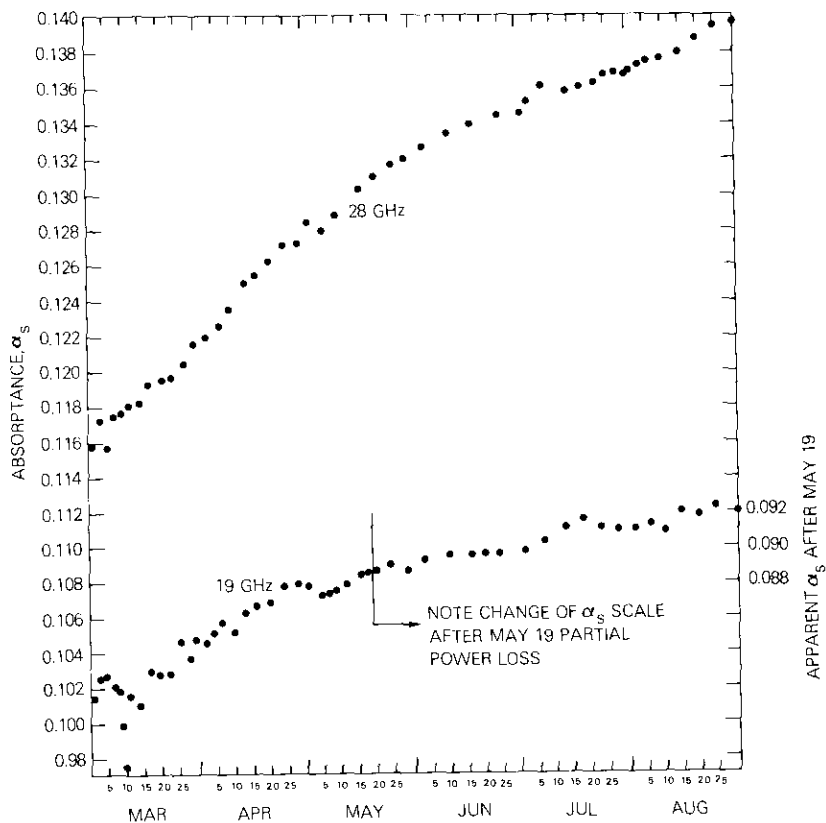


Figure 2. α_s History of Beacon Radiators on D-4 COMSTAR

has an inherent shortcoming, however, since the D-4 time span (from shortly after the February 21 launch through August) corresponds to time spans for the D-1, D-2, and D-3 which are from 8 to 10 months following launch, with a second appropriate span a year later. With an α_s degradation rate gradually decreasing with time (revealed by the D-1, D-2, and D-3 data), this time span mismatch would not allow a fully correct direct comparison of curve shapes and slopes. Thus, when such comparisons are made, it should be recognized that D-1, D-2, and D-3 degradation rates would have been higher had their time spans been as close to launch as that of D-4.

Figure 3 displays the 28-GHz α_s profiles of the D-1, D-2, and D-3 for two year-apart time spans each, together with the two D-4 results. The

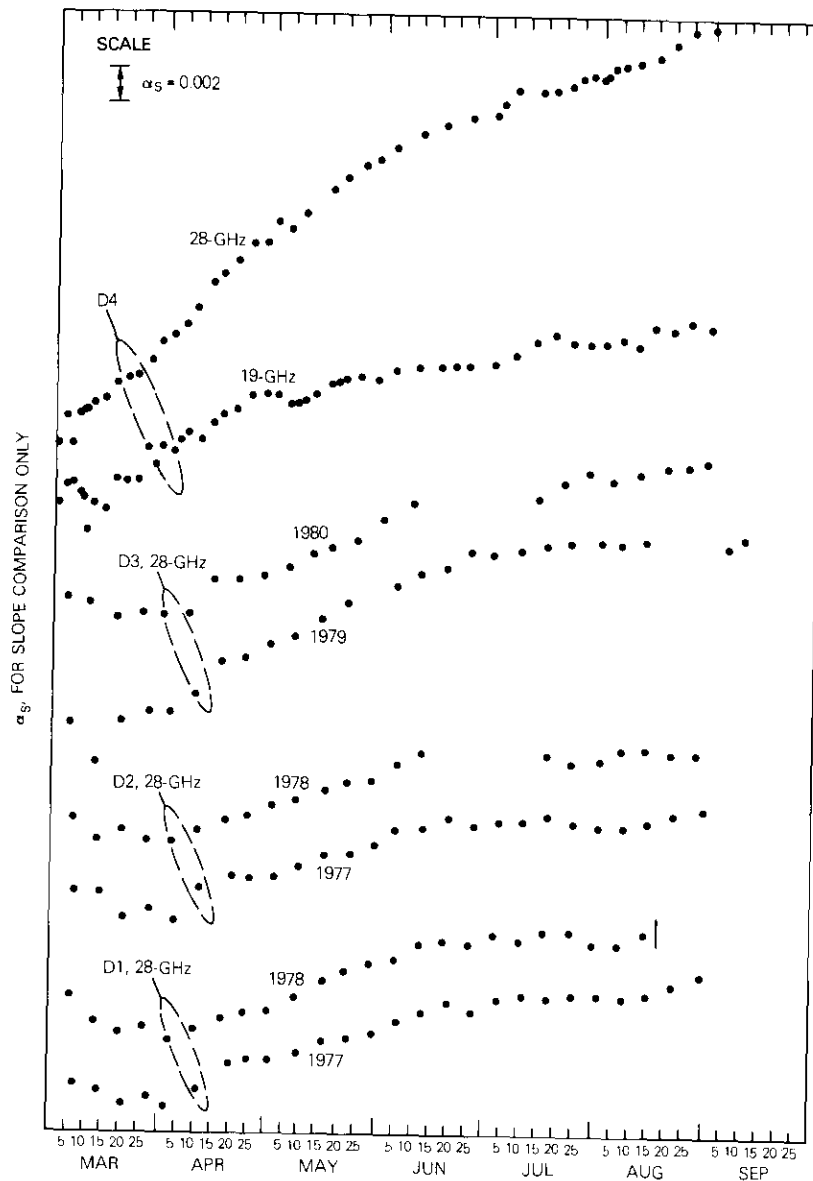


Figure 3. Comparison of D-1, D-2, D-3, and D-4 COMSTAR Beacon Radiator α_s vs Time Slopes During D-4 Time Span (March through August)

various curves are to scale but offset vertically for easier comparison. The first year's profiles for D-1, D-2, and D-3 show essentially constant slopes; during the second year for D-1, the slope decreases just 6 percent; the decrease for D-2 is slightly greater, 9 percent; and for D-3, 11 percent. (The short time spans do not allow an average yearly slope computation.)

Comparison of initial α_s magnitudes from Figure 2 with the corresponding values from Figure 9 of Reference 1 indicates that the D-4 19-GHz value is somewhat lower than those of D-2 and D-3, and appreciably lower than that of D-1. The D-1 initial α_s value is similar to the uncleaned D-4 28-GHz value. These apparently inconsistent results support the conclusion in the reference that the absolute α_s error is of the order of ± 0.01 .

From the referenced study, it is known that α_s increases with increasing solar incidence angle, causing a positive perturbation in the α_s vs time curve between autumnal and vernal equinoxes, when the sun angle is greater than approximately 20° from normal. The D-4 data from early March fall into this time span category. Also, for several weeks following launch, satellite housekeeping functions were not constant, and slight changes in earth-pointing attitude could perturb beacon maximum diurnal temperature. It is also possible that during this March 1981 time frame, a rapid increase in the D-4 α_s occurred, as was observed in the D-3 28-GHz radiator immediately after launch. Because of these three combined irregular influences, it is not surprising that in March some D-4 19-GHz data scatter occurred. These data from the D-4 19-GHz radiator are therefore not used for comparison or explanation.

A comparison of the 5-month (April through August) change in α_s for all beacon radiators is shown in Table 1. The D-4 19-GHz $\Delta\alpha_s$ is approximately equal to that of D-1, slightly higher than that of D-2, and significantly lower than that of D-3. Considering the D-4 time interval (at least 8 months closer to launch than the others), it is expected that a more correct comparison, using the D-4 results 8 months later, would result in a smaller D-4 α_s vs time slope, most likely approximating that of the D-2.

As indicated in the Introduction of this Note, a hoped-for result of leaving one D-4 radiator uncleaned was a measure of the relative contributions to α_s degradation of inadequate prelaunch cleaning and in-orbit contamination. This measure would be possible, however, only if there had been no large differences in α_s histories between

TABLE 1. BEACON RADIATOR α_s INCREASES, APRIL THROUGH AUGUST

COMSTAR	YEAR	$\Delta\alpha_s$	APPROXIMATE INITIAL (POSTLAUNCH) α_s
D-1	1977	0.0074	0.115
	1978	0.0070	
D-2	1977	0.0060	0.104
	1978	0.0055	
D-3	1979	0.0100	0.108
	1980	0.0090	
D-4 (19-GHz cleaned)	1981	0.0075	0.100
	(28-GHz uncleaned)	1981	

cleaned and uncleaned, implying either not much initial contaminant (nothing that could be cleaned off) or an almost totally ineffective cleaning procedure. Such was not the case, and the second question raised in the Introduction remains unanswered.

Conclusions

CLEANED RADIATOR

The main conclusion from this comparison of 6 months of α_s vs time data is that the OSR α_s on the D-4 19-GHz beacon radiator is degrading at a rate approximately equal to that on the D-2 28-GHz; that is, somewhat less than that on the D-1 and appreciably less than that on the D-3. Initial α_s readings after launch are lowest for the D-4 19 GHz.

The reason for this relatively low degradation rate for the D-4 19-GHz radiator is not immediately apparent; the accumulation of surface contaminants on D-4 should be at least as large as on any of the other radiators because of the much longer storage time for D-4. A possible explanation might be that somehow a different cleaning procedure and/or technique was used. (The author did not witness any actual cleaning.) During the $2\frac{2}{3}$ years between D-3 and D-4 cleaning, changes could have been made in the specifications on solvents, procedures, etc., and/or personnel. In addition, a subtle human factor could have prompted a more careful, thorough, and effective cleaning. There may

have been a greater awareness of the importance of D-4 radiator cleaning, since attention was focused on this activity by the specific, unusual instructions for cleaning only one radiator.

UNCLEANED RADIATOR

As shown in Figure 2, the α_s for the uncleaned 28-GHz radiator, unlike the cleaned 19-GHz unit, increases monotonically from early March through August. The total α_s increment over the entire data collection span is more than double that of the 19-GHz radiator. The initial α_s of approximately 0.116 is appreciably higher than the approximately 0.100 for the 19-GHz unit; this difference is of interest despite the relatively high uncertainty in absolute α_s calculations. However, for a 3-week period, from mid-March through the first week in April, the α_s vs time slopes are almost identical for the two radiators. This may indicate that it took about 3 weeks for the D-4 surface contaminants to significantly darken under ultraviolet exposure.

The higher initial α_s and the rate of increase for the 28-GHz radiator were expected, but a quantitative comparison (*i.e.*, the α_s increase twice that of the 19-GHz) cannot be readily interpreted into a definitive measure of the nature or extent of prelaunch OSR surface contamination. The general conclusion is that more contaminant was initially present on the uncleaned 28-GHz radiator in orbit; the prelaunch cleaning of the 19-GHz radiator was, by this type of measure, effective.

A quantitative conclusion is an upper limit on OSR α_s degradation as a result of poor cleaning procedures. No matter how deficient OSR cleaning, α_s degradation should be no worse than that presented here.

Reference

- [1] N. L. Hyman, "Solar Absorptance Degradation of the COMSTAR Satellite Centimeter Wave Beacon Thermal Radiators," *COMSAT Technical Review*, Vol. 11, No. 1, Spring 1981, pp. 159-177.

19- and 28-GHz high power/efficiency IMPATT amplifiers*

SU MIN CHOU

(Manuscript received July 22, 1981)

Introduction

This note presents the results of experiments on an improved design for 19- and 28-GHz IMPATT solid-state amplifiers for possible Beacon application on future INTELSAT satellites. In this design, double-drift region silicon diodes replace the single-drift region silicon IMPATT diodes used in the COMSTAR Beacons built at COMSAT Laboratories [1]-[3]. The new amplifier design also simplifies assembly and tuning procedures considerably.

Advances in device technology have made it possible to improve the DC to RF conversion efficiency and reliability of IMPATT amplifiers. Three different kinds of IMPATT diodes (NEC's single- and double-drift silicon, and Varian's GaAs Read-profile) were tested as oscillators at 19 GHz. Results showed that Varian's GaAs IMPATT diode delivers 1-W RF power with 15-percent efficiency. The NEC double-drift silicon IMPATT diode delivers 1.4 W with 10-percent efficiency, and the NEC single-drift silicon diode delivers 750-mW RF power with less than 6.5-percent efficiency.

Of all the devices tested, the Varian GaAs Read diode was the most efficient. However, NEC's double-drift silicon diode was selected over Varian's diode because the NEC diodes appear to be better adapted for

*This note is based upon work performed at COMSAT Laboratories under the sponsorship of INTELSAT.

Su Min Chou is senior staff scientist in the Microwave Communications Laboratory, COMSAT Laboratories.

space flight. A single-diode IMPATT module operating as the final stage of a 19-GHz output amplifier, and a single-diode IMPATT module operating as the final stage of a 28.6-GHz output amplifier were developed and tested. NEC double-drift region silicon IMPATT diodes ND8020W-5H and ND8030W-1N were employed in the 19-GHz and 28.6-GHz amplifiers, respectively. In these diodes, diamond heat sinks allow for efficient diode junction heat dissipation. Output powers of 1 W at 28.6 GHz (with 10-percent efficiency) and 2 W at 19 GHz (with more than 13-percent efficiency) were achieved when the diodes operated at optimum efficiency. At these output power levels, the amplifiers showed a 5.5 ± 0.2 dB gain with a bandwidth of more than 5 percent.

19-GHz single-diode IMPATT amplifier

The 19-GHz single-diode IMPATT amplifier design is novel in many respects. The main body of the amplifier module is in one piece, making the amplifier more compact and easier to fabricate and assemble. The reduced-height waveguide through the block is fabricated by electric discharge techniques. The diode is soldered into a diode mount, which is held in place with a retainer nut. A spring-loaded, low-pass filter section insures a positive pressure bias contact to the diode. Figure 1 shows a cross-section view of the amplifier module.

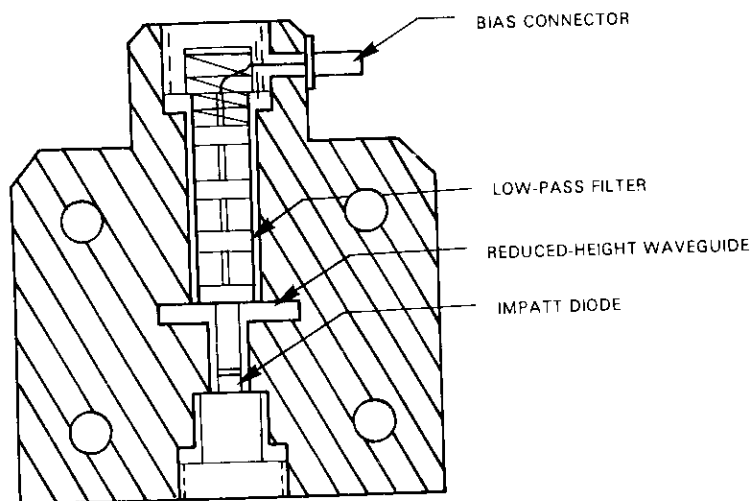


Figure 1. Cross-Section View of 19-GHz Amplifier Module

An external view of the single-stage breadboard amplifier module is shown in Figure 2. The diode module is connected to a five-port circulator through a waveguide transformer. The current regulator box, which can support two amplifier stages (only one regulator is wired), is shown on the right. The insertion loss of the circulator is less than 0.3 dB per path and the return loss for each port is 23 dB minimum.

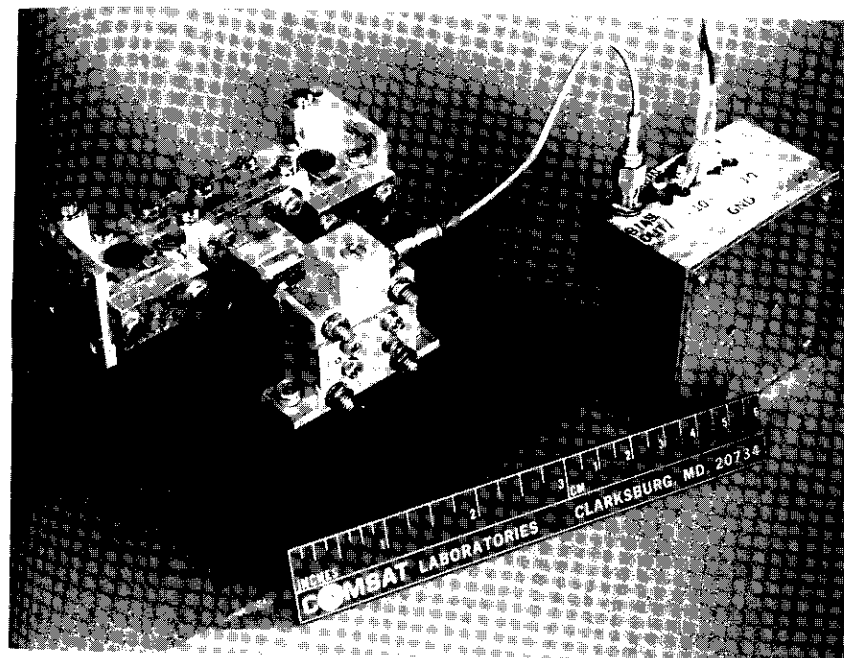


Figure 2. 19-GHz Single-Stage IMPATT Amplifier

Manual measurements were carried out by the test procedure shown in the block diagram in Figure 3. At different input power levels, the gain, output power, and power-added efficiency of the amplifier were measured and plotted against various bias current conditions. Results are shown in Figures 4, 5, and 6. A typical plot of gain, output power, and power-added efficiency vs the input power level is shown in Figure 7. When the amplifier operates at 160-mA bias current, the junction temperature rise is less than 140°C . The amplifier delivers

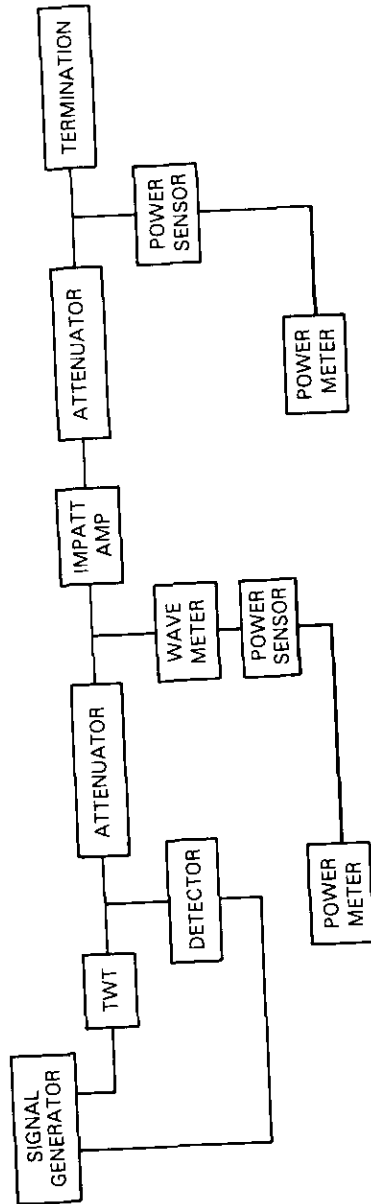


Figure 3. IMPATT Amplifier Test Set-Up

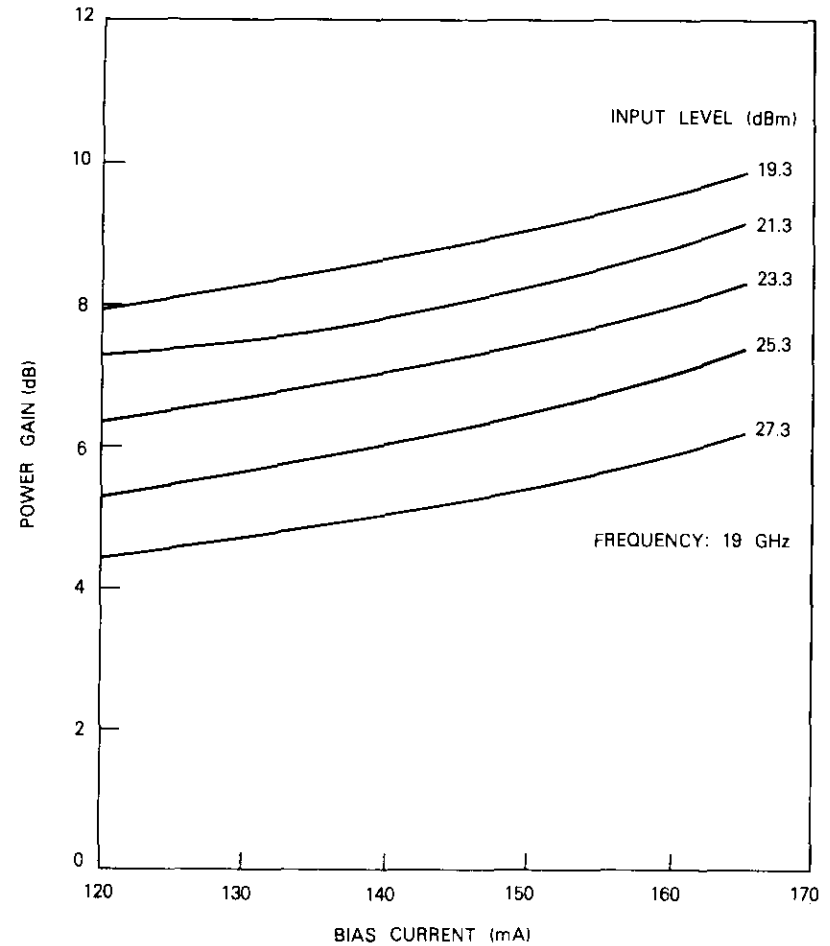


Figure 4. Amplifier Gain vs Bias Current

more than 33 dBm at 19 GHz with a 5.7-dB gain and more than a 13-percent power-added efficiency.

The amplifier was tested for broadband performance. Plots of the gain vs frequency and output power vs frequency at different input power levels are shown in Figures 8 and 9. For example, at 27-dBm input power level, the amplifier provides 5.8 ± 0.2 dB gain and 1.4-GHz bandwidth centered at 19 GHz.

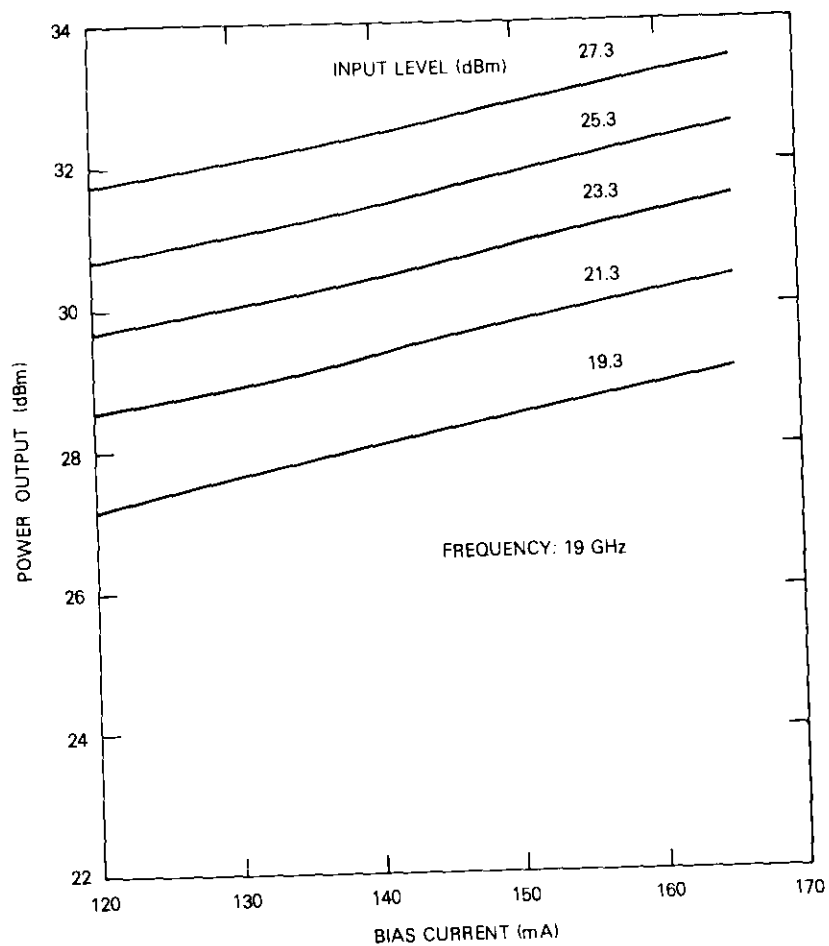


Figure 5. Power Output vs Bias Current

28-GHz single-diode IMPATT amplifier

Figure 10 shows the external view of a 28-GHz single-diode amplifier with input and output isolators. Its basic construction is similar to that of the 19-GHz IMPATT amplifier. The NEC double-drift silicon IMPATT diode ND8030W was used, and the current regulator design was the same as that of the 19-GHz amplifiers.

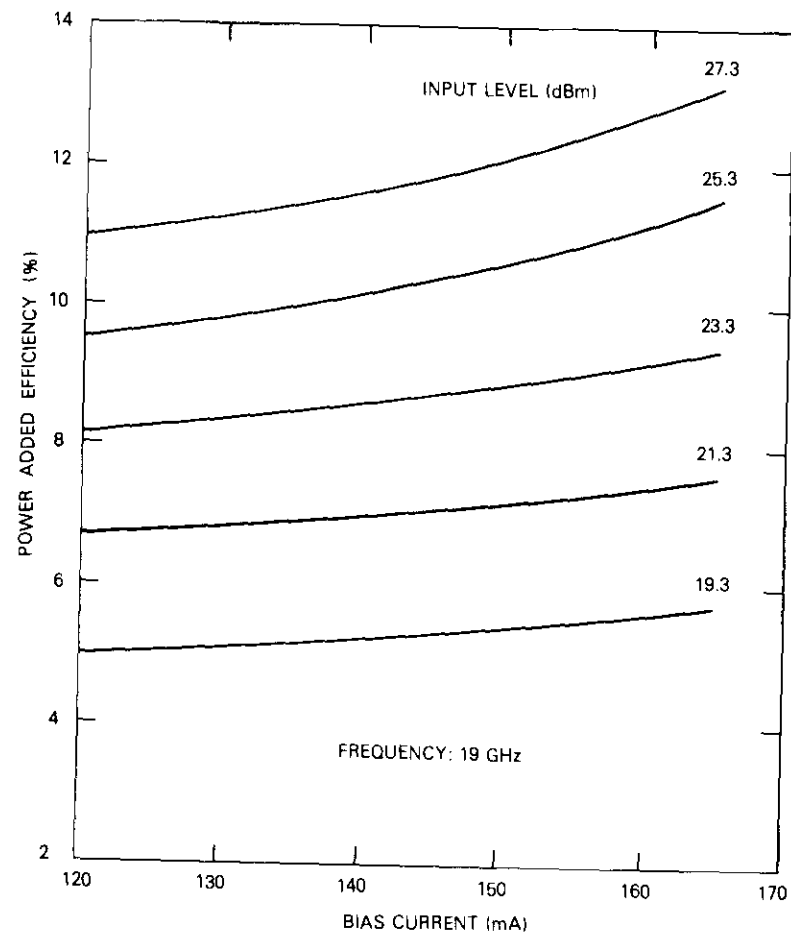


Figure 6. Power-Added Efficiency vs Bias Current

Figures 11, 12, and 13 show plots of typical gain, output power, and efficiency vs bias current at 28.6 GHz. The amplifier delivers 1-W RF power with 5.3-dB gain and 9.5-percent power-added efficiency. The gain and output power vs frequency at various input power levels is also illustrated in Figures 14 and 15. The amplifier shows more than

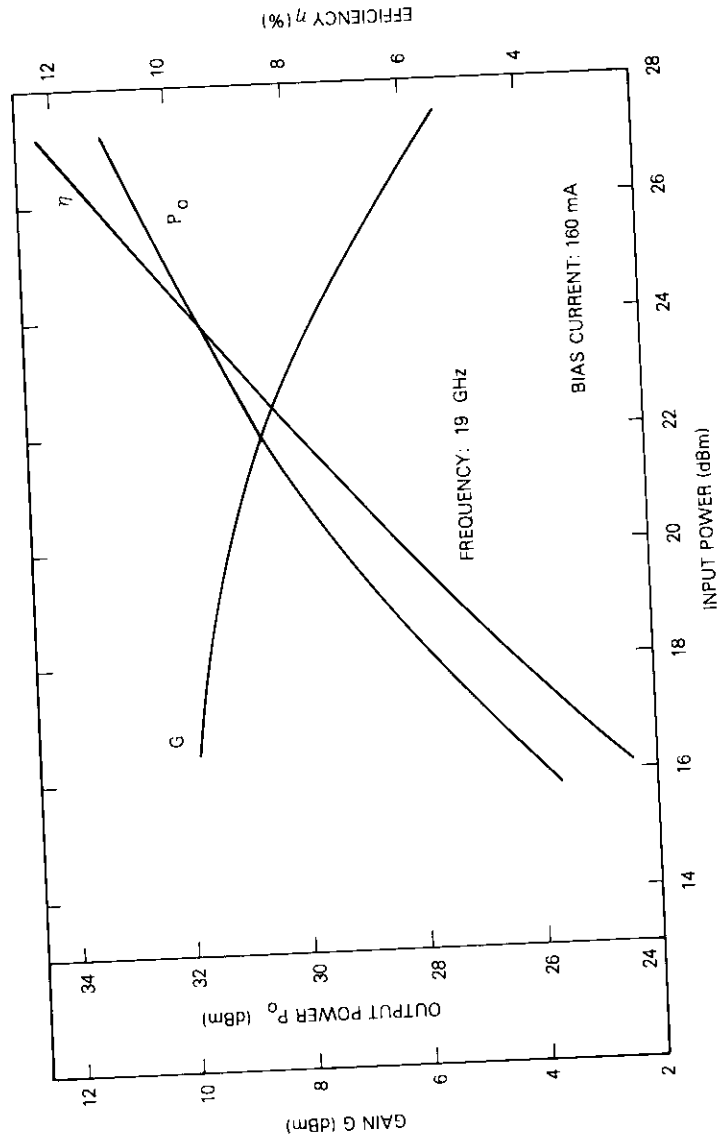


Figure 7. A Typical Plot of Gain, Output Power, and Power-Added Efficiency vs Input Power

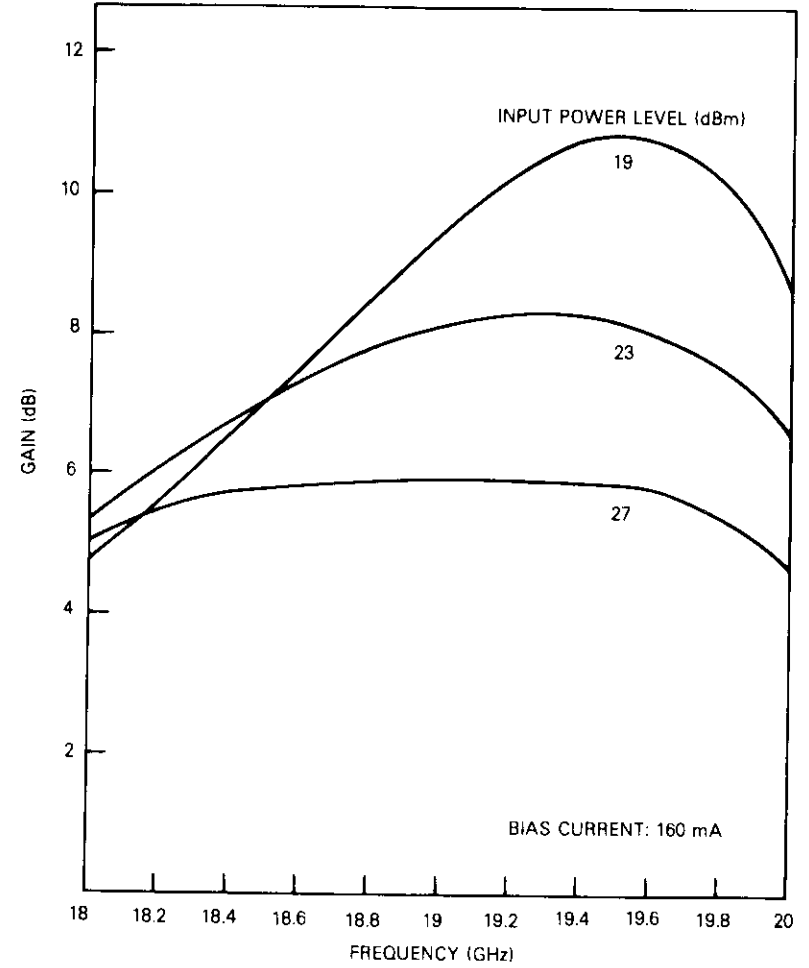


Figure 8. Amplifier Gain vs Frequency

a 1-GHz bandwidth with a 5.0 ± 0.2 dB gain at 1-W output power level centered at 28.6 GHz.

A plot of typical output power, efficiency, and gain vs input power level, is also shown in Figure 16. The bias condition at which these particular data were taken was 130 mA and 55.3 V.

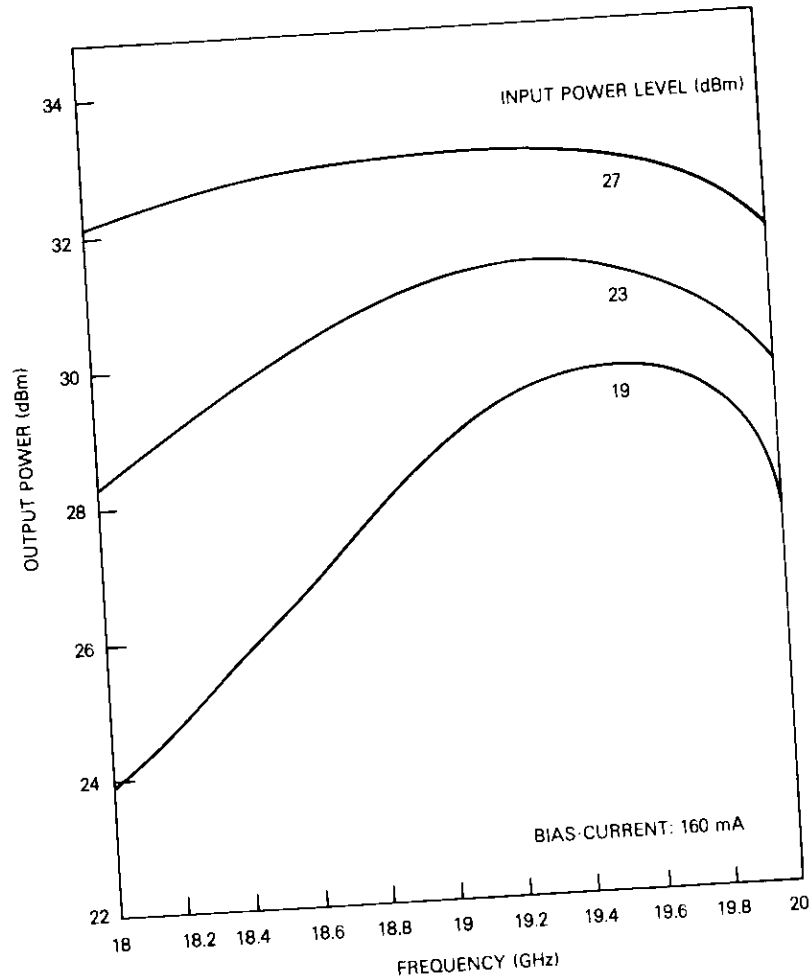


Figure 9. Amplifier Output Power vs Frequency

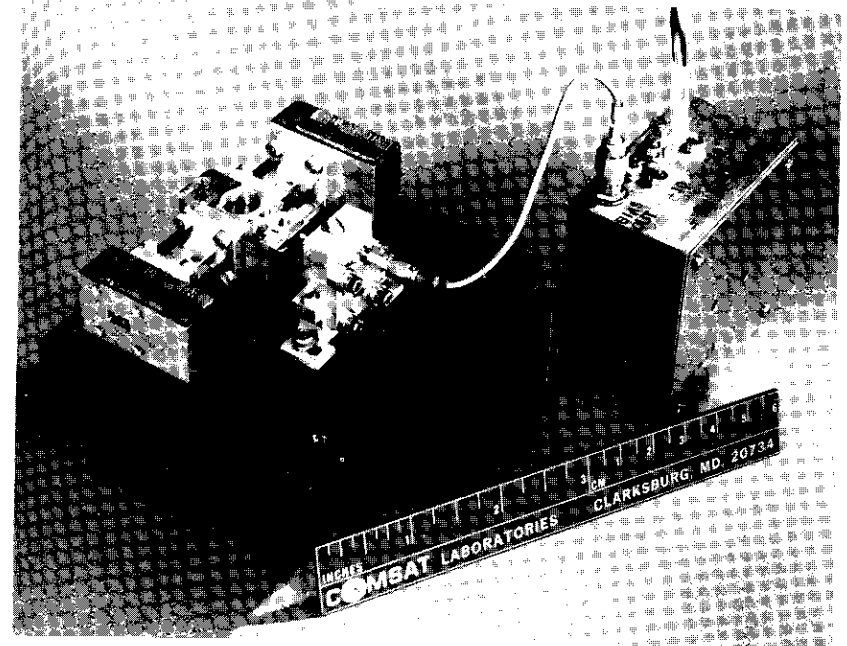


Figure 10. External View of a 28-GHz IMPATT Amplifier

Conclusions

The overall performance of single-stage, single-diode IMPATT amplifiers is summarized in Table 1. COMSTAR amplifier data are listed for comparison.

Typical results obtained from the same 19-GHz IMPATT amplifier indicate that the IMPATT diode can be operated somewhat less efficiently if less RF output power and lower DC power consumption are desired.

The new design requires minimum tuning, and affords easy replacement of the diode. Three amplifier modules of the 19- and 28-GHz kind

TABLE 1. SUMMARY OF SINGLE-DIODE AMPLIFIER PERFORMANCE

PERFORMANCE PARAMETERS		AMPLIFIERS			
		19 GHz (COMSTAR)	19 GHz (NEW)	28 GHz (COMSTAR)	28 GHz (NEW)
Output Power	(W)	0.87	2.0	0.3	1.0
Gain	(dB)	5.2	6.1	6.7	5.3
Operating Bias					
V_{op}	(V)	48	76.2	37	55
I_{op}	(mA)	180	165	98	130
DC Power	(W)	8.64	12.5	3.6	7.2
Bandwidth					
(± 0.2 dB)	(GHz)		1.4		1.0
Power-Added Efficiency	(%)	7	13.1	6.6	9.5
Junction Temperature Rise	($^{\circ}$ C)	160	160		170

have been built and more than five diodes have been tested in each module. Amplifier performance can be kept the same with slight tuning adjustment to compensate for the differences among individual diodes.

The amplifiers tested were stable and did not exhibit any spurious signals or out-of-band oscillations up to 40 GHz. Under a no-drive condition, the input VSWR of both amplifiers was better than 1.2:1. The amplifiers showed no measurable effect from load variations.

Acknowledgments

The author wishes to acknowledge the valuable comments and critique by M. Barrett and W. Getsinger, and to thank M. Urcuyo for the measurements.

References

- [1] M. J. Barrett, "19- and 28-GHz IMPATT Amplifiers," *COMSAT Technical Review*, Vol. 7, No. 1, Spring 1977, p. 129.
- [2] L. Pollack, "Centimeter Wave Beacons for COMSTAR Satellites," *COMSAT Technical Review*, Vol. 7, No. 1, Spring 1977, p. 103.
- [3] W. J. Getsinger, "Centimeter Wave Beacon Transmitter Design," *COMSAT Technical Review*, Vol. 7, No. 1, Spring 1977, p. 109.

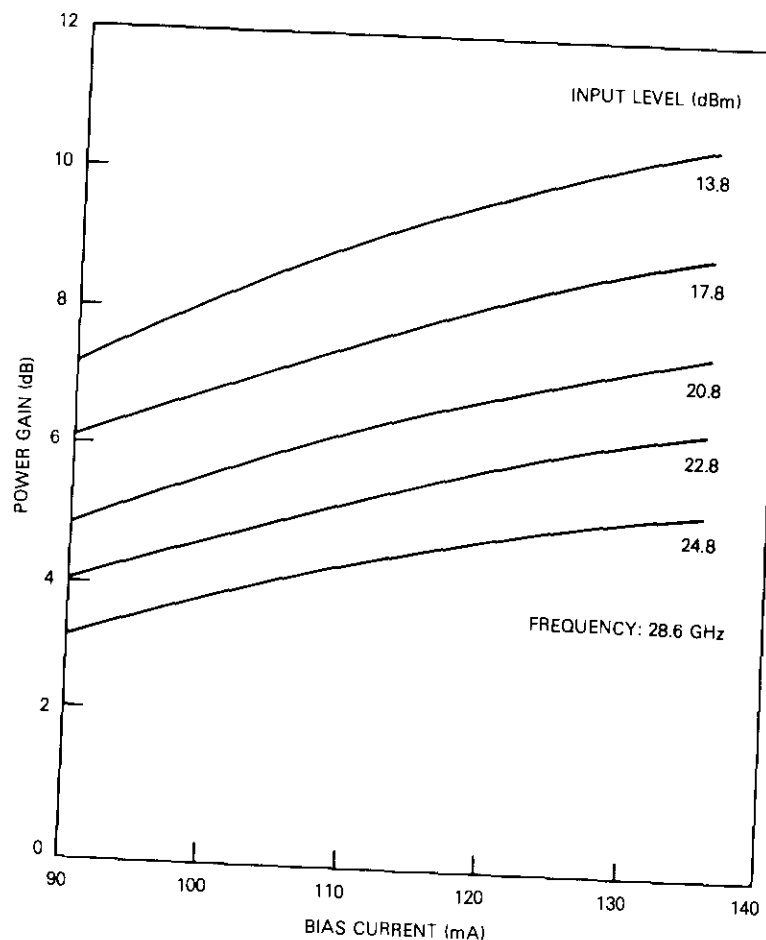


Figure 11. Power Gain vs Bias Current

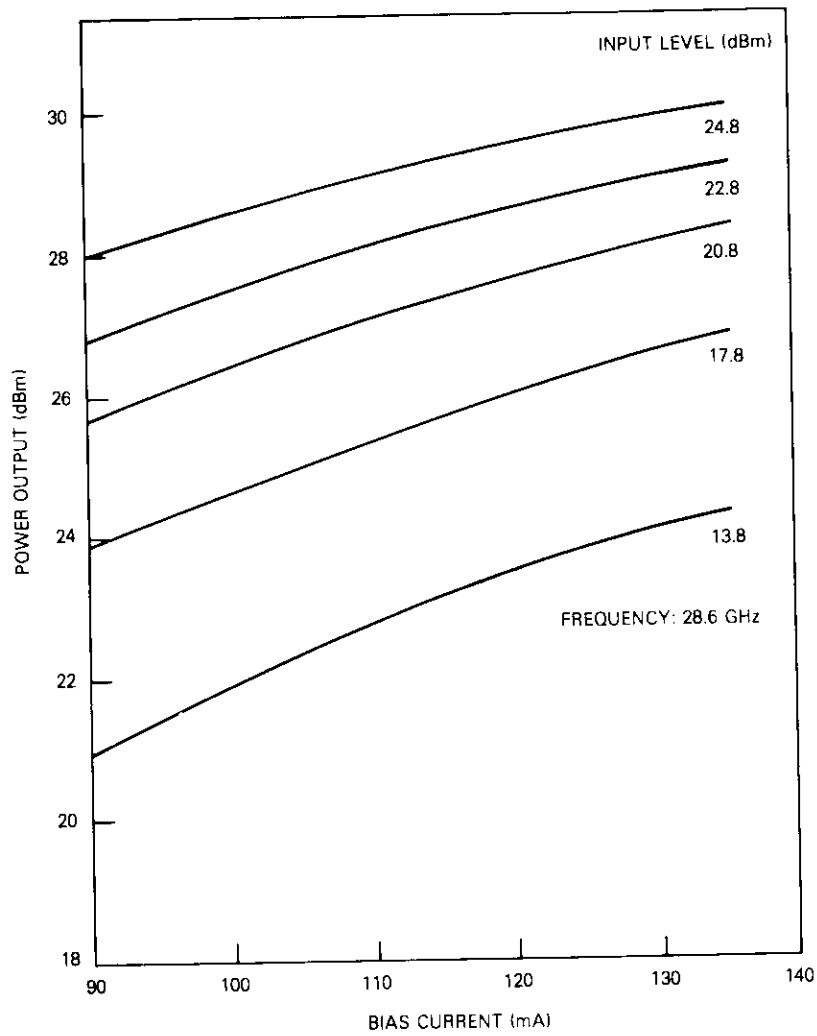


Figure 12. Output Power vs Bias Current

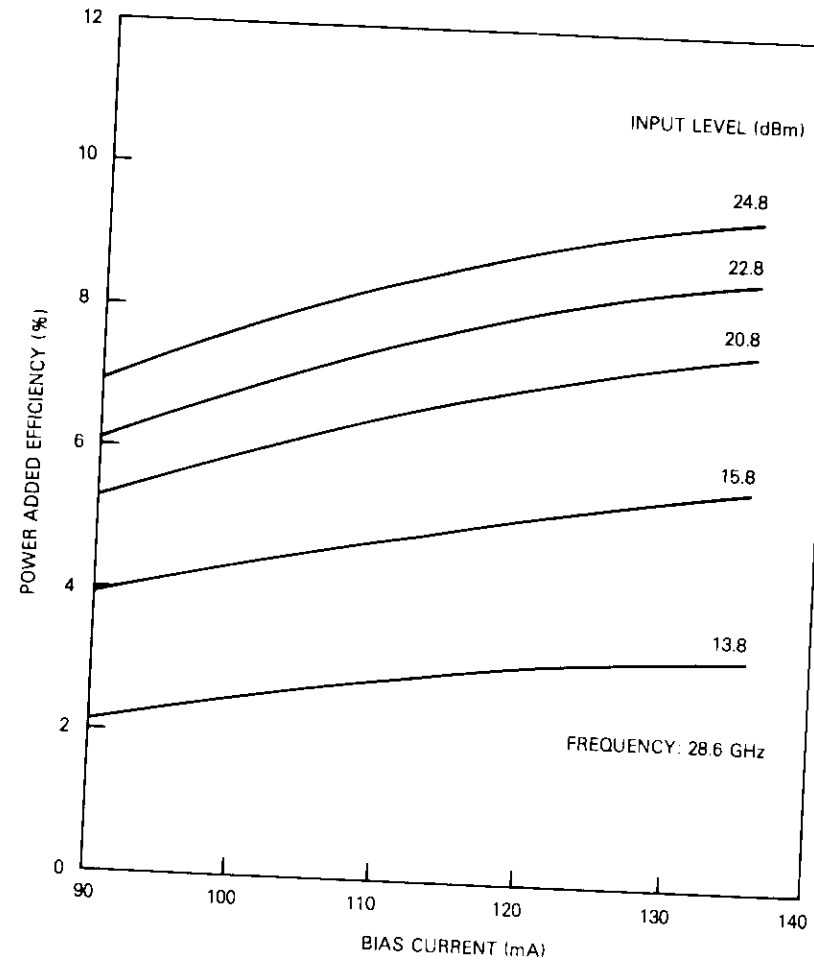


Figure 13. Power-Added Efficiency vs Bias Current

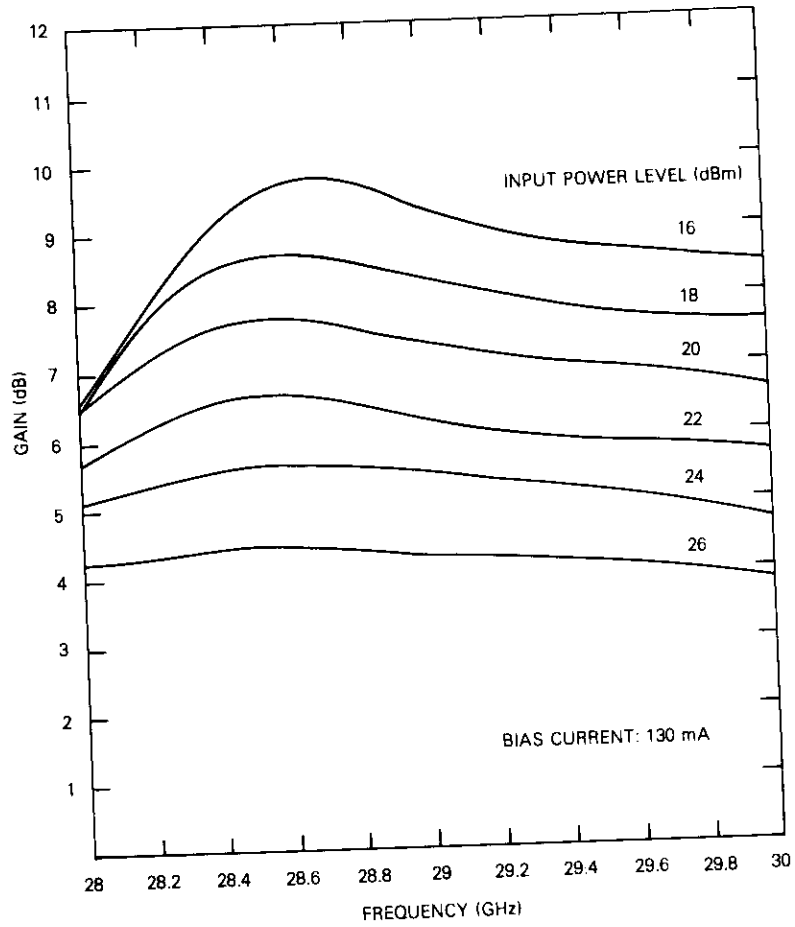


Figure 14. Power Gain vs Frequency

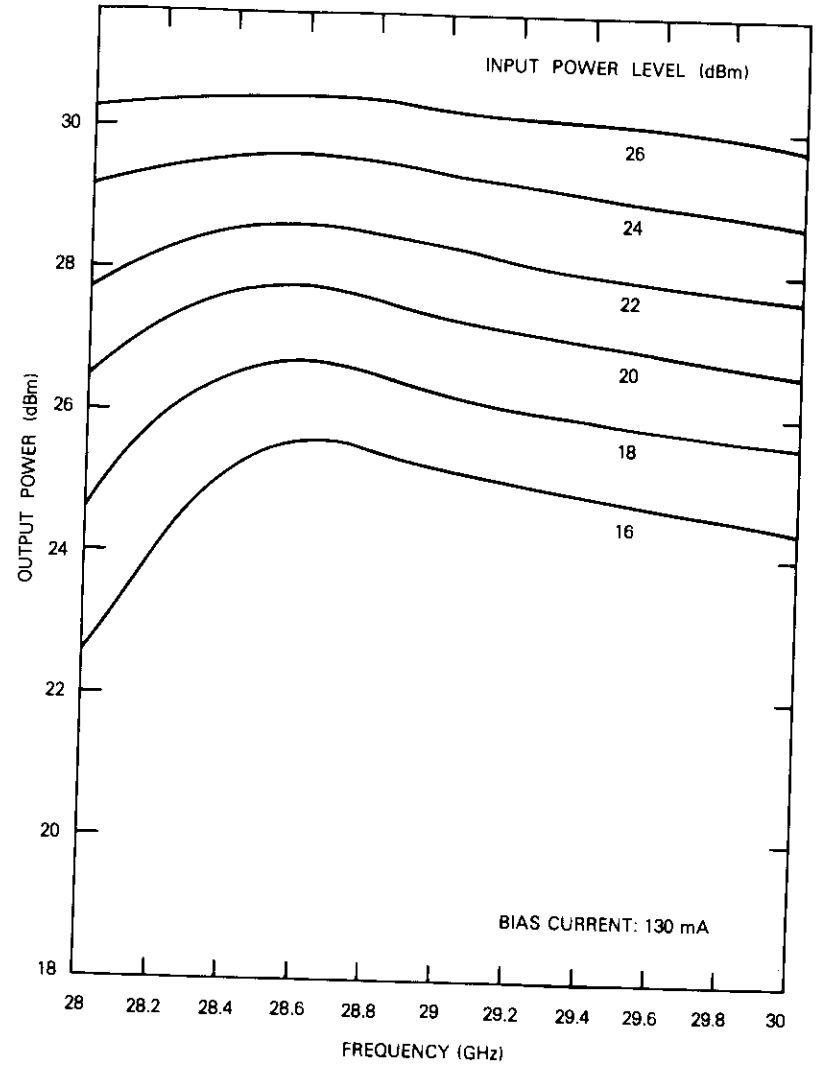


Figure 15. Output Power vs Frequency

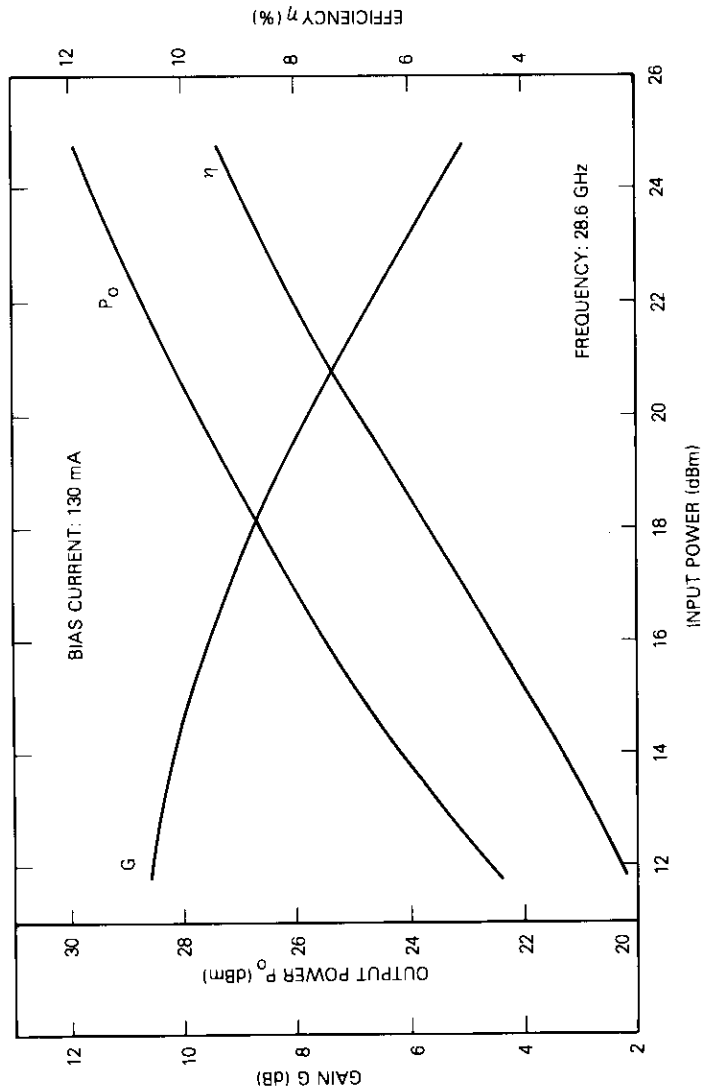


Figure 16. A Typical Plot of Power Output, Gain, and Efficiency vs Input Power Level

Translations of Abstracts in this issue

Système à satellite de radiodiffusion directe pour les Etats-Unis

L.M. KEANE, *Rédacteur*

Sommaire

Les articles de cette série décrivent le premier service commercial de radiodiffusion directe par satellite proposé pour les Etats-Unis. Les articles définissent les éléments du système tels qu'ils sont conçus à l'heure actuelle, et décrivent les principaux compromis techniques que l'on a dû faire au cours de l'élaboration de la configuration du système. On y indique les services qui seront offerts, et quels en seront les caractéristiques. Les articles envisagent l'utilisation de l'orbite et du spectre à la lumière des conférences mondiales sur la planification des satellites de radiodiffusion directe. On y présente également des analyses et des mesures pour déterminer quel serait le moyen le plus efficace permettant au service de radiodiffusion directe par satellite et aux autres services nationaux (terrestres fixes) de partager éventuellement les mêmes bandes de fréquences.

Evolution du système SBS

W.H. CURRY, JR.

Sommaire

Au début de 1981, la société Satellite Business Systems (SBS) a lancé ses nouveaux services à domicile. Elle met désormais à la disposition des clients des réseaux privés commutables permettant une transmission intégrée de la téléphonie, des données numériques et de l'image par l'intermédiaire de liaisons par satellite entre stations terriennes situées à domicile.

La SBS projette de faire évoluer les possibilités du système de façon à permettre l'introduction du partage des services par les clients dont les besoins